UNIVERSITY OF CALIFORNIA

Los Angeles

Characterizing miR-146a and miR-34a in B-cell lymphomagenesis

A dissertation submitted in partial satisfaction of the requirements for the degree

Doctor of Philosophy in Cellular and Molecular Pathology

by

Jorge Rafael Contreras

2016

ABSTRACT OF THE DISSERTATION

Characterizing miR-146a and miR-34a in B-cell lymphomagenesis

by

Jorge Rafael Contreras

Doctor of Philosophy in Cellular and Molecular Pathology

University of California, Los Angeles, 2016

Professor Dinesh Subba Rao, Chair

B-cell development is punctuated by developmental stages that rely on precise expression of regulatory genes and gene rearrangements necessary to advance the developing cell. MicroRNAs (miRNAs) function at the post-transcriptional level by targeting mRNA transcripts adding a layer of gene expression modulation previously unappreciated. miRNAs have been demonstrated to be intricately involved in each of the developmental stages of the B-cell. These small non-coding RNAs have been shown to either promote malignant transformation or suppress it. Hence, some miRNAs have been dubbed oncomiRs while others are called tumor suppressors. In samples of B-cell lymphoma dysregulated expression of numerous miRNAs is well documented, but functional roles for many of these remain to be elucidated.

miR-146a is an NF-κB responsive gene that modulates the inflammatory response. Early studies identified IRAK1, and TRAF6 as targets of this miRNA. Since these two proteins are adaptor molecules of the NF-κB pathway they complete a negative feedback loop between miR-146a and NF-κB. Studies on the effects of deficiency of miR-146a demonstrated a role in

myeloid, T- and B-cell malignancy as these animals developed all three given enough time. Several malignancies including breast cancer, papillary thyroid carcinoma, prostate cancer, and pancreatic cancer models have demonstrated the functional relevance of this miRNA suppressing proliferation, invasion, and migration. In B-cell malignancies the question remained does miR-146a modulate lymphomagenesis and if so is it through NF-κB. In our study using animals overexpressing c-Myc and deficient for miR-146a we observed reduced survival, increased lymph node involvement, differential involvement of the spleen, and malignancies of a mature B-cell phenotype. High throughput sequencing identified differentially expressed genes enriched for targets of the EGR1 transcription factor. Furthermore ectopic miR-146a expression in B-cell malignancies showed reduced proliferation with a concomitant decrease of EGR1 at the transcriptional as well as the translational level. Finally, EGR1 was identified as a bona fide target of miR-146a.

In response to cellular insults p53 induces various genes involved in cell cycle control, DNA repair, and apoptosis. Initial high throughput sequencing studies identified numerous miRNAs upregulated upon induction of p53. Among the miRNAs upregulated upon p53 induction is miR-34a. miR-34a can modulate genes involved in cell cycle progression, cell growth, and apoptosis. Developmental studies show miR-34a ectopic expression can arrest B-cells at the pro-B stage. Additionally, osteosarcoma and ovarian cancer samples demonstrate reduced expression of miR-34a. Given miR-34a's role in B cell development and its dysregulation in numerous malignancies we were interested in characterizing its role in B-cell lymphomagenesis. To answer this question we opted to use the well-established Eμ-Myc transgenic mouse line. High-throughput sequencing of c-Myc driven B-cell malignancies sufficient/deficient for miR-34a identified novel targets Csf1r, Jhy and Fgfr1. GSEA analysis of c-Myc driven B-cell malignancies revealed enrichment of miR-34a putative targets. miR-34a ectopic expression in B-cell lymphoma cell lines demonstrated reduced proliferation, as well as

novel targets Csf1r, Jhy, and Fgfr1. These findings identify novel targets of miR-34a in the context of B-cell malignancies.

This thesis identifies novel targets for both miR-146a and miR-34a that modulate B-cell oncogenesis demonstrated their roles as tumor suppressors. These studies pave the way for novel therapeutic approaches for c-Myc driven B-cell malignancies.

The dissertation of Jorge Rafael Contreras is approved.

Gay M. Crooks

Aldons J. Lusis

Samuel Wheeler French

Dinesh Subba Rao, Committee Chair

University of California, Los Angeles

2016

DEDICATION

This dissertation is dedicated to my family: my parents, Blanca and Jorge Sr.; my brother, Moises; my Queen, Teri; and the jewels of my heart, Val and Sam.

TABLE OF CONTENTS

FIGURES AND TABLES

ACKNOWLEDGEMENTS

First and foremost, I would like to thank God for without him none of this would be possible. I want to thank my advisor Dr. Dinesh Rao for giving me the opportunity to carry out my research studies and providing support, guidance, and mentorship through these years. I am sincerely grateful to have worked in his lab. I would like to thank my committee for their guidance and advice in my career. Also, I want to thank all the members of the Rao Lab through the years that have taught me, guided me, supported me, and lent a hand. In particular, Tiffany Tran, Thilini Fernando, Jayanth Palanichamy, Norma Rodriguez-Malave, Neha Goswami, Ella Waters, Parth Patel, Jasmine Gajeton, Jaime Anguiano, Kim Pioli, and Mike Alberti, and Nolan Ung.

The work presented in this thesis was supported in part by the Eugene V. Cota-Robles Fellowship from UCLA and the Tumor Immunology Training Grant (NIH T32CA009120). Additional support was given by an R01CA166450–01 and a Career Development Award K08CA133521, the Sidney Kimmel Translational Scholar Award SKF-11-013, the Irving Feintech Family Foundation/Tower Cancer Research Foundation Research Grant, the University of California Cancer Research Coordinating Committee, the Stein-Oppenheimer Endowment Award, and the UCLA Broad Stem Cell Research Center to Dr. Dinesh Rao.

The work presented in Chapter I is a version of Contreras and Rao “MicroRNAs in inflammation and immune responses” published in December 2011 with permission from Leukemia. The work presented in Chapter II is a reprint of Contreras et al. “MicroRNA-146a modulates B-cell oncogenesis by regulating Egr1” published in April 2015 with permission from Oncotarget. The research was carried out under the direction of PI Dinesh S. Rao. I led, conceptualized, planned, executed, and interpreted the experiments. Completion of the manuscript was made possible by the important experimental contributions from Jayanth

Palanichamy, Tiffany Tran, Thilini Fernando, Norma Rodriguez-Malave, Neha Goswami, Valerie Arboleda, and David Casero. Contribution to result interpretation and construction of the manuscript were made by Dinesh S. Rao.

The work presented in Chapter III is a version of Contreras et al. “Functional characterization of miR-34a in B-cell lymphomagenesis”. The research was done under the direction of PI Dinesh S. Rao. I led, conceptualized, planned, executed, and interpreted the experiments. Experimental contributions were made by, Thilini R. Fernando, Tiffany Tran, Jayanth K. Palanichamy, David Casero, Norma Rodriguez-Malave, Jaime Anguiano, Kimanh T. Pioli, and Dinesh S. Rao. Contribution to result interpretation and construction of the manuscript were made by Dinesh S. Rao.

The works included in the appendices are reprints of Palanichamy et al. “RNA-binding protein IGF2BP3 targeting of oncogenic transcripts promotes hematopoietic progenitor proliferation” and of Rodriguez-Malave et al. “BALR-6 regulates cell growth and cell survival in B-lymphoblastic leukemia” with permission from the Journal of Clinical Investigation and Molecular Cancer, respectively. I contributed to the experimental design, execution, data analysis, and the overall construction of these articles in both appendix I and II.

Finally, I would like to thank all my friends and family at LPE for their unconditional love and support. I could not have accomplished this without you.

VITA

Jorge R Contreras

EDUCATION

2010-2016 PhD Candidate University of California Los Angeles, CA

Cellular and Molecular Pathology Program

2007-2010 Bachelors in Science (B.S.) Cal State Dominguez Hills Los Angeles, CA

General Biology

PUBLICATIONS

- Fernando T.R., **Contreras J.R.**, Zampini M., Rodriguez-Malave N.I., Palanichamy J.K., Gajeton J., Ung N., Tran T.M., Anguiano J., Aros C., Waters E., Casero D., Basso G., Pigazzi M., Rao D.S. (**2016**) "The lncRNA CASC15 regulates SOX4 expression in RUNX1-rearranged acute leukemia". Submitted (addressing reviews)
- Palanichamy, J.K., Howard, J.M., Tran, T.M., **Contreras, J.R.**, Fernando, T.R., Sterne-Weiler, T., Katzman, S., Tolou, M., Yan, W., Basso, G., Pigazzi, M., Sanford, J.R., Rao, D.S. *RNA-binding protein IGF2BP3 targeting of oncogenic transcripts promotes hematopoietic progenitor proliferation.* J Clin Invest, 2016. **126**(4): p. 1495-511. (PMID: 26974154)
- Rodriguez-Malave, N.I., Fernando, T.R., Patel, P.C., **Contreras, J.R.**, Palanichamy, J.K., Tran, T.M., Anguiano, J., Davoren, M.J., Alberti, M.O., Pioli, K.T., Sandoval, S., Crooks, G.M., Rao, D.S. *BALR-6 regulates cell growth and cell survival in B-lymphoblastic leukemia.* Mol Cancer, 2015. **14**: p. 214. (PMID: 26694754)
- **Contreras, J.R.**, Palanichamy, J.K., Tran, T.M., Fernando, T.M., Rodriguez-Malave, N.I., Goswami, N., Arboleda, V.A., Casero, D., Rao, D.S. *MicroRNA-146a modulates B-cell oncogenesis by regulating Egr1.* Oncotarget, 2015. **6**(13): p. 11023-37. (PMID: 25906746)

- **Contreras, J.** and D.S. Rao, *MicroRNAs in inflammation and immune responses.* Leukemia, 2012. **26**(3): p. 404-13. (PMID: 22182919)

RESEARCH EXPERIENCE

July 2011-Dec 2015 **University of California** **Los Angeles, CA**

Graduate Student Researcher Principal Investigator**: Dinesh S. Rao, MD, PhD.**

Primary Project: Characterizing the role of miR-146a and miR-34a in B-cell lymphomagenesis.

Aug 2009-Jul 2010 **Cal State Dominguez Hills** **Los Angeles, CA**

Student Researcher, Principal Investigators: **Helen H. Chun PhD.**

Primary Project: Characterizing the role ATM autophosphorylation regulation by PP2A.

ADDITIONAL EXPERIENCE

Sept 2013-Dec 2013 **University of California** **Los Angeles, CA**

Teaching Assistant, PATH 222

Jan 2012-Mar 2012 **University of California** **Los Angeles, CA**

Teaching Assistant, LS4

AWARDS AND FELLOWSHIPS

Apr 2012–June 2016 **University of California** **Los Angeles, CA**

Tumor Immunology Training Grant

Sep 2010–June2012 **University of California** **Los Angeles, CA**

Eugene Cota-Robles Fellowship

CHAPTER I:

Introduction:

“microRNAs in B cell malignancies”

Abstract

MicroRNAs (miRNAs) are important regulators of gene expression in all compartments of the immune system. In B cell development they regulate essential pathways that include: B cell receptor (BCR) signaling, cell to cell interactions, and class switching of immunoglobulins. They are necessary to the normal development of cells, and data suggests that the deregulation of specific miRNAs is involved in malignant transformation due to their function as oncogenes or tumor suppressors. Amplification and overexpression of either 'oncomiRs' or genetic loss of tumor suppressor miRNAs is associated with disease and sufficient to potentiate tumorigenesis in mouse models. Additionally, global miRNA deficiency mediated by alterations in the biogenesis machinery is oncogenic. Taken together this data indicates the importance of deregulation of specific miRNAs in cancer. Here we studied two miRNAs namely miR-146a, and miR-34a due to their role in association with oncogenesis as established by previous studies.

Introduction

First discovered by the laboratories of Victor Ambros and Gary Ruvkun in Caenorhabditis elegans, miRNAs are the first extensively studied class of noncoding RNAs.[1, 2] There are thousands miRNAs that have been cataloged, with various degrees of conservation. It is now clear that there are likely species-specific miRNAs, and the most current listing in miRBase lists 2588 miRNAs in humans.[3] miRNA biogenesis is a highly regulated process that allows for their expression in particular cellular and functional contexts. miRNAs are encoded within the cellular genome in three main ways: (1) as unique genes (2) as intronic sequences within protein-coding genes and (3) as polycistronic miRNAs, or a single transcript encoding multiple miRNAs.[4, 5] This variable encoding renders complex possibilities for their regulation, through alternative processing or miRNA processing. The canonical miRNA biogenesis path- way involves transcription of these genes by RNA polymerase II, which allows

for regulation by transcription factors.[6] Following transcription, the primary miRNA transcript is processed by the endoribonucleases Drosha/DGCR8 in the nucleus before transport into the cytoplasm.[7, 8] The resulting pre-miRNA is further processed by the endoribonuclease Dicer.[9, 10] Dicer acts by cleaving the looped end of the miRNA precursor and 'dicing' the RNA at 20–25 base-pair intervals thereafter. This results in the formation of a short double-stranded RNA consisting of the miRNA and its complementary sequence. This is unwound and loaded onto the RNA-induced silencing complex (RISC) where the mature miRNA binds to target sequences (reviewed in Czech and Hannon[11])

Recently, a second, non-Dicer-dependent pathway of miRNA biogenesis has been discovered.[12, 13] This alternative pathway relies on a component of the RISC complex, namely the Argonaute protein Ago2, to mediate the final processing of the miRNA. Several miRNAs are thought to be processed by this pathway. Interestingly, the secondary structure of the pre-miRNA seems to be important in determining the pathway of biogenesis, with distinct loop and hairpin structures determining whether the miRNA precursor is cleaved by Dicer or Ago2. Of these, miR-451 is the best characterized, and it contains a very small, distinctive loop structure.

Following its maturation via endoribonucleolytic cleavage, the miRNA is unwound and the thermodynamically more stable strand is loaded onto the RISC, a complex composed of multiple proteins and RNAs. Here, the miRNA encounters and binds to a target mRNA sequence. The basis of targeting is thought to be Watson-Crick base-pairing via a six-nucleotide seed sequence located within the 3' untranslated region of the target mRNA. This seems to be the most well-accepted model for targeting, and several target prediction algorithms are based on this model.[14-17] Usually, there are also areas of complementarity along the 3' end of the miRNA, leading to a central region of noncomplementarity or 'bulge' sequence. In contrast to this, small interfering RNAs bind to target sequences with perfect complementarity, leading to

endoribonucleolytic cleavage of the target mRNA via the Slicer function of Ago2.[18, 19] The mechanism of miRNA repression of the targeted transcript is thought to involve a combination of mRNA destabilization and exoribonucleolytic activity as well as translational repression (reviewed in Nilsen[20]). Recent work suggests that mRNA levels are an accurate way to determine the degree of repression caused by miRNA expression.[21]

Because repression is thought to be mediated through a short 'seed' sequence, miRNAs are predicted to target numerous mRNAs within a cell, from tens to hundreds. This has been partially validated by high-throughput techniques that show that miRNA gain and loss of function can lead to the repression or derepression of numerous genes, respectively.[21, 22] This has led investigators seeking targets for miRNAs to use a combination of high-throughput

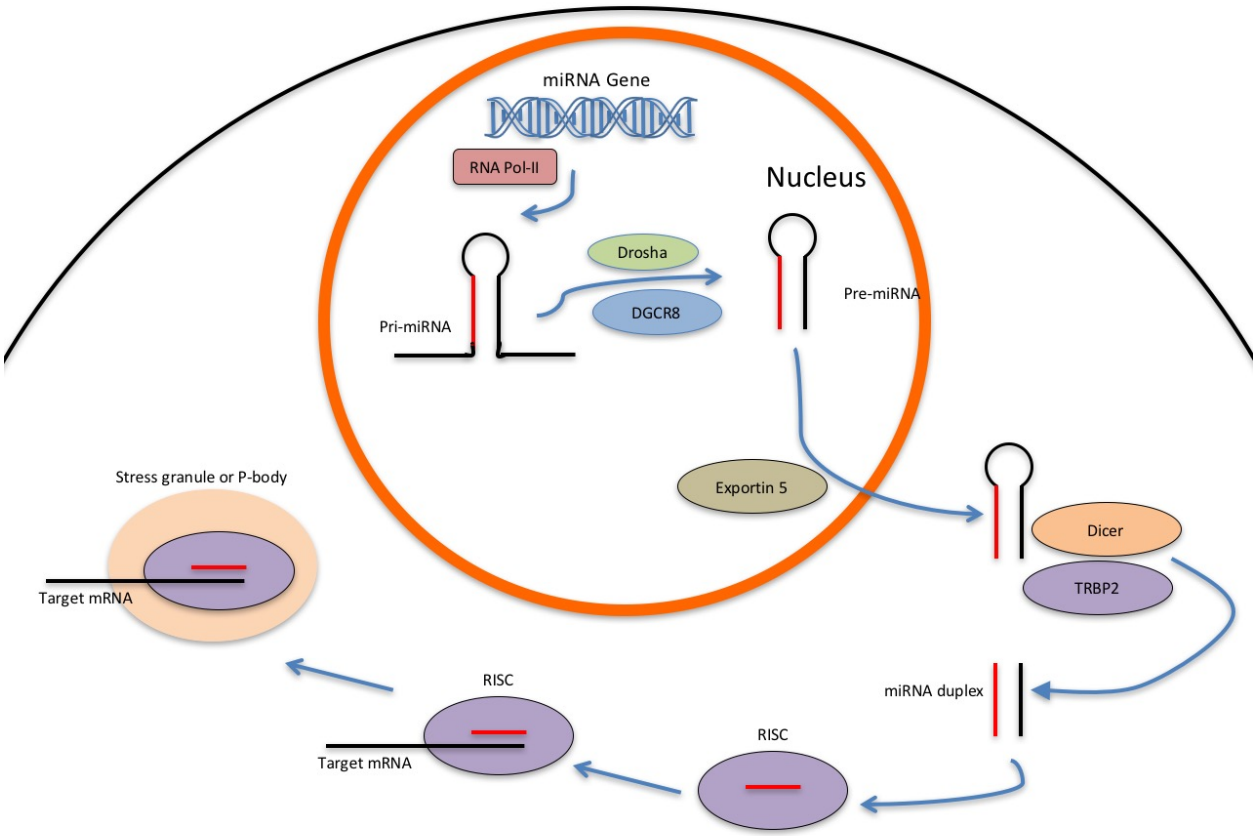

Figure 1: Schematic of miRNA biogenesis.

experimental techniques and bioinformatics-based predictive algorithms to delineate direct miRNA targets.[23] Other recent methodological advances include crosslinking of miRNAs with the RISC complex followed by immunoprecipitation3 and high-throughput sequencing to identify mRNA targets in the relevant biochemical context, the so-called Argonaute HITS-CLIP.[24] These technological advances have rendered possible the identification of various pathways regulated by miRNAs. Overall, the multiplicity of targeting by miRNAs has led to the idea that they can regulate large sets of genes and thus have profound effects on gene expression.

MicroRNAs in B-cell activation

B cells are a central component of the adaptive immune system responsible for the production of long-lived antibodies, which are the main determinant of long-term specific immunity.[25] B cells develop in the bone marrow and achieve a remarkable diversity of antigen specificities by rearrangement of their immunoglobulin loci by V(D)J recombination. Once they have matured in the bone marrow, they seed secondary lymphoid organs where they are activated by antigens that their B-cell receptors (surface immunoglobulin) recognize. Once they are activated, they undergo proliferation and further differentiation. The outcome of antigenic activation is differentiation into either plasma cells that secrete highly specific antibodies or memory B cells that can be reactivated for future protection.[26] Once an antigen comes into contact with the B-cell receptor, a signalosome consisting of the B-cell receptor and of intracellular signaling kinases such as Phospholipase C-2 gamma, phosphatidyl inositol 3-kinase, Bruton's tyrosine kinase and Vav as well as B-cell adaptor Blnk is assembled.[26] Although conventional B cells (B2 B cells) require CD4þ T-cell activation, B1 B cells do not. It is thought that B1 B cells are activated by a TLR microbial detection pathway.[27]

The overall importance of miRNAs in hematopoiesis was established by a seminal study that showed that miR-181 was highly expressed in B cells and guided B-cell development when

constitutively expressed.[28] Mice with an early B-cell-specific deletion of Dicer demonstrated a lack of B-cell development past the pro-B-cell stage.[29] This seemed to be mediated via increased apoptosis, and the protein targets, bcl-2 interacting mediator of cell death and phosphatase and tensin homolog, were thought to be responsible for the phenotype. miR-150 constitutive expression has an effect on B-cell development, as does miR-34a constitutive expression.[30-32] Both miRNAs must normally be downregulated at the pro-B to pre-B transition and their continued expression leads to inhibition of their respective targets, c-Myb and Foxp1 (forkhead box P1), which are required for further B-cell development.

miRNAs are now known to play a clear role in controlling the activation of mature B cells. At the global level, Dicer ablation in mature B cells (as opposed to early precursor B cells) resulted in an increase in marginal zone B cells and a decrease in follicular B cells.[33] It was also determined that these mice had an increased titer of autoimmune antibodies with autoimmune disease in female mice. This study also hinted that the relevant target was Bruton's tyrosine kinase, which is important in controlling B-cell activation.

In B-2 cells, miR-155 plays a major role in regulating the response in germinal center cells, where B cells undergo a second round of DNA rearrangement, followed by selection.[34, 35] miR-155-deficient mice show marked defects in both antibody secretion and class-switch recombination upon immunization.[36, 37] miR-155 represses over 60 target genes in B cells, including Pu.1, SHIP1 and AID.[37] In fact, Pu.1 seems to be at least partially responsible for the defects in B-cell activation seen in these mice.[37] The role of AID, which mediates class-switch recombination and somatic hypermutation, was further explored by two groups who generated a highly specific disruption of the miR-155 target site in the Aicda 3' untranslated region.[38, 39] Disruption of the miR-155/AID interaction led to persistent/increased somatic hypermutation, including abnormal translocations, and decreased high-affinity antibodies in immunized mutant mice. This result suggests that the majority of miR-155-mediated phenotypic

effects in B cells are not mediated by AID, but that the AID/miR-155 interaction has an important function. One possibility is that miR-155 inhibition of Aicda may represent a delayed negative regulatory switch, which allows for the proper temporal control of somatic hypermutation and positive selection. Interestingly, miR-181b overexpression in B cells was found to reduce the class-switch recombination rates, possibly by also downregulating AID.[40] In another study, miR-150 deficient mice show an expansion of B1 B cells accompanied by dramatic increases in steady-state antibodies.[30] miR-150 deficient mice also showed an enhanced response to immunization with T-dependent antigens, indicating an effect on follicular (B2) B cells. Together, these studies have revealed an important function for miRNAs in B-cell development and activation. The finding of autoimmune or immunodysregulated phenotypes in miRNA-disrupted mice should provide an impetus to search for B-cell-mediated mechanisms of autoimmune disease.

MicroRNAs in leukemia

Many profiling studies have led to a wealth of information about dysregulated miRNA expression in various tumors of the hematolymphoid system. This has led to the concept of 'oncomiRs', or oncogenic miRNAs, and tumor-suppressor miRNAs. miR-155, miR-34, miR-29, miR-15/16 cluster, miR181, and miR17-92 are a group of miRNAs most frequently dysregulated in chronic lymphocytic leukemia (CLL). Identification of their targets has uncovered their functional role in oncogenic progression.

When overexpressed in mice, miR-155 causes a myeloproliferative disorder; miR-125b leads to a chronic myeloproliferative disease that evolves into an acute leukemia. miR-29a was also recently reported to cause an acute myeloid leukemia when overexpressed in mice, whereas overexpression of miR-21 resulted in an acute lymphoblastic leukemia.[41, 42] These studies highlight that several oncomiRs are capable of transforming hematopoietic cells. Despite

these similarities in induction of malignant phenotypes, the functions of these miRNAs in immune cells may be quite different; for example, TLR signaling induces miR-155 and miR-21 but it downregulates miR-125b.

In CLL deletions at 11q, 17p, and 13q are frequently seen leading to loss of miR-34b/c, p53, and miR-15/16-1 respectively. miR-15/16-1 and miR-34a/b/c have binding sites for p53 in their promoters and interestingly target p53, and ZAP-70 respectively.[43] The targets of these miRNAs play a balancing act that when shifted towards increased p53 levels leads to an anti-apoptotic program, but if ZAP-70 is increased a poorer prognosis of CLL is observed.[44, 45] The seminal hematopoietic miRNA, miR-181, is suppressed in CLL as the disease progresses and in the context of indolent vs. aggressive CLL miR-181 is higher in indolent cases.[46-48]

In addition to oncomiRs, several tumor-suppressor miRNAs may have important roles in leukemogenesis. Perhaps the most elegantly studied tumor-suppressor miRNA is the previously mentioned miR-15a/16 polycistron, which was initially identified as being located at the 13q14 chromosomal locus deleted in chronic lymphocytic leukemia.[49] Initial studies identified several important targets of miR-15a/16 including oncogenes such as BCL2 and TCL1.[47, 50] Experimentally, deletion of (1) the miRNA-containing segment of the gene, (2) the larger noncoding RNA that contained the miRNAs and of (3) the entire homologous locus in mice led to successively more severe phenotypes, and all recapitulated chronic lymphocytic leukemia to some degree.[51] Overall, the observations made regarding the functional role of miRNAs in leukemogenesis suggest that replacement of tumor-suppressor miRNAs and inhibition of oncomiRs may have an important role in future therapeutic approaches.

MicroRNAs in lymphoma

The pioneering study that demonstrated the role of miRNAs in the development/progression of lymphomas used the polycistronic cluster of miR-17-92 in

conjunction with the Eμ-myc mouse model.[52] Here the authors demonstrated that miRNAs can accelerate lymphomagenesis in the context of c-Myc overexpression. Due to the driving force of c-Myc oncogenesis the question remained whether miRNAs alone can confer a significant advantage in transforming normal B cells. This question was answered using an Eμ-miR-17-92 transgenic animal that developed aggressive B cell malignancies consisting of B1-cell proliferating disease, aggressive CLL-like disease, and a diffuse large B cell lymphoma (DLBCL) like disease.[53] In these animals a proportion of the phenotype can be attributed to the repression of PTEN and BIM by miR-17-92.[54, 55]

The miR17-92 cluster is one of the most potent oncomiRs in non-Hodgkin lymphomas of B cell origin. In B-cell non-Hodgkin lymphomas samples this cluster is often amplified or upregulated, yet the expression of the individual miRNAs is disparate for reasons unknown. The functional relevance of the different members of this cluster is context dependent due to variability in from cell type to cell type. Though they have been observed to counteract each other in a functional manner creating a model yet to be elucidated.[56]

miR-155 has been characterized in B cell development and malignant transformation it is known to be deregulated in ABC type DLBCL, follicular lymphoma (FL), CLL, and mantle cell lymphoma.[57-60] To address the role of this miRNA in oncogenesis a previous approach was employed generating an Eμ-miR-155 animals.[61] Using these transgenic mice novel targets of miR-155 were revealed to be SHIP1, and C/EBPβ both regulators of B cell development and known to modulation of IL6. Additionally, in these mice the B cells were blocked at the pro-B cell stage giving rise to a polyclonal lymphoproliferation.[62] As mention SHIP1 is a target of miR-155 but it also modulates AKT activity that in these Eμ-miR-155 animals is left unchecked due to SHIP1 being suppressed culminating in altered BCR signaling.

Both NF-κB and MYB two well know transcription factors modulate miR-155 expression, interestingly in DLBCL, where NF-κB is known to be dysregulated, miR-155 is also

deregulated.[60, 63] In these same DLBCL samples B-cell development modulators PU.1, and CD10 are repressed believed to be due to this NF-κB/miR-155/PU.1 axis.[64]

miR-21 is another miRNA that is consistently observed to be dysregulated in lymphoid malignancies such as ABC-DLBCL and AIDS related DLBCL.[57, 65, 66] To determine the role this miRNA plays in-vivo a conditional mouse overexpressing miR-21 in hematopoietic cells was created.[42] These mice developed pre-B cell malignancies that if deprived of this miRNA led to tumor regression accompanied by increased apoptosis, and growth arrest. (Medina2010) On the other hand when a global deletion model of this miRNA was created no abnormal phenotype was observed in B cell development.[67]

In malignant B-cells miR-21 has been demonstrated to target the tumor suppressor PTEN not unlike miR-19.[68] In DLBCL cell lines miR-21 repression leads to increased sensitivity of these cells to cyclophosphamide, doxorubicin, vincristine and prednisone (CHOP) a classic drug combination in treating these types of tumors with the tumor suppressor PDCD4 identified in these cell types.[68, 69] Furthermore, knockdown of miR-21 in cell lines reduced their proliferation and invasive capacity demonstrating the oncogenic potential of this microRNA.[69]

On the basis of these studies it would appear miR-21 overexpression in malignancies would indicate a poor prognosis but this remains debatable. In DLBCL patients with high miR-21 there appears to be longer relapse-free survival while in CLL patients high expression indicates a worse prognosis.[57, 60, 65, 70]

A typical oncomiR miR-21 mediates its effects by inhibiting the expression of phosphatases that would otherwise regulate expression of the AKT and MAPK pathways. miR-21 is a NF-κB responsive gene that represses tumor suppressor such as PTEN and PDCD4. The latest studies on miR-21have postulated a link between inflammation and cancer.[71] In this

study an inflammatory stimulus initiates a positive feedback loop that has sustained miR-21 expression accompanied by NF-κB activation ultimately leading to oncogenic transformation.

miR-34a is a p53 transactivated miRNA and one of the first to be characterized as a DNA damage responsive microRNA.[72] Early studies found this miRNA to contain reduced basal expression in CLL patients with mutated or absent p53.[73] Additionally, p53 deficient cells failed to induces this microRNA even in the presence of DNA insult.[74] Conversely, CLL samples containing wild type p53 also showed low levels of miR-34a postulating an alternative regulatory pathway for miR-34a.[72, 74, 75] In cases of DLBCL, CLL, MCL, and mucosa associated lymphoid tissue lymphomas low miR-34a expression has the poorest prognosis.

In B-cells miR-34a is upregulated upon p53 stabilization subsequently repressing B-MYB and indirectly decreasing E2F1 leading to cell-cycle arrest.[76] AXL is a receptor tyrosine kinase recently ascribed be upregulated in CLL, and shown to be a direct target of miR-34a.[77] In cells receiving chemotherapeutic treatment AXL reduction was observed and is likely due to engagement of the p53/miR-34a pathway. SIRT1 is a NAD-dependent deacytelase blocking apoptosis through deactivation of p53, and recently it has been validated as a target of miR-34a.[78, 79] These discoveries imply that a positive feedback loop exists when p53 is activated miR-34a helps sustains p53 via direct repression of SIRT1.[79]

The well know proto-oncogene MYC is also known to bind the miR-34a promoter, and in the context of c-Myc overexpressing malignancies miR-34a is repressed.[80] In DLBCL miR-34a knockdown led to cell proliferation by derepression of germinal center transcription factors FOXP1 and BCL6.[80, 81] Conversely, miR-34a upregulation is known to suppress cell migration as well as induce apoptosis by repression of SIRT1, and BCL2 in solid tumors.[78] If miR-34a can recapitulate these functions in B cell lymphomas is a question that remains to be answered. Taken together these studies point towards a function for miR-34a both in DNA damage response and therapeutic applications. Confounding the role of miR-34a in B-cells a

recent study demonstrated that its overexpression indirectly repressed p53.[82] In this context MYC was targeted causing repression of ARF and subsequently upregulating MDM2. Applying these results to a MYC driven lymphoma it would indicate miR-34a ectopic expression can have anti-apoptotic effects by targeting the pathway MYC-ARF-MDM2-p53.[82]

miR-34a is a well characterized tumor suppressor its low abundance has been observed in many tumor tissues including B-cell non-Hodgkin lymphomas.[75, 83] Several studies have demonstrated its ability to target oncogenes and pro-survival proteins including NOTCH1, MYC, BCL2, SIRT1, Survivin, CCL22, MDM4, YY1, and AXL. As mentioned previously the question is whether these targets play a role in the context of malignant B cells due to the dynamic expression of miR-34a in B-cell development.

miR-146a was first identified as an NF-κB responsive gene in the monocytic cell line THP-1.[84] In this same study it was uncovered that miR-146a is part of a negative feedback loop by targeting adapter molecules of the NF-κB pathway, IRAK1 and TRAF6. Transgenic animals deficient for this miRNA were found to develop myeloid expansions, autoimmune disease as well as B- and T-cell tumors.[85] In these animals hematopoietic stem and progenitor cell (HSPC) homeostasis was found to be dysregulated in part due to abnormal lymphocyte development.[86]

In breast cancer, and androgen independent prostate cancer cells with ectopic expression of miR-146a a reduced migratory, invasive and metastatic potential has been observed.[87-89] While in pancreatic cancer cells induction of miR-146a leads to reduced cell invasion and metastasis.[90] Additionally, an anaplastic thyroid carcinoma cell line with miR-146a upregulation reduced the oncogenic potential of these cells while increasing their susceptibility to chemotherapeutic reagents.[91] In bone marrow transplant experiments suppressing miR-146a in conjunction with miR-145 produces a phenotype reminiscent of the 5q syndrome.[92]

At the genomic level a polymorphism in the pre-miRNA sequence of miR-146a was identified in papillary thyroid carcinoma samples with a C allele demonstrating a reduction in miR-146a biogenesis and conferring an increased risk of disease.[93] In hepatocellular carcinoma samples the G allele conferred an increased biogenesis of this miRNA and in males conferred an increased risk of disease.[94]

To date numerous targets have been uncovered for miR-146a in pathways regulating development, apoptosis, and proliferation among others.[89, 91, 95, 96] In the context of hematopoietic development miR-146a regulates HSPC's longevity and quality.[86] Of great interest is the role this miRNA plays in malignant transformation as can be seen in all studies performed to date.[85, 87-91] Taken together these studies demonstrate the importance of miR-146a both in development and tumorigenesis.

Conclusions and speculations

The field of miRNA research has undergone a tremendous expansion in the past decade, and these studies have changed fundamentally how we look at gene expression. For example, the unique temporal regulation properties that are possible with miRNAs would not be possible with transcription factors. Furthermore, although not reviewed here, coexpression of a host protein coding gene and an intronic miRNA can produce a unique regulatory module.[97] Further insights into miRNA function continue to be made – a recent study that examined gene expression using single-cell imaging studies reveal that the changes in target gene expression are highly dependent on abundance in a miRNA-expressing cell.[98] There seems to be a threshold level below which repression by miRNA can be close to complete. Around the threshold value, miRNAs can modulate significant but subtotal repression of the target. Well above the threshold value, miRNAs do not change target gene expression at all. At the

population level, such effects would amplify differences in gene expression between low- and high expressing cells.

In malignant transformation, we have reviewed the centrality of miRNAs as oncogenic, as well as tumor suppressors. Acting as oncogenes (such as miR-155 promoting acute leukemia), and as tumor suppressor (such as miR-15/16-1 suppressing oncogenes BCL2), miRNAs add a layer of gene regulation previously unappreciated in malignant transformation.

However, the function of a single miRNA in different cell lineages is still incompletely understood, as highlighted by miR-34a, which can repress components of the cell survival pathway in colon cancer cells such as E2F3, while alternatively in BJAB cells cell survival was unaffected.[99] miRNAs may have different functions in different cell lineages, because of the exquisite sensitivity of miRNA regulation to the concentration, or lack thereof, of its target mRNA. Future research with exacting loss of function of specific miRNAs in subsets of malignant cells, as well as deletions of miRNA target sites, will be required to precisely understand the function of miRNAs during immune responses.

In addition to these detailed mechanistic studies to delineate miRNA function, research tapping into the therapeutic applications of these miRNAs has begun. Indeed, small RNA delivery has already been demonstrated in a few human trials, and small RNA inhibition in animal models can be achieved with anti-miRNAs or antagomirs.[100, 101] These studies demonstrate the potential of these therapeutics in tuning down miRNA function. A related theme of research, replacing miRNAs, is also gaining traction. For example, delivery of miR-146a or miR-21 may be able to tune down oncogenes. The technology for such delivery may entail using double-stranded small RNA molecules, but delivery into the right cell types and tissues remains a challenge. One method is suggested by the recent observation that some miRNAs can pass between cells via exosome-mediated transfer.[102] It is also tempting to speculate that such cell-to-cell communications may regulate immune cell function.

miRNA research in the immune system has progressed a great deal in just a few short years. Their evolutionary conservation-these mechanisms are present in simple multicellular animals and plants in addition to mammals-is remarkable and suggests an ancient function. Some have suggested that they may have arisen as a primitive antiviral response and that these miRNAs may be particularly important in the immune system. Regardless of their origin, it is clear that miRNAs have diverse and important functions in gene expression. Exciting developments and unexpected twists undoubtedly remain as we continue our efforts to understand the function and develop the therapeutic potential of these enigmatic regulators of gene expression.

References

1. Lee, R.C., R.L. Feinbaum, and V. Ambros, The C. elegans heterochronic gene lin-4 encodes small RNAs with antisense complementarity to lin-14. Cell, 1993. **75**(5): p. 843-54.
2. Wightman, B., I. Ha, and G. Ruvkun, Posttranscriptional regulation of the heterochronic gene lin-14 by lin-4 mediates temporal pattern formation in C. elegans. Cell, 1993. **75**(5): p. 855-62.
3. Kozomara, A. and S. Griffiths-Jones, miRBase: integrating microRNA annotation and deep-sequencing data. Nucleic Acids Res, 2011. **39**(Database issue): p. D152-7.
4. Kim, V.N., J. Han, and M.C. Siomi, Biogenesis of small RNAs in animals. Nat Rev Mol Cell Biol, 2009. **10**(2): p. 126-39.
5. Winter, J., et al., Many roads to maturity: microRNA biogenesis pathways and their regulation. Nat Cell Biol, 2009. **11**(3): p. 228-34.
6. Lee, Y., et al., MicroRNA genes are transcribed by RNA polymerase II. EMBO J, 2004. **23**(20): p. 4051-60.
7. Lee, Y., et al., The nuclear RNase III Drosha initiates microRNA processing. Nature, 2003. **425**(6956): p. 415-9.
8. Gregory, R.I., et al., The Microprocessor complex mediates the genesis of microRNAs. Nature, 2004. **432**(7014): p. 235-40.
9. Bernstein, E., et al., Role for a bidentate ribonuclease in the initiation step of RNA interference. Nature, 2001. **409**(6818): p. 363-6.
10. Ketting, R.F., et al., Dicer functions in RNA interference and in synthesis of small RNA involved in developmental timing in C. elegans. Genes Dev, 2001. **15**(20): p. 2654-9.
11. Czech, B. and G.J. Hannon, Small RNA sorting: matchmaking for Argonautes. Nat Rev Genet, 2011. **12**(1): p. 19-31.

12. Cheloufi, S., et al., A dicer-independent miRNA biogenesis pathway that requires Ago catalysis. Nature, 2010. **465**(7298): p. 584-9.
13. Cifuentes, D., et al., A novel miRNA processing pathway independent of Dicer requires Argonaute2 catalytic activity. Science, 2010. **328**(5986): p. 1694-8.
14. Lewis, B.P., et al., Prediction of mammalian microRNA targets. Cell, 2003. **115**(7): p. 787-98.
15. Lewis, B.P., C.B. Burge, and D.P. Bartel, Conserved seed pairing, often flanked by adenosines, indicates that thousands of human genes are microRNA targets. Cell, 2005. **120**(1): p. 15-20.
16. Grimson, A., et al., MicroRNA targeting specificity in mammals: determinants beyond seed pairing. Mol Cell, 2007. **27**(1): p. 91-105.
17. Bartel, D.P., MicroRNAs: target recognition and regulatory functions. Cell, 2009. **136**(2): p. 215-33.
18. Liu, J., et al., Argonaute2 is the catalytic engine of mammalian RNAi. Science, 2004. **305**(5689): p. 1437-41.
19. Song, J.J., et al., Crystal structure of Argonaute and its implications for RISC slicer activity. Science, 2004. **305**(5689): p. 1434-7.
20. Nilsen, T.W., Mechanisms of microRNA-mediated gene regulation in animal cells. Trends Genet, 2007. **23**(5): p. 243-9.
21. Baek, D., et al., The impact of microRNAs on protein output. Nature, 2008. **455**(7209): p. 64-71.
22. Guo, H., et al., Mammalian microRNAs predominantly act to decrease target mRNA levels. Nature, 2010. **466**(7308): p. 835-40.
23. O'Connell, R.M., et al., MicroRNA-155 is induced during the macrophage inflammatory response. Proc Natl Acad Sci U S A, 2007. **104**(5): p. 1604-9.

24. Chi, S.W., et al., Argonaute HITS-CLIP decodes microRNA-mRNA interaction maps. Nature, 2009. **460**(7254): p. 479-86.

25. Hardy, R.R. and K. Hayakawa, B cell development pathways. Annu Rev Immunol, 2001. **19**: p. 595-621.

26. Harwood, N.E. and F.D. Batista, Early events in B cell activation. Annu Rev Immunol, 2010. **28**: p. 185-210.

27. Montecino-Rodriguez, E. and K. Dorshkind, New perspectives in B-1 B cell development and function. Trends Immunol, 2006. **27**(9): p. 428-33.

28. Chen, C.Z., et al., MicroRNAs modulate hematopoietic lineage differentiation. Science, 2004. **303**(5654): p. 83-6.

29. Koralov, S.B., et al., Dicer ablation affects antibody diversity and cell survival in the B lymphocyte lineage. Cell, 2008. **132**(5): p. 860-74.

30. Xiao, C., et al., MiR-150 controls B cell differentiation by targeting the transcription factor c-Myb. Cell, 2007. **131**(1): p. 146-59.

31. Zhou, B., et al., miR-150, a microRNA expressed in mature B and T cells, blocks early B cell development when expressed prematurely. Proc Natl Acad Sci U S A, 2007. **104**(17): p. 7080-5.

32. Rao, D.S., et al., MicroRNA-34a perturbs B lymphocyte development by repressing the forkhead box transcription factor Foxp1. Immunity, 2010. **33**(1): p. 48-59.

33. Belver, L., V.G. de Yebenes, and A.R. Ramiro, MicroRNAs prevent the generation of autoreactive antibodies. Immunity, 2010. **33**(5): p. 713-22.

34. Cozine, C.L., K.L. Wolniak, and T.J. Waldschmidt, The primary germinal center response in mice. Curr Opin Immunol, 2005. **17**(3): p. 298-302.

35. Wolniak, K.L., S.M. Shinall, and T.J. Waldschmidt, The germinal center response. Crit Rev Immunol, 2004. **24**(1): p. 39-65.

36. Thai, T.H., et al., Regulation of the germinal center response by microRNA-155. Science, 2007. **316**(5824): p. 604-8.

37. Vigorito, E., et al., microRNA-155 regulates the generation of immunoglobulin class-switched plasma cells. Immunity, 2007. **27**(6): p. 847-59.

38. Teng, G., et al., MicroRNA-155 is a negative regulator of activation-induced cytidine deaminase. Immunity, 2008. **28**(5): p. 621-9.

39. Dorsett, Y., et al., MicroRNA-155 suppresses activation-induced cytidine deaminase-mediated Myc-Igh translocation. Immunity, 2008. **28**(5): p. 630-8.

40. de Yebenes, V.G., et al., miR-181b negatively regulates activation-induced cytidine deaminase in B cells. J Exp Med, 2008. **205**(10): p. 2199-206.

41. Han, Y.C., et al., microRNA-29a induces aberrant self-renewal capacity in hematopoietic progenitors, biased myeloid development, and acute myeloid leukemia. J Exp Med, 2010. **207**(3): p. 475-89.

42. Medina, P.P., M. Nolde, and F.J. Slack, OncomiR addiction in an in vivo model of microRNA-21-induced pre-B-cell lymphoma. Nature, 2010. **467**(7311): p. 86-90.

43. Auer, R.L., S. Riaz, and F.E. Cotter, The 13q and 11q B-cell chronic lymphocytic leukaemia-associated regions derive from a common ancestral region in the zebrafish. Br J Haematol, 2007. **137**(5): p. 443-53.

44. Merkel, O., et al., Interdependent regulation of p53 and miR-34a in chronic lymphocytic leukemia. Cell Cycle, 2010. **9**(14): p. 2764-8.

45. Fabbri, M., et al., Association of a microRNA/TP53 feedback circuitry with pathogenesis and outcome of B-cell chronic lymphocytic leukemia. JAMA, 2011. **305**(1): p. 59-67.

46. Calin, G.A., et al., A MicroRNA signature associated with prognosis and progression in chronic lymphocytic leukemia. N Engl J Med, 2005. **353**(17): p. 1793-801.

47. Pekarsky, Y., et al., Tcl1 expression in chronic lymphocytic leukemia is regulated by miR-29 and miR-181. Cancer Res, 2006. **66**(24): p. 11590-3.

48. Santanam, U., et al., Chronic lymphocytic leukemia modeled in mouse by targeted miR-29 expression. Proc Natl Acad Sci U S A, 2010. **107**(27): p. 12210-5.

49. Calin, G.A., Y. Pekarsky, and C.M. Croce, The role of microRNA and other non-coding RNA in the pathogenesis of chronic lymphocytic leukemia. Best Pract Res Clin Haematol, 2007. **20**(3): p. 425-37.

50. Calin, G.A., et al., MicroRNA profiling reveals distinct signatures in B cell chronic lymphocytic leukemias. Proc Natl Acad Sci U S A, 2004. **101**(32): p. 11755-60.

51. Klein, U., et al., The DLEU2/miR-15a/16-1 cluster controls B cell proliferation and its deletion leads to chronic lymphocytic leukemia. Cancer Cell, 2010. **17**(1): p. 28-40.

52. He, L., et al., A microRNA polycistron as a potential human oncogene. Nature, 2005. **435**(7043): p. 828-33.

53. Sandhu, S.K., et al., B-cell malignancies in microRNA Emu-miR-17~92 transgenic mice. Proc Natl Acad Sci U S A, 2013. **110**(45): p. 18208-13.

54. Ventura, A., et al., Targeted deletion reveals essential and overlapping functions of the miR-17 through 92 family of miRNA clusters. Cell, 2008. **132**(5): p. 875-86.

55. Xiao, C., et al., Lymphoproliferative disease and autoimmunity in mice with increased miR-17-92 expression in lymphocytes. Nat Immunol, 2008. **9**(4): p. 405-14.

56. Olive, V., Q. Li, and L. He, mir-17-92: a polycistronic oncomir with pleiotropic functions. Immunol Rev, 2013. **253**(1): p. 158-66.

57. Lawrie, C.H., et al., MicroRNA expression distinguishes between germinal center B cell-like and activated B cell-like subtypes of diffuse large B cell lymphoma. Int J Cancer, 2007. **121**(5): p. 1156-61.

58. Eis, P.S., et al., Accumulation of miR-155 and BIC RNA in human B cell lymphomas. Proc Natl Acad Sci U S A, 2005. **102**(10): p. 3627-32.

59. Roehle, A., et al., MicroRNA signatures characterize diffuse large B-cell lymphomas and follicular lymphomas. Br J Haematol, 2008. **142**(5): p. 732-44.

60. Vargova, K., et al., MYB transcriptionally regulates the miR-155 host gene in chronic lymphocytic leukemia. Blood, 2011. **117**(14): p. 3816-25.

61. Costinean, S., et al., Pre-B cell proliferation and lymphoblastic leukemia/high-grade lymphoma in E(mu)-miR155 transgenic mice. Proc Natl Acad Sci U S A, 2006. **103**(18): p. 7024-9.

62. Costinean, S., et al., Src homology 2 domain-containing inositol-5-phosphatase and CCAAT enhancer-binding protein beta are targeted by miR-155 in B cells of Emicro-MiR-155 transgenic mice. Blood, 2009. **114**(7): p. 1374-82.

63. Thompson, R.C., I. Vardinogiannis, and T.D. Gilmore, Identification of an NF-kappaB p50/p65-responsive site in the human MIR155HG promoter. BMC Mol Biol, 2013. **14**: p. 24.

64. Thompson, R.C., et al., NF-kappaB down-regulates expression of the B-lymphoma marker CD10 through a miR-155/PU.1 pathway. J Biol Chem, 2011. **286**(3): p. 1675-82.

65. Lawrie, C.H., et al., Detection of elevated levels of tumour-associated microRNAs in serum of patients with diffuse large B-cell lymphoma. Br J Haematol, 2008. **141**(5): p. 672-5.

66. Thapa, D.R., et al., B-cell activation induced microRNA-21 is elevated in circulating B cells preceding the diagnosis of AIDS-related non-Hodgkin lymphomas. AIDS, 2012. **26**(9): p. 1177-80.

67. Ma, X., et al., Loss of the miR-21 allele elevates the expression of its target genes and reduces tumorigenesis. Proc Natl Acad Sci U S A, 2011. **108**(25): p. 10144-9.

68. Bai, H., et al., MicroRNA-21 regulates the sensitivity of diffuse large B-cell lymphoma cells to the CHOP chemotherapy regimen. Int J Hematol, 2013. **97**(2): p. 223-31.

69. Gu, L., et al., Inhibition of miR-21 induces biological and behavioral alterations in diffuse large B-cell lymphoma. Acta Haematol, 2013. **130**(2): p. 87-94.

70. Rossi, S., et al., microRNA fingerprinting of CLL patients with chromosome 17p deletion identify a miR-21 score that stratifies early survival. Blood, 2010. **116**(6): p. 945-52.

71. Iliopoulos, D., et al., STAT3 activation of miR-21 and miR-181b-1 via PTEN and CYLD are part of the epigenetic switch linking inflammation to cancer. Mol Cell, 2010. **39**(4): p. 493-506.

72. He, X., L. He, and G.J. Hannon, The guardian's little helper: microRNAs in the p53 tumor suppressor network. Cancer Res, 2007. **67**(23): p. 11099-101.

73. Mraz, M., et al., miR-34a, miR-29c and miR-17-5p are downregulated in CLL patients with TP53 abnormalities. Leukemia, 2009. **23**(6): p. 1159-63.

74. Zenz, T., et al., Detailed analysis of p53 pathway defects in fludarabine-refractory chronic lymphocytic leukemia (CLL): dissecting the contribution of 17p deletion, TP53 mutation, p53-p21 dysfunction, and miR34a in a prospective clinical trial. Blood, 2009. **114**(13): p. 2589-97.

75. Asslaber, D., et al., microRNA-34a expression correlates with MDM2 SNP309 polymorphism and treatment-free survival in chronic lymphocytic leukemia. Blood, 2010. **115**(21): p. 4191-7.

76. Zauli, G., et al., miR-34a induces the downregulation of both E2F1 and B-Myb oncogenes in leukemic cells. Clin Cancer Res, 2011. **17**(9): p. 2712-24.

77. Boysen, J., et al., The tumor suppressor axis p53/miR-34a regulates Axl expression in B-cell chronic lymphocytic leukemia: implications for therapy in p53-defective CLL patients. Leukemia, 2014. **28**(2): p. 451-5.

78. Li, L., et al., MiR-34a inhibits proliferation and migration of breast cancer through down-regulation of Bcl-2 and SIRT1. Clin Exp Med, 2013. **13**(2): p. 109-17.

79. Yamakuchi, M., M. Ferlito, and C.J. Lowenstein, miR-34a repression of SIRT1 regulates apoptosis. Proc Natl Acad Sci U S A, 2008. **105**(36): p. 13421-6.

80. Craig, V.J., et al., Myc-mediated repression of microRNA-34a promotes high-grade transformation of B-cell lymphoma by dysregulation of FoxP1. Blood, 2011. **117**(23): p. 6227-36.

81. Rizzo, M., et al., The over-expression of miR-34a fails to block DoHH2 lymphoma cell proliferation by reducing p53 via c-MYC down-regulation. Nucleic Acid Ther, 2012. **22**(4): p. 283-8.

82. Sotillo, E., et al., Myc overexpression brings out unexpected antiapoptotic effects of miR-34a. Oncogene, 2011. **30**(22): p. 2587-94.

83. Navarro, A., et al., microRNA expression profiles identify subtypes of mantle cell lymphoma with different clinicobiological characteristics. Clin Cancer Res, 2013. **19**(12): p. 3121-9.

84. Taganov, K.D., et al., NF-kappaB-dependent induction of microRNA miR-146, an inhibitor targeted to signaling proteins of innate immune responses. Proc Natl Acad Sci U S A, 2006. **103**(33): p. 12481-6.

85. Boldin, M.P., et al., miR-146a is a significant brake on autoimmunity, myeloproliferation, and cancer in mice. J Exp Med, 2011. **208**(6): p. 1189-201.

86. Zhao, J.L., et al., MicroRNA-146a acts as a guardian of the quality and longevity of hematopoietic stem cells in mice. Elife, 2013. **2**: p. e00537.

87. Bhaumik, D., et al., MicroRNAs miR-146a/b negatively modulate the senescence-associated inflammatory mediators IL-6 and IL-8. Aging (Albany NY), 2009. **1**(4): p. 402-11.

88. Lin, S.L., et al., Loss of mir-146a function in hormone-refractory prostate cancer. RNA, 2008. **14**(3): p. 417-24.

89. Hurst, D.R., et al., Breast cancer metastasis suppressor 1 up-regulates miR-146, which suppresses breast cancer metastasis. Cancer Res, 2009. **69**(4): p. 1279-83.

90. Li, Y., et al., Up-regulation of miR-146a contributes to the inhibition of invasion of pancreatic cancer cells. Cancer Res, 2010. **70**(8 Suppl): p. 5703.

91. Pacifico, F., et al., Nuclear factor-{kappa}B contributes to anaplastic thyroid carcinomas through up-regulation of miR-146a. J Clin Endocrinol Metab, 2010. **95**(3): p. 1421-30.

92. Starczynowski, D.T., et al., Identification of miR-145 and miR-146a as mediators of the 5q- syndrome phenotype. Nat Med, 2010. **16**(1): p. 49-58.

93. Jazdzewski, K., et al., Common SNP in pre-miR-146a decreases mature miR expression and predisposes to papillary thyroid carcinoma. Proc Natl Acad Sci U S A, 2008. **105**(20): p. 7269-74.

94. Xu, T., et al., A functional polymorphism in the miR-146a gene is associated with the risk for hepatocellular carcinoma. Carcinogenesis, 2008. **29**(11): p. 2126-31.

95. Labbaye, C., et al., A three-step pathway comprising PLZF/miR-146a/CXCR4 controls megakaryopoiesis. Nat Cell Biol, 2008. **10**(7): p. 788-801.

96. Curtale, G., et al., An emerging player in the adaptive immune response: microRNA-146a is a modulator of IL-2 expression and activation-induced cell death in T lymphocytes. Blood, 2010. **115**(2): p. 265-73.

97. Small, E.M. and E.N. Olson, Pervasive roles of microRNAs in cardiovascular biology. Nature, 2011. **469**(7330): p. 336-42.

98. Mukherji, S., et al., MicroRNAs can generate thresholds in target gene expression. Nat Genet, 2011. **43**(9): p. 854-9.

99. Forte, E., et al., The Epstein-Barr virus (EBV)-induced tumor suppressor microRNA MiR-34a is growth promoting in EBV-infected B cells. J Virol, 2012. **86**(12): p. 6889-98.

100. DeVincenzo, J., et al., A randomized, double-blind, placebo-controlled study of an RNAi-based therapy directed against respiratory syncytial virus. Proc Natl Acad Sci U S A, 2010. **107**(19): p. 8800-5.

101. Krutzfeldt, J., et al., Silencing of microRNAs in vivo with 'antagomirs'. Nature, 2005. **438**(7068): p. 685-9.

102. Valadi, H., et al., Exosome-mediated transfer of mRNAs and microRNAs is a novel mechanism of genetic exchange between cells. Nat Cell Biol, 2007. **9**(6): p. 654-9.

CHAPTER II:

"MicroRNA-146a modulates B-cell oncogenesis by regulating Egr1"

(reprint)

MicroRNA-146a modulates B-cell oncogenesis by regulating Egr1

Jorge R. Contreras[1,2], Jayanth Kumar Palanichamy[1], Tiffany M. Tran[1], Thilini R. Fernando[1], Norma I. Rodriguez-Malave[1,2], Neha Goswami[1], Valerie A. Arboleda[1], David Casero[1], Dinesh S. Rao[1,3,4]

[1]Department of Pathology and Laboratory Medicine, UCLA, Los Angeles, CA USA

[2]Cellular and Molecular Pathology Ph.D. Program, UCLA, Los Angeles, CA USA

[3]Jonsson Comprehensive Cancer Center, UCLA, Los Angeles, CA USA

[4]Broad Stem Cell Research Center, UCLA, Los Angeles, CA USA

Correspondence to:
Dinesh S. Rao, **e-mail:** drao@mednet.ucla.edu

Keywords: *microRNA, B-cell, lymphoma, leukemia, c-Myc*

Received: *January 26, 2015* ***Accepted:*** *February 24, 2015* ***Published:*** *April 13, 2015*

ABSTRACT

miR-146a is a NF-κB induced microRNA that serves as a feedback regulator of this critical pathway. In mice, deficiency of miR-146a results in hematolymphoid cancer at advanced ages as a consequence of constitutive NF-κB activity. In this study, we queried whether the deficiency of miR-146a contributes to B-cell oncogenesis. Combining miR-146a deficiency with transgenic expression of c-Myc led to the development of highly aggressive B-cell malignancies. Mice transgenic for c-Myc and deficient for miR-146a were characterized by significantly shortened survival, increased lymph node involvement, differential involvement of the spleen and a mature B-cell phenotype. High-throughput sequencing of the tumors revealed significant dysregulation of approximately 250 genes. Amongst these, the transcription factor Egr1 was consistently upregulated in mice deficient for miR-146a. Interestingly, transcriptional targets of Egr1 were enriched in both the high-throughput dataset and in a larger set of miR-146a-deficient tumors. miR-146a overexpression led to downregulation of Egr1 and downstream targets with concomitant decrease in cell growth. Direct targeting of the human EGR1 by miR-146a was seen by luciferase assay. Together our findings illuminate a bona fide role for miR-146a in the modulation of B-cell oncogenesis and reveal the importance of understanding microRNA function in a cell- and disease-specific context.

INTRODUCTION

MicroRNAs (miRNAs) are a class of small non-coding RNAs, 21–22 nucleotides in length, which have physiological roles in many developmental systems [1]. miRNAs primarily act through post-transcriptional repression of target mRNAs via short complementary sequences in the 3'untranslated region (UTR) of mRNA transcripts [2, 3]. It has been reported that nearly 2000 miRNAs exist in the human genome and more than half of protein-coding genes are potential targets for miRNAs [4]. Both oncogenic and tumor suppressive miRNAs have been described in oncogenesis, acting via repression of tumor-suppressive and growth-promoting targets, respectively [5–8]. It is important to note, however, that miRNA regulation of gene expression is highly context-dependent: they regulate a cell type-specific transcriptome generated by a set of oncogenic or developmental transcriptional regulators. Hence, uncovering the oncogenic role of a miRNA requires the study of lineage specific transcriptional dysregulation.

miR-146a was discovered as a transcriptional target of the NF-κB pathway acting as a negative feedback regulator of this pathway and repressing some key components, such as *Traf6* and *Irak1* [9–13]. In line with its function in the NF-κB pathway, miR-146a deficiency in mice results in the development of a hyper inflammatory phenotype characterized by myeloid proliferation, lymphoid

hyperplasia, T-cell hyper activation and autoantibody production [9, 11, 14, 15]. Subsequently, aged knockout mice develop myeloid and lymphoid malignancies [9, 11]. These phenotypes are characterized by a dependence on constitutive NF-κB activity, as demonstrated by the correction of many phenotypes by deletion of elements of NF-κB signaling or downstream mediators [11, 16].

Constitutive NF-κB activity is a hallmark of many different types of cancer including B-cell malignancies [17]. The activated B-cell type of diffuse large B-cell lymphoma (ABC-DLBCL), which demonstrates constitutive NF-κB activation, is more aggressive and leads to worse outcomes in patients. Currently, several components of the NF-κB pathway have been found mutated in DLBCL, producing activation of NF-κB [18, 19]. The role of miR-146a as a negative regulator of this critical pathway, along with the development of B-cell malignancies in knockout mice, suggest that loss of miR-146a via undefined mechanisms may represent a pathogenetic event in B-cell malignancies that contributes to constitutive NF-κB activity.

In addition to being regulated by NF-κB, miR-146a has been shown to be positively regulated by the potent oncogene, *c-Myc*, in a melanoma cell line [20]. In contrast, primary samples of B-cell lymphoma with high levels of *c-Myc* expression show dramatic downregulation of miR-146a expression, and additional studies demonstrate negative regulation of miR-146a by c-Myc [21–23]. This led us to question the role that miR-146a plays in *c-Myc*-mediated oncogenesis in the B-cell lineage. Since *c-Myc* is a powerful transcriptional regulator with a specific transcriptome, we hypothesized that miR-146a mediated effects on the *c-Myc* gene expression program would reveal unique cancer relevant pathways. To test our hypotheses, we intercrossed the Eμ-Myc mouse with miR-146a-deficient animals. We found that miR-146a deficiency accelerates oncogenesis, decreases survival, and alters the differentiation stage of the tumors that are formed in the resulting mice. Histopathologic and flow cytometric analyses revealed a distinctive pattern of involvement in miR-146a-deficient animals. Mechanistically, few genes were significantly differentially regulated between wild-type and miR-146a-deficient, *c-Myc* driven tumors. Of these, *Egr1* and its downstream mediators were identified as a novel pathway regulated by miR-146a in B-cells. Our findings promise to open up a new area of research and demonstrate a tumor suppressive function for miR-146a in B-cell oncogenesis.

RESULTS

miR-146a deficiency decreases survival of Eμ-Myc transgenic mice

Given the proposed roles for miR-146a in tumor suppression and negative feedback regulation of the NF-κB pathway, we examined whether miR-146a deficiency would synergize with *c-Myc* during B-cell oncogenesis. miR-146a-deficient and Eμ-Myc transgenic mice were bred to yield cohorts of mice that carried the Eμ-Myc transgene with wild-type, heterozygous or homozygous knockout alleles of miR-146a (Figure 1a–1b). Most tumors that formed in Eμ-Myc mice showed a lymphoblastic morphology with numerous mitotic figures and apoptotic bodies on H&E sections (Figure 1c–1e). Conversely, tumors from the miR-146a-deficient mice demonstrated a more heterogeneous appearance. Many tumors had lymphoblastic morphology, but others showed a plasmacytoid appearance, including eosinophilic cytoplasmic concretions, suggestive of immunoglobulin deposits (Figure 1e inset shows cells with immunoglobulin concretions). Eμ-Myc miR-146a$^{+/-}$ mice did not have a significant reduction in their survival (Figure 1f). On the other hand, homozygous deficiency caused a decrease in survival from 104.5 days to 82.5 days (Figure 1f). Gender differences were noted, with female miR-146a$^{-/-}$ mice showing significant differences in survival, while males only showed a trend towards reduced survival (Supplementary Figure 1a–1d). Finally, virtually all mortality in both sets of mice was attributable to tumor formation (data not shown).

miR-146a-deficient tumors demonstrate differential anatomic patterns of involvement

Anatomically, tumors in both sets of mice showed differential patterns of involvement of hematopoietic and lymphoid organs, with virtually all mice showing thymic involvement. 31% of Eμ-Myc miR-146a$^{+/+}$ did not show any lymph node involvement, whereas all of the miR-146a$^{-/-}$ did show involvement (Figure 2a). While the majority of mice in both groups showed small numbers of circulating tumor cells in the peripheral blood, 6/10 Eμ-Myc miR-146a$^{-/-}$ mice examined showed frank leukemia (defined as a white blood cell count of greater than 30,000/μL) (Figure 2b–2d). This was in contrast to the lower numbers of Eμ-Myc miR-146a$^{+/+}$ mice that demonstrated leukemia by blood counts (4/14). Amongst mice with predominantly solid tumors, miR-146a deficiency caused a statistically significant increase in peripheral blood CD11b+ myeloid cells but not in B220+ B-cells, CD3ε+ T-cells, hemoglobin or platelets (Supplementary Figure 2a–2f). This may represent the propensity of miR-146a-deficient hematopoietic progenitors to produce increased numbers of myeloid cells. Bone marrow analysis of these mice found similar proportions of myeloid cells, erythroid cells, and B- lymphocytes (Supplementary Figure 2g–2i).

Mice in both groups demonstrated enlarged spleens, with average weights of approximately 400 mg (SupplementaryFigure 3a). In Eμ-Myc miR-146a$^{+/+}$ mice there was involvement of the white pulp with contiguous spread between the lymphoid follicles (Figure 2e, dotted area). High power views showed the malignant cells in both the white and red pulp (Supplementary Figure 3b–3c). On the other hand, Eμ-Myc miR-146a$^{-/-}$ mice showed

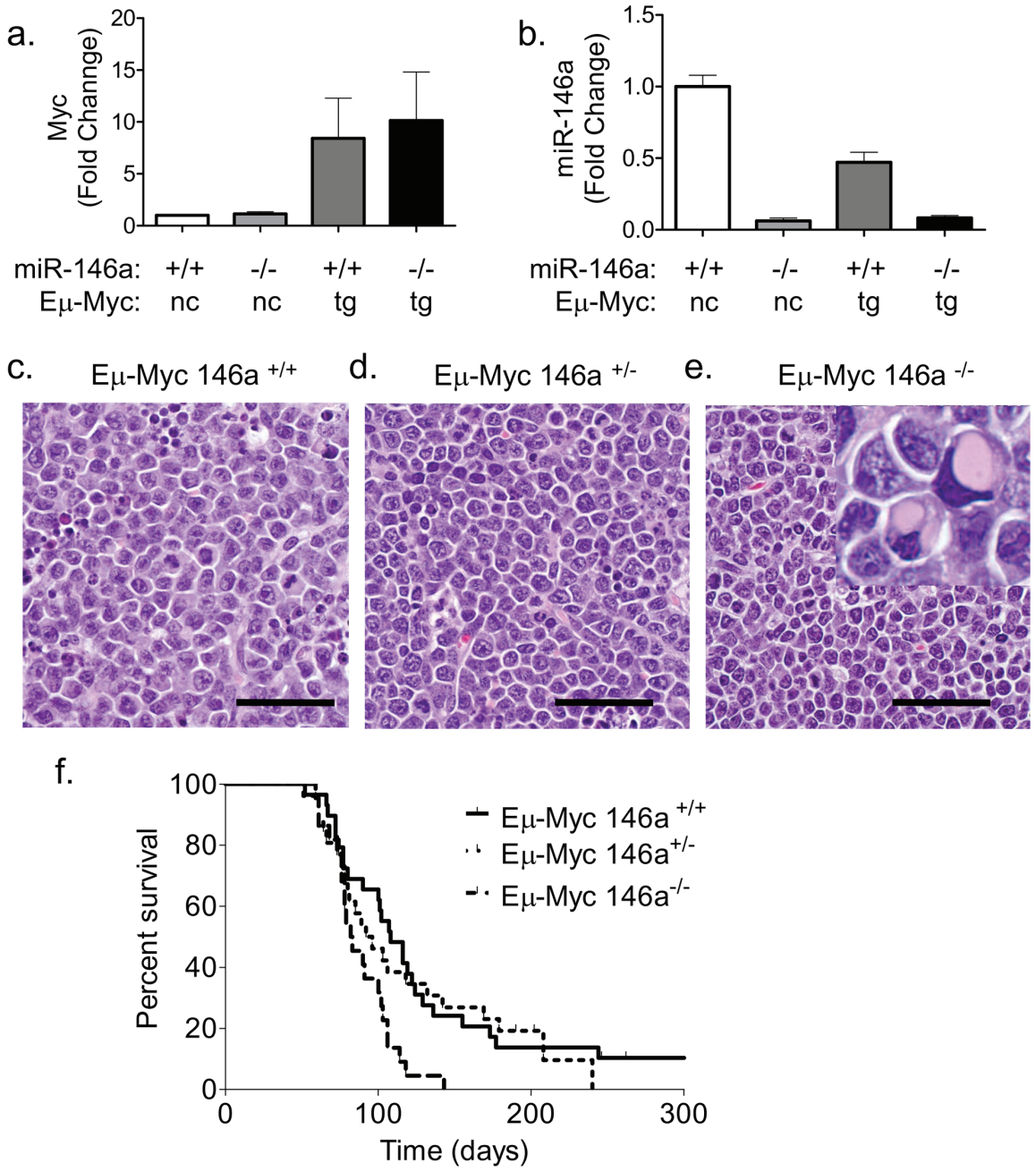

Figure 1: miR-146a deficiency causes increased mortality in Eμ-Myc mice. (a) RT-qPCR for c-Myc was performed on splenic B-cells from WT and miR-146a$^{-/-}$ mice or tumor samples from Eμ-Myc miR-146a$^{+/+}$and Eμ-Myc miR-146a$^{-/-}$ animals (n = 3, 3, 12, 11 respectively) (nc: non-carrier; tg: transgene). **(b)** RT-qPCR for miR-146a was performed from the same samples as for c-Myc. **(c–e)** Hematoxylin and Eosin (H&E) stained sections of lymph node tumors derived from Eμ-Myc miR-146a$^{+/+}$, Eμ-Myc miR-146a$^{+/-}$and Eμ-Myc miR-146a$^{-/-}$mice, respectively. The inset in (e) shows a subset of cells with immunoglobulin concretions. Scale bar for Figures 1c-e, 40 μm. **(f)** Kaplan Meier survival curve of mice with Eμ-Myc oncogene and wild-type, heterozygous, or homozygous deficiency of miR-146a (n = 26 for Eμ-Myc miR-146a$^{+/+}$(Solid line in graph), n = 23 for Eμ-Myc miR-146a$^{+/-}$ (Dotted line on graph), n = 22 for Eμ-Myc miR-146a$^{-/-}$ (Dashed line on graph);w.t. vs. het comparison, Log-Rank Test, p = 0.6725; w.t. vs. k.o. comparison, Log-Rank Test, p = 0.0027).

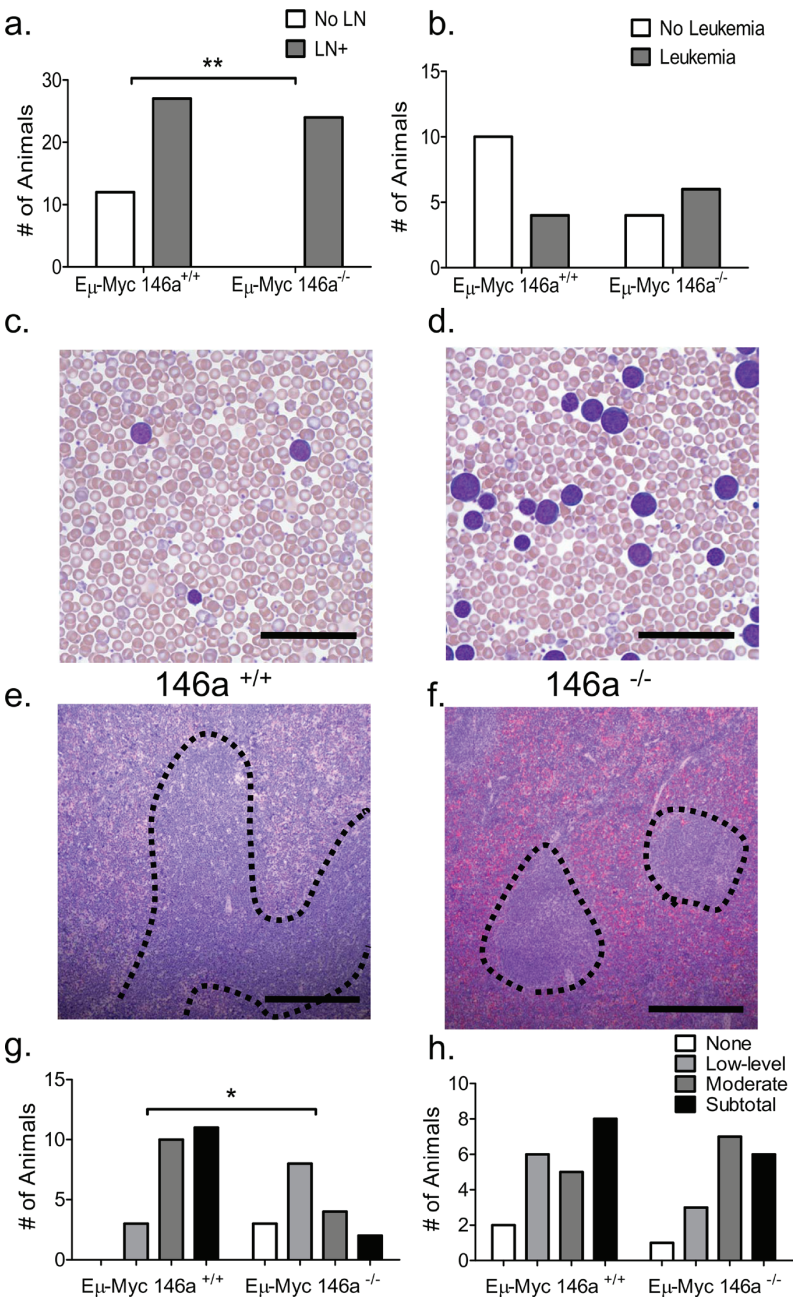

Figure 2: miR-146a-deficient tumors show a differential pattern of anatomic involvement. (a) Macroscopic lymph node involvement is significantly increased in miR-146a$^{-/-}$ deficient mice (n = 39 for Eμ-Myc miR-146a$^{+/+}$ and n = 24 for Eμ-Myc miR-146a$^{-/-}$; Fisher's exact test, p = 0.002). **(b)** Quantitation of the incidence of leukemia, defined as a peripheral white blood cell count of greater than 30, 000/μL, in these mice, shows a trend towards statistical significance between the groups (n = 14 for Eμ-Myc miR-146a$^{+/+}$ and n = 10 for Eμ-Myc miR-146a$^{-/-}$; Fisher's exact test, p = 0.21). **(c–d)** Wright stained peripheral blood smears from mice with miR-146a-sufficient and deficient Eμ-Myc driven tumors. Scale bar, 40 μm. **(e)** H&E stained section of Eμ-Myc miR-146$^{+/+}$spleen, low power image. Dotted lines delineate expanded white pulp. Scale bar, 400 μm. **(f)** Low power view of an H&E stained section showing relative sparing of the white pulp (dotted lines) in Eμ-Myc miR-146a$^{-/-}$ mice. Scale bar, 400 μm. **(g)** Quantitation of splenic white pulp involvement in Eμ-Myc miR-146a$^{+/+}$and Eμ-Myc miR-146a$^{-/-}$ mice on an ordinal 4-point scale going from no involvement to subtotal involvement of the spleen (n = 24 for Eμ-Myc miR-146a$^{+/+}$$n$ = 17 for Eμ-Myc miR-146a$^{-/-}$; Chi Square Test, p = 0.004). **(h)** Quantitation of splenic red pulp involvement in Eμ-Myc miR-146a$^{+/+}$and Eμ-Myc miR-146a$^{-/-}$ mice on an ordinal 4-point scale going from no involvement to subtotal involvement of the spleen (n = 24 for Eμ-Myc miR-146a$^{+/+}$$n$ = 17 for Eμ-Myc miR-146a$^{-/-}$; Chi Square Test, p = 0.671).

extensive involvement of the red pulp with relative sparing of the white pulp (Figure 2f). Using a semi-quantitative 4-point scale to grade involvement, we found that white pulp involvement was significantly higher in Eμ-Myc miR-146a$^{+/+}$ mice compared to knockout mice (Figure 2g). Red pulp involvement was not different between the two groups (Figure 2h). Despite these differential patterns of involvement, the relative numbers of B-cells, T-cells and myeloid cells in the spleen were equivalent between the two groups of mice (Supplementary Figure 3d–3k). Together, the data suggest similar overall infiltration of the spleen (given similar weights and cellular composition), but a predilection for the red pulp when miR-146a is deficient, suggesting that the deficiency of miR-146a may change the homing properties of the malignant B-cells. The patterns of involvement are somewhat reminiscent of certain subtypes of B-cell lymphoma/leukemia that show peripheral blood involvement and red pulp involvement in the spleen, but are not correlated with NF-κB activity or histologic subtype in humans.

miR-146a-deficient tumors demonstrate a mature B-cell phenotype

To further characterize the increased mortality seen in the miR-146a-deficient mice, we undertook immunophenotypic analyses. The tumors in both sets of mice were predominantly of B-cell phenotype (Figure 3a–3b). Similarly, Eμ-Myc mice with a heterozygous deficiency for miR-146a also developed B-cell tumors (Supplementary Figure 4a–4d). To examine the stage of differentiation, we examined expression of IgM, finding that greater than 70% of tumors from Eμ-Myc miR-146a$^{+/+}$ mice were IgM-. In contrast, only 42% of tumors from Eμ-Myc miR-146a$^{-/-}$ mice were IgM- (Figure 3c–3d). Amongst IgM- tumors, several were plasmacytic, shown by morphology and staining for CD138 (Figure 3e). Next, we dichotomized the data by mean fluorescent intensity (MFI), finding that CD138+ tumors were more frequently seen in the miR-146a-deficient background (Figure 3f). When we combined positivity for CD138 and IgM, most miR-146a-deficient tumors showed a mature B-cell phenotype (either IgM+ or CD138+) whereas miR-146a-sufficient tumors were negative for both IgM and CD138 (Figure 3). Tumor cells from miR-146a-deficient mice showed lower expression of memory B-cell/activation related antigen, CD80 (Supplementary Figure 4e–4f), but similar expression of CD44 (Supplementary Figure 4g–4h). To further characterize the stage of B-cell differentiation in these tumors, we performed RT-qPCR to quantitate the expression of genes involved in B-cell differentiation. We found that transcripts for Blimp1, CD43, Bcl6 and Ighδ were all more highly expressed in tumors from miR-146a-deficient mice (Figure 3h–3k). Interestingly, female mice, which showed a statistically significant difference in survival, showed similar trends in their immunophenotypic profiles (Supplementary Figure 5a–5f) as well as in gene expression of maturation-related B-cell transcripts (Supplementary Figure 5g–5j) when compared to the group overall. Together these findings indicate that miR-146a-deficient tumors are composed of malignant B-cells that derive from a different stage of differentiation than tumors sufficient for miR-146a.

miR-146a-deficient tumors show a limited difference in transcriptome expression, including many putative targets of miR-146a

To define a mechanistic basis for miR-146a-deficient B-lymphomagenesis, we performed RNA-sequencing on four miR-146a sufficient and two miR-146a-deficient tumors. Based on this comparison, we arrived at a list of 249 genes that were differentially regulated with an adjusted *p*-value of 0.05 or lower (Figure 4a). We then searched the dataset for miR-146a targets predicted by TargetScan [2, 3]. Of the differentially regulated genes, 53 genes are predicted to be miR-146a targets (Figure 4b). When we examined the genes that were upregulated, 29 out of 140 genes were predicted miR-146a targets (Figure 4c), and this did not represent a statistical enrichment. Next, we confirmed some of the findings by RT-qPCR in the larger set of tumor samples that we had collected. Four of the top ten genes from RNA sequencing had significantly different expression levels in the tumors when assayed by qPCR. These genes include *Jhy* and *Camk2b* (Figure 4d and 4f). *Jhy* is a recently described novel gene with no known function in oncogenesis or hematopoiesis; while *Camk2b* has a previously described putative role in epithelial cancer [24]. The gene *Dtx3*, which showed differential regulation by RNA-sequencing, was not differentially expressed in the larger set of tumor samples (Figure 4h). Other genes that were differentially expressed included the putative target *Egr1*, with *Nrp2* showing a trend towards differential expression (Figure 4e and 4g). A third predicted target, *Axl*, failed to show differential regulation by qPCR in this larger set of samples (Figure 4i). Hence, the transcriptome data provided us with a starting point for understanding tumorigenesis, uncovering putative miR-146a targets in the setting of B-cell oncogenesis.

The transcriptome regulated by EGR1 is differentially regulated in miR-146a-deficient tumors

The early growth response-1 gene (*Egr1)*, has previously described functions in hematopoietic differentiation [25, 26]. Given that *Egr1* is overexpressed in miR-146a-deficient tumors, we undertook an analysis to determine whether the *Egr1* transcriptome is differentially regulated. Using a publically available ChIP-Seq dataset, we gathered a list of EGR1 transcription factor binding

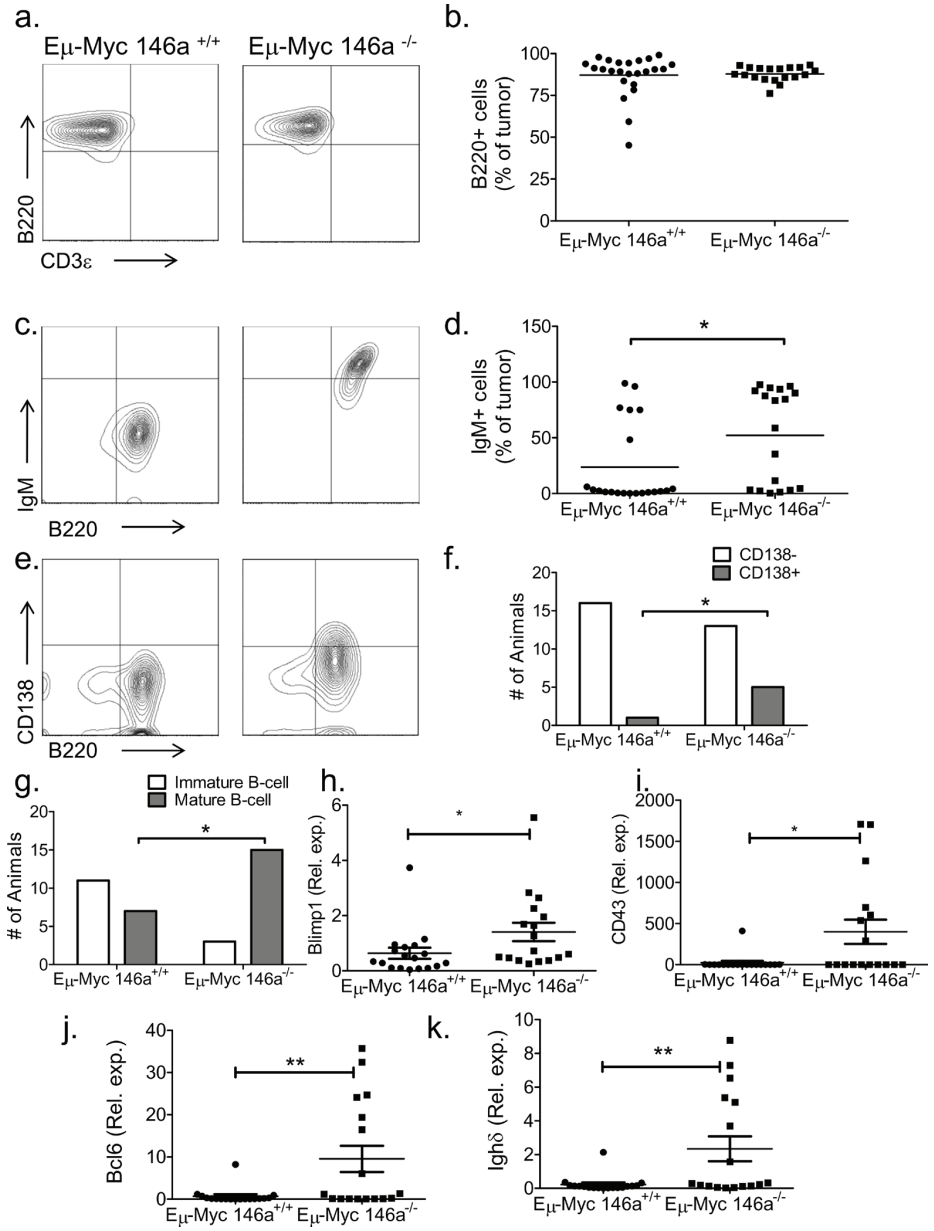

Figure 3: miR-146a deficiency causes a mature B-cell phenotype in Eμ-Myc mice. (a) Representative FACS plot showing staining for B220 and CD3ε in Eμ-Myc miR-146a$^{+/+}$ and Eμ-Myc miR-146a$^{-/-}$mice. **(b)** FACS shows that both groups of mice demonstrate B-cell tumors (n = 24 for Eμ-Myc miR-146a$^{+/+}$ and n = 19 for Eμ-Myc miR-146a$^{-/-}$; t-test p = 0.794). **(c)** Representative FACS plots stained for B220 and IgM from tumors derived from Eμ-Myc miR-146a$^{+/+}$ and Eμ-Myc miR-146a$^{-/-}$ mice. **(d)** Percentage of IgM positive cells in tumors from both cohorts showing increased IgM positivity in Eμ-Myc miR-146a$^{-/-}$ tumors (n = 25 for Eμ-Myc miR-146a$^{+/+}$ and n = 17 for Eμ-Myc miR-146a$^{-/-}$; t-test, p = 0.03). **(e)** Representative FACS plots stained for B220 and CD138 from tumors derived from Eμ-Myc miR-146a$^{+/+}$ and Eμ-Myc miR-146a$^{-/-}$ mice. **(f)** Dichotomized CD138 expression data (see methods for details on dichotomization), showing animals with CD138+ versus CD138- tumors (n = 18 for Eμ-Myc miR-146a$^{+/+}$ and n = 18 for Eμ-Myc miR-146a$^{-/-}$; Chi-square test, one-sided p = 0.04). **(g)** Tumors were dichotomized as being either immature (double negative for CD138 and IgM) or mature (having expression of either marker) (n = 18 for Eμ-Myc miR-146a$^{+/+}$ and n = 18 for Eμ-Myc miR-146a$^{-/-}$; Chi-square test, p = 0.0062). **(h–k)** RT-qPCR data for Blimp1, CD43, Bcl6, and Ighδ in tumors from Eμ-Myc miR-146a$^{+/+}$ (n = 18)and Eμ-Myc miR-146a$^{-/-}$ mice (n = 17). All comparisons showed statistically significant differences by T-test (p = 0.05 for Blimp1 (h), p = 0.014 for CD43 (i), p = 0.0070 for Bcl6 (j), and p = 0.0067 for Ighδ(k).

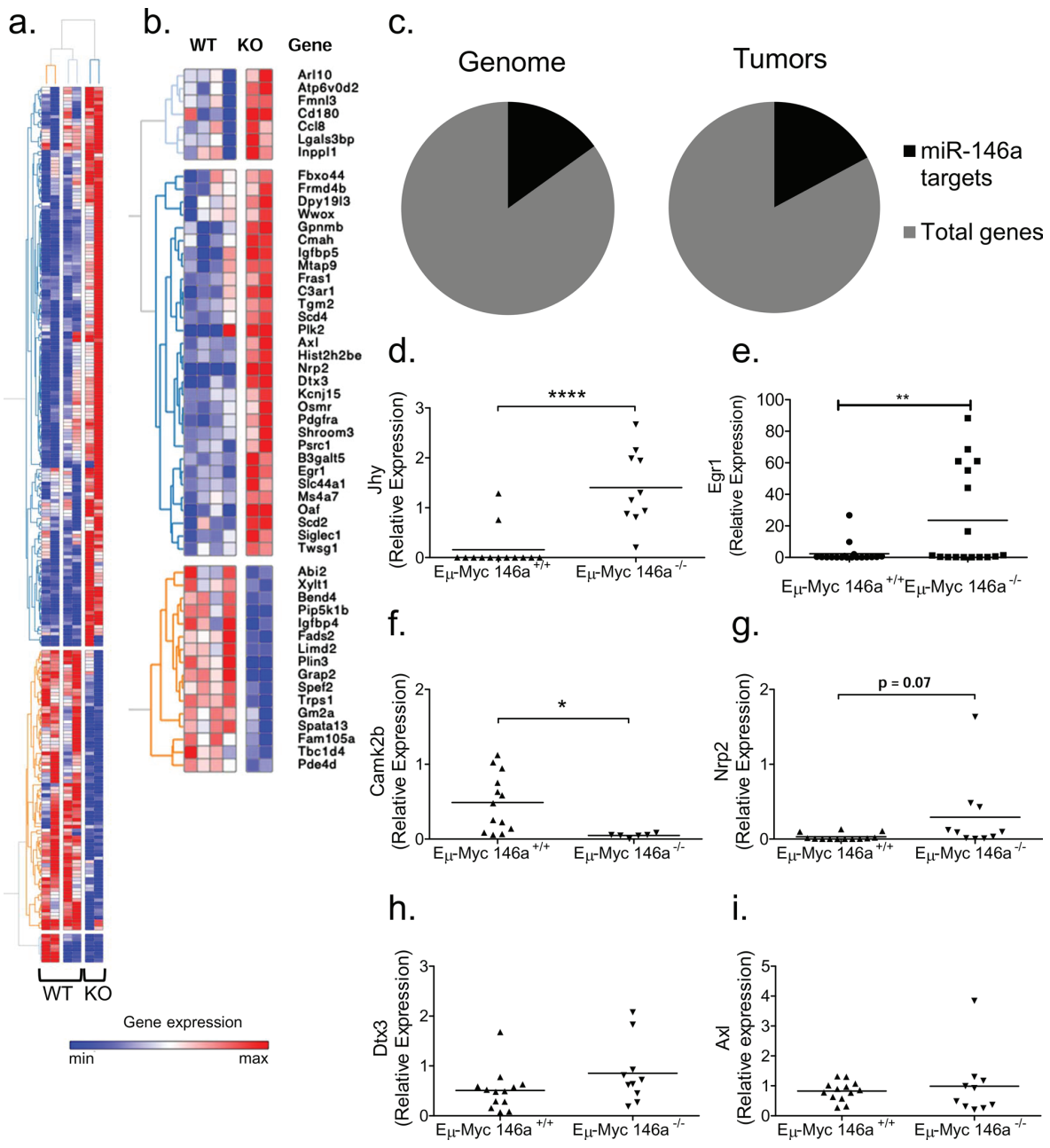

Figure 4: Gene expression analyses of Eμ-Myc driven tumors with miR-146a deficiency. (a) Genes differentially expressed between Eμ-Myc miR-146a$^{+/+}$ and Eμ-Myc miR-146a$^{-/-}$ tumors. **(b)** Differentially expressed genes with miR-146a sites in their UTR as predicted by the TargetScan algorithm. The heat map color scale represents, for each gene, the relative expression level using the average mean gene expression as a reference. **(c)** Graphical representation of the percentage of the genome (left) predicted to be targeted by miR-146a (2773 predicted targets out of 18, 393 annotated UTRs), compared with the percentage of upregulated genes in the tumor dataset (right) that are predicted miR-146a targets (29 predicted targets out of 169 upregulated genes). No statistically significant enrichment was found (Chi-square test). **(d–i)** RT-qPCR of genes found to be differentially regulated by RNA-sequencing analysis, including *Jhy* (d; *t*-test, $p < 0.0001$), *Egr1* (e; *t*-test, $p = 0.0086$), *Camk2b* (f; *t*-test, $p = 0.01$), *Nrp2* (g; *t*-test, $p = 0.0743$), *Dtx3* (h; *t*-test, $p = 0.127$) and *Axl* (i; *t*-test, $p = 0.616$). The three genes on the left (*Jhy, Camk2b and Dtx3*) were amongst the most differentially regulated genes between the miR-146a sufficient and deficient tumors by RNA sequencing. The three genes on the right (*Egr1, Nrp2 and Axl*) represent putative targets of miR-146a (For RT-qPCR analysis $n = 13$ for Eμ-Myc miR-146a$^{+/+}$and $n = 10$ for Eμ-Myc miR-146a$^{-/-}$ for panels d, g, h, i; $n = 13$ for Eμ-Myc miR-146a$^{+/+}$and $n = 6$ for Eμ-Myc miR-146a$^{-/-}$ for panel f; $n = 18$ for Eμ-Myc miR-146a$^{+/+}$ and $n = 17$ for Eμ-Myc miR-146a$^{-/-}$ for panel e).

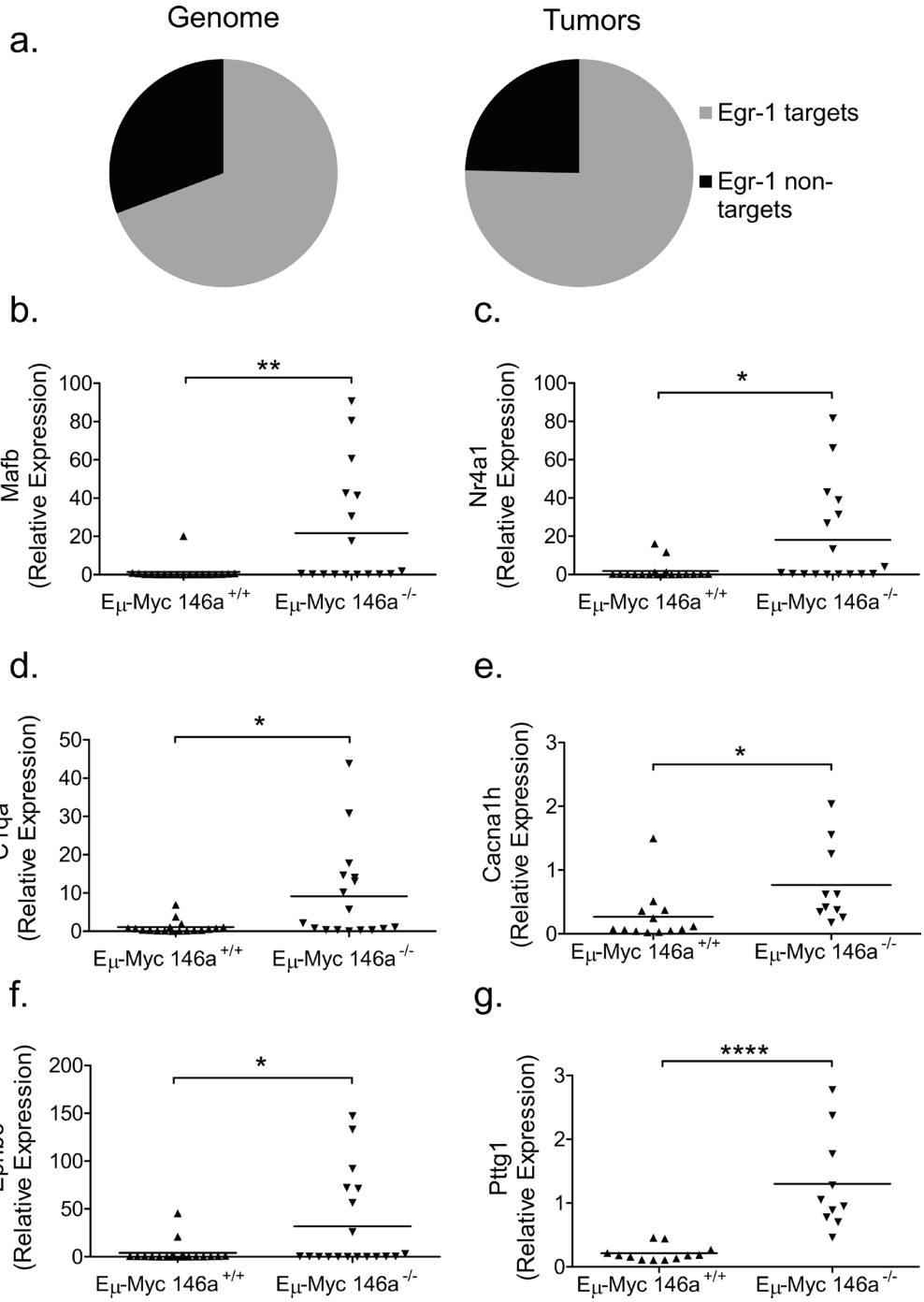

Figure 5: Genes with EGR1 transcription factor binding sites are enriched in Eμ-Myc driven tumors with miR-146a deficiency. (a) Graphical representation of the percentage of the genome (left) containing EGR1 TFBS (11136 TFBS out of 16288 genes that were conserved between human and mouse), compared with the percentage of differentially regulated genes in the tumor dataset (right) that show EGR1 TFBS (153 with TFBS out of 203 differentially regulated genes that are conserved between mouse and human). This difference was found to be statistically significant (Chi-square test, one-sided $p = 0.0353$). **(b–g)** RT-qPCR confirmation of differentially regulated genes that show EGR1 TFBS, including *Mafb* (b; *t*-test, $p = 0.0093$), *Nr4a1* (c, *t*-test, $p = 0.0126$), *C1qa* (d; *t*-test, $p = .0101$), *Cacna1 h* (e; *t*-test, $p = .0308$), *Ephb6* (f; *t*-test, $p = .0248$), *Pttg1* (g; *t*-test, $p < 0.0001$). For these RT-qPCR analyses, $n = 18$ for Eμ-Myc miR-146a$^{+/+}$and $n = 17$ for Eμ-Myc miR-146a$^{-/-}$.

sites (TFBS) around known protein coding genes in three different human cell lines (K562, GM12878, and H1-hESC) [27]. This dataset was compared to the list of differentially regulated genes in miR-146a-deficient tumors that have human homologs (Supplementary Figure 6a–6b). Remarkably, genes that show TFBS for EGR1 were statistically overrepresented in the differentially regulated gene set from miR-146a-deficient tumors (Figure 5a). We then confirmed several targets of EGR1 that (i) were differentially regulated in the RNA-sequencing dataset and (ii)had been previously shown in the literature to be EGR1 targets or had EGR1 binding sites based on the ChIP-Seq datasets. Several genes that are important in hematopoiesis and/or cancer were profiled in the larger set of tumors and showed a significantly differential regulation. These genes included *Mafb* (Figure 5b), *Nr4a1* (Figure 5c), *C1qa* (Figure 5d), *Cacna1 h* (Figure 5e), *Ephb6* (Figure 5f) and *Pttg1* (Figure 5g and Supplementary Figure 6c). Changes in gene expression in Egr1 and a subset of its targets were conserved in the subset of tumors derived from female mice, hinting that these molecular changes may underlie the increased lethality in the knockout mice (Supplementary Figure 5k–5n). Together, these findings indicate that miR-146a-regulated *Egr1* may represent a critical target that leads to the elaboration of a gene expression signature and the more aggressive phenotype observed during miR-146a-deficient, Eμ-Myc-mediated oncogenesis.

Egr1 is regulated by miR-146a and overexpression of miR-146a has an anti-growth effect on B-cell lymphoma cell lines

To elucidate whether miR-146a targets *Egr1*, we examined the 3' untranslated region (UTR) of the cDNA transcript. In the human *EGR1* sequence, there is a miR-146a 7-mer binding site located at position 111–117 of the 3' UTR (Figure 6a). The DNA sequence surrounding this area is somewhat conserved between the human and the mouse, but the complete 7-mer site is not present in the mouse (Supplementary Figure 6d). To examine direct targeting, we cloned a 996 bp segment of the human *EGR1* 3′UTR into the pmiRGlo vector. Co-transfection of a miR-146a over- expression vector along with the luciferase-*EGR1* 3′UTR fusion construct showed significant repression of luciferase activity, compared to the empty vector, similar to that observed for *Traf6*. Mutation of the binding site for miR-146a in the EGR1 3' UTR derepressed luciferase expression. A similar repression was not consistently observed for the murine Egr1 3'UTR (Figure 6b). Stable overexpression of miR-146a using a retroviral vector in the murine leukemia cell lines, 70Z/3 and WEHI-231 led to a repression of *Egr1* at both the transcript and protein levels (Figure 6c–6e, 6i–6j, 6l). In addition, overexpression of miR-146a led to decreased growth of both cell lines at baseline and following serum starvation (Figure 6f–6g, 6m–6n). Moreover, we observed repression of the EGR1 target, *Nr4a1* (Figure 6h, 6k), implicating the same sequence of regulation with miR-146a overexpression as that observed with miR-146a deficiency in the tumors. Moreover, miR-146a overexpressing cells showed a downregulation of Blimp1 and Bcl6 (Supplementary Figure 6i–6l), in line with the observations made in the tumors. In the human DLBCL cell line, SUDHL2, miR-146a overexpression led to repression of EGR1 as well as the expected target of miR-146a, TRAF6 (Figure 6o). Nrp2 was validated as an additional target of miR-146a (Supplementary Figure 6e–6h). These findings imply a role for miR-146a in the regulation of B-cell leukemia/lymphoma cell growth and demonstrate that in the human, miR-146a directly targets EGR1 via canonical 3' UTR-mediated targeting. Hence, miR-146a overexpression and knockout results in significant effects on Egr1 and downstream gene expression, suggesting a conserved regulatory module in the human and mouse.

DISCUSSION

In this manuscript we describe the modulation of tumorigenesis by the NF-κB induced tumor suppressor microRNA, miR-146a. miR-146a plays a very important role in immune cells and seems to be critical in modulating feedback inhibition of the NF-κB pathway. Its role in T-cells, myeloid cells and hematopoietic stem cells is well-established, with deletion of this miRNA leading to T-cell hyper activation, myeloid hyperplasia and tumors, and stem cell exhaustion [9, 11, 14, 16]. The role of miR-146a in the developmental sequence of B-cells is less understood. In young miR-146a-deficient mice, B-cell development appears to proceed normally, but by the age of six months, lymphoid follicles in the spleen and other lymphoid tissue demonstrate hyperplasia [9, 28]. Following this phase, myeloproliferative disease becomes the dominant phenotype and B-cell numbers drop as the mice age. Nonetheless, aged miR-146a-deficient mice show an increased incidence of B-cell malignancies. Interestingly, these tumors show a predilection for the lymph nodes, similar to what we have observed here with Eμ-Myc driven tumors.

miR-146a-deficient Eμ-Myc transgenic mice develop mature B-cell neoplasms with IgM and/or CD138 expression, leading to a higher proportion of lymph node tumors and leukemia in the peripheral blood. There is some heterogeneity in the proportion of Eμ-Myc mice reported to develop IgM+ tumors in the literature [29, 30], but our results have been consistently in the 20–30% range. The immunophenotypic differences, along with concordant gene expression changes (e.g., Blimp1 and Bcl6), indicate that miR-146a deficiency may alter the stage of B-cell development that is most susceptible to transformation by *c-Myc*. This is an interesting observation as B-cell neoplasms in humans that have increased levels of *c-Myc* can also derive from different stages of development (for example, B-lymphoblastic leukemia, Burkitt's lymphoma,

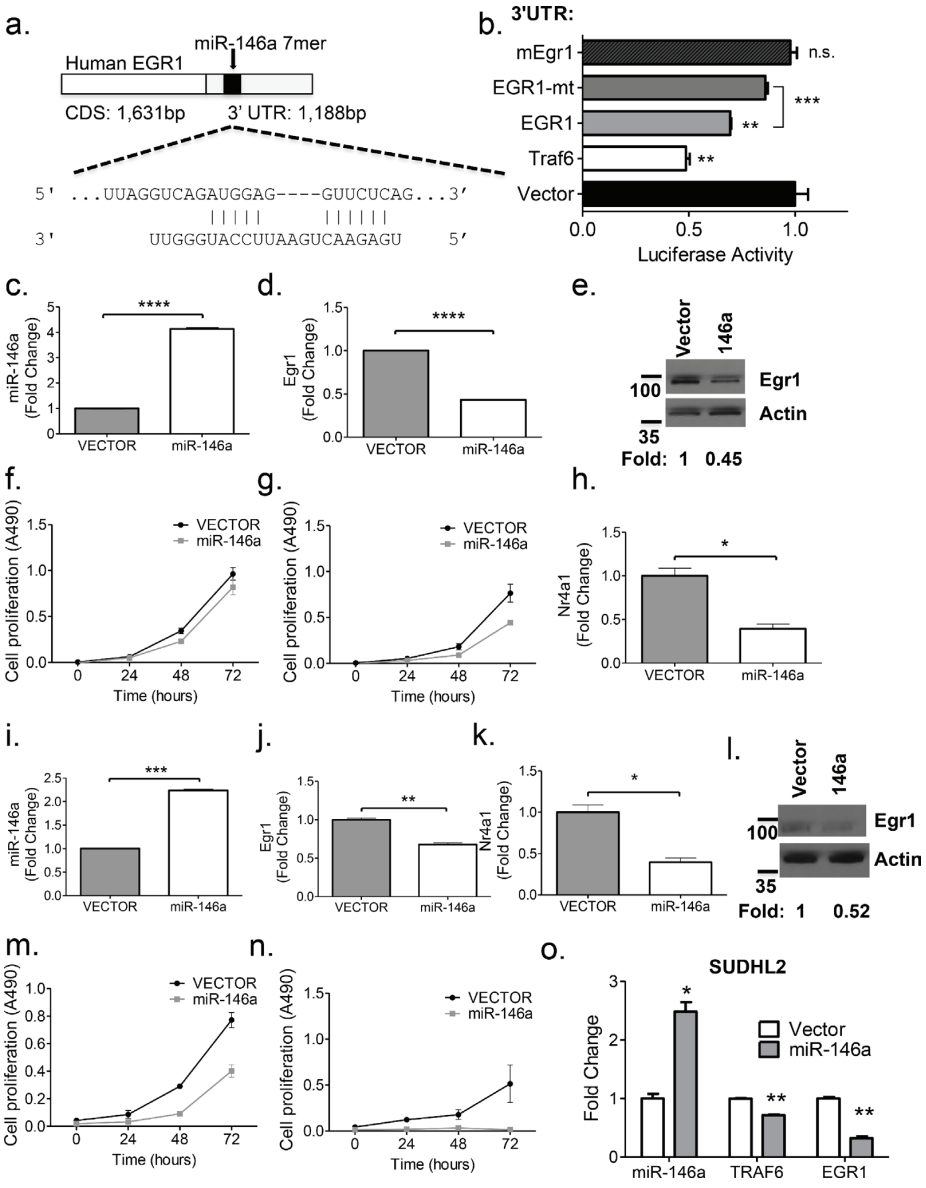

Figure 6: Egr1 is regulated by miR-146a. **(a)** The human EGR1 cDNA contains a 1, 188 bp 3'UTR that contains an intact miR-146a 7-mer binding site. Shown is a schematic of the binding between EGR1 and miR-146a. **(b)** Luciferase assays quantitating repression with MGP/miR-146a co-transfection relative to MGP alone for each of the UTRs depicted. Each measurement is representative of firefly luciferase normalized to renilla luciferase, and was performed in duplicate, with the experiment was repeated at least three times (*T*-test; Traf6 v Vector, $p = 0.0013$; EGR1 vs. vector, $p = 0.0077$; EGR1 vs. mutant EGR1, $p = 0.0002$). **(c–d)** RT-qPCR analyses of miR-146a and *Egr1*, respectively in the murine 70Z/3 cell line. **(e)** Western Blot analysis confirms EGR1 repression with miR-146a over expression in the 70Z/3 cell line. Fold repression was computed using ImageJ software. **(f–g)**. Cell proliferation (MTS) assays were performed using 70Z/3 cells transduced with either empty vector (MGP) or miR-146a over expressing vector (MGP-miR-146a). Basal growth is shown in (f), while growth in samples following 24 hours of serum starvation is shown in (g). **(h)** RT-qPCR of the EGR1 target gene, *Nr4a1*, shows repression in miR-146a overexpressing cells. **(i–k)**. RT-qPCR analyses of miR-146a, *Egr1* and *Nr4a1*, respectively, in the murine WEHI-231 cell line. **(l)** Western Blot analysis, as in (e), using the WEHI-231 cell line **(m–n)**. Cell proliferation (MTS) assays were used to measure basal growth and growth following 4 hours of serum starvation **(o)** miR-146a overexpression in a human DLBCL cell line, SUDHL2 results in the repression of TRAF6 and EGR1. All comparisons were made with *T*-test for Figure 6c-o, with the following legend: $*p < 0.05$; $**p < 0.005$; $***p < 0.0005$; $****p < 0.0001$.

DLBCL, and plasma cell myeloma) [31–35]. Here, the expression of a miRNA in an experimental model of Myc-mediated oncogenesis does alter the stage of B-cell oncogenesis. Although the relevance to human disease remains to be established, it is interesting to speculate that miRNA expression may have an important role in defining the cellular composition of lymphoma from a given driver mutation.

An important question raised by this study is whether the observed phenotypes occur as a consequence of cell-intrinsic or cell-extrinsic mechanisms. The primary tumor sites showed primarily B-cells, and histologically, the tumors appeared to be quite homogeneous. In miR-146a-deficient mice, T-cell activation is thought to occur as a consequence of repeated bouts of subclinical infection and inflammation without the "recalibrating" effects of miR-146a expression. We do not think this is a likely cause for the augmentation of oncogenesis, since the development of tumors under specific pathogen free conditions do not occur early in life in miR-146a singly-deficient mice. Heterozygotes did not show increased mortality in the presence of Eμ-Myc, whereas miR-146a heterozygosity alone causes inflammatory changes [9]. Hence, it is likely that increased tumorigenesis in our mice occurs primarily as a consequence of B-cell intrinsic mechanisms. However, we cannot entirely exclude a cell-extrinsic process driven by benign but hyperactivated T-cells. Future studies to address this issue will include producing B-cell specific knockouts and knock-ins of miR-146a to study disease progression, but are beyond the scope of the current study.

In an effort to further characterize tumorigenesis in these mice, we undertook gene expression analysis by high-throughput sequencing. We have found that a small set of genes are significantly differentially regulated between miR-146a sufficient and deficient Eμ-Myc tumors. While the functional analysis did not reveal an overall pattern to the differentially regulated gene set, the individual genes do seem to be important in various aspects of tumorigenesis (Supplementary Table 2) [36, 37]. Amongst the differentially regulated genes, many have roles in oncogenesis and B-cell development. Perhaps the most interesting gene to be identified by our analysis is *Egr1*, a factor known to promote differentiation in the hematopoietic lineage. EGR1 transcriptionally induces a range of genes, and the differentially regulated gene set in miR-146a-deficient mice was enriched for these targets. Indeed, some of the most differentially regulated genes in our dataset were previously described targets of EGR1 or putative targets as defined by the presence of transcription factor binding sites. Critically, miR-146a regulates *Egr1*, and provides an explanation for the observed phenotypic differences in the tumors from these mice. However, we must note that direct targeting was only seen with the human EGR1 3'UTR, and hence the mechanism of this regulation in the mouse may be indirect. This could include non-canonical mechanisms of miRNA targeting (such as in the 5'UTR) and/or indirect regulation.

miR-146a overexpression changes the growth of murine B-cell lines, suggesting the importance of the EGR1-mediated transcription program in maintaining growth of these cells. Notably, miR-146a overexpression also led to the repression of certain mRNAs that are important in B-cell differentiation including Blimp1 and Bcl6, once again supporting the notion of miR-146a playing a role in the maturation stage of the tumor cells. This is line with prior reports showing that expression of an Egr1 transgene supported the development of progenitor cells into mature, IgM-expressing B-cells [26]. Interestingly, some of the genes that contain TFBS for EGR1 are also regulated by miR-146a (for example, *Nrp2*), suggesting that miR-146a may target several points in the same pathway during B-cell oncogenesis. Downstream, genes without a defined role in B-cell neoplasms were also identified. *Pttg1* is overexpressed in a wide variety of endocrine and non-endocrine tumors, modulates tumor invasiveness and recurrence in several systems, and has functions in chromatid separation and cell cycle progression [38]. *Jhy* is another gene we identified whose deficiency causes juvenile hydrocephalus in mice [39]. It will be of great interest to study how miR-146a deficiency causes differential regulation of these novel genes and what their roles are in normal and malignant B-lymphopoiesis.

Our findings also point to the cell-type specific nature of miRNA mediated regulation. The targets uncovered in a malignant B-cell are different than those found in an activated T-cell or a myeloid cell. For example, our findings suggest that *Traf6* and *Irak1*, which are highly important in the elaboration of myeloid phenotypes, may not be as important in B-cell oncogenesis, particularly that induced by *c-Myc*, as these genes were not differentially regulated in the tumors that we examined (data not shown). These findings highlight the need for experimental work in carefully defined physiological and pathological systems to comprehensively understand miRNA function.

In summary, we show that concurrent *c-Myc* overexpression coupled with the absence of a *bona fide* tumor suppressor miRNA leads to more aggressive tumor due to a small set of genes that are regulated directly or indirectly by miR-146a. . Our novel set of targets may indicate that miR-146a regulates components of signaling networks other than the NF-κB inflammatory pathway. Hence, our work opens the door to new areas of investigation in B-cell oncogenesis and miRNA biology.

MATERIALS AND METHODS

Mice

miR-146a-deficient (miR-146a$^{-/-}$) mice were developed as previously described [9, 11, 16]. Eμ-Myc mice were purchased from Jackson laboratories and housed under pathogen free conditions at the University of California, Los Angeles [40]. Eμ-Myc and miR-146a$^{-/-}$mice

were bred to obtain Eμ-Myc miR-146a$^{+/-}$mice with further miR-146a$^{-/-}$ intercross producing Eμ-Myc miR-146a$^{-/-}$ mice. Mice were monitored for tumors and sacrificed when they became pre-moribund indicated by the following criteria: tumors larger than 1.5cm, emaciation, or any other signs of distress. All mouse studies were approved by the UCLA Office of Animal Research Oversight.

Flow cytometry

Blood, bone marrow, spleen, and lymph node tumors were collected from the mice under sterile conditions. Single cell suspensions were lysed in red blood cell lysis buffer. Fluorochrome conjugated antibodies against B220, CD3ε, CD11b, Ter119, CD19, IgM, CD80, CD138, CD44, CD21, CD23, and CD5 were used for staining (all antibodies obtained from Biolegend). Flow cytometry was performed on a FACSAria and analysis performed using FlowJo software. Dichotomization of flow cytometric measurements was accomplished by visual inspection of the data and identification of clusters within the data. These were then validated by comparison of the means and averages of the two clusters. For CD138, this was accomplished by examining the Mean Fluorescence Intensity and determining that the low expression cluster had a mean MFI, 154.0 ± 13.96 (N = 30) and 557.6 ± 71.87 (N = 7) for the high CD138 samples (p <0.0001 for this comparison).

Histopathology

Organs were collected after necropsy and fixed in 10% neutral buffered formalin. These were then embedded in paraffin, processed for hematoxylin and eosin staining by the Translational Pathology Core Laboratory at UCLA. Histopathologic analysis was performed by a board certified hematopathologist (D.S.R). The degree of splenic involvement was scored on a 4-point scale for red and white pulp involvement. Analysis of dichotomized or ordinal-type histopathologic data was accomplished by the use of Fisher's Exact Test.

Statistical analyses

Figures are graphed as mean with the standard deviation of the mean (SD) for continuous numerical data. Bar graphs are employed to show dichotomized or ordinal-type histopathologic data. Student's t-test, Fisher's exact test, Chi square test, and Kaplan-Meier survival analysis were performed using GraphPad Prism software, applied to each experiment as described in the figure legends.

RNA-sequencing and analysis

Total RNA was extracted from tumors using Trizol combined with Qiagen miRNEasy mini kit with additional on column DNAse I digestion. Following isolation of RNA, cDNA libraries were built using the Illumina(San Diego, CA) TrueSeq RNA Sample Preparation kit V2 (RS-122–2001). An Agilent Bioanalyzer was used to determine RNA quality (RIN > 8) prior to sequencing. RNA-Seq libraries were sequenced on an Illumina HiSeq 2000 (single-end 100bp). Raw sequence files were obtained using Illumina's proprietary software and are available at NCBI's Gene Expression Omnibus resource (GEO Series accession number GSE67113; http://www.ncbi.nlm.nih.gov/geo/query/acc.cgi?acc=GSE67113) resource. RNA-Seq reads were aligned using STAR v2.3.0 [41]. The GRCm38 assembly (mm10) of the mouse genome and the junction database from Ensembl's gene annotation (release 71) were used as reference for STAR. The count matrix for genes in Ensembl's genome annotation (excluding rRNAs, Mt_rRNAs and Mt_tRNAs) was generated with HTSeq-count v0.5.4p3 (http://www-huber.embl.de/users/anders/HTSeq/) and normalized using the geometric mean across samples [42]. DESeq v1.14.0 [42] was used to classify genes as differentially expressed (Benjamini-Hochberg adjusted p-value < 0.05). Moderate fold changes between conditions were obtained from variance-stabilized data [42]. Functional annotation of differentially expressed genes was generated through the use of DAVID [36, 37]. Hierarchical gene clustering was performed with GENE-E (http://www.broadinstitute.org/cancer/software/GENE-E/). To display the heatmap, the expression levels were re-scaled so that, for each gene, the limits of the color scale correspond to the minimum and maximum expression levels across all samples.

EGR1 transcription factor binding site analysis

Publically available ENCODE data for EGR1 Transcription Factor Binding Site ChIP-Seq Uniform Peak analysis was downloaded from the UCSC Genome Browser for the K562, H1-hESC, and GM12878 cell lines [27]. For each line, the locations for all EGR1 Transcription Factor Binding Sites (TFBS) were grouped based on the closest known gene based using the UCSC Main (hg19) ccds gene list. The genes with one or more TFBS were compared to the mouse (mm10) RNASeq data set to identify genes that were differentially expressed in the miR-146a-deficient tumors and also had at least one EGR1 TFBS in close proximity to the gene (defined as 3 kb). A Chi-Square test was performed with one degree of freedom to compare the relative frequency of EGR1 TFBS in the differentially expressed dataset (Observed) with the frequency across the genome (Expected). Only the mouse genes with a human homolog (total of 16288 genes) were used.

RT-qPCR

RNA collected from the murine tumors was reverse transcribed using qScript reagent and PerfeCTa SYBR Green FastMix reagent (Quanta Biosciences) or TaqMan MicroRNA Assay (Life Technologies). Primer sequences used are listed in Supplementary Table 1.

Western blot

Tumor cell suspensions were lysed in RIPA buffer (Boston BioProducts) supplemented with Halt Protease and Phosphatase Inhibitor Cocktail (Thermo Scientific). Equal amounts of protein lysate (as quantified by using bicinchoninic acid protein assay, BCA (Thermo Scientific)) were electrophoresed on a 5–12% SDS–PAGE and electroblotted onto a nitrocellulose membrane. Antibodies used were c-MYC Rabbit polyclonal (#9402), EGR1 (44D5) Rabbit monoclonal (all antibodies from Cell Signaling), and ß-Actin (AC15) mouse monoclonal antibody (Sigma Aldrich). Secondary HRP-conjugated antibodies were purchased from Santa Cruz Biotechnology.

MTS assay

Cell proliferation was measured using the Promega Cell Titer 96 Aqueous Non-Radioactive Cell Proliferation Assay kit. After addition of reagent according to the manufacturer's protocol, cells were incubated at 37°, 5% CO_2 for 4 hours and absorbance was measured at 490 nm.

Luciferase assays

A 996-bp segment of the human *EGR1* 3'UTR containing the miR-146a site was cloned into the pmiRGlo dual luciferase vector (Promega). A similar cloning strategy was used to clone murine Egr1 3'UTR and the Nrp2 UTR (see Supplementary Table 1). For mutation of the miR-146a binding site, we utilized site-directed mutagenesis as previously described using the primers shown in Supplementary Table 1 [43]. Co-transfections were performed with Lipofectamine 2000 (Life Technologies) as per the manufacturer's instructions. Cells were lysed after 24 hours, substrate was added and luminescence was measured on a Glomax-Multi Jr (Promega).

Genotyping for miR-146a mice and c-Myc mice

Mice were genotyped for miR-146a deletion and Eμ-Myc presence using DNA extracted from tail samples. Genotyping for miR-146a deletion was done as described previously [11]. Primers are listed in Supplementary Table 1.

ACKNOWLEDGMENTS

We thank members of the Rao lab for helpful discussions regarding the research. This work was supported by an R01CA166450–01 and Career Development Award K08CA133521 from the National Institutes of Health (DSR). DSR was a Sidney Kimmel Scholar supported by the Sidney Kimmel Foundation for Cancer Research (Translational Award SKF-11–013). JRC was supported by the Eugene V. Cota-Robles Grant and by a training award from the institutional Tumor Immunology training Grant (NIH T32CA009120). TRF was supported by Tumor Biology Training Grant NIH T32CA009056 from the National Institute of Health. NIRM was supported by the Eugene V. Cota-Robles Fellowship from UCLA and the Graduate Research Fellowship Program from the National Science Foundation. Flow cytometry was performed in the UCLA Jonsson Comprehensive Cancer Center (JCCC) and Center for AIDS Research Flow Cytometry Core Facility that is supported by National Institutes of Health awards AI-28697, and award number P30CA016042, the JCCC, the UCLA AIDS Institute, and the David Geffen School of Medicine at UCLA. We would like to acknowledge the ENCODE project and in particular the EGR1 Transcription Factor Binding Site Chip-Seq data, generated and analyzed by the Hudson Alpha Institute in Huntsville, AL.

CONFLICTS OF INTEREST

The authors declare no conflicts of interest.

REFERENCES

1. O'Connell RM, Rao DS, Chaudhuri AA, Baltimore D. Physiological and pathological roles for microRNAs in the immune system. Nature reviews Immunology. 2010; 10:111–122.
2. Bartel DP, Chen CZ. Micromanagers of gene expression: the potentially widespread influence of metazoan microRNAs. Nature reviews Genetics. 2004; 5:396–400.
3. Bartel DP. MicroRNAs: target recognition and regulatory functions. Cell. 2009; 136:215–233.
4. Griffiths-Jones S, Grocock RJ, van Dongen S, Bateman A, Enright AJ. miRBase: microRNA sequences, targets and gene nomenclature. Nucleic Acids Res. 2006; 34:D140–144.
5. Calin GA, Dumitru CD, Shimizu M, Bichi R, Zupo S, Noch E, Aldler H, Rattan S, Keating M, Rai K, Rassenti L, Kipps T, Negrini M, Bullrich F, Croce CM. Frequent deletions and down-regulation of micro- RNA genes miR15 and miR16 at 13q14 in chronic lymphocytic leukemia. Proc Natl Acad Sci U S A. 2002; 99:15524–15529.
6. Klein U, Lia M, Crespo M, Siegel R, Shen Q, Mo T, Ambesi-Impiombato A, Califano A, Migliazza A, Bhagat G, Dalla-Favera R. The DLEU2/miR-15a/16–1 cluster controls B cell proliferation and its deletion leads to chronic lymphocytic leukemia. Cancer Cell. 2010; 17:28–40.
7. O'Connell RM, Rao DS, Chaudhuri AA, Boldin MP, Taganov KD, Nicoll J, Paquette RL, Baltimore D. Sustained expression of microRNA-155 in hematopoietic stem cells causes a myeloproliferative disorder. The Journal of experimental medicine. 2008; 205:585–594.
8. O'Connell RM, Chaudhuri AA, Rao DS, Baltimore D. Inositol phosphatase SHIP1 is a primary target of miR-155. Proc Natl Acad Sci U S A. 2009; 106:7113–7118.

9. Boldin MP, Taganov KD, Rao DS, Yang L, Zhao JL, Kalwani M, Garcia-Flores Y, Luong M, Devrekanli A, Xu J, Sun G, Tay J, Linsley PS, Baltimore D. miR-146a is a significant brake on autoimmunity, myeloproliferation, and cancer in mice. J Exp Med. 2011.
10. Taganov KD, Boldin MP, Chang KJ, Baltimore D. NF-kappaB-dependent induction of microRNA miR-146, an inhibitor targeted to signaling proteins of innate immune responses. Proc Natl Acad Sci U S A. 2006; 103:12481–12486.
11. Zhao JL, Rao DS, Boldin MP, Taganov KD, O'Connell RM, Baltimore D. NF-kappaB dysregulation in microRNA-146a-deficient mice drives the development of myeloid malignancies. Proc Natl Acad Sci U S A. 2011; 108:9184–9189.
12. Starczynowski DT, Kuchenbauer F, Argiropoulos B, Sung S, Morin R, Muranyi A, Hirst M, Hogge D, Marra M, Wells RA, Buckstein R, Lam W, Humphries RK, Karsan A. Identification of miR-145 and miR-146a as mediators of the 5q- syndrome phenotype. Nat Med. 2010; 16:49–58.
13. Starczynowski DT, Kuchenbauer F, Wegrzyn J, Rouhi A, Petriv O, Hansen CL, Humphries RK, Karsan A. MicroRNA-146a disrupts hematopoietic differentiation and survival. Exp Hematol. 2010.
14. Yang L, Boldin MP, Yu Y, Liu CS, Ea CK, Ramakrishnan P, Taganov KD, Zhao JL, Baltimore D. miR-146a controls the resolution of T cell responses in mice. The Journal of experimental medicine. 2012; 209:1655–1670.
15. Lu LF, Boldin MP, Chaudhry A, Lin LL, Taganov KD, Hanada T, Yoshimura A, Baltimore D, Rudensky AY. Function of miR-146a in controlling Treg cell-mediated regulation of Th1 responses. Cell. 2010; 142:914–929.
16. Zhao JL, Rao DS, O'Connell RM, Garcia-Flores Y, Baltimore D. MicroRNA-146a acts as a guardian of the quality and longevity of hematopoietic stem cells in mice. eLife. 2013; 2:e00537.
17. Alizadeh AA, Eisen MB, Davis RE, Ma C, Lossos IS, Rosenwald A, Boldrick JC, Sabet H, Tran T, Yu X, Powell JI, Yang L, Marti GE, Moore T, Hudson J, Jr., Lu L, et al. Distinct types of diffuse large B-cell lymphoma identified by gene expression profiling. Nature. 2000; 403:503–511.
18. Ngo VN, Young RM, Schmitz R, Jhavar S, Xiao W, Lim KH, Kohlhammer H, Xu W, Yang Y, Zhao H, Shaffer AL, Romesser P, Wright G, Powell J, Rosenwald A, Muller-Hermelink HK, et al. Oncogenically active MYD88 mutations in human lymphoma. Nature. 2011; 470:115–119.
19. Compagno M, Lim WK, Grunn A, Nandula SV, Brahmachary M, Shen Q, Bertoni F, Ponzoni M, Scandurra M, Califano A, Bhagat G, Chadburn A, Dalla-Favera R, Pasqualucci L. Mutations of multiple genes cause deregulation of NF-kappaB in diffuse large B-cell lymphoma. Nature. 2009; 459:717–721.
20. Forloni M, Dogra SK, Dong Y, Conte D, Jr., Ou J, Zhu LJ, Deng A, Mahalingam M, Green MR, Wajapeyee N. miR-146a promotes the initiation and progression of melanoma by activating Notch signaling. eLife. 2014; 3:e01460.
21. Robertus JL, Kluiver J, Weggemans C, Harms G, Reijmers RM, Swart Y, Kok K, Rosati S, Schuuring E, van Imhoff G, Pals ST, Kluin P, van den Berg A. MiRNA profiling in B non-Hodgkin lymphoma: a MYC-related miRNA profile characterizes Burkitt lymphoma. Br J Haematol. 2010; 149:896–899.
22. Chang TC, Yu D, Lee YS, Wentzel EA, Arking DE, West KM, Dang CV, Thomas-Tikhonenko A, Mendell JT. Widespread microRNA repression by Myc contributes to tumorigenesis. Nat Genet. 2008; 40:43–50.
23. Chang TC, Zeitels LR, Hwang HW, Chivukula RR, Wentzel EA, Dews M, Jung J, Gao P, Dang CV, Beer MA, Thomas-Tikhonenko A, Mendell JT. Lin-28B transactivation is necessary for Myc-mediated let-7 repression and proliferation. Proc Natl Acad Sci U S A. 2009; 106:3384–3389.
24. Johansson FK, Goransson H, Westermark B. Expression analysis of genes involved in brain tumor progression driven by retroviral insertional mutagenesis in mice. Oncogene. 2005; 24:3896–3905.
25. Kharbanda S, Nakamura T, Stone R, Hass R, Bernstein S, Datta R, Sukhatme VP, Kufe D. Expression of the early growth response 1 and 2 zinc finger genes during induction of monocytic differentiation. J Clin Invest. 1991; 88:571–577.
26. Dinkel A, Warnatz K, Ledermann B, Rolink A, Zipfel PF, Burki K, Eibel H. The transcription factor early growth response 1 (Egr-1) advances differentiation of pre-B and immature B cells. The Journal of experimental medicine. 1998; 188:2215–2224.
27. Bernstein BE, Birney E, Dunham I, Green ED, Gunter C, Snyder M. An integrated encyclopedia of DNA elements in the human genome. Nature. 2012; 489:57–74.
28. Hu R, Kagele DA, Huffaker TB, Runtsch MC, Alexander M, Liu J, Bake E, Su W, Williams MA, Rao DS, Moller T, Garden GA, Round JL, O'Connell RM. miR-155 promotes T follicular helper cell accumulation during chronic, low-grade inflammation. Immunity. 2014; 41:605–619.
29. Frenzel A, Labi V, Chmelewskij W, Ploner C, Geley S, Fiegl H, Tzankov A, Villunger A. Suppression of B-cell lymphomagenesis by the BH3-only proteins Bmf and Bad. Blood. 2010; 115:995–1005.
30. Nemajerova A, Petrenko O, Trumper L, Palacios G, Moll UM. Loss of p73 promotes dissemination of Myc-induced B cell lymphomas in mice. J Clin Invest. 2010; 120:2070–2080.
31. Kuehl WM, Brents LA, Chesi M, Huppi K, Bergsagel PL. Dysregulation of c-myc in multiple myeloma. Current topics in microbiology and immunology. 1997; 224:277–282.
32. Dalla-Favera R, Bregni M, Erikson J, Patterson D, Gallo RC, Croce CM. Human c-myc onc gene is located on the region of chromosome 8 that is translocated in Burkitt lymphoma cells. Proc Natl Acad Sci U S A. 1982; 79:7824–7827.

33. Adams JM, Gerondakis S, Webb E, Corcoran LM, Cory S. Cellular myc oncogene is altered by chromosome translocation to an immunoglobulin locus in murine plasmacytomas and is rearranged similarly in human Burkitt lymphomas. Proc Natl Acad Sci U S A. 1983; 80:1982–1986.
34. Battey J, Moulding C, Taub R, Murphy W, Stewart T, Potter H, Lenoir G, Leder P. The human c-myc oncogene: structural consequences of translocation into the IgH locus in Burkitt lymphoma. Cell. 1983; 34:779–787.
35. Rabbitts TH, Hamlyn PH, Baer R. Altered nucleotide sequences of a translocated c-myc gene in Burkitt lymphoma. Nature. 1983; 306:760–765.
36. Huang da W, Sherman BT, Zheng X, Yang J, Imamichi T, Stephens R, Lempicki RA. Extracting biological meaning from large gene lists with DAVID. Curr Protoc Bioinformatics. 2009; . Chapter 13:Unit 13 11.
37. Huang da W, Sherman BT, Lempicki RA. Systematic and integrative analysis of large gene lists using DAVID bioinformatics resources. Nat Protoc. 2009; 4:44–57.
38. Salehi F, Kovacs K, Scheithauer BW, Lloyd RV, Cusimano M. Pituitary tumor-transforming gene in endocrine and other neoplasms: a review and update. Endocr Relat Cancer. 2008; 15:721–743.
39. Appelbe OK, Bollman B, Attarwala A, Triebes LA, Muniz-Talavera H, Curry DJ, Schmidt JV. Disruption of the mouse Jhy gene causes abnormal ciliary microtubule patterning and juvenile hydrocephalus. Dev Biol. 2013; 382:172–185.
40. Adams JM, Harris AW, Pinkert CA, Corcoran LM, Alexander WS, Cory S, Palmiter RD, Brinster RL. The c-myc oncogene driven by immunoglobulin enhancers induces lymphoid malignancy in transgenic mice. Nature. 1985; 318:533–538.
41. Dobin A, Davis CA, Schlesinger F, Drenkow J, Zaleski C, Jha S, Batut P, Chaisson M, Gingeras TR. STAR: ultrafast universal RNA-seq aligner. Bioinformatics. 2013; 29:15–21.
42. Anders S, Huber W. Differential expression analysis for sequence count data. Genome Biol. 2010; 11:R106.
43. Rao DS, O'Connell RM, Chaudhuri AA, Garcia-Flores Y, Geiger TL, Baltimore D. MicroRNA-34a perturbs B lymphocyte development by repressing the forkhead box transcription factor Foxp1. Immunity. 2010; 33:48–59.

SUPPLEMENTARY FIGURES AND TABLES

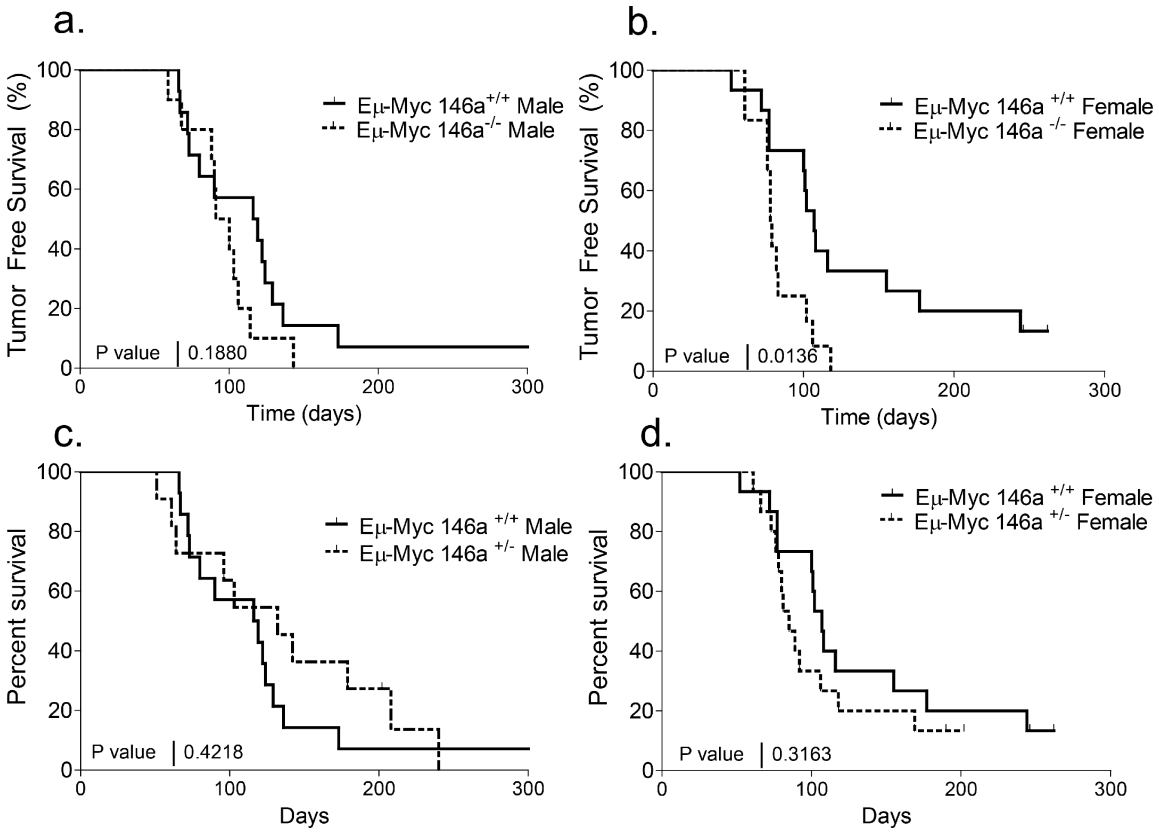

Supplementary Figure S1: miR-146a deficiency causes increased mortality in female Eμ-Myc mice. (a) Tumor-free survival curve of male mice with Eμ-Myc oncogene and either wild-type or homozygous deficiency of miR-146a (n = 14 for Eμ-Myc miR-146a$^{+/+}$ n = 10 for Eμ-Myc miR-146a$^{-/-}$: Log-Rank Test, p = 0.1880). **(b)** Tumor-free survival curve of female mice with Eμ-Myc oncogene and either wild-type or homozygous deficiency of miR-146a (n = 15 for Eμ-Myc miR-146a$^{+/+}$, n = 12 for Eμ-Myc miR-146a$^{-/-}$; Log-rank Test, p = 0.0136). **(c)** Tumor-free survival curve of male mice with Eμ-Myc oncogene and either wild-type or heterozygous deficiency of miR-146a (n = 14 for Eμ-Myc miR-146a$^{+/+}$, n = 11 for Eμ-Myc miR-146a$^{+/-}$; Log-Rank Test, p = 0.4218). **(d)** Tumor free survival curve of female mice with Eμ-Myc oncogene and either wild-type or heterozygous deficiency of miR-146a (n = 15 for Eμ-Myc miR-146a$^{+/+}$, n = 15 for Eμ-Myc miR-146a$^{+/-}$; Log-Rank Test, p = 0.3163).

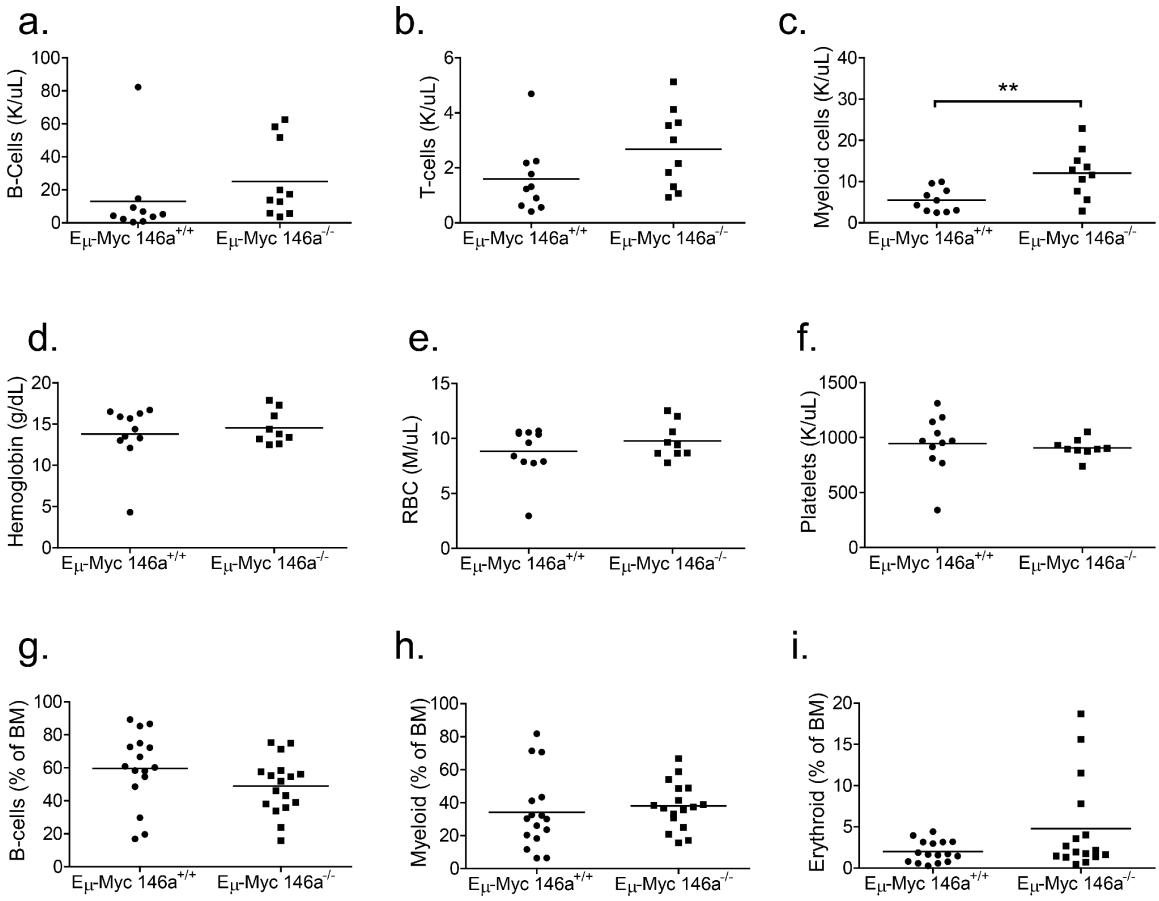

Supplementary Figure S2: Blood and bone marrow composition in Eμ-Myc animals at the time of death. (a–c) Quantitation of absolute number of B-cells (a), T-cells (b), and Myeloid cells (c) based on CBC and FACS analysis of blood at time of death (n = 10 Eμ-MycmiR-146a$^{+/+}$, and n = 10 Eμ-Myc miR-146a$^{-/-}$; t-test p = 0.2719, 0.0904 and 0.0052 respectively). **(d–i)** Hemoglobin levels, red blood cell, and platelet counts at time of death (n = 11 Eμ-MycmiR-146a$^{+/+}$, and n = 9 Eμ-Myc miR-146a$^{-/-}$; t-test, p = 0.5663, 0.3150 and 0.6521 respectively). Percentage of B-cells (g), Myeloid (h), and Erythroid (i) cells in the bone marrow of mice at time of death (n = 16 Eμ-Myc miR-146a$^{+/+}$, and n = 17 Eμ-Myc miR-146a$^{-/-}$; t-test, p = 0.1250, 0.5529 and 0.0635 respectively).

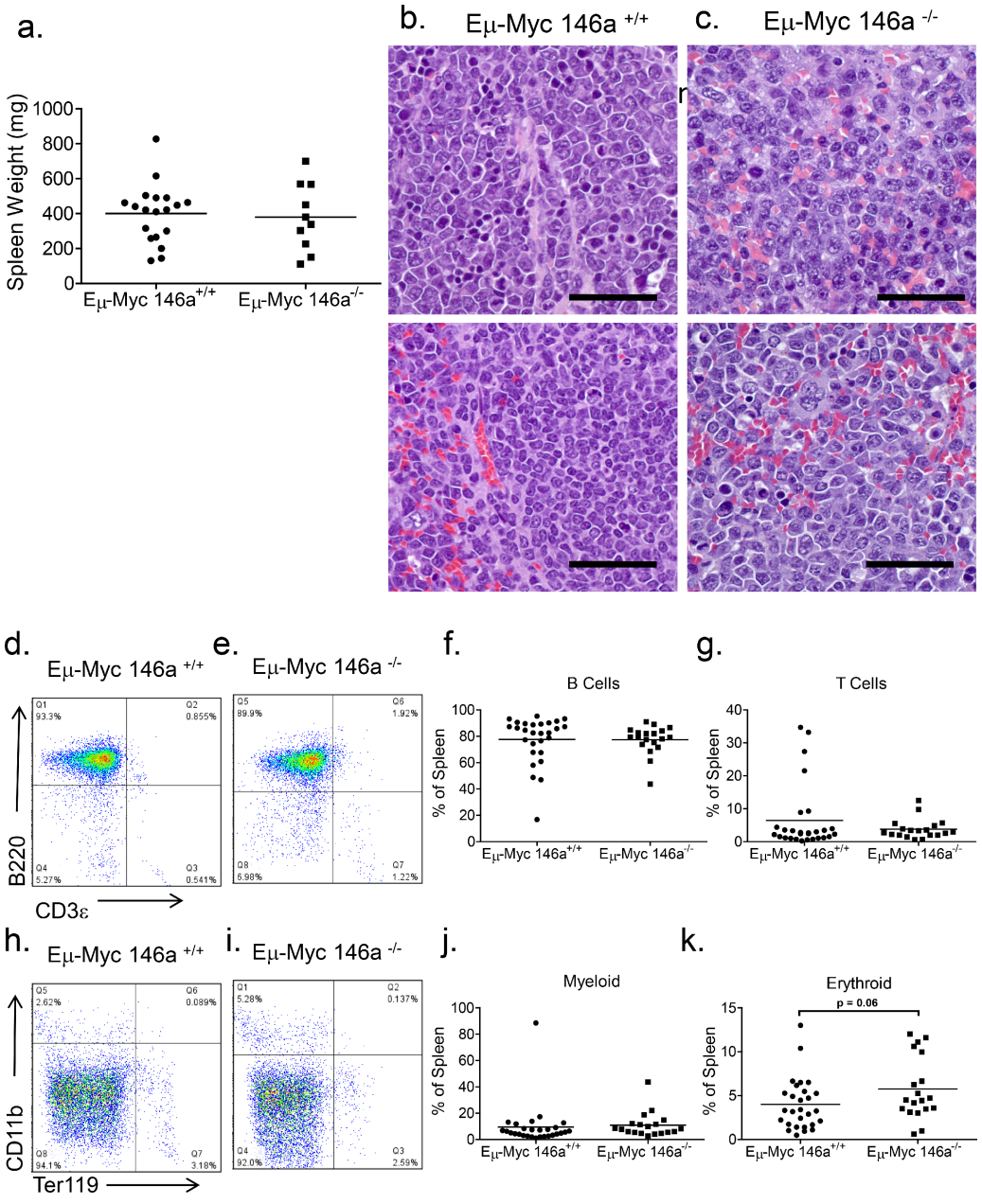

Supplementary Figure S3: Analysis of spleens from Eμ-Myc animals deficient for miR-146a. **(a)** Spleen weights at the time of death for all animals where data was available (n = 19 Eμ-Myc miR-146a$^{+/+}$ and n = 10 Eμ-Myc 146a$^{-/-}$; t-test, p = 0.7662). **(b–c)** Representative high power images of paraffin embedded H&E stained tumor samples showing red (top panels), and white (bottom panels) pulp of splenic tumors from Eμ-Myc animals sufficient or deficient for miR-146a. **(d–e, h–i)** Representative FACS plots from Eμ-Myc miR-146a$^{+/+}$ and Eμ-MycmiR-146a$^{-/-}$ spleens stained with B220 and CD3e, or CD11b and Ter119, respectively. **(f–g, j–k)** Quantitation of the percentage of B-lymphocytes, T-lymphocytes, Myeloid or Erythroid cells in the spleens of Eμ-Myc miR-146a$^{+/+}$ and Eμ-MycmiR-146a$^{-/-}$ mice, based on FACS (n = 28, Eμ-Myc miR-146a$^{+/+}$, and n = 19, Eμ-Myc miR-146a$^{-/-}$; t-test, p = 0.9505, 0.2568, 0.7114, and 0.0600 respectively).

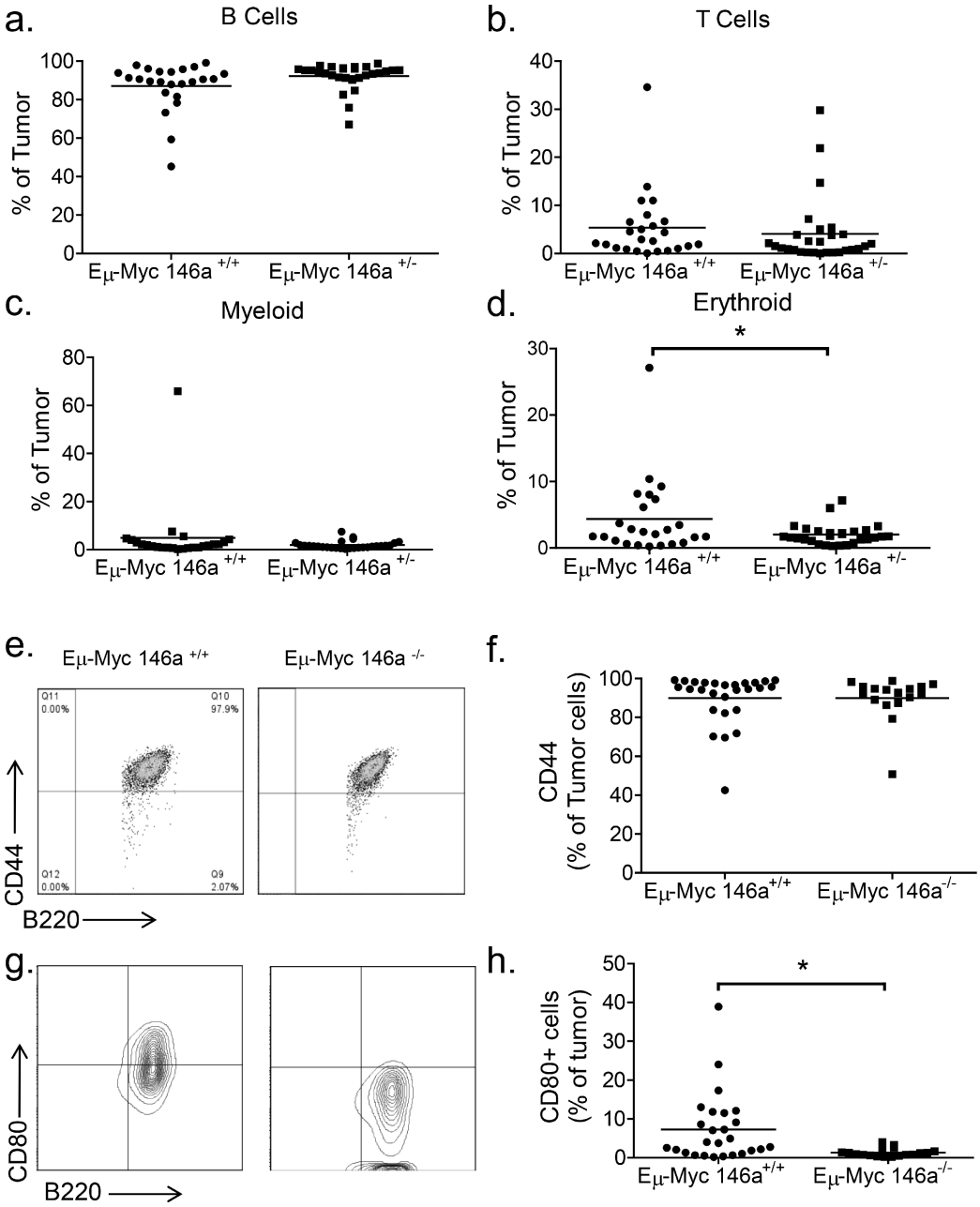

Supplementary Figure S4: Immunophenotypic properties of tumors in mice with heterozygous and homozygous deficiency of miR-146a. (a–d) B-, T-, myeloid, and erythroid cells, respectively, quantitated by FACS in tumors from mice carrying the Eμ-Myc oncogene and wild-type or heterozygous for miR-146a ($n = 24$ for Eμ-Myc miR-146a$^{+/+}$ and $n = 28$ for Eμ-Myc miR-146a$^{+/-}$; t-test $p = 0.0704$, 0.5164 and 0.2368, 0.0427 respectively). **(e)** Representative FACS plots from Eμ-Myc 146a$^{+/+}$ or Eμ-Myc 146a$^{-/-}$ tumors stained with CD44 and B220. **(f)** Quantitation of all mice where data was available for the percent of CD44 positive cells in tumors from Eμ-Myc 146a$^{+/+}$ or Eμ-Myc 146a$^{-/-}$ ($n = 27$ Eμ-Myc 146a$^{+/+}$ and $n = 17$ Eμ-Myc 146a$^{-/-}$; T-Test, $p = 0.9922$). **(g)** Representative FACS plots from Eμ-Myc 146a$^{+/+}$ or Eμ-Myc 146a$^{-/-}$ tumors stained with CD80 and B220. **(h)** Quantitation of all mice where data was available for the percent of CD44 positive cells in tumors from Eμ-Myc 146a$^{+/+}$ or Eμ-Myc 146a$^{-/-}$ ($n = 27$ Eμ-Myc 146a$^{+/+}$ and $n = 17$ Eμ-Myc 146a$^{-/-}$; T-Test, $p = 0.0069$).

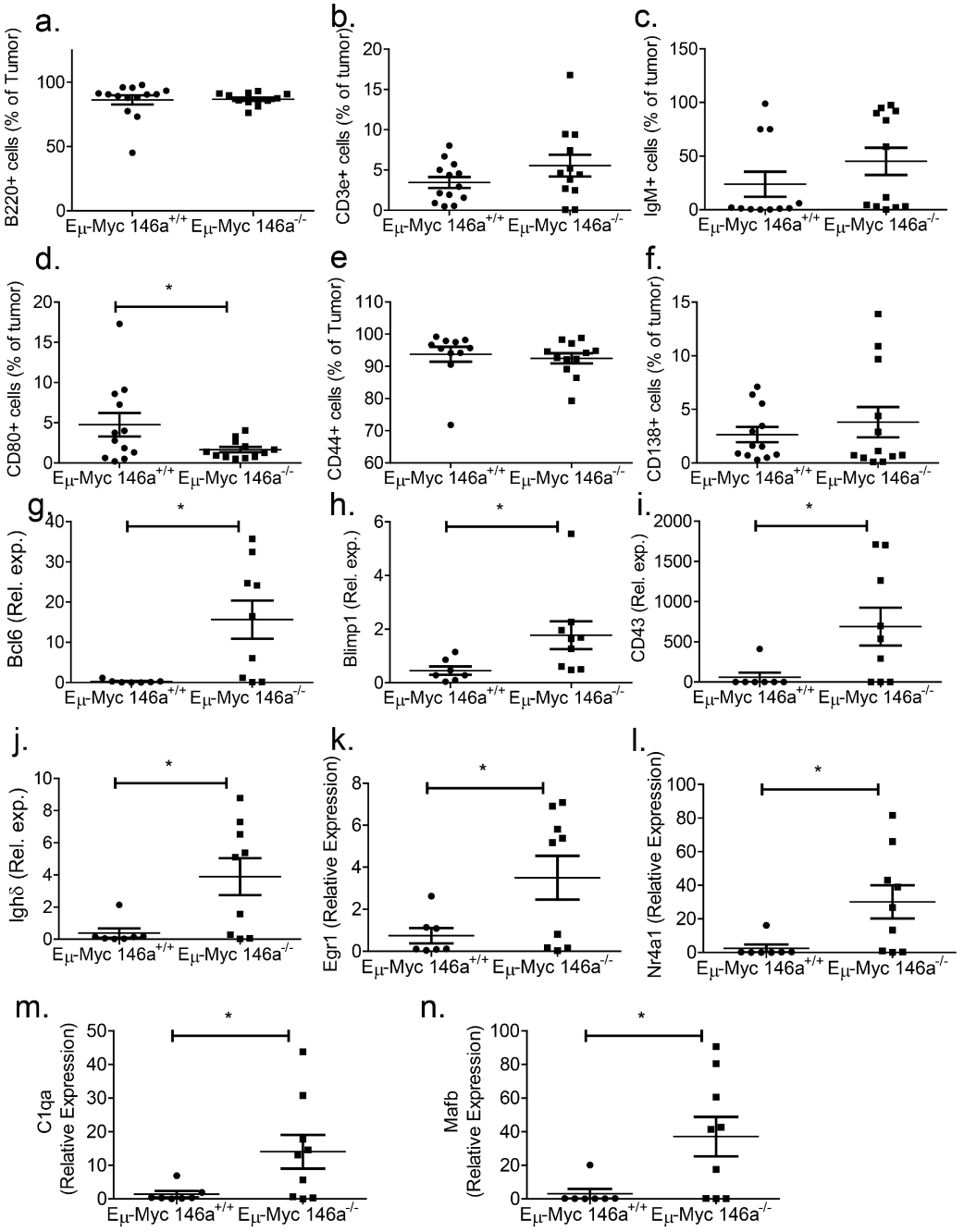

Supplementary Figure S5: Analysis of immunophenotypic and gene expression features of tumors from female Eμ-Myc 146a$^{-/-}$ mice. (a–f) Quantitation of B220+ (a), CD3e+ (b), IgM+ (c), CD80+ (d), CD44+ (e) and CD138+ (f) cells from female mice that carry the Eμ-Myc transgene and are either sufficient or deficient for miR-146a. Only CD80 expression is significantly different (*T*-test, $p = 0.0487$). This may be due to the reduced numbers of animals available for the analysis ($n = 12$ Eμ-Myc 146a$^{+/+}$ and $n = 12$ Eμ-Myc 146a$^{-/-}$). **(g–j)** RT-qPCR analyses of B-cell maturation associated transcripts from female mice that carry the Eμ-Myc transgene and are either sufficient or deficient for miR-146a. All comparisons showed a statistically significant difference ($p < 0.05$ for all comparisons between the mice; $n = 7$ Eμ-Myc 146a$^{+/+}$ and $n = 9$ Eμ-Myc 146a$^{-/-}$). **(k–n)**. RT-qPCR analyses of Egr1 and putative Egr1-regulated transcripts from female mice that carry the Eμ-Myc transgene and are either sufficient or deficient for miR-146a. All comparisons showed a statistically significant difference ($p < 0.05$ for all comparisons between the mice; $n = 7$ Eμ-Myc 146a$^{+/+}$ and $n = 9$ Eμ-Myc 146a$^{-/-}$).

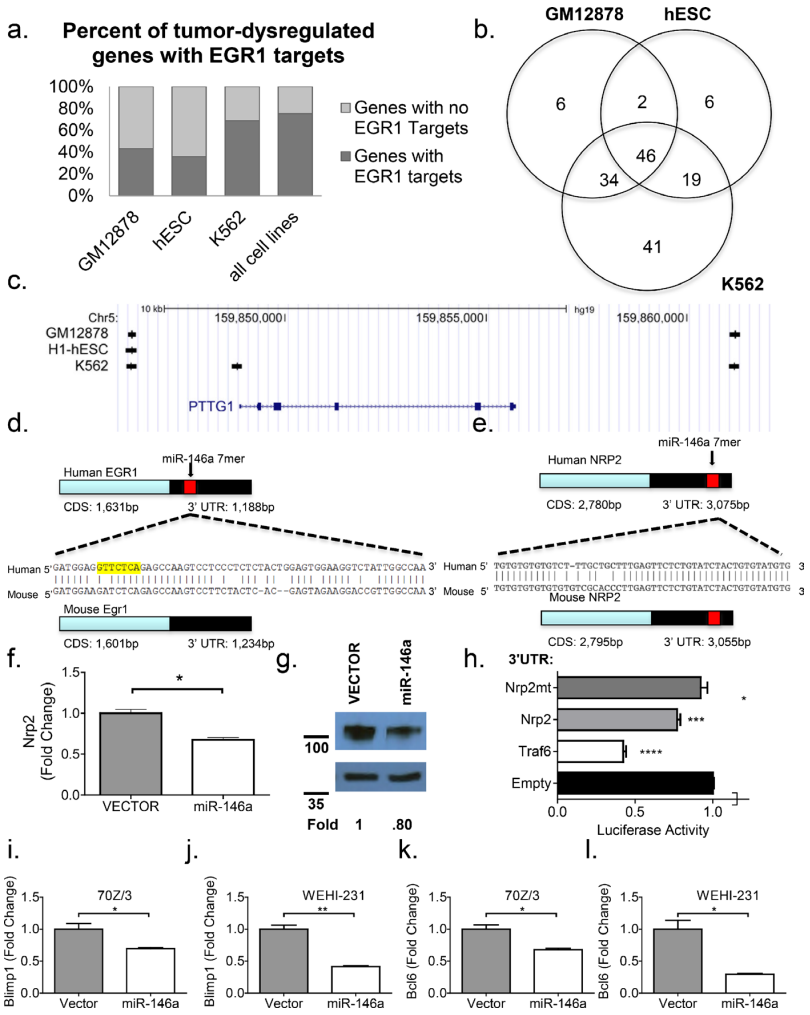

Supplementary Figure S6: High throughput analyses for EGR1 TFBS and demonstration of a novel miR-146a target, *Nrp2*. **(a)** Plot showing the numbers of genes that were differentially regulated in miR-146a deficient tumors that have EGR1 binding sites in the three different cell lines. Note that the K562 cell line had the highest number of binding sites. The cell lines displayed a wide range in the total number of EGR1 transcription factor binding sites (TFBS). The K562 cell line had a total of 36,367 sites representing 12,741 genes, the GM12878 line had 16,530 sites representing 9,170 genes, and the H1-hESC line had only 8, 818 sites representing 6,349 genes. There exists a wide range in the total number of EGR1 TFBS sites as well as the total genes with EGR1 binding sites. In the K562 cell line, 62% of total protein coding genes are putatively regulated by EGR1. In the H1-hESC line 31% of genes have EGR1 TFBS and in GM12878 line 45% of genes have EGR1 TFBS sites. When all three cell lines are combined, there are a total of 62,071 sites representing 13,944 unique genes. **(b)** Intersection of differentially regulated genes from the RNA-Seq dataset overlaid with the genes containing EGR1 TFBS obtained from ChIP-Seq data of the three different cell lines. **(c)** *Pttg1* is a differentially regulated gene in miR-146a deficient tumors. It is found on chromosome 5 and has EGR1 transcription factor binding sites based on the reanalyzed ChIP-Seq data presented above. **(d)** Schematic representation of human and mouse *Egr1* gene showing the miR-146a binding site in the 3′UTR. **(e)** Schematic representation of human and mouse *Nrp2* gene showing the miR-146a binding site in the 3′UTR. **(f)** RT-qPCR analysis of *Nrp2* in 70Z/3 cell lines either expressing MGP or MGP-miR-146a vector (*t*-test, $p = 0.0148$). **(g)** Western blot analysis for NRP2 after miR-146a shows reduction in the protein levels in 70Z/3 cells when compared to the reference gene actin (upper panel: Nrp2 and lower panel, β-actin). Shown below are fold repression computed using ImageJ software. **(h)** Luciferase assays showing repression seen with MGP/miR-146a co-transfection relative to MGP alone for each of the UTRs depicted. Each measurement is representative of firefly luciferase normalized to renilla luciferase, and was performed in duplicate, with the experiment was repeated at least three times (*T*-test; Traf6 v Vector, $p < 0.0001$; Nrp2 vs. vector, $p = 0.0005$; Nrp2 vs. mutant Nrp2, $p = 0.033$). **(i–l)**. RT-qPCR analyses of Blimp1 and Bcl6 in 70Z/3 and WEHI-231 cells that are overexpressing miR-146a. All comparisons showed statistically significant downregulation of these genes in miR-146a overexpressing cell lines (*$p < 0.05$; **$p < 0.005$).

Supplementary Table S1: RT-qPCR primers and genotyping primers used. Listed are the primers used for RNAseq data validation, genotyping miR-146a and Eμ-Myc allele, and cloning. 5'*P** indicates phosphorylated 5' end.

RT-qPCR primers	Direction	Sequence
Jhy	FOW	5′ GGTGCCGGCAGGATGAATAA 3′
	REV	5′ AAGTTGGTGTGATGGACGGG 3′
Cacna1h	FOW	5′ ATGCTTGGGAACGTGCTTCTT 3′
	REV	5′ GTCTGGTAGTATGGCCGCAA 3′
Camk2b	FOW	5′ TGGTGGAACAAGCCAAGAGTTT 3′
	REV	5′ GAGGGAGAGATCCTTTGGGG 3′
Myo18b	FOW	5′ AGAACAATGGAGTCCGCTGG 3′
	REV	5′ GCTGGCTGTGGATCTTCTGT 3′
Pttg1	FOW	5′ CCCTCCAACCAAAACAGCC 3′
	REV	5′ TCCCTTACCAGATTCCCATGAT 3′
Axl	FOW	5′ GTGGTTTCCAGACAACCTACG 3′
	REV	5′ CGGATGTGATACGGGGTGTG 3′
Egr1	FOW	5′ TTGTGGCCTGAACCCCTTTT 3′
	REV	5′ AGATGGGACTGCTGTCGTTG 3′
Oaf	FOW	5′ GAAGGGGCAGAGTCAGTTCC 3′
	REV	5′ GTTTTTCTGCCGGAGCTTGG 3′
Nrp2	FOW	5′ GCTGGCTACATCACTTCCCC 3′
	REV	5′ CAATCCACTCACAGTTCTGGTG 3′
Dtx3	FOW	5′ ACCCAATGTCATCACTTGGAAC 3′
	REV	5′ CCTCTTGCACCCTAGTCAGGT 3′
Mafb	FOW	5′TGGATGGCGAGCAACTACC3′
	REV	5′CCAGGTCATCGTGAGTCACA3′
Nr4a	FOW	5′TTGAGTTCGGCAAGCCTACC3′
	REV	5′GTGTACCCGTCCATGAAGGTG3′
C1qa	FOW	5′AAAGGCAATCCAGGCAATATCA3′
	REV	5′TGGTTCTGGTATGGACTCTCC3′
Bcl6	FOW	5′CCGGCACGCTAGTGATGTT3′
	REV	5′TGTCTTATGGGCTCTAAACTGCT3′
IgD	FOW	5′CTTAGCTGCCGAGAGGGATG3′
	REV	5′ACACTGTGCTCGAAGGTGTT3′
IgM	FOW	5′AACATTGCTGGCAGGGGTAG3′
	REV	5′ACCAGAGGTTGTCCCTCCTT3′
CD43	FOW	5′GACCCACTTCCTTTCCCCCT3′
	REV	5′CGTACCCAGCAAGATCATACCC3′

(*Continued*)

RT-qPCR primers	Direction	Sequence
Bcl6	FOW	5′CCGGCACGCTAGTGATGTT3′
	REV	5′TGTCTTATGGGCTCTAAACTGCT3′
Blimp1	FOW	5′TTCTCTTGGAAAAACGTGTGGG3′
	REV	5′GGAGCCGGAGCTAGACTTG3′
Traf6	FOW	5′GCACAAGTGCCCAGTTGAC3′
	REV	5′TGCAAAATTGTCGGGAAACAGT3′
EGR1	FOW	5′GGTCAGTGGCCTAGTGAGC3′
	REV	5′GTGCCGCTGAGTAAATGGGA3′
mmu-miR-146a		5′ UGAGAACUGAAUUCCAUGGGUU 3′
Cloning primers		
Egr1 CDS	FOW	5′AGCTAGA-AGATCT-TTCTCCAGCTCGCTGGTCC3′
	REV	5′AGCATCT-CTCGAG-TTCCTGCCTCTCCCTTTGCT3′
Egr1-3′-UTR	FOW	5′TAATCTGGTTTAAACGAGCTCTGGAAGATCTCAGAGCCAAG3′
	REV	5′TCGAATCCCTGCAGGCTCGAGGAACTTCATGTTCATAACATAC AAAAA3′
Egr1-3′-UTR-Mutant	FOW	5′P*ATGTCCACTGGACTGTCACCTC3′
	REV	5′P*GGCTGTTTCAGGCAGCTGAAG3′
EGR1-3′-UTR	FOW	5′TAATCTGGTTTAAACGAGCTCGAGGAGATGGCCATAGGAGA3′
	REV	5′TCGAATC-CCTGCAGGCTCGAGTACAAAAATCGCCGCCTACT3′
EGR1-3′-UTR-Mutant	FOW	5′P*GATGGAGCTGGACTGGAGCCAA3′
	REV	5′P*TGACCTAAGAGGAACCCTCC3′
Nrp2-3′-UTR	FOW	5′TAATCTGGTTTAAACGAGCTCACTGTGGTGGCCAAGTGAAT3′
	REV	5′TCGAATCCCTGCAGGCTCGAGCAGCACTGAGTCCCACGTTA3′
Nrp2-3′-UTR-Mutant	FOW	5′P*ACCCTTGCTGGACTGTGTATCT3′
	REV	5′P*GCGACACACACACACACACA3′
Traf6-3′-UTR	FOW	5′TAATCTGGTTTAAAGAGCTCTGAAAATCACCACTGCCTGT3′
	REV	5′TCGAATCCCTGCAGGCTCGAGGGATCCCCTCTGCTTCCTTA3′
Traf6-3′-UTR-Mutant	FOW	5′P*GGTGTTGCTGGACTGTTTAGTT3′
	REV	5′P*AGAGCGGTAACTTCTCTACTG3′
Bcl6-3′-UTR	FOW	5′TAATCTG- GTTTAAAC-GAGCTC-CCAGCCCCTTCTCAGAATC3′
	REV	5′TCGAATC-CCTGCAGG-CTCGAG CAACGCACTAATGCAGTTTAGA3′
Genotyping primers		
miR-146a WT	FOW	5′ CTTGGACCAGCAGTCCTCTTGATGCACCTT 3′
miR-146a KO	FOW	5′ ATCGCGGCCGCTTTAAGTGTAGAGAGGGGGTCAAGTA 3′
	REV	5′ ATTGCTCAGCGGTGCTGTCCATCTGCACGA 3′
Eμ-Myc	FOW	5′ ACCCAGGCTAAGAAGGCAAT 3′
	REV	5′ GCTCCGGGGTGTAAACAGTA 3′

Supplementary Table S2: Functional annotation results for gene expression data from miR-146a deficient tumors. Genes that were differentially expressed between tumors from Eμ-Myc 146a$^{+/+}$ and for Eμ-Myc 146a$^{-/-}$ were used as the input in the DAVID Functional Annotation Tool for Functional Annotation Analysis. Listed are keywords associated with subgroups of genes.

Term	Count	%	*P*-Value
disulfide bond	67	28.5106383	4.68E–11
signal	74	31.4893617	1.45E–10
Secreted	47	20	2.36E–10
glycoprotein	79	33.61702128	1.03E–08
innate immunity	11	4.680851064	1.82E–08
complement pathway	7	2.978723404	4.80E–07
immune response	12	5.106382979	1.23E–05
collagen	8	3.404255319	6.11E–05
transmembrane protein	15	6.382978723	1.35E–04
inflammatory response	7	2.978723404	3.21E–04
Growth factor binding	4	1.70212766	6.67E–04
chemotaxis	6	2.553191489	8.23E–04
Immunoglobulin domain	15	6.382978723	8.25E–04
inflammation	4	1.70212766	9.79E–04
extracellular matrix	10	4.255319149	9.99E–04
gpi-anchor	7	2.978723404	0.003569296
cell adhesion	12	5.106382979	0.005673897
hydroxylation	5	2.127659574	0.006928978
thiolester bond	3	1.276595745	0.007127014
immunoglobulin c region	3	1.276595745	0.007127014
sulfation	4	1.70212766	0.007435725
phosphoprotein	93	39.57446809	0.007720982
ATP	7	2.978723404	0.009174195
membrane	81	34.46808511	0.01649583
Fatty acid biosynthesis	4	1.70212766	0.01701409
cell membrane	31	13.19148936	0.018684946
tumor suppressor	5	2.127659574	0.020455856
calmodulin-binding	5	2.127659574	0.033890063
sh3 domain	7	2.978723404	0.034520031
ubl conjugation	12	5.106382979	0.047435024
lipoprotein	13	5.531914894	0.047618299
duplication	5	2.127659574	0.054099645
oxidoreductase	12	5.106382979	0.077770979

(*Continued*)

Term	Count	%	*P*-Value
thioester bond	2	0.85106383	0.079863592
Proto-oncogene	4	1.70212766	0.08178812
Pyrrolidone carboxylic acid	3	1.276595745	0.088004782
metalloprotease inhibitor	2	0.85106383	0.090742103

Supplementary Table S3: RT-qPCR analyses of individual animals for expression of B-cell maturation related antigens.

Animal	Genotype	Gender	Bcl6	Blimp1	CD43	IgM	IgD
1451	wt	f	0.271339	1.145588	0.705806	0.709198	0.177013
1454	wt	m	0.038736	0.093968	0.066144	0.558738	0.029974
1460	wt	m	8.20188	0.721423	3.902207	0.250748	0.014211
1520	wt	m	0.033797	0.174896	0.127757	0.456917	0.124269
1521	wt	m	0.135677	0.924525	0.16494	0.277375	0.037454
1523	wt	f	0.028054	0.095877	0.048391	0.195235	0.039226
1526	wt	f	0.120526	0.28323	0.324306	0.401445	0.050215
1656	wt	m	0.053368	0.108736	0.284504	0.226677	0.057909
1659	wt	m	0.161924	0.551277	0.297023	0.653097	0.130972
1749	wt	m	0.701637	3.735392	2.918962	0.750918	0.105922
1915	wt	m	0.095955	0.336614	0.960706	0.451744	0.13981
2223	wt	f	0.283138	0.463385	0.426341	0.613296	0.160568
1910	wt	f	0.030032	0.043638	0.063009	0.120665	0.021617
1655	wt	m	0.923301	0.619757	0.666354	0.397616	0.31778
1524	wt	f	1.150118	0.856506	411.4145	0.382629	2.139207
2937	wt		0.19628	0.954403	0.433843	1.408135	0.364334
2378	wt	f	0.065022	0.283746	0.193816	0.22365	0.137365
2962	wt	m	0.020592	0.077438	0.069717	0.213156	0.038049
3088	ko		0.130181	0.372912	0.349963	0.264002	0.127249
3091	ko		0.071145	0.721328	0.395792	0.820457	0.138954
1650	ko	f	24.11388	5.552898	698.29	0.549226	5.102985
1946	ko	m	19.37964	2.64538	603.3702	0.383629	3.693471
1947	ko	f	24.67962	2.261896	1709.758	0.580115	6.531063
1948	ko	f	32.45105	1.64023	1704.209	0.528875	7.289359
1954	ko	m	1.312308	2.83128	0.386467	1.10656	0.11313
2037	ko	f	16.44691	1.268977	536.9497	0.668309	5.380701
2038	ko	f	35.71832	1.959675	1262.413	0.664103	8.780564

(*Continued*)

Animal	Genotype	Gender	Bcl6	Blimp1	CD43	IgM	IgD
2222	ko	f	6.066195	1.687667	290.3511	0.311407	1.574364
1958	ko	f	0.133845	0.609388	0.570343	0.496057	0.051101
2320	ko	m	0.043995	0.332472	0.113839	0.673455	0.321443
2581	ko	m	0.044904	0.251925	0.063658	0.500618	0.190218
2590	ko	f	0.092365	0.496068	0.172707	0.88351	0.284531
2843	ko	m	0.203623	0.472634	0.582692	1.103613	0.227785
2949	ko	f	1.158255	0.482188	0.921204	0.36023	0.031063
2589	ko	m	0.070043	0.372983	0.223328	0.789975	0.045549

CHAPTER III:

"Functional characterization of miR-34a in B-cell lymphomagenesis"

Abstract

Background: The p53 DNA damage response pathway induces the miR-34 family consisting of miR-34a, b, and c. Of the three family members, miR-34a is known to modulate a number of cancer-related pathways in a wide range of malignancies from prostate cancer to neuroblastoma. Additionally, in B-cell malignancies, miR-34a has been shown to be dysregulated, via silencing or deletion events. In B-cell development miR-34a ectopic expression can arrest B-cells by targeting the FOXP1 transcription factor necessary for cells to transition from the pro-B to the pre-B cell stage. Given the functional background miR-34a plays in B-cell development, the dysregulated expression in malignancy, and association with the p53 pathways it remains to be addressed miR-34a absence leads to B-cell lymphomagenesis.

Results: Here, we performed a series of experiments to define the function of miR-34a in B-cell malignancies. In-vivo deletion of miR-34a in c-Myc driven B-cell malignancies did not show modulation of tumor phenotype or aggressiveness. Additionally, we performed high-throughput sequencing on tumors either sufficient or deficient for miR-34a and identified novel targets Csf1r, Jhy, and Fgfr1. Using 3'UTR-linked luciferase reporter assays, we found that Csf1r, Jhy and Fgfr1 are direct targets of miR-34a. Finally, ectopic expression of miR-34a in established cell lines reduced proliferation and repressed novel targets Csf1r, Jhy, and Fgfr1.

Conclusions: Our findings show a role for miR-34a in modulating B cell malignancies in the context of c-Myc oncogenesis. The novel targets identified in this study add to the pathways miR-34a modulates in malignant transformation albeit in this case for B-cells. Taken together this study identifies additional targets for therapeutic approaches in B-cell malignancies with c-Myc lesions and possibly future development of drugs aimed at these.

Background

Lymphomas comprise a heterogeneous group of malignancies derived from B- and T-cells.[1] In these cell types aberrant biological events occur at the genetic, epigenetic, and

proteomic level driving malignant transcriptional programs. Classical translocations in B cell malignancies include the c-Myc translocaction characterized from Burkitt lymphomas (BL), which show a juxtaposition of the c-Myc proto-oncogene with the immunoglobulin heavy chain gene (IgH) or the light chain gene (IgK, IgL). (Bornkamm2009) Additional oncogenic lesions observed in B-cell malignancies include BCL6 and BCL2 translocations to promoters of the IgH, IgL.[2] The genesis of these translocations appears to be related to “accidents” during B-cell development, that normally mediate the rearrangement of the IGH locus. Recent studies have demonstrated a interplay between c-Myc and p53 in DLBCL’s that remains to be functionally studied. (Scheifer2015)

B-cell development relies upon balanced expression of transcription factors in addition to various checkpoints that serve to eliminate aberrant B-cells such as those that carry the previously described translocations. MicroRNAs have demonstrated their capacity to regulate hematopoietic development and play an important role in malignant transformation. To date numerous oncomiRs as well as tumor suppressive miRNAs have been identified and characterized. Of importance is miR-34a which is a part of the miR-34 family that consists of miR-34a, b, and c who share the same seed sequence as miR-449.[3] miR-34a is also part of the p53 DNA damage response network and as such is capable of inducing apoptosis, proliferation and cell cycle arrest.[4-7] Consequently, suppression of miR-34a by p63 has been shown to allow progression of the cell cycle.[8] Independent of p53, miR-34a can also be activated by ELK1 in the context of cell senescence, wher it has been shown totarget and repress c-Myc.[9]

Various cancers have inactivation of miR-34a due to events culminating in deletion or repression of this miRNA.[10-12] Studies in chronic lymphocytic leukemia (CLL) patients have demonstrated that inactivation of miR-34a accompanies p53 deletion/inactivating mutations and conversely that ectopic expression leads to induction of apoptosis in cell lines.[13] In gastric diffuse large B-cell lymphomas (gDLBCL) miR-34a was repressed in the presence of increased

MYC expression. MYC knockdown in DLBCL leads to increased expression of miR-34a which is accompanied by reduced proliferation.[14] Methylation studies have shown that a significant proportion of hematologic malignancies have hypermethylation of the miR-34a locus, includingNK/T cell lymphomas.[12] Despite the large amount of data that demonstrate a tumor-suppressive role for miR-34a, one recent study demonstrated that knockdown of this miRNA led to reduced proliferation.[15]

To definitively address the functional role of miR-34a in B-cell lymphomagenesis we sought to knockout miR-34a in B-cell specific c-Myc driven lymphomagenesis, as well as overexpression studies of miR-34a. We found that in the context of c-Myc driven B-lymphomagenesis, miR-34a deficiency does not alter the incidence or type of B-cell lymphoma. High-throughput sequencing of lymphoma samples deficient/sufficient for miR-34a revealed an enrichment of predicted miR-34a targets and identified the novel targets Csf1r, Jhy, and Fgfr1. Gene set enrichment analysis (GSEA) using publicly available datasets of WT, pre-malignant, and malignant c-Myc driven murine B-cell malignancies demonstrated an enrichment of putative miR-34a targets. Ectopic expression of miR-34a in murine and human established B-cell lines demonstrated a reduction in proliferation with a concomitant repression of Csf1r, Jhy and Fgfr1. Together these findings identify a role for miR-34a in the regulation of gene expression in c-Myc driven B-cell malignancies. Furthermore, these studies identify novel putative targets for the treatment of c-Myc driven lymphomas.

Results

miR-34a deficiency does not alter survival in c-Myc driven lymphomagenesis

To study the role of miR-34a in a B-cell specific context of tumorigenesis we employed the use of the Eμ-Myc murine model. These transgenic mice overexpress the c-Myc oncogene under the control of the Eμ enhancer restricting expression of this oncogene to B-cells.[16] We crossbred Eμ-Myc animals with miR-34a deficient mice to obtain cohorts of animals sufficient

and deficient for miR-34a. Most tumors that formed in Eμ-Myc mice showed a lymphoblastic morphology with numerous mitotic figures and apoptotic bodies on H&E sections (data not shown). In miR-34a deficient tumors this morphological pattern, and time to tumor presentation in animals remained unchanged. All mortality in these animals was attributed to tumor formation, but miR-34a deficiency did not affect overall survival (Figure. 1).

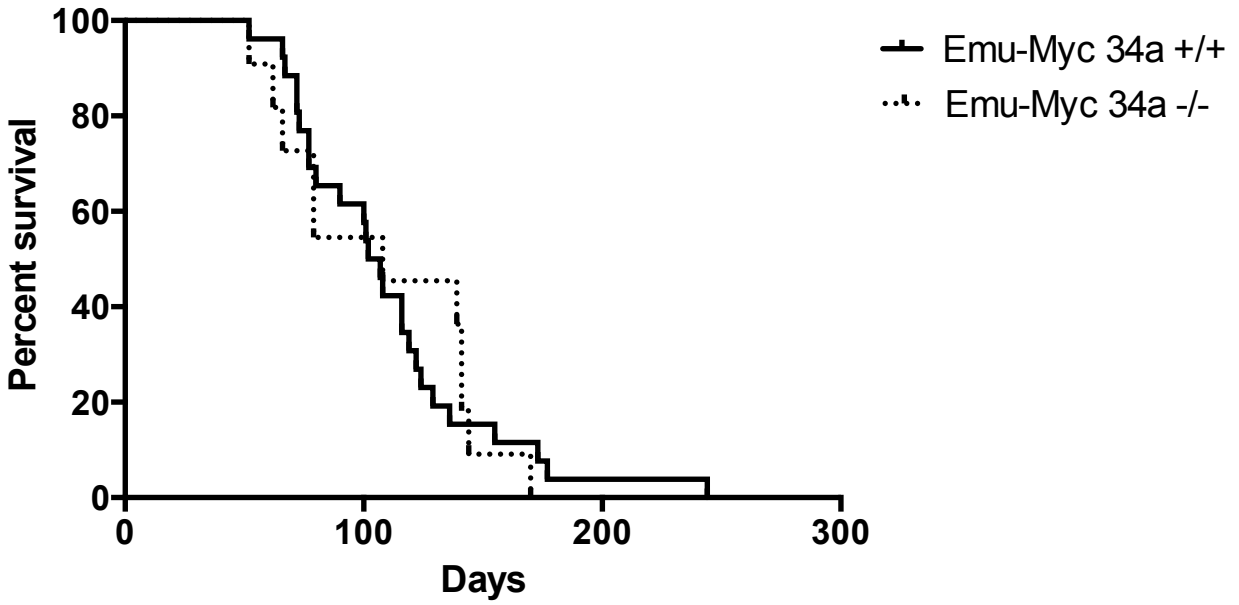

Figure 1: miR-34a deficiency does not alter survival in c-Myc driven B-cell malignancies. (**a**) Kaplan Meier survival curve of mice with Eμ-Myc oncogene and wild-type, or homozygous deficiency of miR-34a (n = 26 for Eμ-Myc miR-34a+/+(Solid line in graph), n = 10 for Eμ-Myc miR-34a–/– (Dashed line on graph); w.t. vs. k.o. comparison, Log-Rank Test, P = 0.9798).

miR-34a deficiency alters the c-Myc driven transcriptome

At the transcriptional level we were interested to know if miR-34a deletion led to changes in gene expression. To answer this question we performed high-throughput sequencing on a small cohort of Eμ-Myc tumors either sufficient or deficient for miR-34a. Only a small set of genes was significantly differentially expressed (DE) between these two genotypes (Figure 2a). To validate our results, we selected genes from our DE dataset and performed RT-qPCR analysis on a larger cohort of tumors (Figure 2c-e). DE genes identified by RNAseq were also

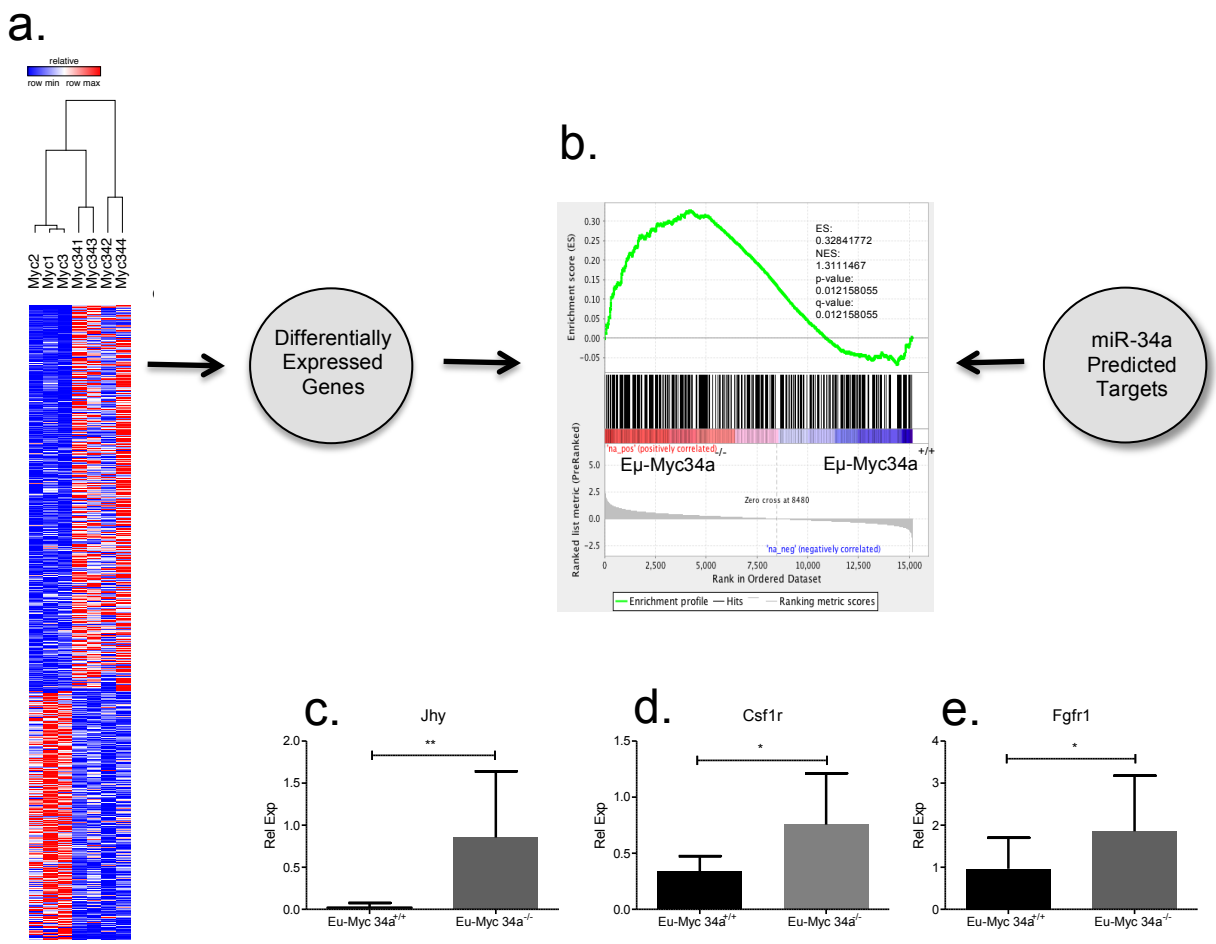

Figure 2: miR-34a deficiency alters c-Myc driven B-cell transcriptome. (**a**) Genes differentially expressed between Eμ-Myc miR-34a+/+ and Eμ-Myc miR-34a–/– tumors. The heat map color scale represents, for each gene, the relative expression level using the average mean gene expression as a reference (**b**) Enrichment plot from gene set enrichment analysis (GSEA) genes DE between Eμ-Myc miR-34a+/+ and Eμ-Myc miR-34a–/– tumors who enrichment for miR-34a putative targets (normalized enrichment score = 1.3111, q-value = 0.0121) (**c-e**) RT-qPCR of genes found to be differentially regulated by RNA-sequencing analysis, including Jhy (c; t-test, p = 0.0031), Csf1r (e; t-test, p = 0.0212), Fgfr1 (e; t-test, p = 0.0460). These three genes represent putative targets of miR-34a (For RT-qPCR analysis n = 12 for Eμ-Myc miR-34a+/+and n = 16 for Eμ-Myc miR-34a–/– for panels c, d, e).

differentially expressed in our larger cohort of tumors. We were also interested to know if miR-34a putative targets made up a significant proportion of these DE genes identified our analysis. To answer this we performed gene set enrichment analysis (GSEA) for putative miR-34a targets in our DE geneset. As expected DE genes were enriched for putative targets of miR-34a (Figure 2b).

c-Myc driven B-cell malignancies are enriched for miR-34a putative targets

Previous studies in DLBCL have shown that c-Myc is capable of repressing miR-34a indicating a possible dysregulation of miR-34a targets.[14] Furthermore, there are reports that miR-34a represses c-Myc. To understand the overlap between Myc and miR-34a regulated pathways, we performed the following bioinformatics analyses. Briefly, we wanted to answer the question of whether miR-34a putative targets were overrepresented in c-Myc-driven B-cell oncogenesis. To answer this we turned to a publicly available c-Myc ChIP-seq dataset (Sabo et al. 2015 [17]). This dataset contained lists of genes targeted by c-Myc in B-cells from either pre-malignant or malignant Eμ-Myc mice as well as WT animals. We performed GSEA for putative miR-34a targets obtained from Targetscan release 7.0 in each of these conditions. Indeed we found that c-Myc driven B-cell malignancies were enriched for putative miR-34a targets (Figure 3c) while premalignant genes contained a trend towards enrichment (Figure 3b) WT B-cells had no enrichment (Figure 3a). These findings suggested to us that transformation induced by Myc is partially dependent on the dysregulation of miR-34a targets, and that the study of genes targeted by both Myc and miR-34a may yield important insights into oncogenesis.

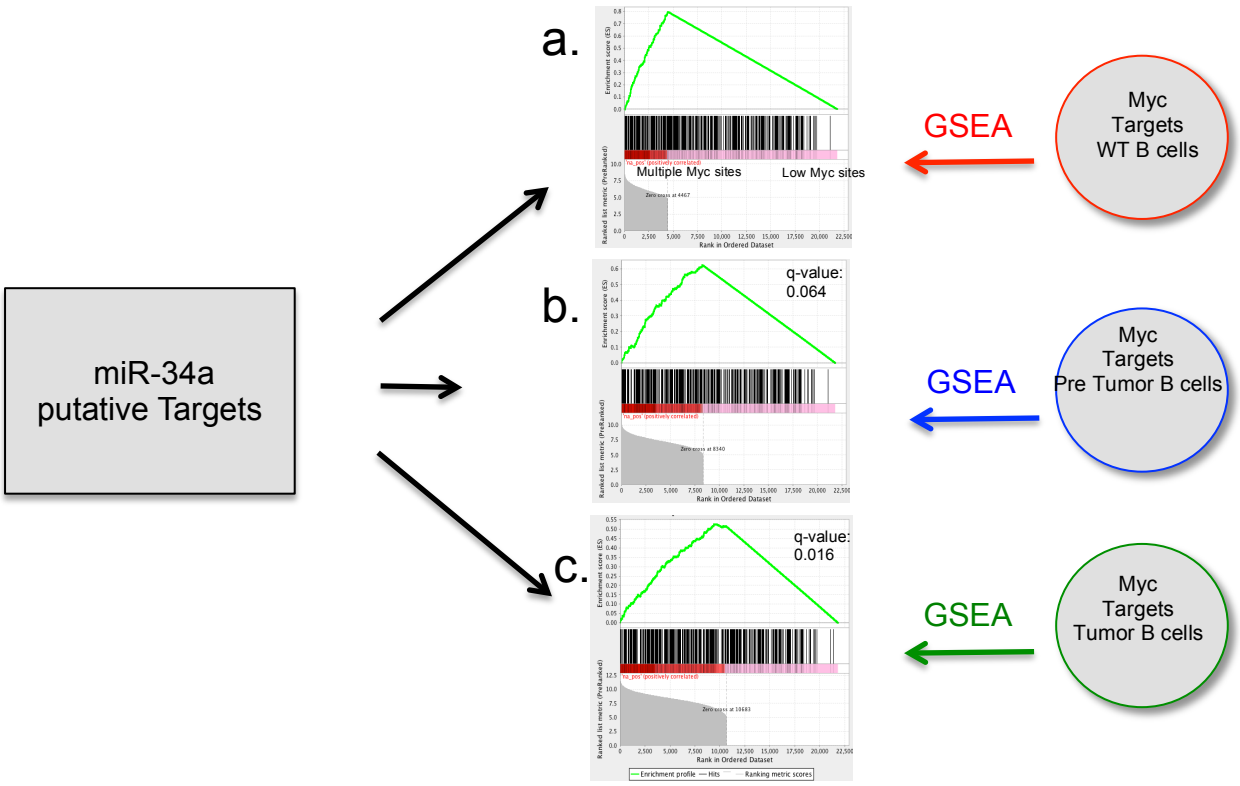

Figure 3: miR-34a putative targets are enriched in c-Myc driven B-cell malignancies. (**a-c)** Enrichment plot from gene set enrichment analysis (GSEA). (a) Genes with binding sites for c-Myc in WT B-cells did not show significant enrichment for miR-34a putative targets (q-value = 0.3520). (b) Genes with binding sites in pre-malignant B-cells show a trend towards enrichment of miR-34 putative targets (q-value = 0.064). (c) Genes with binding sites for c-Myc in tumors show significant enrichment for miR-34a putative targets (q-value = 0.016).

miR-34a suppresses cell proliferation and represses putative mRNA targets in B-cell lymphoma lines

Multiple studies have shown cell lines from different tissues have demonstrated that ectopic miR-34a expression leads to reduced proliferation.[7, 9, 10, 18, 19] Conversely, other studies have demonstrated a pro-growth role for miR-34a and yet others show no effect with miR-34a replacement.[15, 20] To clarify whether miR-34a overexpression can modulate cellular growth, we turned to using both B-cell and myeloid leukemia cell lines. Indeed, ectopic expression resulted in a reduction in cell proliferation as well as repression in putative targets of miR-34a (only Reh shown Figure 4a-d).

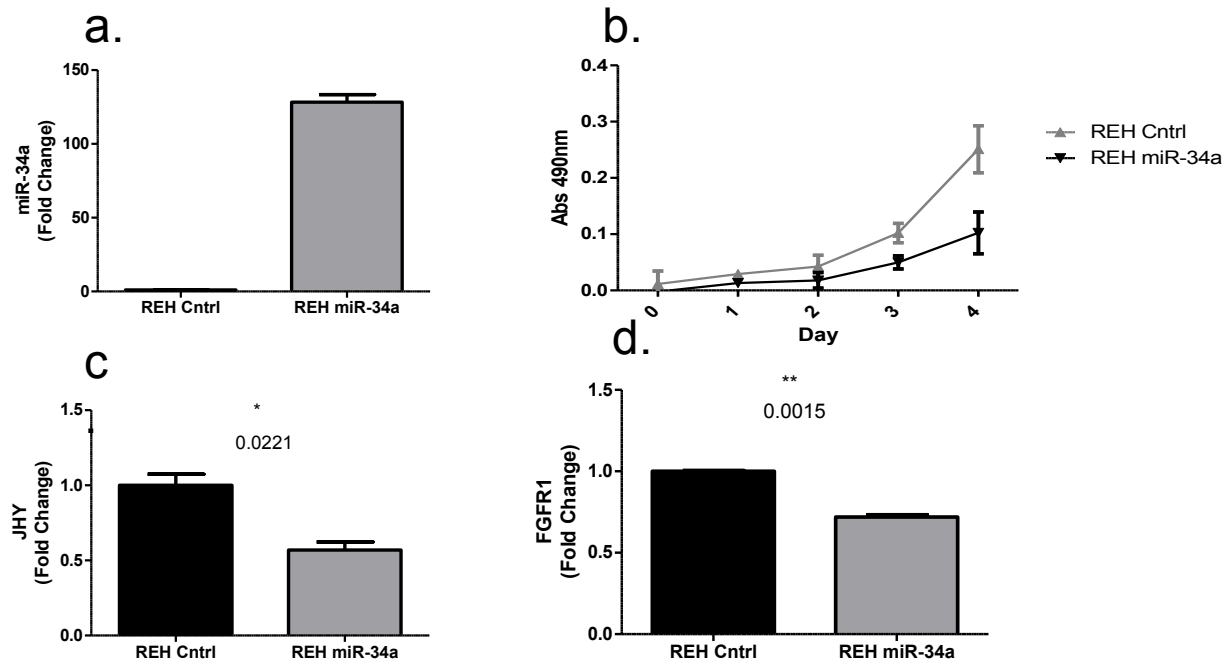

Figure 4: miR-34a overexpression suppresses proliferation and putative targets in B-cell lymphoma lines. (**A**) miR-34a expression in ectopic expression cell lines by qRT-PCR. Normalized to RNU48. (**B**) Decreased cell proliferation upon miR-34a overexpression in REH cells as measured by MTS (**C**) Quantitation of JHY by RT-qPCR in REH cell lines (**D**) qRT-PCR quantification of FGFR1 in Reh cell

lines transduced with vector control, or miR-34a. Normalized to ACTIN. Evaluations were made using a two-tailed T-test, p<0.05 (*); p<0.005 (**); p<0.0005 (***); p<0.0001 (****).

Csf1r, Jhy and Fgfr1 are novel targets of miR-34a

miRNAs function via targeting of the 3'UTR portion of mRNA transcripts. To date numerous miR-34a targets that are involved in various cellular functions have been uncovered.[7, 21-39] To validate Csf1r, Jhy and Fgfr1 as bona fide targets of miR-34a we performed 3'UTR-linked luciferase assays using WT and mutated 3'UTRs from the respective genes. Briefly, the 3'UTR for each of these genes, Jhy, Fgfr1, and Csf1r, contain evolutionarily conserved binding sites for miR-34a. These segments of the respective UTRs were cloned into the previously described luciferase reporter vector system, following which the site for miR-34a binding was mutated using site-directed mutagenesis. Luciferase assays were performed using these reporters with and without expression of miR-34a that was co-transfected into 293T cells. The results demonstrate that expression of miR-34a led to a repression of luciferase activity in the wild-type, but not the mutated 3'UTR in these assays (Figure 5).

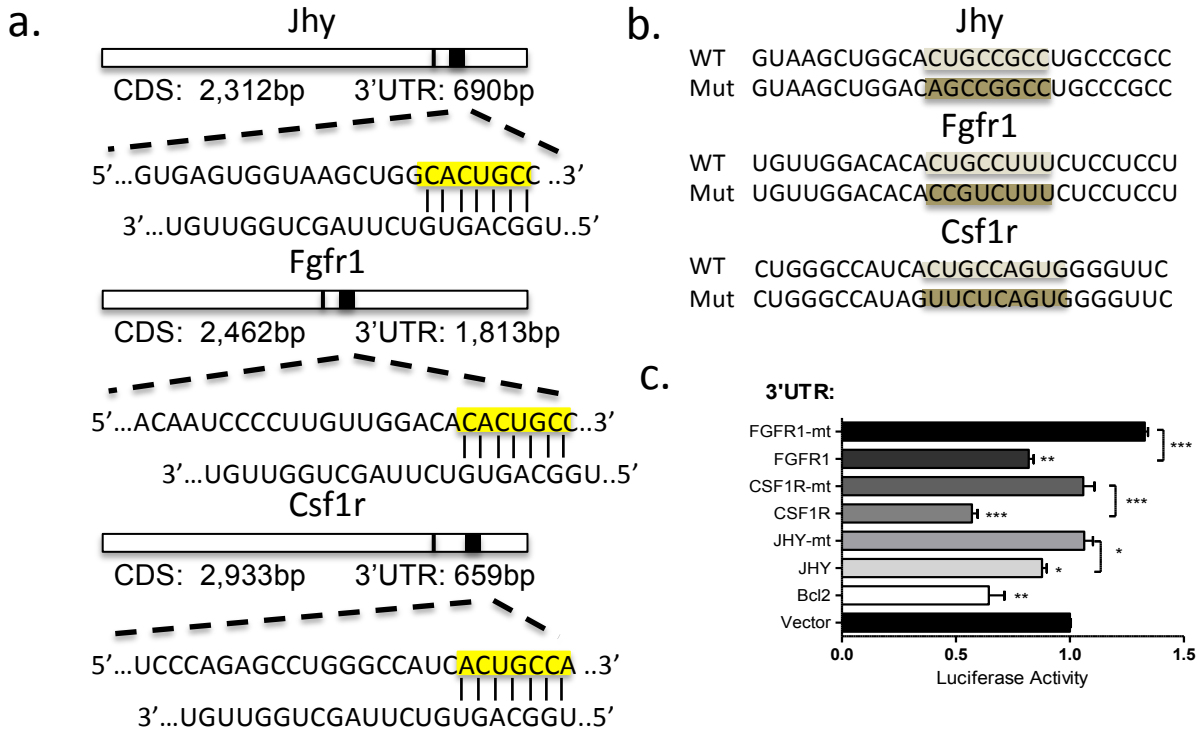

Figure 5: CSF1R, JHY, and FGFR1 are novel targets of miR-34a. (**a**) Shown is a schematic of the binding between Jhy, Fgfr1, and Csf1r and miR-34a. (**b**) Shown is a schematic of site directed mutagenesis in Jhy, Fgfr1, and Csf1r. (**c**) Luciferase assays quantitating repression with MGP/miR-34a co-transfection relative to MGP alone for each of the UTRs depicted. Each measurement is representative of firefly luciferase normalized to renilla luciferase, and was performed in duplicate, with the experiment repeated at least three times. Evaluations were made using a two-tailed T-test, $p<0.05$ (*); $p<0.005$ (**); $p<0.0005$ (***); $p<0.0001$ (****).

Discussion

In this study we demonstrate that the deletion of miR-34a in Myc driven B-cell oncogenesis resulted in no significant change in latency of disease onset, mortality or the phenotype of B-cell tumors. This stands in stark contrast to our results with miR-146a (see chapter 2). Myc-driven oncogenesis was accelerated with the deletion of miR-146a, and this was correlated with increased maturity of the B-cell neoplasms that developed in these mice. Likely, this is due to the fact that miR-34a and miR-146a regulate different transcriptomes, given their distinct specificity in targeting. Indeed, some of our further analysis bore out this possibility. Also, genetic redundancy is a possibility, as miR-34a family miRNAs are more numerous than miR-146 family miRNAs. Hence, the presence of other family members that are also induced upon p53 activation and share common targets may temper the effects of miR-34a deletion.

Interestingly, gene expression analysis demonstrated that putative miR-34a targets were enriched in the differentially expressed gene set when comparing Myc tumors that were either miR-34a sufficient or deficient. This, again, was in contrast to the analyses we carried out with miR-146a. miR-146a targets, as a class, were not significantly enriched in the differentially expressed gene set (Contreras et al 2015), and instead, a single target, Egr1, was found to lead to the many downstream changes in gene expression. This leads us to believe that miR-34a may act as a fine-tuner of gene expression, causing small changes in many different genes, and the deregulation of these genes by knockout of miR-34a was insufficient to cause a significant increase in oncogenesis.

An additional reason for the lack of a phenotypic effect of miR-34a deletion may relate to how the pathways regulated by miR-34a and miR-146a relate to the Myc-related transcriptome. We found that the transcriptome regulated by Myc during oncogenesis (as defined by ChIP-seq data) is enriched in miR-34a targets, suggesting that there may be an interplay between the two pathways. Hence, targets that are being massively upregulated by Myc overexpression may not incur an increment significant enough to cause a phenotypic change in oncogenesis via deletion of miR-34a. In contrast, miR-146a is thought to regulate NFkB pathway related targets- and miR-146a deficient Myc-driven oncogenesis may therefore have more severe consequences.

Our work also allowed us to extract novel direct miR-34a targets, which lay the foundation for our future work. Interestingly, the gene Jhy was found to be deregulated in both miR146a and miR-34a deficient c-Myc driven tumors. Hence, it will be of great interest to determine how this gene plays a role in B-cell oncogenesis. The role of Csf1r is well-established in the myeloid lineage (indeed, this is the cellular version of the viral oncogene, fms). However, how this may act to regulate B-cell oncogenesis is an open question, and one that opens up therapeutic possibilities if it is found to be deregulated in human B-cell tumors. The Fgfr1 is another receptor tyrosine kinase that is known to play a role in the growth of various mesenchymal cells, and disruptions of this receptor have been discovered in plasma cell neoplasms.[40] These novel targets of miR-34a may therefore have varying roles in the regulation of B-cell malignancies.

In addition to clarifying a role for miR-34a in the regulation of certain novel targets, our work also confirms the general tumor suppressive role for miR-34a in the B-cell and myeloid lineages. Therapeutic possibilities are suggested for constitutively expressing miR-34a in various hematolymphoid tumors, as we demonstrate that cell lines with overexpression have decreased survival. Moreover, our analyses suggest that in Myc-driven oncogenesis, miR-34a overexpression may counter the effects of Myc, given that miR-34a targets are overrepresented as Myc transcriptional targets. Hence, we will examine whether miR-34a delivery via retroviral

overexpression in the bone marrow or via delivery as a chemically modified oligonucleotide can serve a therapeutic purpose. Our future studies in this direction may lay the groundwork for future work in therapeutics in this area.

Methods

Mice

miR-34a deficient (miR-34a–/–) mice were donated and generated as previously described.[41] Eμ-Myc mice were purchased from Jackson laboratories and housed under pathogen free conditions at the University of California, Los Angeles.[16] Eμ-Myc and miR-34a–/– mice were bred to obtain Eμ-Myc miR-34a+/–mice with further miR-34a–/– intercross producing Eμ-Myc miR-34a–/– mice. Mice were monitored for tumors and sacrificed when they became pre-moribund indicated by the following criteria: tumors larger than 1.5cm, emaciation, or any other signs of distress. The UCLA Office of Animal Research Oversight approved all mouse studies.

Statistical Analysis

Figures are graphed as mean with the standard deviation of the mean (SD) for continuous numerical data. Bar graphs are employed to show dichotomized or ordinal type histopathologic data. Student's t-test, Fisher's exact test, Chi square test, and Kaplan-Meier survival analysis were performed using GraphPad Prism software, applied to each experiment as described in the figure legends.

RT-qPCR

RNA collected from the murine tumors was reverse transcribed using qScript reagent and PerfeCTa SYBR Green FastMix reagent (Quanta Biosciences) or TaqMan MicroRNA Assay (Life Technologies). Primer sequences used are listed in Supplementary Table 1.

Cloning and Cell culture

mmu-miR-155 formatted miR-34a constructs were cloned into BamHI and XhoI sites in the MSCV vector using the strategy that we have previously described to generate knockdown vectors.[29, 42, 43] Primer sequences used are listed in Supplemental Table 1 or mentioned previously.[43] RS4;11, Reh (TEL-AML1-translocated; CRL-8286, Nalm-6 , 70Z/3 (ATCC TIB-158) murine pre B-cell leukemic cell line, and the HEK 293T cell line (ATCC CRL-11268) were grown in their corresponding media at 37oC in a 5% CO_2 incubator as previously described [16, 53].

Transduction and sorting of cell lines

Lentiviruses and MSCV-based retroviruses were produced to generate knockdown constructs as previously described.[29, 42, 43] In brief, 5.0 x 10^5 cells were spin-infected at 30^{o}C for 90 minutes in the presence polybrene (4 μg/mL). Transduced cell lines were sorted for high green expression using a BD FACSAriaII cell sorter, and analysis was performed using BD FACSDiva software.

Biological assays

For MTS proliferation assays, cells were cultured for at least 5 days before plating. Cells were plated at a density of 2,500 cells per 100 μl of media in each well of a 96 well plate. Reagents were added according to the manufacturer's instructions (Promega CellTiter 96 Aqueous Non-Radioactive Cell Proliferation Assay kit) and cells were incubated at 37°C, 5% CO_2 for 4 hours before absorbance was measured at 490 nm.

Co-transfections were performed with BioT (Bioland Scientific LLC) in 24 well plates as per the manufacturer's instructions. Cells were lysed after 48 hours and supernatant lysate was collected as per manufacturer's instructions (Promega). The dual luciferase assay kit (Promega)

was used as substrates for Renilla and firefly luciferase activity. Luminescence was measured on a Glomax-Multi Jr (Promega). The ratio of firefly to Renilla luciferase activity was calculated for all samples. The luminescence for the sample co-transfected with MSCV empty vector and pCMV3 empty vector, was used as a normalization control.

Histology

Organs were collected after necropsy and fixed in 10% neutral buffered formalin. These were then embedded in paraffin, processed for hematoxylin and eosin staining by the Translational Pathology Core Laboratory at UCLA. Histopathologic analysis was performed by a board certified hematopathologist (D.S.R). The degree of splenic involvement was scored on a 4-point scale for red and white pulp involvement. Analysis of dichotomized or ordinal-type histopathologic data was accomplished by the use of Fisher's Exact Test.

RNA-sequencing and analysis

Total RNA was extracted from tumors using Trizol combined with Qiagen miRNEasy mini kit with additional on column DNAse I digestion. Following isolation of RNA, cDNA libraries were built using the Illumina (San Diego, CA) TrueSeq RNA Sample Preparation kit V2 (RS-122–2001). An Agilent Bioanalyzer was used to determine RNA quality (RIN > 8) prior to sequencing. RNA-Seq libraries were sequenced on an Illumina HiSeq 2000 (single-end 100bp). Raw sequence files were obtained using Illumina's proprietary software and are available at NCBI's Gene Expression Omnibus resource (GEO Series accession number) resource. RNA-Seq reads were aligned using STAR v2.3.0 [41]. The GRCm38 assembly (mm10) of the mouse genome and the junction database from Ensembl's gene annotation (release 71) were used as reference for STAR. The count matrix for genes in Ensembl's genome annotation (excluding rRNAs, Mt_rRNAs and Mt_tRNAs) was generated with HTSeq-count v0.5.4p3 (http://www-huber.embl.de/users/anders/ HTSeq/) and normalized using the geometric mean across

samples [42]. DESeq v1.14.0 [42] was used to classify genes as differentially expressed (Benjamini-Hochberg adjusted p-value < 0.05). Moderate fold changes between conditions were obtained from variance-stabilized data [42]. Functional annotation of differentially expressed genes was generated through the use of DAVID [36, 37]. Hierarchical gene clustering was performed with GENE-E (http://www. broadinstitute.org/cancer/software/GENE-E/). To display the heatmap, the expression levels were re-scaled so that, for each gene, the limits of the color scale correspond to the minimum and maximum expression levels across all samples.

Flow cytometry of samples

Blood, bone marrow, spleen, and lymph node tumors were collected from the mice under sterile conditions. Single cell suspensions were lysed in red blood cell lysis buffer. Fluorochrome conjugated antibodies against B220, CD3ε, CD11b, Ter119, CD19, IgM, CD80, CD138, CD44, CD21, CD23, and CD5 were used for staining (all antibodies obtained from Biolegend). Flow cytometry was performed on a FACSAria and analysis performed using FlowJo software. Dichotomization of flow cytometric measurements was accomplished by visual inspection of the data and identification of clusters within the data. These were then validated by comparison of the means and averages of the two clusters. For CD138, this was accomplished by examining the Mean Fluorescence Intensity and determining that the low expression cluster had a mean MFI, 154.0 ± 13.96 (N = 30) and 557.6 ± 71.87 (N = 7) for the high CD138 samples ($p < 0.0001$ for this comparison)

All antibodies were procured from eBiosciences (San Diego, CA) or Biolegend (San Diego, CA).

References

1. Sabattini, E., et al., WHO classification of tumours of haematopoietic and lymphoid tissues in 2008: an overview. Pathologica, 2010. 102(3): p. 83-7.
2. Basso, K. and R. Dalla-Favera, Roles of BCL6 in normal and transformed germinal center B cells. Immunol Rev, 2012. 247(1): p. 172-83.
3. Kozomara, A. and S. Griffiths-Jones, miRBase: annotating high confidence microRNAs using deep sequencing data. Nucleic Acids Res, 2014. 42(Database issue): p. D68-73.
4. Chang, T.C., et al., Transactivation of miR-34a by p53 broadly influences gene expression and promotes apoptosis. Mol Cell, 2007. 26(5): p. 745-52.
5. Raver-Shapira, N., et al., Transcriptional activation of miR-34a contributes to p53-mediated apoptosis. Mol Cell, 2007. 26(5): p. 731-43.
6. Tarasov, V., et al., Differential regulation of microRNAs by p53 revealed by massively parallel sequencing: miR-34a is a p53 target that induces apoptosis and G1-arrest. Cell Cycle, 2007. 6(13): p. 1586-93.
7. Ji, Q., et al., Restoration of tumor suppressor miR-34 inhibits human p53-mutant gastric cancer tumorspheres. BMC Cancer, 2008. 8: p. 266.
8. Antonini, D., et al., Transcriptional repression of miR-34 family contributes to p63-mediated cell cycle progression in epidermal cells. J Invest Dermatol, 2010. 130(5): p. 1249-57.
9. Christoffersen, N.R., et al., p53-independent upregulation of miR-34a during oncogene-induced senescence represses MYC. Cell Death Differ, 2010. 17(2): p. 236-45.
10. Corney, D.C., et al., Frequent downregulation of miR-34 family in human ovarian cancers. Clin Cancer Res, 2010. 16(4): p. 1119-28.
11. Hermeking, H., The miR-34 family in cancer and apoptosis. Cell Death Differ, 2010. 17(2): p. 193-9.

12. Chim, C.S., et al., Epigenetic inactivation of the miR-34a in hematological malignancies. Carcinogenesis, 2010. 31(4): p. 745-50.

13. Asslaber, D., et al., microRNA-34a expression correlates with MDM2 SNP309 polymorphism and treatment-free survival in chronic lymphocytic leukemia. Blood, 2010. 115(21): p. 4191-7.

14. Craig, V.J., et al., Myc-mediated repression of microRNA-34a promotes high-grade transformation of B-cell lymphoma by dysregulation of FoxP1. Blood, 2011. 117(23): p. 6227-36.

15. Forte, E., et al., The Epstein-Barr virus (EBV)-induced tumor suppressor microRNA MiR-34a is growth promoting in EBV-infected B cells. J Virol, 2012. 86(12): p. 6889-98.

16. Harris, A.W., et al., The E mu-myc transgenic mouse. A model for high-incidence spontaneous lymphoma and leukemia of early B cells. J Exp Med, 1988. 167(2): p. 353-71.

17. Sabo, A., et al., Selective transcriptional regulation by Myc in cellular growth control and lymphomagenesis. Nature, 2014. 511(7510): p. 488-92.

18. Dalgard, C.L., et al., Differential microRNA-34a expression and tumor suppressor function in retinoblastoma cells. Invest Ophthalmol Vis Sci, 2009. 50(10): p. 4542-51.

19. Ji, Q., et al., MicroRNA miR-34 inhibits human pancreatic cancer tumor-initiating cells. PLoS One, 2009. 4(8): p. e6816.

20. Rizzo, M., et al., The over-expression of miR-34a fails to block DoHH2 lymphoma cell proliferation by reducing p53 via c-MYC down-regulation. Nucleic Acid Ther, 2012. 22(4): p. 283-8.

21. Welch, C., Y. Chen, and R.L. Stallings, MicroRNA-34a functions as a potential tumor suppressor by inducing apoptosis in neuroblastoma cells. Oncogene, 2007. 26(34): p. 5017-22.

22. He, L., et al., A microRNA component of the p53 tumour suppressor network. Nature, 2007. 447(7148): p. 1130-4.

23. Sun, F., et al., Downregulation of CCND1 and CDK6 by miR-34a induces cell cycle arrest. FEBS Lett, 2008. 582(10): p. 1564-8.

24. Yamakuchi, M., M. Ferlito, and C.J. Lowenstein, miR-34a repression of SIRT1 regulates apoptosis. Proc Natl Acad Sci U S A, 2008. 105(36): p. 13421-6.

25. Wei, J.S., et al., The MYCN oncogene is a direct target of miR-34a. Oncogene, 2008. 27(39): p. 5204-13.

26. Ichimura, A., et al., MicroRNA-34a inhibits cell proliferation by repressing mitogen-activated protein kinase kinase 1 during megakaryocytic differentiation of K562 cells. Mol Pharmacol, 2010. 77(6): p. 1016-24.

27. Pang, R.T., et al., MicroRNA-34a suppresses invasion through downregulation of Notch1 and Jagged1 in cervical carcinoma and choriocarcinoma cells. Carcinogenesis, 2010. 31(6): p. 1037-44.

28. Kojima, K., et al., MiR-34a attenuates paclitaxel-resistance of hormone-refractory prostate cancer PC3 cells through direct and indirect mechanisms. Prostate, 2010. 70(14): p. 1501-12.

29. Rao, D.S., et al., MicroRNA-34a perturbs B lymphocyte development by repressing the forkhead box transcription factor Foxp1. Immunity, 2010. 33(1): p. 48-59.

30. Heinemann, A., et al., Tumor suppressive microRNAs miR-34a/c control cancer cell expression of ULBP2, a stress-induced ligand of the natural killer cell receptor NKG2D. Cancer Res, 2012. 72(2): p. 460-71.

31. Kim, N.H., et al., A p53/miRNA-34 axis regulates Snail1-dependent cancer cell epithelial-mesenchymal transition. J Cell Biol, 2011. 195(3): p. 417-33.

32. Wang, X., et al., Upregulation of p18Ink4c expression by oncogenic HPV E6 via p53-miR-34a pathway. Int J Cancer, 2011. 129(6): p. 1362-72.

33. Weeraratne, S.D., et al., miR-34a confers chemosensitivity through modulation of MAGE-A and p53 in medulloblastoma. Neuro Oncol, 2011. 13(2): p. 165-75.

34. Chen, H., et al., Mir-34a is upregulated during liver regeneration in rats and is associated with the suppression of hepatocyte proliferation. PLoS One, 2011. 6(5): p. e20238.

35. Mudduluru, G., et al., Regulation of Axl receptor tyrosine kinase expression by miR-34a and miR-199a/b in solid cancer. Oncogene, 2011. 30(25): p. 2888-99.

36. Bai, H., et al., MicroRNA-21 regulates the sensitivity of diffuse large B-cell lymphoma cells to the CHOP chemotherapy regimen. Int J Hematol, 2013. 97(2): p. 223-31.

37. Vo, D.T., et al., The oncogenic RNA-binding protein Musashi1 is regulated by tumor suppressor miRNAs. RNA Biol, 2011. 8(5): p. 817-28.

38. de Antonellis, P., et al., MiR-34a targeting of Notch ligand delta-like 1 impairs CD15+/CD133+ tumor-propagating cells and supports neural differentiation in medulloblastoma. PLoS One, 2011. 6(9): p. e24584.

39. Yang, J., et al., MiR-34 modulates Caenorhabditis elegans lifespan via repressing the autophagy gene atg9. Age (Dordr), 2013. 35(1): p. 11-22.

40. Bain, B.J., Myeloid and lymphoid neoplasms with eosinophilia and abnormalities of PDGFRA, PDGFRB or FGFR1. Haematologica, 2010. 95(5): p. 696-8.

41. Choi, Y.J., et al., miR-34 miRNAs provide a barrier for somatic cell reprogramming. Nat Cell Biol, 2011. 13(11): p. 1353-60.

42. Fernando, T.R., et al., LncRNA Expression Discriminates Karyotype and Predicts Survival in B-Lymphoblastic Leukemia. Mol Cancer Res, 2015. 13(5): p. 839-51.

43. Contreras, J.R., et al., MicroRNA-146a modulates B-cell oncogenesis by regulating Egr1. Oncotarget, 2015. 6(13): p. 11023-37.

CHAPTER IV:

Conclusions and Future Directions

Oncogenesis

B-cell neoplasms are a heterogeneous group of diseases capable of arising at any stage of B-cell development. As mentioned previously, rearrangements of transcription factors, such as c-Myc and Bcl6, with immunoglobulin genes is a commonly found feature in these neoplasms.[1] More recently, the discovery and characterization of oncomiRs and tumor suppressive miRNAs has elucidated their importance in post-transcriptional regulation in tumor progression.[2-5] miR-146a is an NF-κB responsive gene initially found to modulate the innate immune response to inflammatory insult in monocytes.[6] In transgenic animals deficient for this miRNA, a complex phenotype arose consisting of a myeloproliferative disease characterized by increased numbers of myeloid cells and infiltration in various tissues.[7] Given enough time, these animals also develop B- and T-cell lymphoid malignancies.[8] In this study, we sought to characterize the role of miR-146a in c-Myc driven B-cell oncogenesis using transgenic mice. Deletion of miR-146a in these transgenic mice gave rise to more aggressive B-cell malignancies, as demonstrated by a reduction in survival and differential levels of involvement in the lymph nodes and spleen. Histopathologically, tumors of miR-146a deficient animals appeared similar to controls but, upon closer examination, experimental tumors contained cells of a more mature type as demonstrated by cells with immunoglobulin concretions. This would indicate miR-146a modulates B-cell maturation in addition to HSCs as shown by Zhao et al. In vitro studies further demonstrated miR-146a can serve as a tumor suppressor. Upon overexpression of miR-146a in established cell lines, we observed a reduction in proliferation. The in vivo as well as the in vitro studies here demonstrate that miR-146a does indeed modulate B-cell oncogenesis— warranting further studies to fully characterize its function.

Identified as a downstream target of the genome guardian p53, miR-34a is induced upon genotoxic stress.[9-11] Once activated, it is capable of targeting genes involved in cell cycle progression and apoptosis such as E2F3 and BCL2, among others.[12, 13] In B-cell

development, miR-34a targets the transcription factor FOXP1 allowing cells to transition from the pro-B to pre-B cell stage.[14] Its overexpression in numerous malignant cell lines is known to reduce proliferation, yet in others it is has no effect.[15, 16] In this study, we aimed to characterize miR-34a deficiency in c-Myc driven B-cell oncogenesis. Using transgenic animals overexpressing c-Myc and sufficient or deficient for miR-34a, we found miR-34a deficiency does not alter c-Myc driven B-cell oncogenesis. Upon histopathological examination of tumors from both genotypes, we found no difference between the two. Overexpression studies of miR-34a corroborated previous studies, demonstrating stunted cell proliferation in overexpressing lines. Taken together, these studies demonstrate miR-34a is dispensable in c-Myc driven oncogenesis, but miR-34a plays an unknown role in B-cell neoplasms.

Novel Targets

Over a decade ago, a seminal study was able to subgroup a panel of diffuse large B-cell (DLBCL) type lymphomas using gene expression profiles.[17] miRNAs act as post-transcriptional gene regulators by binding to partially complementary sequences in the 3' UTR on target messenger RNAs, thereby causing downregulation of the target.[18] Studies on established cell lines have demonstrated miRNAs ability to modulate the transcriptome in malignant cells.[15, 19] In this study, we aimed to identify novel targets for miR-146a in a B-cell transcriptome driven by c-Myc oncogenesis. To do this, we performed high-throughput sequencing (HT-seq) on c-Myc driven malignancies sufficient or deficient for miR-146a. We identified 249 significantly differentially expressed (DE) genes between the two genotypes. Although we did not see enrichment of putative targets, we did identify novel targets of miR-146a in B-cell lymphomas. One of these novel targets is Egr1, which previous studies have shown is a positive regulator of B-cell development. Given this gene's role as a transcription factor, this reveals a pathway for further studies in B-cell malignancies. Given the functional

targets identified in various tumor types such as pancreatic cancer, breast cancer, etc., we were interested to find novel targets of miR-34a in B-cell oncogenesis.[20] Similar to our miR-146a study, we used c-Myc driven lymphomas sufficient or deficient for miR-34a to perform HT-seq and found 24 genes DE between the two genotypes. Upon manual examination of this dataset, we identified the following putative targets of miR-34a: Csf1r, Jhy, and Fgfr1. Taken together, this study has identified previously unknown downstream targets of miR-34a in c-Myc driven oncogenesis. These targets are novel and specific to B-cell oncogenesis that will warrant further analysis.

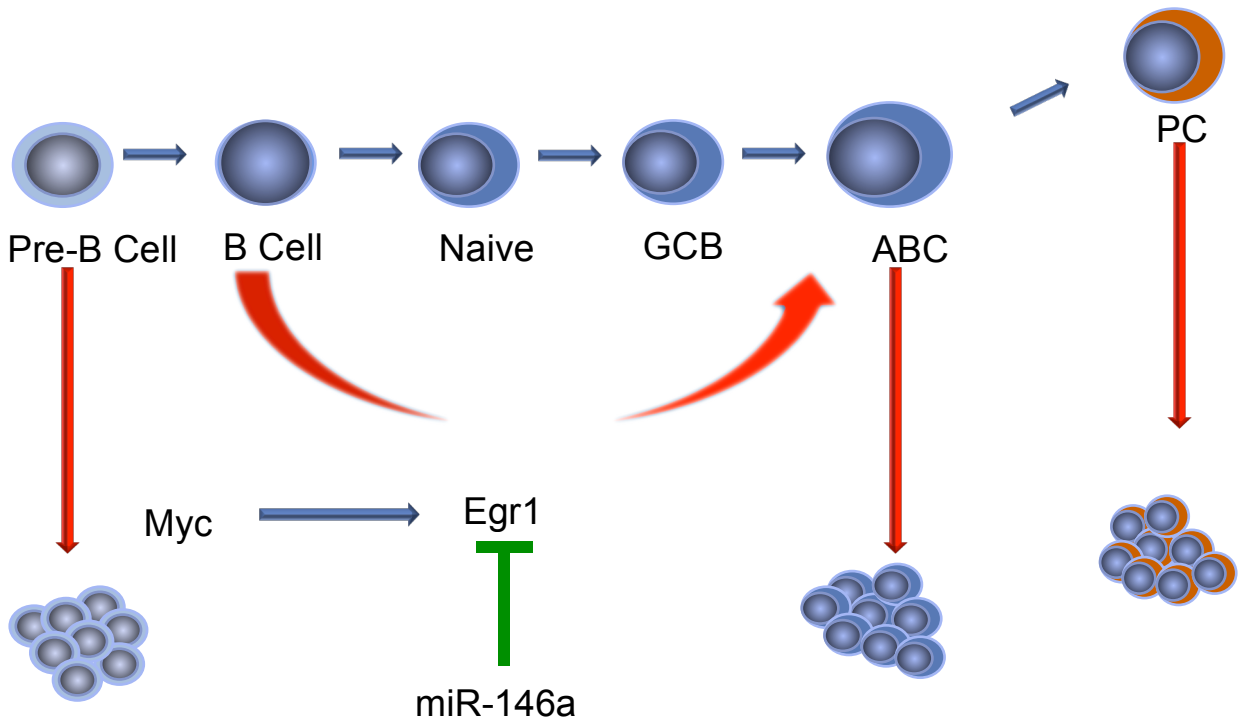

Figure 1: Schematic of miR-146a/Egr1 model in Eμ-myc mice. In Eμ-myc tumors miR-146a represses Egr1 and these mice primarily develop pre-B cell tumors. In Eμ-myc/miR-146a$^{-/-}$ tumors Egr1 is derepressed and in these mice predominantly develop mature B-cell tumors.

Contextual study

Prior studies have demonstrated the changes in gene expression profiles (GEP) of mRNAs as well as microRNAs as B-cells mature.[21-23] Not surprisingly malignant B-cells can be subset by both their mRNA, and microRNA GEP's.[17, 23] Given how miRNAs function, the context in which miRNAs are studied is very important for two reasons; 1) a microRNA can only modulate mRNAs that are being expressed, 2) microRNAs mainly function as fine tuning mechanism. In these studies, we sought to characterize the role of miR-146a and miR-34a in the context of B-cell malignancies. For these miRNAs, previous studies established their role as tumor suppressors in different cell lineages. Here, we were interested in delineating their tumor suppressor capabilities in B-cell malignancies. For miR-146a, we found accelerated oncogenesis as demonstrated by reduced survival of animals deficient for this miRNA. In miR-34a, we characterized its tumor suppressive capabilities in established B-cell and myeloid leukemia cell lines. Interestingly, for miR-34a we found that the c-Myc oncogene deregulates several miR-34a putative targets, as identified by our GSEA analysis of c-Myc driven malignancies. Not surprisingly, when we deleted miR-34a in this context we found miR-34a did not modulate c-Myc driven oncogenesis. Nonetheless, in B-cell leukemia cell lines we found that miR-34a replacement does inhibit proliferation with a concomitant repression of newly identified targets in this study. As mentioned previously the context of miRNA study is fundamental to the outcome for the two reasons mentioned. In our miR-146a study we identified a novel result due to genes regulated by miR-146a being expressed in our model but tempered by this microRNA. As shown in Fig. 1 in plain Eμ-myc mice Egr1 is suppressed by miR-146a and consequently a majority of tumors derive from the pre-B cell stage. When we remove miR-146a Egr1 is derepressed and alters the transcriptome leading to a majority of tumors coming from a more mature B-cell stage. In our miR-34a study we found that in our model a significant proportion of miR-34a targets are upregulated due to c-Myc. As the function of most miRNAs appears to fine tune the transcriptome it is not surprising that deletion of this miRNA failed to modulate c-Myc

oncogenesis. In this case deficiency of miR-34a is overshadowed by the c-Myc lesion, or put another way miR-34a deficiency and c-Myc overexpression modulate similar pathways.

Future directions

In this study, we have uncovered the novel targets Egr1, Jhy, Csf1r, and Fgfr1 which have established novel pathways or, at the least, downstream effectors of previously identified pathways in miR-146a and miR-34a. In order to fully comprehend the role that these targets play in B-cell oncogenesis, future studies need to be undertaken such as knockdown of these genes in the presence of their respective miRNAs to characterize complementation. In the case of Jhy, Csf1r, and Fgfr1, we are currently attempting a CRISPR-Cas9-mediated deletion of these targets in leukemia cell lines. In these cell lines, we will characterize cell proliferation, apoptosis, and cell cycle progression to further delineate this pathway regulated by miR-34a.

As we have discovered a deregulation of miR-34a putative targets in the context of c-Myc driven B-cell oncogenesis, the next step is to characterize miR-34a replacement therapy in Eμ-myc animals. To this end, we have begun a series of bone marrow transplant experiments in conjunction with ectopic expression of miR-34a. In these animals, we suspect miR-34a will reduce the aggressiveness of c-Myc driven tumors.

References

1. Seifert, M., R. Scholtysik, and R. Kuppers, Origin and pathogenesis of B cell lymphomas. Methods Mol Biol, 2013. **971**: p. 1-25.
2. Calin, G.A., et al., A MicroRNA signature associated with prognosis and progression in chronic lymphocytic leukemia. N Engl J Med, 2005. **353**(17): p. 1793-801.
3. Cimmino, A., et al., miR-15 and miR-16 induce apoptosis by targeting BCL2. Proc Natl Acad Sci U S A, 2005. **102**(39): p. 13944-9.
4. He, L., et al., A microRNA polycistron as a potential human oncogene. Nature, 2005. **435**(7043): p. 828-33.
5. Xiao, C., et al., Lymphoproliferative disease and autoimmunity in mice with increased miR-17-92 expression in lymphocytes. Nat Immunol, 2008. **9**(4): p. 405-14.
6. Taganov, K.D., et al., NF-kappaB-dependent induction of microRNA miR-146, an inhibitor targeted to signaling proteins of innate immune responses. Proc Natl Acad Sci U S A, 2006. **103**(33): p. 12481-6.
7. Zhao, J.L., et al., NF-kappaB dysregulation in microRNA-146a-deficient mice drives the development of myeloid malignancies. Proc Natl Acad Sci U S A, 2011. **108**(22): p. 9184-9.
8. Boldin, M.P., et al., miR-146a is a significant brake on autoimmunity, myeloproliferation, and cancer in mice. J Exp Med, 2011. **208**(6): p. 1189-201.
9. Wei, C.L., et al., A global map of p53 transcription-factor binding sites in the human genome. Cell, 2006. **124**(1): p. 207-19.
10. Bommer, G.T., et al., p53-mediated activation of miRNA34 candidate tumor-suppressor genes. Curr Biol, 2007. **17**(15): p. 1298-307.
11. Chang, T.C., et al., Transactivation of miR-34a by p53 broadly influences gene expression and promotes apoptosis. Mol Cell, 2007. **26**(5): p. 745-52.

12. Ji, Q., et al., Restoration of tumor suppressor miR-34 inhibits human p53-mutant gastric cancer tumorspheres. BMC Cancer, 2008. **8**: p. 266.
13. Tazawa, H., S. Kagawa, and T. Fujiwara, MicroRNAs as potential target gene in cancer gene therapy of gastrointestinal tumors. Expert Opin Biol Ther, 2011. **11**(2): p. 145-55.
14. Rao, D.S., et al., MicroRNA-34a perturbs B lymphocyte development by repressing the forkhead box transcription factor Foxp1. Immunity, 2010. **33**(1): p. 48-59.
15. Tazawa, H., et al., Tumor-suppressive miR-34a induces senescence-like growth arrest through modulation of the E2F pathway in human colon cancer cells. Proc Natl Acad Sci U S A, 2007. **104**(39): p. 15472-7.
16. Forte, E., et al., The Epstein-Barr virus (EBV)-induced tumor suppressor microRNA MiR-34a is growth promoting in EBV-infected B cells. J Virol, 2012. **86**(12): p. 6889-98.
17. Alizadeh, A.A., et al., Distinct types of diffuse large B-cell lymphoma identified by gene expression profiling. Nature, 2000. **403**(6769): p. 503-11.
18. Grimson, A., et al., MicroRNA targeting specificity in mammals: determinants beyond seed pairing. Mol Cell, 2007. **27**(1): p. 91-105.
19. Sun, F., et al., Downregulation of CCND1 and CDK6 by miR-34a induces cell cycle arrest. FEBS Lett, 2008. **582**(10): p. 1564-8.
20. Kastl, L., I. Brown, and A.C. Schofield, miRNA-34a is associated with docetaxel resistance in human breast cancer cells. Breast Cancer Res Treat, 2012. **131**(2): p. 445-54.
21. Hoffmann, R., et al., Changes in gene expression profiles in developing B cells of murine bone marrow. Genome Res, 2002. **12**(1): p. 98-111.
22. Jima, D.D., et al., Deep sequencing of the small RNA transcriptome of normal and malignant human B cells identifies hundreds of novel microRNAs. Blood, 2010. **116**(23): p. e118-27.

23. Zanette, D.L., et al., miRNA expression profiles in chronic lymphocytic and acute lymphocytic leukemia. Braz J Med Biol Res, 2007. **40**(11): p. 1435-40.

APPENDICES

APPENDIX I:

RNA-binding protein IGF2BP3 targeting of oncogenic transcripts promotes hematopoietic progenitor proliferation (reprint)

RNA-binding protein IGF2BP3 targeting of oncogenic transcripts promotes hematopoietic progenitor proliferation

Jayanth Kumar Palanichamy,[1] Tiffany M. Tran,[1,2] Jonathan M. Howard,[3] Jorge R. Contreras,[1] Thilini R. Fernando,[1] Timothy Sterne-Weiler,[3] Sol Katzman,[3] Masoud Toloue,[4] Weihong Yan,[5] Giuseppe Basso,[6] Martina Pigazzi,[6] Jeremy R. Sanford,[3] and Dinesh S. Rao[1,2,7,8]

[1]Department of Pathology and Laboratory Medicine, David Geffen School of Medicine at UCLA, Los Angeles, California, USA. [2]Department of Molecular, Cellular and Integrative Physiology, UCLA, Los Angeles, California, USA. [3]Department of Molecular, Cellular and Developmental Biology, UCSC, Santa Cruz, California, USA. [4]Bioo Scientific Corporation, Austin, Texas, USA. [5]Department of Chemistry and Biochemistry, UCLA, Los Angeles, California, USA. [6]Department of Women's and Children's Health SDB, University of Padova, Padova, Italy. [7]Jonsson Comprehensive Cancer Center (JCCC) and [8]Broad Stem Cell Research Center, UCLA, Los Angeles, California, USA.

Posttranscriptional control of gene expression is important for defining both normal and pathological cellular phenotypes. In vitro, RNA-binding proteins (RBPs) have recently been shown to play important roles in posttranscriptional regulation; however, the contribution of RBPs to cell specification is not well understood. Here, we determined that the RBP insulin-like growth factor 2 mRNA-binding protein 3 (IGF2BP3) is specifically overexpressed in mixed lineage leukemia–rearranged (MLL-rearranged) B-acute lymphoblastic leukemia (B-ALL), which constitutes a subtype of this malignancy associated with poor prognosis and high risk of relapse. IGF2BP3 was required for the survival of B-ALL cell lines, as knockdown led to decreased proliferation and increased apoptosis. Enforced expression of IGF2BP3 provided murine BM cells with a strong survival advantage, led to proliferation of hematopoietic stem and progenitor cells, and skewed hematopoietic development to the B cell/myeloid lineage. Cross-link immunoprecipitation and high throughput sequencing uncovered the IGF2BP3-regulated transcriptome, which includes oncogenes *MYC* and *CDK6* as direct targets. IGF2BP3 regulated transcripts via targeting elements within 3′ untranslated regions (3′UTR), and enforced IGF2BP3 expression in mice resulted in enhanced expression of *Myc* and *Cdk6* in BM. Together, our data suggest that IGF2BP3-mediated targeting of oncogenic transcripts may represent a critical pathogenetic mechanism in MLL-rearranged B-ALL and support IGF2BP3 and its cognate RNA-binding partners as potential therapeutic targets in this disease.

Introduction

Oncogenesis in early B cell progenitors results in B cell acute lymphoblastic leukemia (B-ALL), the most prevalent hematological neoplasm in children and young adults (1). The majority of B-ALL cases exhibit genetic alterations, including recurring chromosomal rearrangements, which contribute to the heterogeneity of the observed clinical behavior (2). Specifically, B-ALL with chromosomal rearrangements of the mixed lineage leukemia (*MLL*) gene accounts for 5%–6% of all B-ALL cases and is associated with poor prognosis and risk of early relapse after treatment (3). *MLL*, which encodes a H3K4 methyltransferase, plays a critical role in the transcriptional dysregulation that occurs during leukemogenesis (3, 4). Previously demonstrated targets of MLL include genes critical in cell survival and proliferation, such as *BCL2*, *MYC*, and *CDK6* (5–7). Additionally, MLL is known to regulate hematopoiesis, and its expression correlates with the maintenance of hematopoietic stem cell (HSC) self-renewal and differentiation (8, 9). In line with such a role in normal HSC function, MLL fusion proteins induce *HOXA9* and *MEIS1*, generating leukemia that displays stem cell–like properties (10–12). These findings demonstrate an intimate connection between the dysregulation of gene expression and malignant transformation, and they highlight the importance of investigating key players in the regulation of gene expression.

Simplistically, gene expression may be regulated at the transcriptional and posttranscriptional levels. Recent work has revealed the complexity of the latter mechanism, which not only includes sequences intrinsic to the regulated mRNA but also other factors such as miRs, RNA-binding proteins (RBPs), and noncoding RNA (13). A complex interplay between the protein coding mRNA and the 3′ untranslated region (3′UTR) targeting miRs and RBPs has been reported (14). However, the role of gene expression regulation by RBPs in the malignant transformation of B cells is not understood. In an effort to identify critical RBP-mediated regulation in B-ALL, we began by examining a high throughput dataset generated in our laboratory, identifying the insulin-like growth factor 2 mRNA-binding protein 3 (*IGF2BP3*) as one of the top dysregulated genes in MLL-translocated B-ALL. IGF2BP3 belongs to a family of mRNA-binding proteins that consists of 3 structurally and

Authorship note: J. Kumar Palanichamy, T.M. Tran, and J.M. Howard contributed equally to this work.
Conflict of interest: The authors have declared that no conflict of interest exists.
Submitted: November 17, 2014; **Accepted:** January 26, 2016.
Reference information: *J Clin Invest.* 2016;126(4):1495–1511. doi:10.1172/JCI80046.

functionally related paralogs (IGF2BP1, IGF2BP2, and IGF2BP3) that influence the cytoplasmic fate of mRNAs through localization, stability, and translation (15, 16). IGF2BP3 is an oncofetal protein with high expression during embryogenesis, low expression in adult tissues, and reexpression in malignant tissues. In epithelial cancer, IGF2BP3 expression is associated with a range of neoplastic phenotypes (17–20). However, many of these studies have been largely correlative, and a bona fide functional role of IGF2BP3, or any RBP, in B cell oncogenesis has not been established.

In this study, we sought to delineate the function of IGF2BP3 in B cell leukemogenesis. We overexpressed IGF2BP3 in the BM of lethally irradiated mice and found that it plays a critical role in the proliferation of hematopoietic stem and progenitor cells, recapitulating some features of MLL-rearranged B-ALL. IGF2BP3 provided BM progenitors with a competitive survival advantage and increased their proliferation. We also found that IGF2BP3 was essential for the survival of B-ALL cell lines. We used individual nucleotide resolution cross-linking immunoprecipitation (iCLIP) to capture the in situ specificity of protein-RNA interactions and to reveal the positional context of protein binding sites across the transcriptome. In total, we identified IGF2BP3 binding sites in several hundred transcripts in 2 B-ALL cell lines. IGF2BP3 cross-linking sites are strongly enriched in the 3′UTRs of target transcripts. Of the many IGF2BP3 target transcripts, we demonstrated IGF2BP3-mediated enhancement of the expression of oncogenic targets *CDK6* and *MYC* in B-ALL cells and hematopoietic progenitor cells in vivo. Deletion of the RNA-binding domains of IGF2BP3 abrogated target mRNA binding as well as the hematopoietic stem and progenitor expansion. Together, our studies suggest that IGF2BP3-mediated upregulation of oncogenic targets represents a key pathogenetic mechanism operant in MLL-rearranged B-ALL.

Results

IGF2BP3 is differentially expressed in MLL-rearranged B-ALL. We have previously described a microarray experiment performed on patient B-ALL samples (21). Following correction for multiple-hypotheses testing, we performed unsupervised hierarchical clustering with significantly differentially expressed protein-coding genes (adjusted $P \leq 0.01$). This generated a list of RBPs differentially expressed between the 3 cytogenetic subtypes of B-ALL used in our microarray experiments (ETV-RUNX1, E2A-PBX, and MLL-rearranged). In the list of RBPs whose expression was highest in MLL-rearranged leukemia, *IGF2BP3* was among the top candidates (Figure 1A). MLL-rearranged leukemias show a stem-cell signature with high expression of stemness-associated genes like *HOXA9*, *MEIS1*, and *CD44* (11, 22). Concordant with this, we observed that *HOXA9*, *MEIS1A*, *CDK6*, and *MYC* — putative targets of the oncogenic MLL fusion protein — were significantly overexpressed in the MLL-rearranged group when compared with the other 2 subsets (Supplemental Figure 1, A–D). By performing quantitative PCR (qPCR) on a large cohort of B-ALL patient–derived BMs, we confirmed that *IGF2BP3* and *CD44* were highly expressed in the MLL group (total $n = 134$) (Figure 1, B and C). Additionally, *IGF2BP3* expression was significantly higher in all B-ALL samples when compared with $CD19^+$ B cells isolated from healthy donors (Figure 1B). To examine the dependence of IGF2BP3 on MLL-mediated effects on gene expression, we utilized I-BET151, a bromodomain and extra terminal (BET) domain inhibitor that has recently been shown to inhibit MLL-dependent gene expression (23). Treatment of RS4;11 — an MLL-AF4–expressing human B-ALL cell line — with I-BET151 caused a dose-dependent decrease in the expression of *MYC*, *CDK6*, and *IGF2BP3* (Figure 1D). It also caused cell cycle arrest in the G1-S phase (Figure 1, E and F). These experiments confirm the overexpression of *IGF2BP3* in B-ALL, with the highest expression seen in MLL-rearranged B-ALL. In line with IGF2BP3 being downstream of MLL fusion proteins, a fall in *IGF2BP3* mRNA levels, along with a fall in other MLL-AF4 target levels, is seen after BET inhibition.

IGF2BP3 loss of function causes apoptosis in B-ALL cells. Given the oncogenic expression pattern of IG2BP3 in human B-ALL, we proceeded to examine its expression in 4 different B-ALL cell lines, including 697 (E2A-PBX translocated), RS4;11, REH (ETV-RUNX1 translocated), and NALM6 (Figure 2A). To examine the effects of IGF2BP3 knockdown, we used a lentiviral vector expressing 2 different miR formatted siRNA sequences to transduce RS4;11 cells (Figure 2B). Both siRNAs caused decreased *IGF2BP3* expression by qPCR (Figure 2C). Propidium iodide staining showed an increase in the apoptotic sub-G1 fraction, and 3-(4,5-dimethylthiazol-2-yl)-5-(3-carboxymethoxyphenyl)-2-(4-sulfophenyl)-2H-tetrazolium (MTS) assay showed a significant reduction in cell proliferation with IGF2BP3 knockdown, confirming the dependence of B-ALL cell lines on IGF2BP3 for survival (Figure 2, D and E). Deletion of the *IGF2BP3* locus using the CRISPR-Cas9 system was also undertaken in the RS4;11 cell line. We utilized the LentiCRISPR system (24) with 2 different guide strands, Cr1 and Cr2, to target the *IGF2BP3* locus for deletion. CRISPR-mediated deletion was confirmed by a T7 endonuclease assay (Supplemental Figure 2, D and E) with complete abrogation of IGF2BP3 protein with the guide RNA Cr2, whereas residual protein was detected with Cr1 (Figure 2F). Cr2-mediated deletion resulted in reduced cell proliferation by MTS assay, increased sub-G1 staining, and increased annexin V positivity (Figure 2, G–I). To confirm these findings, we also targeted IGF2BP3 for knockdown in NALM6 cells using a lentiviral siRNA expression system (Supplemental Figure 2A). Reduced *IGF2BP3* mRNA levels were observed with both siRNAs, with si2 giving a stronger reduction in cell proliferation, as seen by the MTS assay (Supplemental Figure 2, B and C). Together, these findings highlight the importance of IGF2BP3 in maintaining cell survival and proliferation in B-ALL.

Enforced expression of IGF2BP3 leads to high levels of engraftment and increased leukocytes. To directly assess the role of IGF2BP3 in the hematopoietic system, we undertook an in vivo experiment to examine the effects of enforced expression. We initially cloned the human or mouse coding sequence of IGF2BP3 into MIG, a murine stem cell virus–based (MSCV-based) retroviral vector (Figure 3A), and confirmed the functionality of the vector in expressing both IGF2BP3 and the GFP marker (Figure 3, B–D, and data not shown). A peripheral bleed of these mice at 4 weeks showed a significant increase in GFP^+ cells that was sustained over time in mice with enforced expression of human and mouse *IGF2BP3*, as measured by the congenic CD45.2 versus CD45.1 FACS markers (Figure 3, E and F). Moreover, significantly increased GFP^+ leukocyte cells were found, confirming increased hematopoietic output attributable to IGF2BP3 expression (Figure 3G). These changes were restricted to

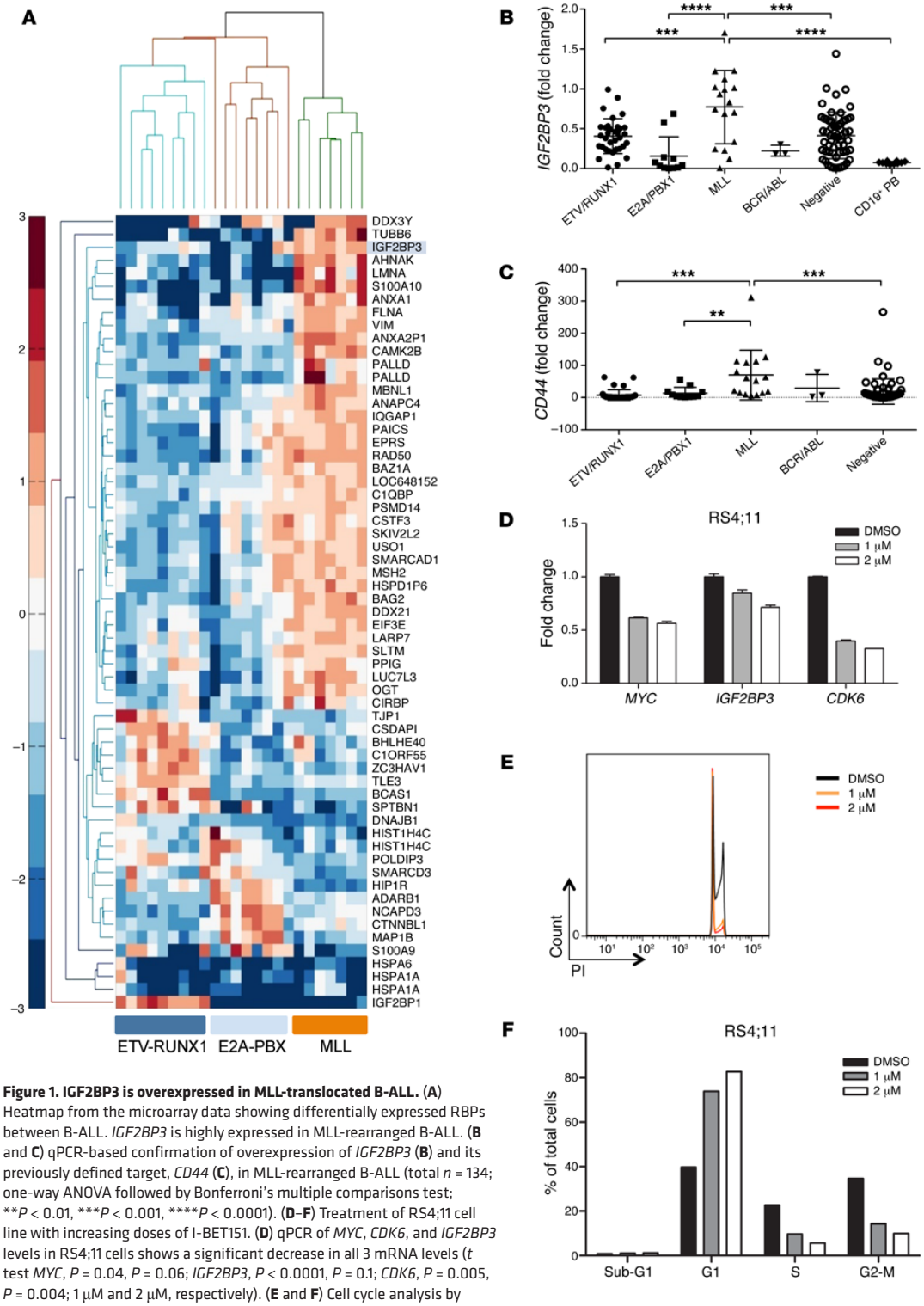

Figure 1. IGF2BP3 is overexpressed in MLL-translocated B-ALL. (**A**) Heatmap from the microarray data showing differentially expressed RBPs between B-ALL. *IGF2BP3* is highly expressed in MLL-rearranged B-ALL. (**B** and **C**) qPCR-based confirmation of overexpression of *IGF2BP3* (**B**) and its previously defined target, *CD44* (**C**), in MLL-rearranged B-ALL (total $n = 134$; one-way ANOVA followed by Bonferroni's multiple comparisons test; $^{**}P < 0.01$, $^{***}P < 0.001$, $^{****}P < 0.0001$). (**D**–**F**) Treatment of RS4;11 cell line with increasing doses of I-BET151. (**D**) qPCR of *MYC*, *CDK6*, and *IGF2BP3* levels in RS4;11 cells shows a significant decrease in all 3 mRNA levels (*t* test *MYC*, $P = 0.04$, $P = 0.06$; *IGF2BP3*, $P < 0.0001$, $P = 0.1$; *CDK6*, $P = 0.005$, $P = 0.004$; 1 μM and 2 μM, respectively). (**E** and **F**) Cell cycle analysis by propidium iodide staining after I-BET151 treatment of RS4;11 cells shows G1 arrest secondary to CDK6 inhibition. Experiments were conducted 3× for validation. qPCR assays were normalized to actin (**B** and **C**) and RNA Pol II (**D**). Data represent mean ±SD. See also Supplemental Figure 1.

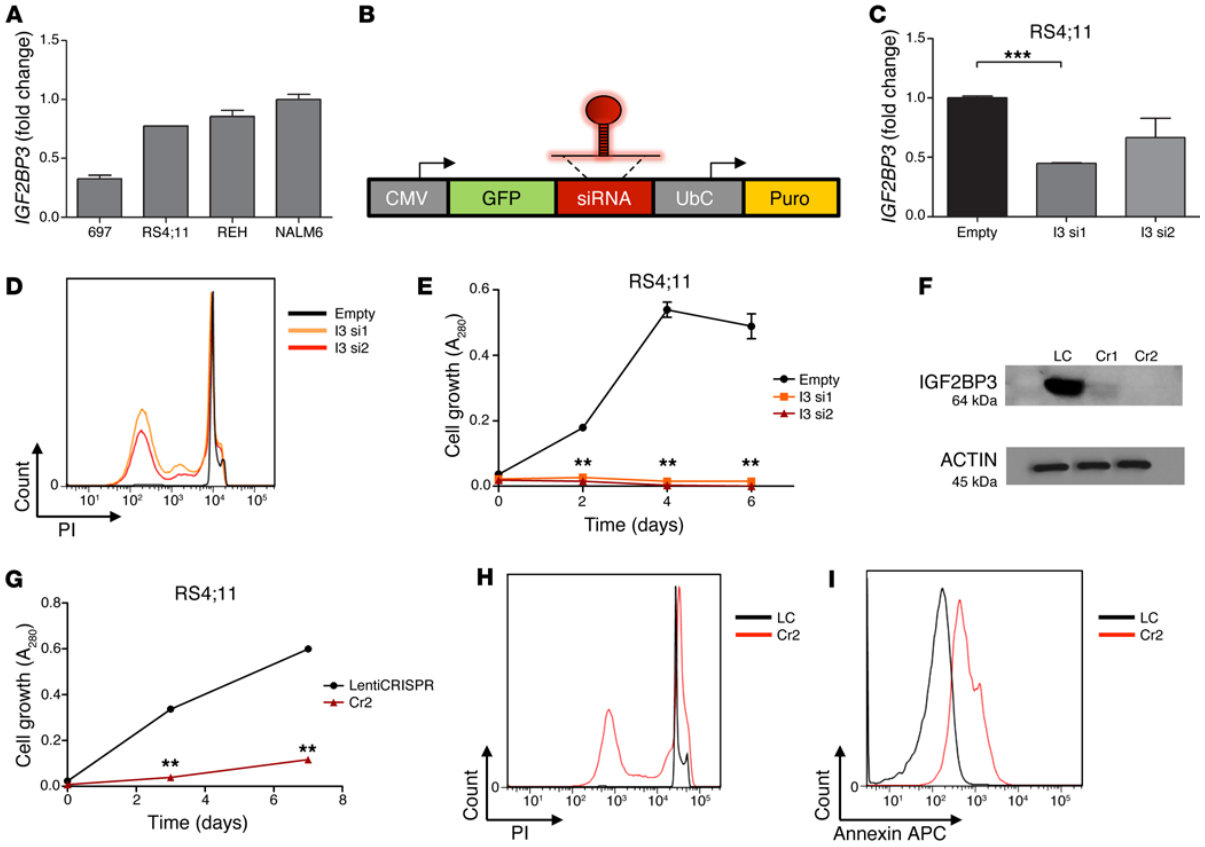

Figure 2. IGF2BP3 knockdown leads to disruptions of cell growth and increased apoptosis. (**A**) *IGF2BP3* expression in human B-ALL cell lines. (**B**) Schematic of lentiviral vector used for IGF2BP3 knockdown. (**C**) *IGF2BP3* knockdown, measured by qPCR shown in RS4;11 cell line (*t* test; ***P = 0.0005). (**D**) Cell cycle analysis with propidium iodide staining. (**E**) MTS assay showing significantly reduced cell proliferation with IGF2BP3 knockdown. (**F**) Western blot showing IGF2BP3 expression after CRISPR-Cas9–mediated targeting using the Cr1 or Cr2 constructs. Cr1-mediated targeting results in some residual protein. β-Actin is used as a loading control. (**G**) MTS assay showing significantly reduced cell proliferation after Cr2 targeting (*t* test; **$P \leq 0.01$ for all marked comparisons). (**H**) Cell cycle analysis by propidium iodide staining showing increased cell death (sub-G1 peak) in Cr2-expressing cells. (**I**) Increased annexin V staining in Cr2-targeted cells with IGF2BP3 KO. I3, IGF2BP3. Experiments were conducted 3× for validation. Data represent mean ±SD. See also Supplemental Figure 2. UbC, ubiquitin C promoter; Puro, puromycin; LC, lentiCRISPR control.

the B cell and myeloid cell counts in the peripheral blood following complete engraftment (Figure 3, H and I). There was no difference in the number of T cells in the periphery (Figure 3J). Interestingly, the number of platelets and red blood cells were significantly lower with IGF2BP3-enforced expression (Figure 3, K and L). Together these findings suggest that IGF2BP3 promotes overall hematopoietic output from the BM and skews BM development toward the B cell/myeloid lineage and away from T-cells, erythroid cells, and megakaryocytes. These findings, notably the preferential increase in B cells and myeloid cells, are interesting in light of the fact that MLL rearrangements are found not only in B-ALL, but also in acute myeloid leukemia and mixed lineage acute leukemia, most commonly expressing both B cell and myeloid markers.

Enforced expression of IGF2BP3 leads to increased progenitors in the BM with higher rates of proliferation. To further characterize these hematopoietic changes, IGF2BP3-overexpressing mice were sacrificed and hematopoietic organs were collected for analysis at 6 months after transplant. The percentage of GFP$^+$ cells was significantly higher in the IGF2BP3-overexpressing BM, similar to the peripheral blood (Supplemental Figure 3, A and B). The overall proportion of myeloid and B cells in the BM were similar between control and IGF2BP3-expressing mice (Supplemental Figure 3, C and D). qPCR from the RNA collected from the mouse BM confirmed human and mouse IGF2BP3 overexpression (Supplemental Figure 3, E and F). These changes led us to query whether there were changes in hematopoietic progenitors in the BM. Indeed, enforced expression of IGF2BP3 led to an increase in the fraction of HSCs, lymphoid-primed multipotent progenitors (LMPPs), and common lymphoid progenitors (CLPs) (Figure 4, A–C). We followed the developmental pathway of B cells by following the schema created by Hardy et al. (25). Among the Hardy fractions, we observed a significant increase in the number of cells in fractions A and B with no significant differences observed in developmentally subsequent stages (Supplemental Figure 3, H, I, and K). Hence, overexpression of IGF2BP3 led to an increase in immature hematopoietic fractions starting at the level of the HSC and on to

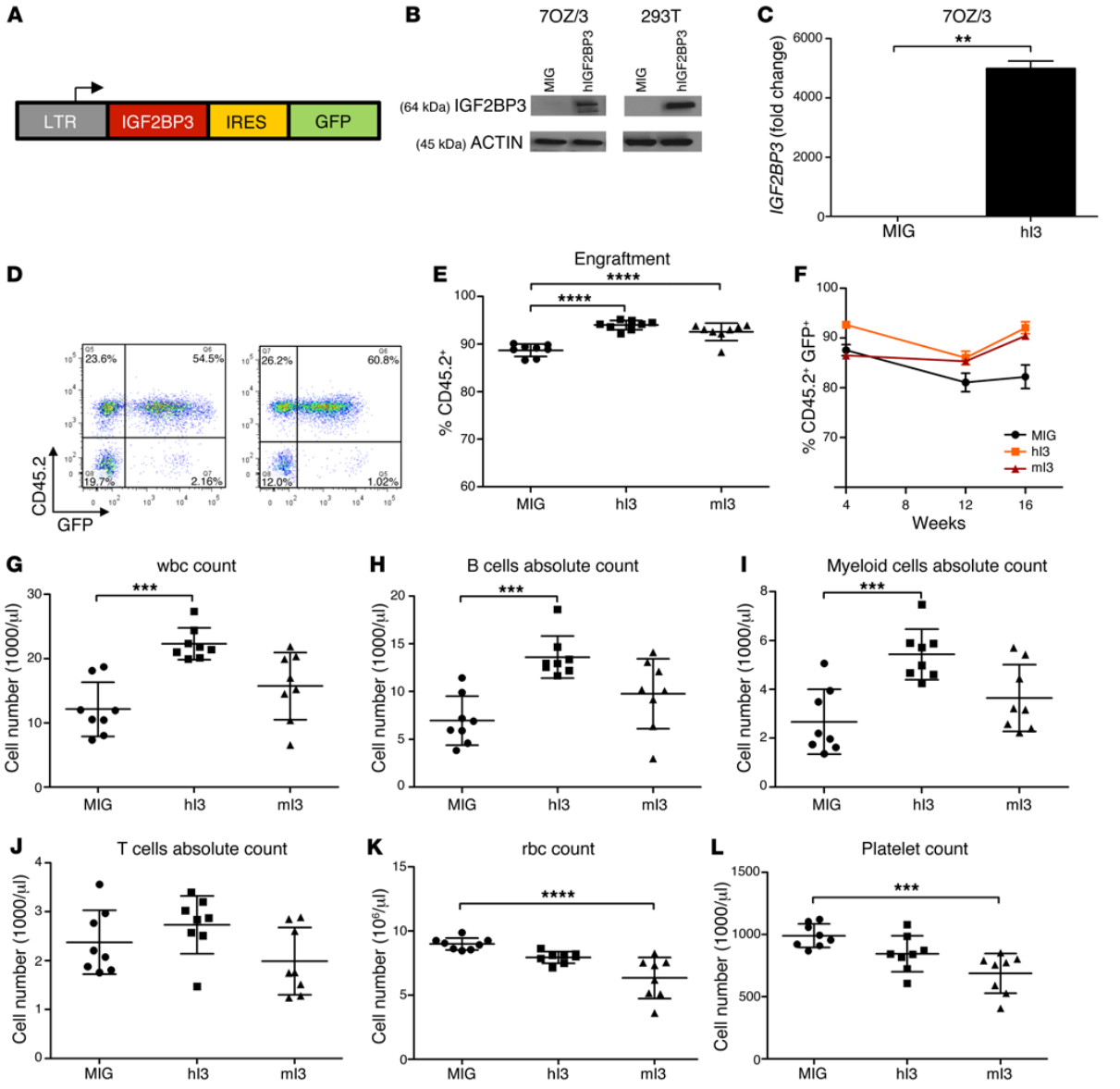

Figure 3. Enforced expression of IGF2BP3 leads to enhanced engraftment and skewing toward B cell/myeloid development. (**A**) Schematic of the bicistronic vector used for enforced expression of IGF2BP3. (**B**) Western blot showing overexpression of IGF2BP3 in the murine pre–B cell line, 7OZ/3, and the human embryonic kidney cell line, 293T. (**C**) qPCR showing overexpression in 7OZ/3 at the mRNA level (*t* test; $^{**}P = 0.0013$). (**D**) FACS analysis of PB from mice 6 weeks after BMT showing successful engraftment and transduction (GFP^+). (**E**) FACS of PB done at 4 weeks after BMT, showing CD45.2 and GFP positivity (one-way ANOVA followed by Bonferroni's test; $^{****}P < 0.0001$). (**F**) Quantitation of GFP expression in the PB between 4 and 16 weeks after transplant shows that the effect is marked and sustained. (**G**) PB leukocyte counts at 16 weeks show increased leukocytes (one-way ANOVA with Bonferroni's test; $^{***}P < 0.001$). (**H** and **I**) Significantly higher numbers of $B220^+$ cells (**H**) and $CD11b^+$ cells (**I**) in PB (one-way ANOVA with Bonferroni's test; $^{***}P < 0.001$). (**J**) FACS-based enumeration of T cells shows no significant change in circulating T cells. (**K** and **L**) Enumeration of RBCs and platelets by CBC show significant reductions (one-way ANOVA with Bonferroni's test; $^{***}P < 0.001$, $^{****}P < 0.0001$). $n = 8$ for all 3 groups. PB, peripheral blood; BMT, BM transplantation; hI3, human IGF2BP3; mI3, murine IGF2BP3; CBC, complete blood count; LTR, long terminal repeat; IRES, internal ribosome entry site. Three separate BMT experiments were completed for validation. Data represent mean ±SD.

the pro–B cell stage. To analyze the proliferation rate of the various progenitor cells in the BM, we performed intracellular staining with Ki67 in conjunction with progenitor cell stains. Ki67 was significantly higher in $Lin^-Sca1^+c\text{-}Kit^+$ (LSK) population and the LMPPs in IGF2BP3-overexpressing BM (Figure 4, D and E). The CLPs did not show a significant difference in Ki67 expression (Supplemental Figure 3, G and J). These findings imply an increase in the proliferation rate of the early progenitors (HSCs and LMPPs),

secondary to increased IGF2BP3 expression. Presumably, this leads to an increase in their numbers and differentiation into more committed downstream progenitors (CLPs and Hardy fractions A and B). Hence, the enforced expression of IGF2BP3 causes a preferential increase in numbers and proliferation of early progenitor populations, leading to the observed B cell– and myeloid biased leukocytosis seen in the periphery.

IGF2BP3 increases the number of B cells in the thymus and myeloid cells in the spleen. The normal mouse thymus is composed mostly of T cell progenitors, but in many murine models of leukemia and lymphoma, it becomes enlarged and overrun by malignant leukocytes (26). On microscopic examination, IGF2BP3 caused thymic medullary expansion with infiltration by large cells. One of the thymi expressing human IGF2BP3 had complete ablation of the cortico-medullary junction (Figure 5A). Hence, IGF2BP3 expression may serve as a precursor to malignant transformation. We observed a significantly higher percentage of GFP^+B220^+ B cells in the thymus when human or mouse IGF2BP3 was overexpressed, with the effect being more pronounced with mouse IGF2BP3 (Figure 5, B and C). Mice with enforced expression of mouse IGF2BP3 also showed a substantial decrease in the number of $CD3\varepsilon^+$ T cells. There was no significant difference in the level of GFP^+ cells in these thymi, indicating a lineage-specific expansion of B cells (Supplemental Figure 4, G–I). Four of 8 of the thymi overexpressing human IGF2BP3 and 1/8 of the thymi overexpressing mouse IGF2BP3 weighed over 50 mg, with no such increase in control mice (data not shown). Interestingly, the spleens were also enlarged following enforced expression of IGF2BP3. Differences in splenic weight were statistically significant for mice with overexpression of human IGF2BP3 with a trend noted for the mouse IGF2BP3 group (Supplemental Figure 4A). IGF2BP3 led to an increase in the number of myeloid cells in the spleen with a significant decrease in the number of $CD3\varepsilon^+$ T cells (Supplemental Figure 4, B–F). Overall, IGF2BP3 appears to tilt the hematopoietic developmental program toward the B cell and myeloid lineages. Hence, the changes seen in the BM — increased numbers and proliferation of B-lymphoid and myeloid progenitors — may result in alterations in hematopoietic homeostasis in the periphery.

IGF2BP3 provides hematopoietic progenitors with a survival advantage. To confirm that IGF2BP3 overexpression equipped the BM progenitors with an advantage while repopulating the irradiated host mouse BM, we performed a formal competitive repopulation transplant assay. Fifty percent of CD45.1 BM cells were mixed with 50% of MIG or IGF2BP3- or HOXA9-overexpressing CD45.2 BM cells and injected into lethally irradiated mice. The IGF2BP3-overexpressing CD45.2 cells had a clear advantage over the MIG- or MIG-HOXA9–expressing cells in engraftment in the peripheral bleeds over time (Figure 5, D and E). Harvesting of the BM revealed that IGF2BP3 conferred a competitive advantage to cells in the BM (Figure 5F). This was also reflected in the thymus (Figure 5G). This corroborates our earlier data showing IGF2BP3 overexpression (Figure 5H) leading to an increase in BM progenitor numbers as well as proliferation rate.

iCLIP identifies the IGF2BP3-RNA interactome in B-ALL cells. The molecular basis of the action of RBPs has recently been investigated using iCLIP and high throughput sequencing. To gain insight into the role of IGF2BP3 in cell growth and MLL-driven leukemogenesis, we performed an iCLIP assay with this protein. iCLIP exploits the photoreactivity of nucleic acid and protein residues and nuclease fragmentation of protein-bound transcripts to capture protein-RNA interactions occurring in situ. Antibodies against IGF2BP3 were used to immunoprecipitate protein-RNA complexes from control or UV-irradiated RS4;11 and REH cells (input shown in Supplemental Figure 5, A and C). As expected, the immunoprecipitated material was antibody dependent and UV dependent, and the electrophoretic mobility of the complex was nuclease sensitive, as predicted for a protein-RNA complex (Supplemental Figure 5, B and D). Coprecipitated RNA was converted to cDNA libraries (Supplemental Figure 5E) and subject to high throughput sequencing. After accounting for PCR duplications, we obtained about 1 million reads per replicate, of which >70% mapped uniquely to the human genome (Supplemental Table 1). Replicate iCLIP sequences from both RS4;11 and REH cells were highly reproducible (Supplemental Figure 6, D and E). Compared with iCLIP cross link sites for heterogeneous ribonucleoprotein A1 (hnRNPA1; HEK cells) and with simulated data drawn randomly from the genome, IGF2BP3 cross-link sites, located at the 5′ end of the iCLIP sequences, were enriched in exons (Figure 6A).

We identified peaks using a negative binomial model (see Methods) in each biological replicate from RS4;11 and REH cells. In total, 849 peaks in 669 genes and 1,937 peaks in 1,149 genes were identified in REH and RS4;11 iCLIP experiments, respectively. Of the peaks called within mRNA sequences, the majority were located within the 3′UTRs (Figure 6B and Supplemental Figure 6, A–C). A search for sequence specificity in cross-linked regions revealed an 8- to 16-fold enrichment of GCAC tetramer–containing motifs over background in both the REH and RS4;11 datasets (Figure 6C). Given the apparent bias of IGF2BP3 binding sites in 3′UTR of target transcripts, we investigated the positional bias of cross-linking sites at a single nucleotide resolution relative to mRNA stop codons. The cross-link density of IGF2BP3 differed from hnRNPA1 in the 3′UTR, reaching its apex just downstream of the stop codon. These data suggested that IGF2BP3 binding sites within the 3′UTR specifically target sequences close to the stop codon in both B-ALL cell lines (Figure 6D).

Based on the distribution of IGF2BP3 cross-linking sites within 3′UTRs (Figure 6D), we hypothesized that IGF2BP3 binding sites may overlap with *cis*-regulatory features associated with 3′UTR-mediated gene regulation. To investigate this possibility, we examined the distribution of IGF2BP3 cross-linking sites relative to miR target sites in the 2 different cell lines. After correcting for the uniform background distribution of simulated cross-link sites, we found that IGF2BP3 cross-link density in both REH and RS4;11 cell lines is highly enriched within a 25-bp window centered on predicted miR target sequences (Figure 6E). By contrast, the density of hnRNPA1 cross-linking sites were uniformly distributed relative to miR target sites. Among the genes with a strong signal by iCLIP-sequencing (CLIP-Seq) were *CDK6* and *MYC*. To confirm our findings demonstrating interaction of IGF2BP3 with these 2 targets by iCLIP (Figure 6, F and G), we utilized RNA immunoprecipitation (RIP; Figure 6H), which showed enrichment of *MYC* and *CDK6* (Figure 6I) in IGF2BP3 RIPs over mouse IgG control. These data demonstrate, for the first time to our knowledge, a comprehensive IGF2BP3 RNA interaction site atlas from human leukemia

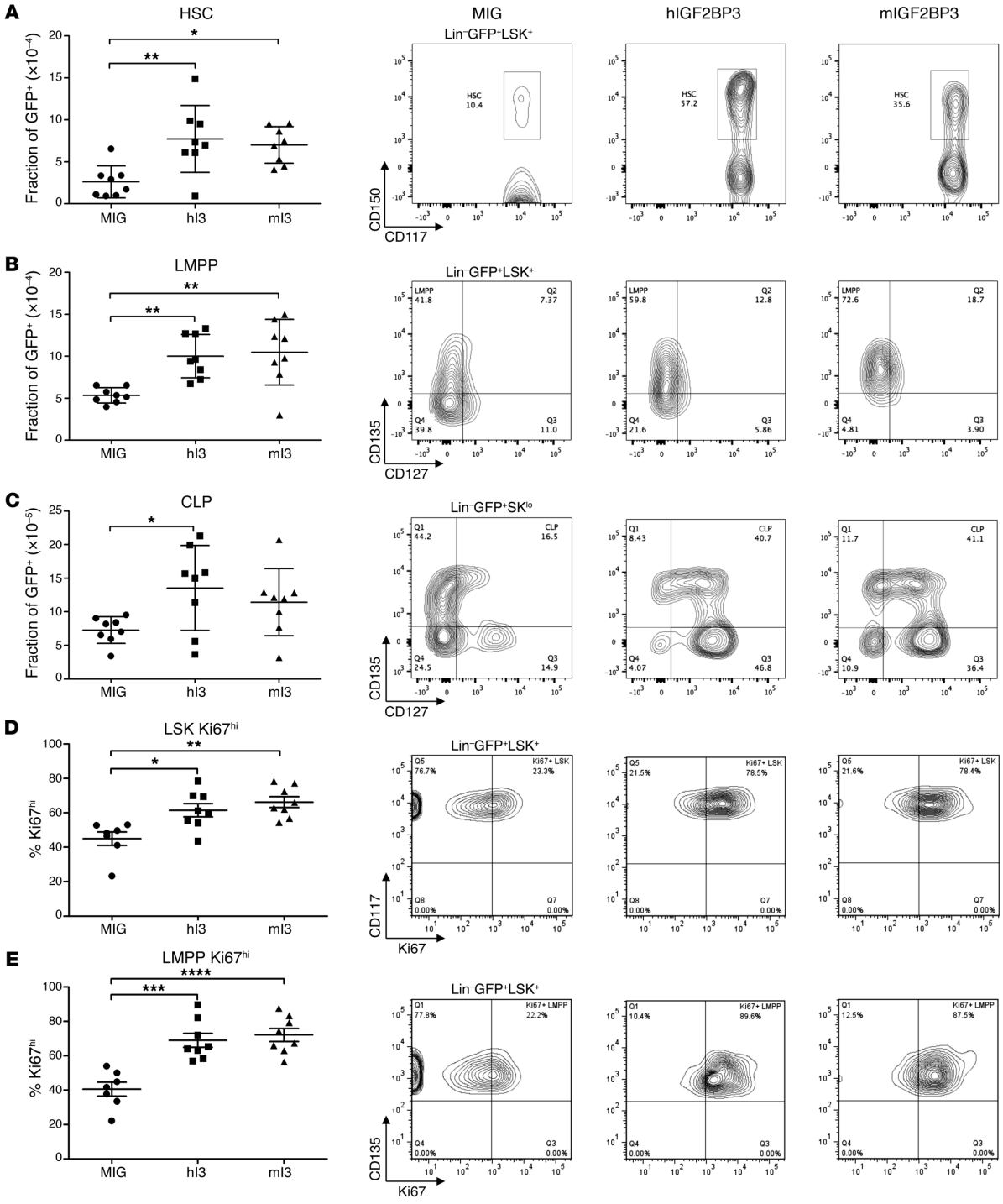

Figure 4. Analysis of BM progenitor populations from IGF2BP3-overexpressing mice. (**A**) Enumeration (left panel) and representative flow cytometry histograms to define HSCs from control vector– (second panel from left), human IGF2BP3– (second from right), and murine IGF2BP3–overexpressing mice (right panel). (**B** and **C**) Analysis for LMPPs and CLPs from mice noted as in **A**. Statistically significant differences were found in LMPPs and CLPs. (**D**) Intracellular Ki67 staining and FACS-based analyses, depicted in the same manner, with enumeration on the left hand side, within the LSK population enriched for HSCs. Significant differences in the high Ki67-expressing population were found. (**E**) Intracellular Ki67 staining and FACS analysis of proliferation in the LMPP population shows significant differences in the proliferative fraction. All comparisons used one-way ANOVA followed by Bonferroni's test. *$P < 0.05$; **$P < 0.01$; ***$P < 0.001$; ****$P < 0.0001$. LSK, Lin$^-$Sca1^{hi}c-Kit^{hi}. Three separate BMT experiments were completed for validation. Data represent mean ±SD. See also Supplemental Figure 3. hI3, human IGF2BP3; mI3, murine IGF2BP3.

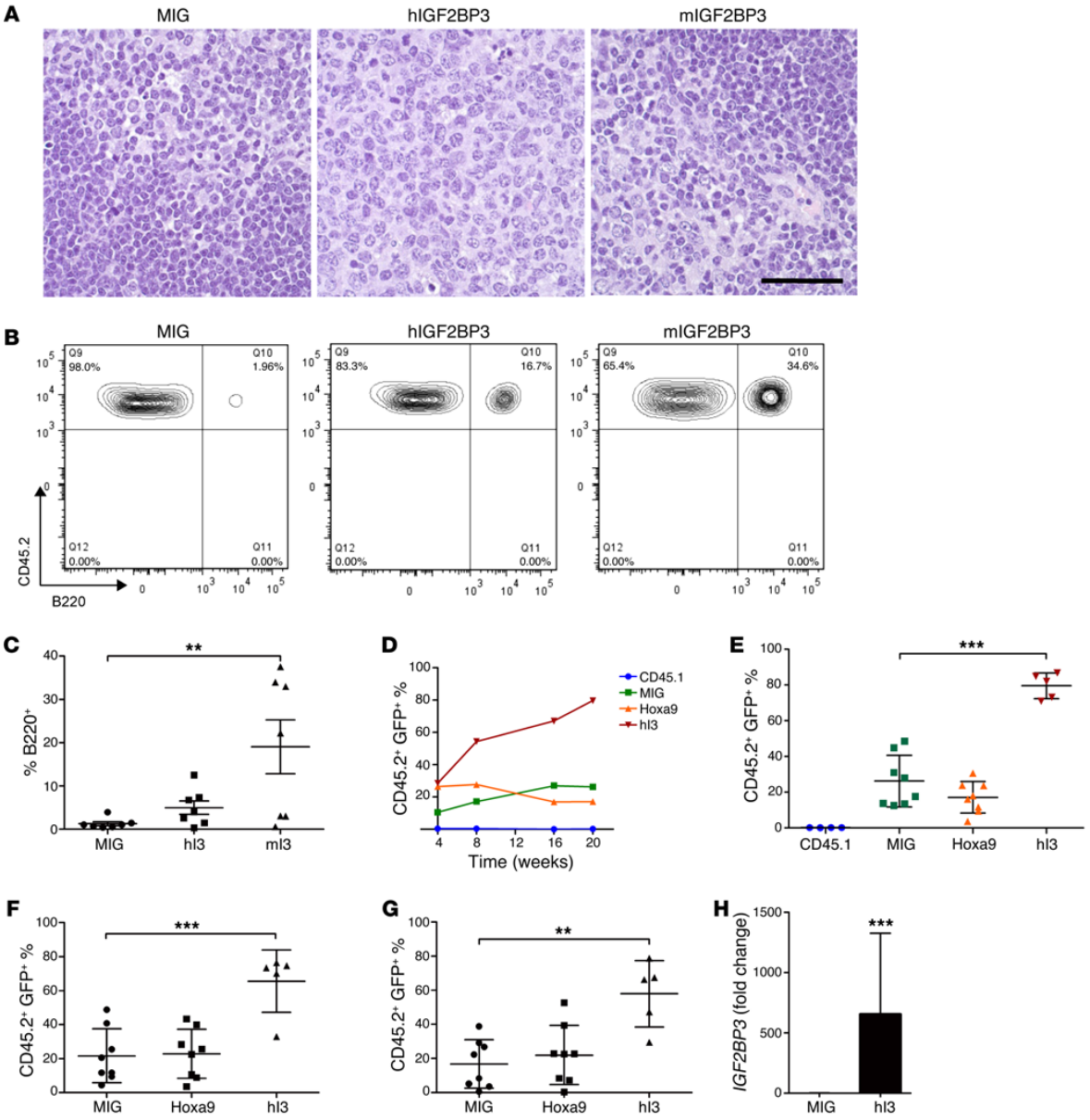

Figure 5. Analysis of thymic cellular composition and competitive repopulation advantage from IGF2BP3-overexpressing mice. (**A**) Histologic images of thymic sections from mice with enforced expression of IGF2BP3. H&E staining. Scale bar: 40 μm. (**B** and **C**) Representative FACS plots and enumeration showing an increase in B220+ cells in the thymus of mice with enforced expression (one-way ANOVA with Bonferroni's test; $^{**}P < 0.01$). See also Supplemental Figure 4. $n = 8$ for all 3 groups. Three separate BMT experiments were completed for validation. (**D**–**H**) Competitive repopulation study. (**D**) Quantitation of GFP expression in the PB between 4 and 20 weeks after transplant in competitive repopulation study of IGF2BP3. (**E**–**G**) FACS of PB (**E**), BM (**F**), and thymus (**G**) done at 20 weeks after BMT, showing CD45.2 and GFP positivity (one-way ANOVA followed by Bonferroni's test; $^{**}P < 0.01$, $^{***}P < 0.001$). (**H**) qPCR confirmation of overexpression of *IGF2BP3* in mouse BM (*t* test; $^{***}P = 0.0006$). $n = 8$ (MIG), $n = 8$ (Hoxa9), $n = 5$ (hI3), and $n = 4$ (100% CD45.1). Competitive repopulation study was completed 3× for validation. Data represent mean ±SD. hI3, human IGF2BP3; mI3, murine IGF2BP3; PB, peripheral blood.

cells. This extensive interaction map reveals a strong preference of IGF2BP3 binding nonuniformly to 3′UTRs with a preference for a GCAC-rich consensus motif near miR target sites.

IGF2BP3 modulates the expression of its targets. The ENRICHR tool (27) was used to functionally classify *IGF2BP3* mRNA targets in REH and RS4;11 cells. In both cell lines, we found that target transcripts were enriched for KEGG pathways related to ribosome biogenesis and translation (Supplemental Table 2). By contrast, transcripts classified by ENRICHR as involved in pathogenic *E. coli* infection, and perhaps most importantly, chronic myeloid

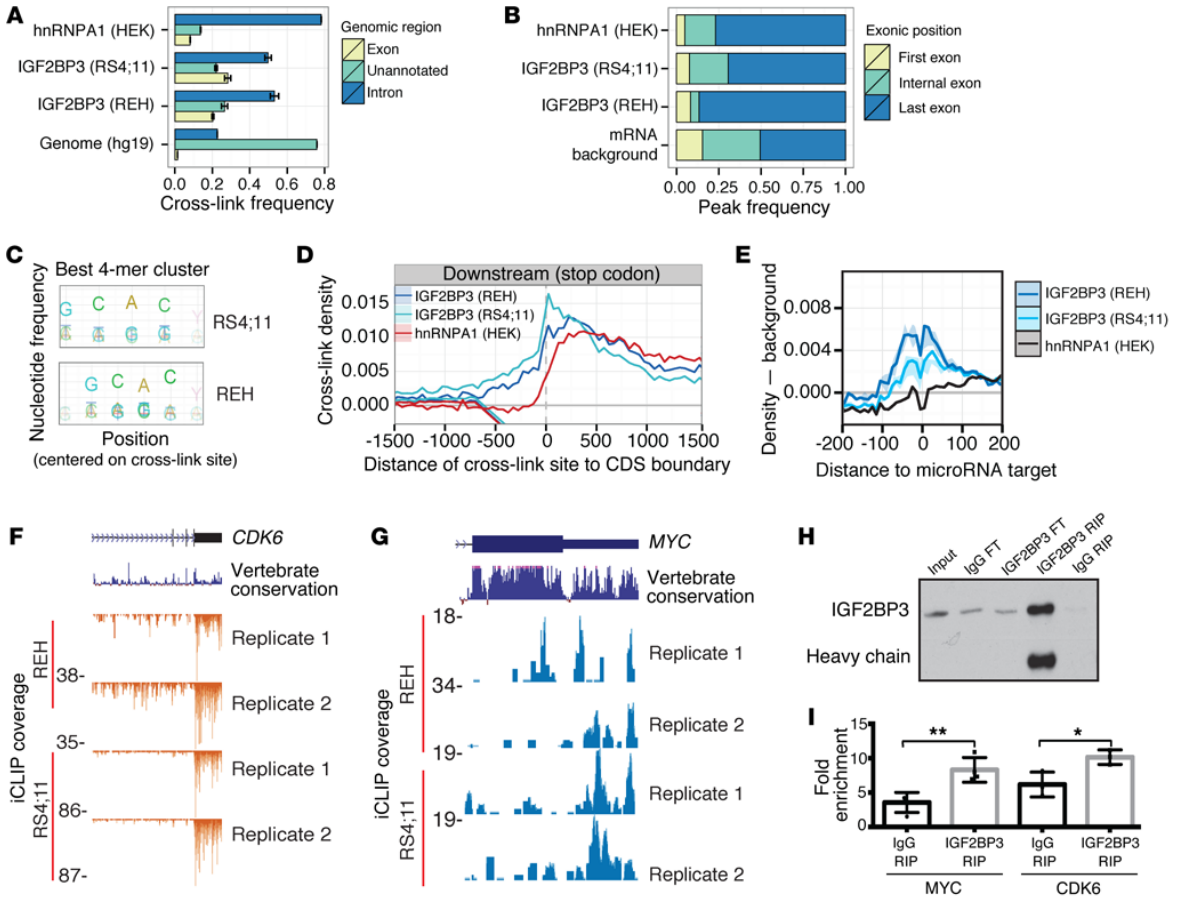

Figure 6. iCLIP analysis of IGF2BP3 in human leukemia cell lines. (**A**) Proportion of IGF2BP3 (REH and RS4;11 cells), hnRNPA1(HEK cells), and simulated (Genome) cross-linking sites observed in exons, introns, or unannotated regions of the human genome. (**B**) Proportion of IGF2BP3 (REH and RS4;11 cells), hnRNPA1 (HEK cells), and simulated (mRNA background) binding sites in coding and noncoding exons. (**C**) Tetramer sequence enrichment at IGF2BP3–cross-linking sites in RS4;11 and REH cells (upper and lower panel, respectively). (**D**) IGF2BP3 (REH, RS4;11) and hnRNPA1 (HEK cells) cross-link site density relative to termination codons. (**E**) IGF2BP3 cross-linking density from REH (dark blue line) and RS4;11 (light blue line) cell lines mapped relative to annotated miR target sites. hnRNPA1 (black line) cross-linking sites from HEK293 cells are included as a control. (**F** and **G**) UCSC Genome Browser snapshot of the *CDK6* and *MYC* 3′UTR loci, respectively. Each panel shows the exon-intron structure of the gene, sequence conservation across vertebrate species, and unique read coverage from 2 iCLIP replicates from each cell line. The maximum number of reads at each position is indicated to the left of each histogram. See also Supplemental Figures 5 and 6. (**H**) Western blot of protein samples from IGF2BP3 RIP. Input refers to RS4;11 cell lysate used for immunoprecipitation. FT is flowthrough of immunoprecipitation from either control (mouse IgG) or IGF2BP3 RIP. RIP is RNA immunoprecipitation from control (mouse IgG) or α-IGF2BP3 antibody (D-7). (**I**) Scatter bar plots comparing the fold-enrichment for *MYC* ($n = 4$, t test; $^{**}P < 0.01$) and *CDK6* ($n = 3$, t test; $^{*}P < 0.05$) in control (mouse IgG) and α-IGF2BP3 antibody RNA immunoprecipitations. Levels of *MYC* and *CDK6* are normalized to input levels from total RNA with 18s rRNA as reference.

leukemia (CML) were enriched in RS4;11 but not the REH dataset (Supplemental Table 2). Hence, we wanted to further explore the functional consequences of IGF2BP3 binding on gene expression at the global level. To determine if IGF2BP3 iCLIP targets (Supplemental Table 3) are regulated by IGF2BP3 expression levels, we performed RNA-Seq on control and IGF2BP3-depleted RS4;11 cells (Supplemental Table 4). Cross-validation of genes differentially expressed by at least 1.5-fold with RS4;11-specific IGF2BP3 iCLIP targets found 216 common genes. Of these targets, the majority showed decreased expression of IGF2BP3 iCLIP targets with IGF2BP3 depletion (157 decreased vs. 59 increased; Figure 7A). Using the ENRICHR tool to classify the common genes cohort, OMIM disease gene ontology analysis (GO analysis) revealed genes associated with leukemogenesis (Figure 7A; black circles), including *CDK6* and *MYC*. GO analysis for downregulated IGF2BP3 iCLIP targets revealed genes associated with posttranscriptional control, hematopoietic cell differentiation, and chromatin modification (Figure 7C). KEGG Pathway analysis also suggested these targets are involved in cell cycle and a variety of cancer pathways (Figure 7C). By contrast, the upregulated IGF2BP3 iCLIP targets revealed genes primarily associated with translation and protein localization (Figure 7B).

CDK6 and MYC mRNAs are targets of IGF2BP3 in vitro and in vivo. Among the many IGF2BP3 mRNA targets, *CDK6* and *MYC*

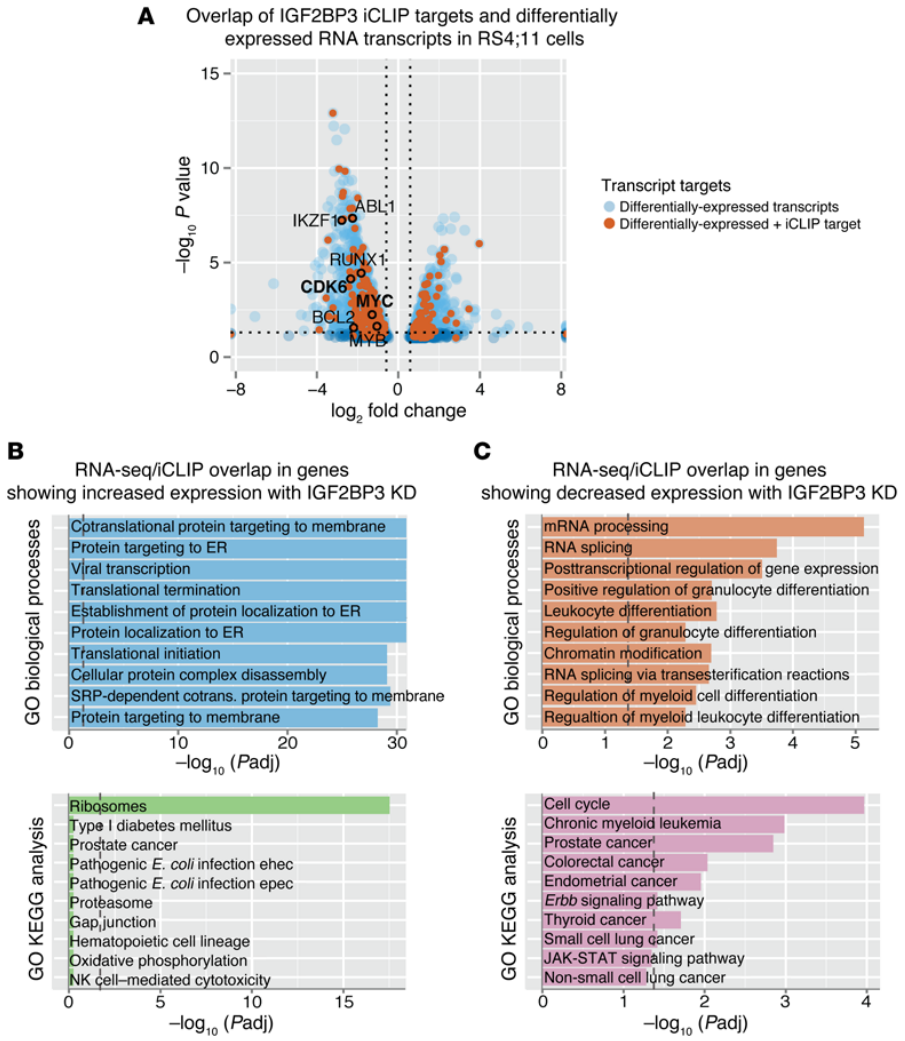

Figure 7. Cross-validation of IGF2BP3 iCLIP targets with IGF2BP3-sensitive differentially expressed genes. (**A**) Volcano plot of differentially expressed genes (blue dots) determined using DESeq analysis on RNA-Seq samples from control and IGF2BP3 knockdown RS4;11 cells (as described in Figure 2). Differentially expressed genes identified as IGF2BP3 targets by iCLIP are highlighted (orange dots). Dots demarcated by black outlines are leukemogenic genes by GO analysis of OMIM-associated disease pathways. Dotted lines represent 1.5-fold–change in expression (vertical lines) and $P < 0.05$ cutoff (horizontal line). (**B** and **C**) GO analysis of gene subgroups showing increased expression (**B**) and decreased expression (**C**) with IGF2BP3 knockdown using ENRICHR gene list enrichment analysis webtool. Term lists used in this analysis were GO_Biological_Processes and KEGG to determine enriched processes and pathways from our cross-validated list of 269 IGF2BP3-targeted and -sensitive genes. Vertical dotted lines represent *P* value cutoff ($P < 0.05$). KD, knockdown.

are very important in the pathogenesis of MLL-translocated B-ALL (6, 7). In our patient data set, MLL-translocated cases of B-ALL demonstrated high levels of these genes, in line with their proposed role as targets bound by and regulated by IGF2BP3 (Supplemental Figure 1, A and B). To test the hypothesis that IGF2BP3 posttranscriptionally regulates the expression of *CDK6* and *MYC* via binding sites in their 3′UTR, we generated a series of vectors using a dual-luciferase reporter system containing the respective UTRs (Figure 8A). The *CDK6* 3′UTR (10 kb) was cloned in 5 separate pieces (CDK6-1 to CDK6-5). Cotransfection of the luciferase vectors with IGF2BP3 resulted in increased luciferase activity in CDK6-3 to CDK6-5, as well as the *MYC* 3′UTR reporters (Figure 8B). This, along with the iCLIP and RNA-Seq data, confirms IGF2BP3 binding to the 3′UTRs of these genes may stabilize the mRNA and/or enhance translation. Mutation of one of the binding sites within the *MYC* 3′UTR, designated MYC Δ3, resulted in a small but reproducible attenuation of IGF2BP3-dependent enhancement of the *MYC* 3′UTR reporter (Figure 8C). However, mutation of individual IGF2BP3 binding sites in the *CDK6* 3′UTRs, followed by IGF2BP3 overexpression and a luciferase assay, did not show any significant difference (data not shown). These findings may result from one of the following possibilities: (i) binding may not be sufficient for alterations of gene expression, or (ii) cooperative binding at multiple sites may be required for an effect on gene expression. Indeed, some parallels have been seen in the case of miRs, where increased repression is seen in targets with multiple binding sites (28). Nonetheless, IGF2BP3 binding would be predicted to lead to increased levels of CDK6 and MYC in cells overexpressing IGF2BP3 and to decreased levels in knockdown cells.

To elucidate whether IGF2BP3 targets CDK6 and MYC in vivo, we performed intracellular staining in BM cells from mice with enforced IGF2BP3 expression and measured mean fluorescence intensity (MFI) by flow cytometry. BM GFP^+ cells derived from human IGF2BP3–expressing mice had increased MFI for CDK6 and MYC (Figure 8, D and F). As a control, GFP^- cells of both groups did not show any difference (Figure 8, E and G). To complement these in vivo data, we analyzed CDK6 and MYC protein levels in cell lines where IGF2BP3 was knocked down using

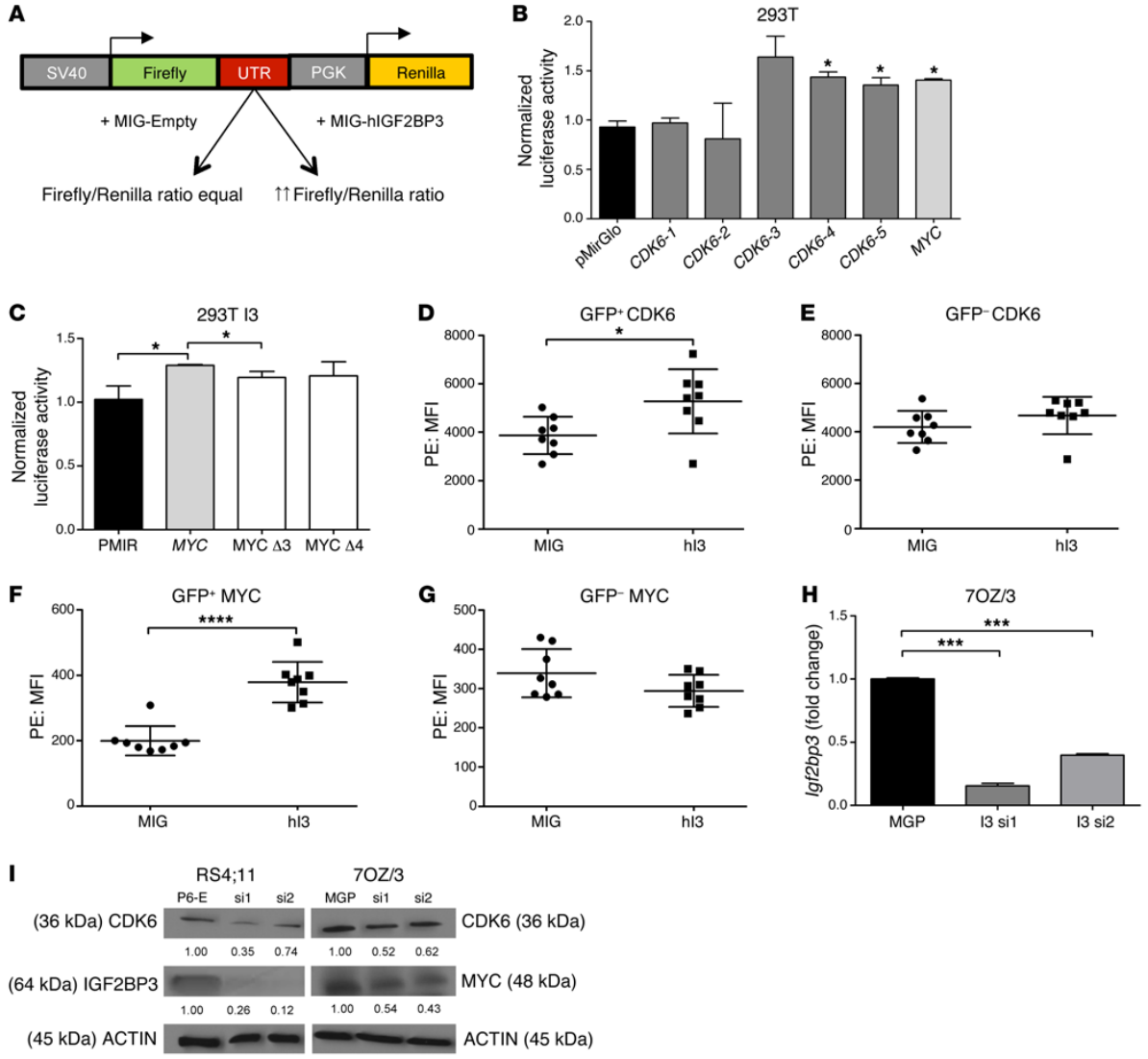

Figure 8. CDK6 and MYC are targeted by IGF2BP3. (**A**) Schematic of the luciferase assay used. (**B**) Luciferase assay showing targeting of the *CDK6* and *MYC* 3′UTRs by IGF2BP3 (*t* test **P* = 0.05; *P* = 0.0250 CDK6-4, *P* = 0.0475 CDK6-5, *P* = 0.0165 MYC). (**C**) Deletion of the *MYC* 3′UTR binding sites of IGF2BP3 led to modest but significantly decreased luciferase activity (*t* test **P* = 0.05; *P* = 0.0120 MYC, *P* = 0.0294 MYC Δ3). (**D** and **E**) CDK6 analysis of BM progenitors shows a significantly increased amount of CDK6 protein in the GFP⁺ BM cells (*t* test; **P* = 0.0213) (**D**) but not in the GFP⁻ (**E**) cells. (**F** and **G**) Intracellular staining for MYC reveals significantly increased levels in the GFP⁺ BM cells after IGF2BP3-enforced expression (*t* test; *****P* < 0.0001) (**F**) but not in the GFP⁻ (**G**) cells. *n* = 8 for all 3 groups. (**H** and **I**) After *Igf2bp3* knockdown in 7OZ/3 cells (*t* test IGF2BP3 si1 and si2, respectively; ****P* = 0.0007, ****P* = 0.0005), there is reduced expression of CDK6 and MYC protein (**H**). In the RS4;11 cell line, Western blot confirmed knockdown of IGF2BP3 protein and reduced expression of CDK6 protein (**I**). Experiments were conducted 3× for validation. Data represent mean ±SD. See also Supplemental Figure 7. hI3, human IGF2BP3; PE, phycoerythrin.

siRNAs previously. There was a substantial decrease in CDK6 protein levels in RS4;11 cells after IGF2BP3 knockdown (Figure 8I). Similarly, *Igf2bp3* knockdown in the murine pre–B 7OZ/3 cell line led to a reduction in CDK6 and MYC protein (Figure 8, H and I). These findings are in agreement with the RNA-Seq data and demonstrate a conserved function for IGF2BP3 (Figure 7A).

At the mRNA level, IGF2BP3 overexpression led to a slight but significant increase in *Myc* mRNA levels, but not in *Cdk6*, in bulk BM (Supplemental Figure 7, A and B). It is possible that an increase in *Cdk6* mRNA may not be detected due to the heterogeneity of the BM cells or because effects on mRNA stability by IGF2BP3 may be mRNA specific. Similarly, murine 7OZ/3 cells showed a modest increase in the *Cdk6* mRNA levels when murine IGF2BP3 was overexpressed (Supplemental Figure 7, C–E). These findings corroborate IGF2BP3 binding and subsequent translational augmentation of these target genes. Overall, these experiments

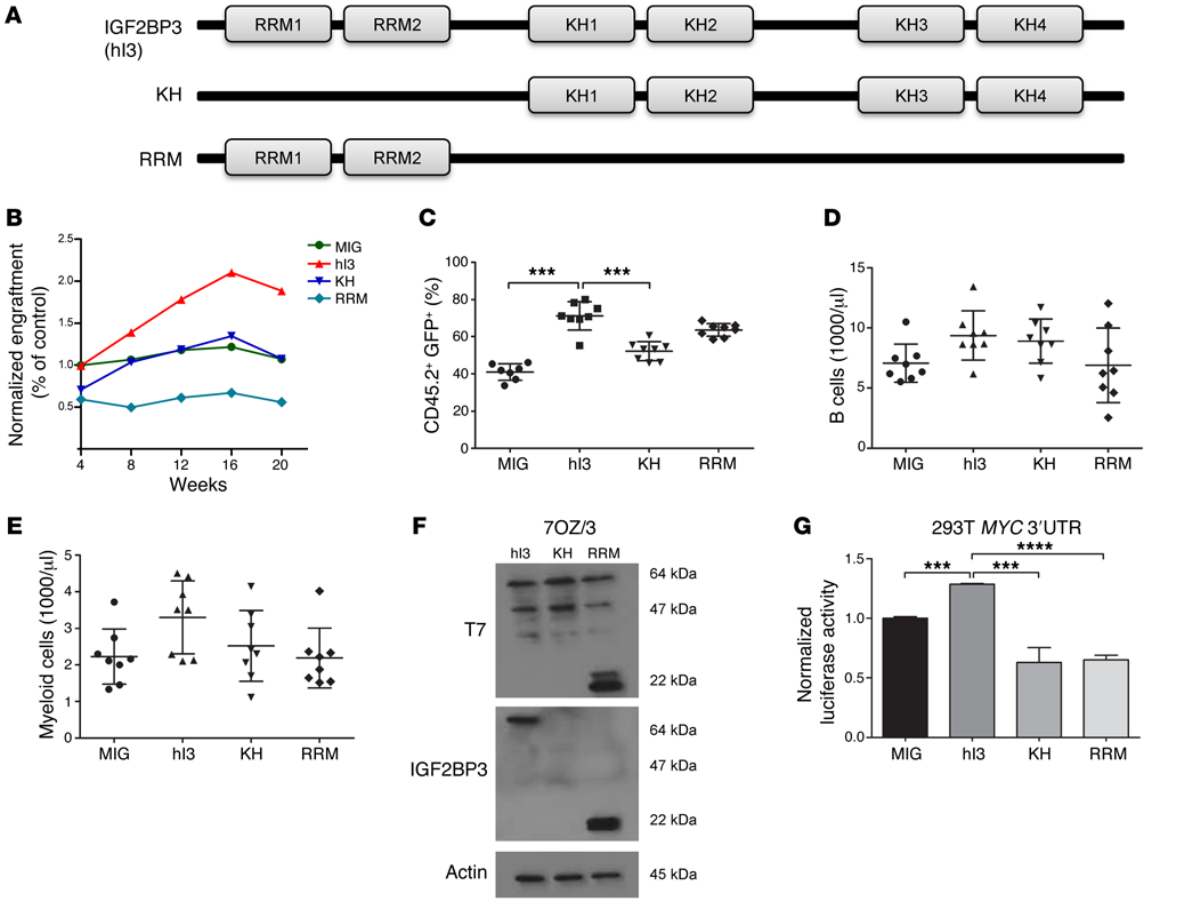

Figure 9. Expression of IGF2BP3 RNA-binding domain mutants in vivo and in vitro. (**A**) Schematic of IGF2BP3 with its binding domains and the respective mutants (KH and RRM). (**B**) Time course of normalized engraftment to MIG in PB between 4 and 20 weeks after transplant. (**C**) FACS of PB done at 4 weeks after BMT, showing CD45.2 and GFP positivity (one-way ANOVA followed by Bonferroni's test; ***$P < 0.001$). (**D**) B cells in PB 16 weeks after transplant. (**E**) Myeloid cells in PB 12 weeks after transplant. $n = 8$ for all groups. Mutant BMT experiment was completed twice for validation. (**F**) Western blot confirmed expression of IGF2BP3 (64 kDa), KH (47 kDa), and RRM (22 kDa) proteins in 7OZ/3 using anti-T7 (top panel) and anti-IGF2BP3 (bottom) antibodies. Actin used as a loading control. (**G**) Luciferase assay shows increased luciferase activity for the *MYC* 3′UTR when cotransfected with hI3 and decreased luciferase activity for the *MYC* 3′UTR when cotransfected with KH and RRM mutants (*t* test hI3, K,H and RRM; ***$P < 0.001$; ****$P < 0.0001$). Experiment was completed 3×. Data represent mean ±SD. hI3, human IGF2BP3; PB, peripheral blood.

demonstrate targeting of CDK6 and MYC by IGF2BP3 in a variety of systems, and that may underlie the observed phenotypic effects of enforced expression.

Mutated IGF2BP3 does not increase hematopoietic progenitor numbers in vivo. IGF2BP3 has 6 RNA-binding domains: 2 RNA recognition motif domain (RRM) and 4 K homology domain (KH) domains that are predicted to mediate the RNA-binding function of IGF2BP3. We created 2 deletion mutants: the KH mutant, containing only the 4 KH domains and devoid of both the RRM domains, and the RRM mutant, containing the 2 RRM domains and lacking the 4 KH domains (Figure 9, A and F). A murine BM transplant was performed with MIG, WT IGF2BP3, KH, and RRM mutants into lethally irradiated recipients. Unlike the WT protein, enforced expression of these mutant proteins failed to cause enhanced hematopoiesis or the skewing toward the B cell and myeloid lineages that we observed previously. The mutant recipient mice showed reduced engraftment (Figure 9, B and C). B cell and myeloid cell counts in the periphery showed a trend toward normalization in IGF2BP3 mutant mice (Figure 9, D and E). A luciferase assay using the *MYC* 3′UTR and comparing WT and mutant IGF2BP3 demonstrated decreased luciferase activity, confirming the idea that these mutants no longer bind to and/or stabilize target mRNAs (Figure 9G). Interestingly, one study reported that the role of KH domains is not well understood in IGF2BP3, among the various IGF2BP family members (29). Although the precise determinants of RNA binding are not known, our findings provide an impetus to perform detailed structure-function analyses to elucidate domains and residues important for IGF2BP3 function. Together with our high throughput data, these experiments provide some of the first comprehensive studies that link the RNA binding function of this protein to organism-level phenotypes.

Discussion

The molecular mechanism of leukemogenesis mediated by MLL-fusion proteins is not completely understood, despite knowledge of the translocation and the resulting fusion proteins for 2 decades. Increasingly, it is recognized that secondary, nongenetic changes are necessary for elaboration of leukemia. For example, deregulation of epigenetic marks by DOT1L, which is recruited by the MLL-AF4 fusion protein, is a key oncogenic mechanism (30). In this study, we found that an RBP, IGF2BP3, is overexpressed in cases of B-ALL that carry a translocation of the *MLL* gene. We propose that posttranscriptional gene expression dysregulation may also play an important role in leukemogenesis. This is borne out by prior studies of another RBP, musashi-2, which demonstrated that it was highly expressed in acute myeloid leukemia and that its overexpression could collaborate with BCR-ABL to promote myeloid leukemogenesis (31). Another recent example is the HuR protein, which is upregulated in multiple epithelial malignancies and is known to stabilize its targets by binding to AU-rich elements within the 3′UTR of target mRNAs (32). Our findings here extend the repertoire of dysregulated RBP expression to B-ALL, providing new insights into this disease.

The mechanism of IGF2BP3 upregulation in MLL-AF4–expressing leukemia is an important question. Our studies showed that a BET domain inhibitor could downregulate IGF2BP3 in RS4;11, and this is thought to specifically target MLL-mediated transcription at low doses (23). Previous reports have also shown IGF2BP3 to be upregulated after MLL-AF4 overexpression in murine BM cells (4). Interestingly, an indirect ChIP-Seq assay done in SEM cells (which carry the MLL-AF4 translocation) showed binding of the fusion protein to the genomic locus containing IGF2BP3 (33). Therefore, it is tempting to speculate that *IGF2BP3* is a direct transcriptional target of MLL fusion proteins. However, IGF2BP3 is also overexpressed in most of the B-ALL cell lines tested, various mature B cell neoplasms (34–37), and a number of epithelial malignancies. Furthermore, differential regulation of this protein has been observed in B-ALL (38). Hence, the mechanism of its upregulation may include other oncogenic pathways.

Previously, knockdown of IGF2BP3 in epithelial cell lines has been shown to reduce cell proliferation and cause apoptosis (18, 37, 39). We found that knockdown or deletion of IGF2BP3 by siRNA or by the CRISPR-Cas9 system led to reduced cell proliferation and increased apoptosis in RS4;11, an MLL-AF4–expressing cell line, and NALM6, another B-ALL cell line that shows high levels of IGF2BP3. These findings highlight the important role that posttranscriptional gene regulation can play in maintaining the malignant behavior of B-ALL cells. It will be of great interest to study whether B-ALL with low expression levels of IGF2BP3 demonstrate an altered RNA-binding repertoire, with an aim toward illuminating key mRNAs that mediate downstream effects of IGF2BP3.

To study the pathogenetic function of this protein, we also created the first in vivo model of IGF2BP3-enforced expression in the murine hematopoietic system. We found that IGF2BP3 increases the number of HSCs, LMPPs, and CLPs in the BM with a concomitant increase in the proliferation rate of HSCs and LMPPs. IGF2BP3 conferred a competitive reconstitution advantage and skewed mouse hematopoiesis toward the B cell and myeloid lineage in the periphery, with leukocytosis in the peripheral blood, atypical B cell infiltration into the thymic medulla, and increased myeloid cells in the spleen. Although the mice did not develop overt leukemia by 6 months after transplantation, these abnormal developmental features are similar to those seen early in MLL-driven leukemogenesis, which include the expansion of the B cell and myeloid lineage. Such IGF2BP3-driven effects on stem and progenitor cells and differentiation fates may extend beyond the hematopoietic system. IGF2BP3 can cause remodeling of the exocrine pancreas when specifically overexpressed in that tissue and is highly expressed in cancer stem cells/tumor-initiating cells in hepatocellular carcinoma (40, 41).

It has been known that IGF2BP3 targets mRNAs for *IGF2*, *CD44*, and the transcription factor *HMGA2* (16, 42). Further reports on HMGA2 and IGF2BPs have suggested that they may play a role in the self-renewal potential of fetal HSCs (43, 44). Let-7 miR has been known to inhibit tumor cell migration and invasion by targeting IGF2BP3 (45). Thus, IGF2BP3 may function in regulating both developmental and oncogenic processes. To examine the molecular mechanism behind the observed disruptions in cellular and hematopoietic homeostasis, we performed iCLIP-Seq analyses. Remarkably, we identified numerous RNA targets of IGF2BP3 in B-ALL cell lines that were known targets of MLL, including *CDK6* and *MYC*. CDK6 has recently been implicated as a highly important target in B-ALL, and inhibition of CDK6 may form the basis of a new therapeutic intervention in B-ALL (7). MYC is a quintessential oncogene, and its overexpression plays a direct, causative role in many B cell leukemias and in lymphoma. Reporter assays confirmed that the interaction of IGF2BP3 with the 3′UTRs of *MYC* and *CDK6* are functionally important. IGF2BP3 with deletions of RNA-binding domains failed to bind and stabilize *MYC* mRNA in the luciferase reporter assay. However, when single IGF2BP3 binding sites were deleted in the *MYC* and *CDK6* 3′UTR, the majority of these deletions failed to reverse the phenotype in the reporter assay. The complexity of 3′UTR targeting is illustrated by the variety of RBPs and noncoding RNAs that have been reported to bind to the *MYC* and *CDK6* 3′UTRs (46–49). Hence, RBP action on its cognate targets is likely dose dependent and cooperative; multiple RBPs have to bind to the same 3′UTR at different locations to exert an effect. In vivo and in vitro targeting of CDK6 and MYC protein was confirmed in the mouse BM and leukemia cell lines, in both the loss- and gain-of-function settings. Hence, we have validated iCLIP as a powerful technique for uncovering disease-relevant targets. It is important to point out that there are likely mRNAs other than *MYC* and *CDK6* that interact with IGF2BP3, including those we identify here, that play important roles in cellular proliferation and/or differentiation. This is illustrated by our attempt to rescue IGF2BP3 knockdown–mediated cell death by cotransducing RS4;11 cells with *MYC* constructs containing or lacking the 3′UTR. MYC alone was not sufficient to rescue changes in the cell cycle engendered by the loss-of-function of IGF2BP3 (data not shown).

The iCLIP-Seq analyses provide a global view of the transcriptome regulated by IGF2BP3. Prior studies have demonstrated single or a few targets for this protein, but our work here shows several hundred mRNAs bound by this protein. To refine our list of possible transcripts, we combined this biochemical target identification with gene expression studies in cells with IGF2BP3 loss

of function. Distinct sets of genes that were bound by IGF2BP3 showed upregulation or downregulation, with downregulated genes demonstrating enrichment for pathways related to cell cycle and leukemia. These findings suggest that IGF2BP3 upregulation in B-ALL serves to stabilize leukemogenic gene expression. Like other modes of posttranscriptional gene expression regulation, the actions of IGF2BP3 are dependent on the cellular transcription program. IGF2BP3 is itself induced by MLL-AF4, and it binds to and upregulates several mRNAs (e.g., *CDK6* and *MYC*) that are also induced by MLL-AF4. In this way, IGF2BP3 may reinforce certain aspects of the gene expression program, thereby sustaining oncogenesis. Interestingly, however, enforced expression of this protein alone also led to proliferation of hematopoietic progenitor cells, suggesting that specificity of RNA stabilization and/or translational enhancement can direct development and influence lineage choice and proliferation.

As oncogenic mutations and translocations are being catalogued via various high throughput sequencing approaches, it is also becoming apparent that single genetic abnormalities are insufficient to cause oncogenesis. Prior work has implicated nongenetic mechanisms, including epigenetic regulation, as key factors in the pathway to full-blown oncogenesis. Here, our studies have uncovered a posttranscriptional mechanism of stabilizing oncogenic gene products such as CDK6 and MYC. This mechanism requires further study and clarification and is likely to yield important insights into the nature of gene expression regulation in leukemogenesis. With targeted therapies emerging against CDK6 and MYC, it will become critical to consider the role of posttranscriptional mechanisms in regulating oncogene-mediated gene expression programs. Moreover, therapeutic avenues are also suggested by the current study, including the generation of sink RNAs to block the binding of IGF2BP3 to its targets or small molecule inhibitors of this protein designed to block its RNA-binding function. Given the expression of IGF2BP3 in many different types of cancer, it will be of great interest to define whether the repertoire of bound mRNAs is similar in tumors of distinct histogenesis and whether conserved oncogenic pathways can be targeted in hematologic and nonhematologic malignancies.

Methods

Patient samples, CD19⁺ cell isolation, and microarray data analysis. All procedures and protocols related to these have been previously described, and the microarray data set has been made publically available (NCBI's Gene Expression Omnibus [GEO GSE65647]) (21).

Apoptosis, proliferation, and cell cycle analysis. To measure cell proliferation, 2,000–4,000 cells per well were cultured in 96-well plates. MTS reagents were added according to the manufacturer's instructions (Promega CellTiter 96 AQ_{ueous} Non-Radioactive Cell Proliferation Assay kit) and cells were incubated at 37°C, 5% CO_2 for 4 hours before absorbance was measured at 490 nm. To measure apoptosis, cells were stained with APC-tagged annexin V and analyzed by flow cytometry. For cell cycle analysis, cells were fixed with 70% ethanol and stained with 1× propidium iodide solution in PBS and analyzed using flow cytometry.

qPCR. RNA collected from human samples was reverse transcribed using iScript reagent (Quanta BioSciences). RNA from cell lines was reverse transcribed using qScript (Quanta BioSciences). qPCR was performed with the StepOne Plus Real-Time PCR System (Applied Biosystems) using PerfeCTa SYBR Green FastMix reagent (Quanta BioSciences). The qPCR primer sequences used are listed in Supplemental Table 5.

Western blot. Cells were lysed in RIPA buffer (Boston BioProducts) supplemented with Halt Protease and Phosphatase Inhibitor Cocktail (Thermo Scientific). Equal amounts of protein lysate (as quantified by using bicinchoninic acid protein assay, BCA [Thermo Scientific]) were electrophoresed on a 5%–12% SDS-PAGE and electroblotted onto a nitrocellulose membrane. Antibodies used were c-MYC rabbit polyclonal (catalog 9402, Cell Signaling Technology), CDK6 rabbit monoclonal (catalog DCS83, Cell Signaling Technology), IGF2BP3 goat polyclonal (catalog sc-47893, Santa Cruz Biotechnology Inc.), T7 rabbit polyclonal (catalog AB3790, Millipore), and β-actin (catalog AC15, Sigma-Aldrich) mouse monoclonal. Secondary HRP-conjugated antibodies (Santa Cruz Biotechnology Inc.) and SuperSignal West Pico kit (Pierce Biotechnology) were used for enhanced chemiluminescence-based detection.

Cell culture, plasmids, and spin infection. mmu-miR-155 or hsa-miR-21 formatted siRNAs were cloned between NotI and BamHI sites of a pHAGE6 lentiviral vector (pHAGE6-CMV-siRNA-UBC-ZsGreen) or between NotI and BamHI sites of a modified pHAGE6 vector downstream of GFP (CMV-GFP-siRNA-UBC-Puromycin). In mouse cell lines, siRNAs and protein-coding inserts were cloned into MGP and MIG vectors (50). The WT IGF2BP3 and deletion mutants (KH and RRM) with a T7 epitope tag were cloned between BglII and XhoI sites in a MIG-based vector (MSCV-T7 tag-Mutant CDS-IRES-GFP; See Supplemental Table 5). For CRISPR-Cas9–mediated targeting, guide RNAs were designed using the Zhang lab website (http://crispr.mit.edu/) and cloned into the LentiCRISPR vector (24). RS4;11 cells were spin-infected at 30°C for 90 minutes in the presence of polybrene. Cells were selected with 5 μg/ml of puromycin for 7 days and used for cell proliferation and apoptosis assays. The human B-ALL cell lines RS4;11 (MLL-AF4 translocated; ATCC CRL-1873), NALM6 (gift from K. Sakamoto, Stanford University, Stanford, California, USA), 697 (E2A-PBX1-translocated; gift from K. Sakamoto), Reh (TEL-AML1-translocated; ATCC CRL-8286), murine pre-B leukemic cell line 7OZ/3 (ATCC TIB-158), and HEK 293T cell line (ATCC CRL-11268) were grown in their corresponding media at 37°C in a 5% CO_2 incubator. Lentiviruses and retroviruses were generated as previously described (50, 51).

BM transplant and competitive repopulation assay. BM was harvested and spin-infected from 8-week-old CD45.2⁺ donor C57BL/6J female mice as previously described (50). We also transplanted donor mice with T7 epitope–tagged IGF2BP3 and mutant constructs, including deletion mutants lacking RNA-bining domains. Eight-week-old CD45.1⁺ recipient B6.SJL-Ptprc-Pep3/BoyJ female mice were lethally irradiated and injected with donor BM 6 hours after irradiation. Eight mice were used per group. In some experiments, the normalized engraftment was calculated as the percent engraftment/transduction efficiency. For competitive repopulation experiments, 8-week-old CD45.1⁺ donor B6.SJL-Ptprc-Pep3/BoyJ female mice and 8-week-old CD45.2⁺ donor C57BL/6J female mice were harvested for BM. CD45.2⁺ BM was infected with viruses overexpressing MIG, HOXA9, or IGF2BP3. CD45.1⁺ and CD45.2⁺ BM cells were mixed in a ratio of 1:1 and injected into lethally irradiated 8-week-old CD45.2⁺ recipient C57BL/6J female mice. A negative control group had 100% CD45.1⁺ BM cells injected into lethally irradiated 8-week-old CD45.2⁺ recipient

C57BL/6J female mice. Mice were bled at 4, 8, 12, 16, and 20 weeks after BM injection for analysis of the peripheral blood. All mice were purchased from the Jackson Laboratory and housed under pathogen-free conditions at UCLA.

Flow cytometry. Blood, BM, thymus, and spleen were collected from the mice under sterile conditions at 27 weeks after transplant. Single cell suspensions were lysed in red blood cell lysis buffer. Fluorochrome-conjugated antibodies were used for staining. The list of antibodies used is provided in Supplemental Table 6. For intracellular staining, after initial staining with surface marker antibodies and fixation with 1% paraformaldehyde (PFA), cells were incubated with antibodies against intracellular antigens (Ki67, Cdk6, and Myc) in 1% Triton containing MACS buffer. After 30 minutes of staining at 4°C, cells were washed twice with PBS and fixed with 1% PFA. Flow cytometry was performed at the UCLA JCCC and at the Broad Stem Cell Research Flow Core. Analysis was performed using FlowJo software.

Histopathology. Fixation and sectioning has been described previously (51). Analysis was performed by a board certified hematopathologist (D.S. Rao).

iCLIP. iCLIP was performed as previously described (52). Briefly, RS4;11 or REH cells were irradiated with UV-C light to form irreversible covalent cross-link proteins to nucleic acids in vivo. After cell lysis, RNA was partially fragmented using micrococcal nuclease, and IGF2BP3-RNA complexes were immunopurified with anti-IGF2BP3 antibody (MBL International Corporation) immobilized on protein A–coated magnetic beads (Invitrogen). After stringent washing and dephosphorylation (FastAP, Fermentas), RNAs were ligated at their 3′ ends to a 3′ preadenylated RNA adaptor, radioactively labeled, run using MOPS-based protein gel electrophoresis, and transferred to a nitrocellulose membrane. Protein-RNA complexes 15–80 kDa above free protein were cut from the membrane, and RNA was recovered by proteinase K digestion under denaturing (3.5 M urea) conditions. The oligonucleotides for reverse transcription contained 2 inversely oriented adaptor regions adapted from the Bioo NEXTflex small RNA library preparation kit (Bioo Scientific), separated by a BamHI restriction site and a barcode region at their 5′ end containing a 4-nt experiment-specific barcode within a 5-nt random barcode to mark individual cDNA molecules. cDNA molecules were size purified using denaturing PAGE, circularized by CircLigase II (Epicenter, Illumina), annealed to an oligonucleotide complementary to the restriction site and cut using BamHI (New England Biolabs Inc.). Linearized cDNAs were then PCR-amplified using Immomix PCR Master Mix (Bioline) with primers (Bioo Scientific) complementary to the adaptor regions and subjected to high throughput sequencing using Illumina HiSeq. A more detailed description of the iCLIP protocol has been published (53). The data discussed in this publication have been deposited in NCBI's GEO (54) (GSE76931).

iCLIP data analysis. Following transcriptomic and genomic alignment with "TopHat2" (55), individual reads were truncated to their 5′ ends to represent the site of cross-linking. To denote specific sites of protein-RNA interaction, 30-bp regions of enrichment over background were determined using "Piranha" (56) in zero-truncated negative binomial mode with a custom local covariate. The covariate was calculated by uniformly distributing the cross-link number of each 30-bp bin across the neighboring 6 bins (3 on each side) to control for regions of overall higher depth as an indication of protein-RNA interaction. Adjacent bins with significant *P* values from Piranha ($\alpha < 0.05$) were combined into single regions. Only overlapping peak regions found to be statistically significant in all 3 replicates were considered biologically reproducible candidates for further analysis. To derive the intragenic distributions of iCLIP-Seq sites, we queried the UCSC Genome Browser MySQL database for hg19 (57) and determined the nearest overlapping gene based first on CCDS gene annotations (58) to determine the canonical ORF and second on Gencode V19 comprehensive for other features (59). Following this, the nearest intragenic anchor (transcription start site, start codon, 5′ splice site, 3′ splice site, stop codon, and polyadenylation site) was recorded, and the spliced distance to the nearest ORF boundary was calculated. As a background control, uniformly distributed cross-link sites were simulated by pseudo-random intervals from hg19 using "bedtools" (60). The intragenic distribution of these sites was determined following the same methodology as the iCLIP cross-link sites.

To determine the binding specificity of IGF2BP3, a 10-nt window surrounding each cross-link site occurring within a biologically reproducible and statistically significant peak from a last exon was extracted, and the counts of each n-mer (4 through 6) were calculated. Random 20-bp intervals from a window of 100–300 nucleotides adjacent to each cross-link site were included as a normalized frequency of n-mers to represent the background probability (p) of observing each n-mer. For each n-mer size, the probability of observing k occurrences of some n-mer out of N total observations is binomially distributed ($k \sim Bin[p, N]$) and Poisson approximated, given sufficiently large values for N (>1,000) and small values of *P* (<0.01). Individual n-mers with Poisson-approximated *P* values significant at a 5% false discovery rate (61) were then aligned with one another and grouped into motifs using k-medoid clustering for optimal values of k (using average silhouette width). The frequency of occurrence of each nucleotide was then plotted in a position-specific manner for each motif cluster.

RNA immunoprecipitation. Protein A Dynabeads (Invitrogen) in 100 mM sodium phosphate buffer (pH 8.1) were treated with either IgG mouse antibody (Jackson ImmunoResearch Laboratories Inc.) or α-IGF2BP3 (Santa Cruz Biotechnology Inc.) for 1 hour at 4°C. Beads were then washed 3× with RSB-100 buffer (10 mM Tris-Cl [pH 7.4], 100 mM NaCl, 2.5 mM $MgCl_2$, 0.5% NP-40). Cytoplasmic lysates were prepared from suspension RS4;11 cells in RSB-100 containing RNase inhibitors. Lysate supernatants were combined with the bead/antibody, rotated at 4°C overnight, and washed, and a portion was removed for Western blot analysis. Pelleted beads were resuspended in Proteinase K buffer (100 mM Tris-HCl [pH 7.4], 50 mM NaCl, 10 mM EDTA [pH 8.0]). Samples were treated with RQ DNase I (Promega) and then treated with Proteinase K (Ambion); both were incubated at 37°C. The RNA was extracted with acid phenol–chloroform and precipitated with sodium acetate, absolute ethanol, and coprecipitate GlycoBlue (Ambion). RNA was recovered by centrifugation, washed, and resuspended in RNase-free water. Quantity and quality were checked with Nanodrop and Total RNA NanoBioanalyzer kit (Agilent Technologies). RNA samples (200 μg of each sample; triplicates of both IgG controls and α-IGF2BP3 immunoprecipitations) were subjected to reverse transcription using the High-Capacity cDNA Reverse Transcription Kit (Thermo Scientific) and subsequent qPCR using the Lightcycler 480 (Roche Diagnostics).

RNA sequencing experiments. RNA was purified from both cytosolic fractions of IGF2BP3-depleted or control RS4;11 cells using TRI-Reagent LS (Sigma-Aldrich), converted to double-stranded libraries

using the NEXTflex Rapid Directional qRNA-Seq Library Prep Kit (Bioo Scientific), and sequenced using Illumina HiSeq 2500 platform. High throughput RNA sequencing data generated by Illumina HiSeq 2500 and corresponded to approximately 30–115 million reads per sample (Supplemental Table 4) was mapped to hg19 build of the human genome (Feb. 2009 GRCh37, NCBI Build 37.1) using Bowtie and TopHat software (62, 63). All data collection and parsing was performed with Perl, and statistical analyses with R, version 2.14.1. All external library packages used are available on CPAN or CRAN. Differentially expressed genes were identified using DESeq. The data are accessible through NCBI's GEO (GSE76931).

Luciferase assays. The *CDK6* 3′UTR is approximately 10-kb long while the *MYC* 3′UTR is approximatley 300 bp. MYC Δ3 and MYC Δ4 are mutant *MYC* 3′UTRs lacking IGF2BP3 binding sites determined from iCLIP data. Primers were designed to exclude these binding sites, fusion PCR was completed, and MYC and MYC Δ 3′UTRs were cloned downstream of firefly luciferase in the pmirGlo vector between the SacI and XhoI sites (64). The *CDK6* 3′UTR was divided into 5 pieces (CDK6 1–5; ~2 kb each) and cloned individually downstream of the firefly luciferase. 293T cells were transfected with the pmirGlo, 3′UTR, or Δ 3′UTR containing reporter vectors along with the MIG empty vector, MIG-hIGF2BP3 overexpression vector, MIG-T7-hIGF2BP3 overexpression vector, or MIG-T7-KH/RRM mutant vectors at a 1:10 ratio (50:500 ng). Cotransfections were performed with Lipofectamine 2000 (Invitrogen) as per the manufacturer's instructions. Cells were lysed after 24 hours, substrate was added, and luminescence was measured on a GloMax-Multi Jr (Promega). The ratio of firefly to Renilla luciferase activity was calculated for all samples. The hIGF2BP3/MIG or mutant/MIG luminescence for the pmirGlo empty vector was used as a normalization control.

Statistics. Data represent mean ±SD for continuous numerical data. One-way ANOVA followed by Bonferroni's multiple comparisons test or 2-tailed Student's *t* tests were performed using GraphPad Prism software and applied to each experiment as described in the figure legends. A *P* value less than 0.05 was considered significant. $^{*}P < 0.05$, $^{**}P < 0.01$, $^{***}P < 0.001$, and $^{****}P < 0.0001$.

Study approval. Written informed consent was obtained from all of the parents of the patients by the Italian Association of Pediatric Hematology and Oncology (AIEOP) and the Berlin-Frankfurt-Muenster (BFM) ALL-2000 trial. The University of Padova IRB approved all procedures, and the study was considered exempt from review at UCLA. Peripheral blood mononuclear cells derived from anonymized donors were obtained from the Center for AIDS Research Virology Core Lab at UCLA or following diagnostic work from the UCLA Department of Pathology and Laboratory Medicine with written consent and IRB approval. All mouse experimental procedures were conducted with the approval of the UCLA Chancellor's Animal Research Committee (ARC).

Author contributions

JKP designed the study, performed the experiments, analyzed the data, and wrote the paper. JRS and DSR designed the study, analyzed the data, and wrote the paper. TMT and JMH performed the experiments, analyzed the data, and wrote the paper. JRC and TRF performed the experiments. TSW, SK, MT, WY, MP, and GB analyzed the data.

Acknowledgments

We thank members of the Rao lab for their helpful discussions. We thank Parth Patel, May Paing, Norma Iris Rodriguez-Malave, Jennifer King, Jaspal Bassi, Kim Pioli, Nolan Ung, and Jaime Anguiano for their technical support. This work was supported by NIH grant R01 CA166450, a seed grant from the UCLA JCCC, and a Career Development Award K08CA133521 (to D.S. Rao), as well as by NIH grants R01GM109146 and R21AG042003 (to J.R. Sanford). J.R. Contreras was supported by the Tumor Immunology Training Grant, NIH T32CA009120. T.R. Fernando was supported by Tumor Biology Training Grant NIH T32CA009056. J.M. Howard was supported by R41HG007336. Flow cytometry was performed in the UCLA JCCC/CFAR Flow Cytometry Core Facility that is supported by NIH AI-28697, P30CA016042, the JCCC, the UCLA AIDS Institute, and the David Geffen School of Medicine at UCLA.

Address correspondence to: Dinesh S. Rao, Department of Pathology and Laboratory Medicine, David Geffen School of Medicine at UCLA, 650 Charles E Young Drive, 12-272 Factor, Los Angeles, California 90095, USA. Phone: 310.825.1675; E-mail: drao@mednet.ucla.edu.

Jayanth Kumar Palanichamy's present address is: Department of Biochemistry, All India Institute of Medical Sciences, New Delhi, India.

1. Mullighan CG. Molecular genetics of B-precursor acute lymphoblastic leukemia. *J Clin Invest*. 2012;122(10):3407–3415.
2. Mullighan CG, Downing JR. Genome-wide profiling of genetic alterations in acute lymphoblastic leukemia: recent insights and future directions. *Leukemia*. 2009;23(7):1209–1218.
3. Krivtsov AV, Armstrong SA. MLL translocations, histone modifications and leukaemia stem-cell development. *Nat Rev Cancer*. 2007;7(11):823–833.
4. Krivtsov AV, et al. H3K79 methylation profiles define murine and human MLL-AF4 leukemias. *Cancer Cell*. 2008;14(5):355–368.
5. Robinson BW, et al. Abundant anti-apoptotic BCL-2 is a molecular target in leukaemias with t(4;11) translocation. *Br J Haematol*. 2008;141(6):827–839.
6. Jiang X, et al. Blockade of miR-150 maturation by MLL-fusion/MYC/LIN-28 is required for MLL-associated leukemia. *Cancer Cell*. 2012;22(4):524–535.
7. Placke T, et al. Requirement for CDK6 in MLL-rearranged acute myeloid leukemia. *Blood*. 2014;124(1):13–23.
8. Jude CD, Climer L, Xu D, Artinger E, Fisher JK, Ernst P. Unique and independent roles for MLL in adult hematopoietic stem cells and progenitors. *Cell Stem Cell*. 2007;1(3):324–337.
9. Ernst P, Mabon M, Davidson AJ, Zon LI, Korsmeyer SJ. An Mll-dependent Hox program drives hematopoietic progenitor expansion. *Curr Biol*. 2004;14(22):2063–2069.
10. Rozovskaia T, et al. Upregulation of Meis1 and HoxA9 in acute lymphocytic leukemias with the t(4: 11) abnormality. *Oncogene*. 2001;20(7):874–878.
11. Imamura T, et al. Frequent co-expression of HoxA9 and Meis1 genes in infant acute lymphoblastic leukaemia with MLL rearrangement. *Br J Haematol*. 2002;119(1):119–121.
12. Somervaille TC, et al. Hierarchical maintenance of MLL myeloid leukemia stem cells employs a transcriptional program shared with embryonic rather than adult stem cells. *Cell Stem Cell*. 2009;4(2):129–140.
13. Palanichamy JK, Rao DS. miRNA dysregulation in cancer: towards a mechanistic understanding. *Front Genet*. 2014;5:54.
14. Abdelmohsen K, et al. 7SL RNA represses p53 translation by competing with HuR. *Nucleic Acids Res*. 2014;42(15):10099–10111.
15. Lederer M, Bley N, Schleifer C, Hüttelmaier S. The role of the oncofetal IGF2 mRNA-binding protein 3 (IGF2BP3) in cancer. *Semin Cancer Biol*.

2014;29:3–12.
16. Bell JL, et al. Insulin-like growth factor 2 mRNA-binding proteins (IGF2BPs): post-transcriptional drivers of cancer progression? *Cell Mol Life Sci*. 2013;70(15):2657–2675.
17. Fadare O, et al. Expression of the oncofetal protein IGF2BP3 in endometrial clear cell carcinoma: assessment of frequency and significance. *Hum Pathol*. 2013;44(8):1508–1515.
18. Suvasini R, et al. Insulin growth factor-2 binding protein 3 (IGF2BP3) is a glioblastoma-specific marker that activates phosphatidylinositol 3-kinase/mitogen-activated protein kinase (PI3K/MAPK) pathways by modulating IGF-2. *J Biol Chem*. 2011;286(29):25882–25890.
19. Schaeffer DF, et al. Insulin-like growth factor 2 mRNA binding protein 3 (IGF2BP3) overexpression in pancreatic ductal adenocarcinoma correlates with poor survival. *BMC Cancer*. 2010;10:59.
20. Kobel M, et al. IGF2BP3 (IMP3) expression is a marker of unfavorable prognosis in ovarian carcinoma of clear cell subtype. *Mod Pathol*. 2009;22(3):469–475.
21. Fernando TR, et al. LncRNA Expression discriminates karyotype and predicts survival in B-lymphoblastic leukemia. *Mol Cancer Res*. 2015;13(5):839–851.
22. Tsutsumi S, et al. Two distinct gene expression signatures in pediatric acute lymphoblastic leukemia with MLL rearrangements. *Cancer Res*. 2003;63(16):4882–4887.
23. Dawson MA, et al. Inhibition of BET recruitment to chromatin as an effective treatment for MLL-fusion leukaemia. *Nature*. 2011;478(7370):529–533.
24. Shalem O, et al. Genome-scale CRISPR-Cas9 knockout screening in human cells. *Science*. 2014;343(6166):84–87.
25. Hardy RR, Shinton SA. Characterization of B lymphopoiesis in mouse bone marrow and spleen. *Methods Mol Biol*. 2004;271:1–24.
26. Aifantis I, Raetz E, Buonamici S. Molecular pathogenesis of T-cell leukaemia and lymphoma. *Nat Rev Immunol*. 2008;8(5):380–390.
27. Chen EY, et al. Enrichr: interactive and collaborative HTML5 gene list enrichment analysis tool. *BMC Bioinformatics*. 2013;14:128.
28. Grimson A, Farh KK, Johnston WK, Garrett-Engele P, Lim LP, Bartel DP. MicroRNA targeting specificity in mammals: determinants beyond seed pairing. *Mol Cell*. 2007;27(1):91–105.
29. Wachter K, Kohn M, Stohr N, Huttelmaier S. Subcellular localization and RNP formation of IGF2BPs (IGF2 mRNA-binding proteins) is modulated by distinct RNA-binding domains. *Biol Chem*. 2013;394(8):1077–1090.
30. Bernt KM, Armstrong SA. A role for DOT1L in MLL-rearranged leukemias. *Epigenomics*. 2011;3(6):667–670.
31. Kharas MG, et al. Musashi-2 regulates normal hematopoiesis and promotes aggressive myeloid leukemia. *Nat Med*. 2010;16(8):903–908.
32. Abdelmohsen K, Gorospe M. Posttranscriptional regulation of cancer traits by HuR. *Wiley Interdiscip Rev RNA*. 2010;1(2):214–229.
33. Guenther MG, et al. Aberrant chromatin at genes encoding stem cell regulators in human mixed-lineage leukemia. *Genes Dev*. 2008;22(24):3403–3408.
34. Tang H, et al. IMP3 as a supplemental diagnostic marker for Hodgkin lymphoma. *Hum Pathol*. 2013;44(10):2167–2172.
35. Hartmann EM, et al. Increased tumor cell proliferation in mantle cell lymphoma is associated with elevated insulin-like growth factor 2 mRNA-binding protein 3 expression. *Mod Pathol*. 2012;25(9):1227–1235.
36. King RL, Pasha T, Roullet MR, Zhang PJ, Bagg A. IMP-3 is differentially expressed in normal and neoplastic lymphoid tissue. *Hum Pathol*. 2009;40(12):1699–1705.
37. Liao B, Hu Y, Herrick DJ, Brewer G. The RNA-binding protein IMP-3 is a translational activator of insulin-like growth factor II leader-3 mRNA during proliferation of human K562 leukemia cells. *J Biol Chem*. 2005;280(18):18517–18524.
38. Stoskus M, Gineikiene E, Valceckiene V, Valatkaite B, Pileckyte R, Griskevicius L. Identification of characteristic IGF2BP expression patterns in distinct B-ALL entities. *Blood Cells Mol Dis*. 2011;46(4):321–326.
39. Lu D, et al. IMP3, a new biomarker to predict progression of cervical intraepithelial neoplasia into invasive cancer. *Am J Surg Pathol*. 2011;35(11):1638–1645.
40. Chen CL, et al. Reciprocal regulation by TLR4 and TGF-β in tumor-initiating stem-like cells. *J Clin Invest*. 2013;123(7):2832–2849.
41. Wagner M, et al. Transgenic overexpression of the oncofetal RNA binding protein KOC leads to remodeling of the exocrine pancreas. *Gastroenterology*. 2003;124(7):1901–1914.
42. Jonson L, Christiansen J, Hansen TV, Vikesa J, Yamamoto Y, Nielsen FC. IMP3 RNP safe houses prevent miRNA-directed HMGA2 mRNA decay in cancer and development. *Cell Rep*. 2014;7(2):539–551.
43. Copley MR, et al. The Lin28b-let-7-Hmga2 axis determines the higher self-renewal potential of fetal haematopoietic stem cells. *Nat Cell Biol*. 2013;15(8):916–925.
44. Toledano H, D'Alterio C, Czech B, Levine E, Jones DL. The let-7-Imp axis regulates ageing of the Drosophila testis stem-cell niche. *Nature*. 2012;485(7400):605–610.
45. Yan L, et al. Regulation of tumor cell migration and invasion by the H19/let-7 axis is antagonized by metformin-induced DNA methylation. *Oncogene*. 2015;34(23):3076–3084.
46. Chen MT, et al. ZFP36L1 promotes monocyte/macrophage differentiation by repressing CDK6. *Sci Rep*. 2015;5:16229.
47. Liu L, et al. Competition between RNA-binding proteins CELF1 and HuR modulates MYC translation and intestinal epithelium renewal. *Mol Biol Cell*. 2015;26(10):1797–1810.
48. Weidensdorfer D, et al. Control of c-myc mRNA stability by IGF2BP1-associated cytoplasmic RNPs. *RNA*. 2009;15(1):104–115.
49. Yang F, et al. Long non-coding RNA GHET1 promotes gastric carcinoma cell proliferation by increasing c-Myc mRNA stability. *FEBS J*. 2014;281(3):802–813.
50. Rao DS, O'Connell RM, Chaudhuri AA, Garcia-Flores Y, Geiger TL, Baltimore D. MicroRNA-34a perturbs B lymphocyte development by repressing the forkhead box transcription factor Foxp1. *Immunity*. 2010;33(1):48–59.
51. O'Connell RM, Balazs AB, Rao DS, Kivork C, Yang L, Baltimore D. Lentiviral vector delivery of human interleukin-7 (hIL-7) to human immune system (HIS) mice expands T lymphocyte populations. *PLoS One*. 2010;5(8):e12009.
52. Konig J, et al. iCLIP reveals the function of hnRNP particles in splicing at individual nucleotide resolution. *Nat Struct Mol Biol*. 2010;17(7):909–915.
53. Huppertz I, et al. iCLIP: protein-RNA interactions at nucleotide resolution. *Methods*. 2014;65(3):274–287.
54. Edgar R, Domrachev M, Lash AE. Gene Expression Omnibus: NCBI gene expression and hybridization array data repository. *Nucleic Acids Res*. 2002;30(1):207–210.
55. Kim D, Pertea G, Trapnell C, Pimentel H, Kelley R, Salzberg SL. TopHat2: accurate alignment of transcriptomes in the presence of insertions, deletions and gene fusions. *Genome Biol*. 2013;14(4):R36.
56. Uren PJ, et al. Site identification in high-throughput RNA-protein interaction data. *Bioinformatics*. 2012;28(23):3013–3020.
57. Meyer LR, et al. The UCSC Genome Browser database: extensions and updates 2013. *Nucleic Acids Res*. 2013;41(Database issue):D64–D69.
58. Pruitt KD, et al. The consensus coding sequence (CCDS) project: Identifying a common protein-coding gene set for the human and mouse genomes. *Genome Res*. 2009;19(7):1316–1323.
59. Harrow J, et al. GENCODE: the reference human genome annotation for The ENCODE Project. *Genome Res*. 2012;22(9):1760–1774.
60. Quinlan AR, Hall IM. BEDTools: a flexible suite of utilities for comparing genomic features. *Bioinformatics*. 2010;26(6):841–842.
61. Klipper-Aurbach Y, et al. Mathematical formulae for the prediction of the residual beta cell function during the first two years of disease in children and adolescents with insulin-dependent diabetes mellitus. *Med Hypotheses*. 1995;45(5):486–490.
62. Trapnell C, Pachter L, Salzberg SL. TopHat: discovering splice junctions with RNA-Seq. *Bioinformatics*. 2009;25(9):1105–1111.
63. Langmead B, Trapnell C, Pop M, Salzberg SL. Ultrafast and memory-efficient alignment of short DNA sequences to the human genome. *Genome Biol*. 2009;10(3):R25.
64. Contreras JR, et al. MicroRNA-146a modulates B-cell oncogenesis by regulating Egr1. *Oncotarget*. 2015;6(13):11023–11037.

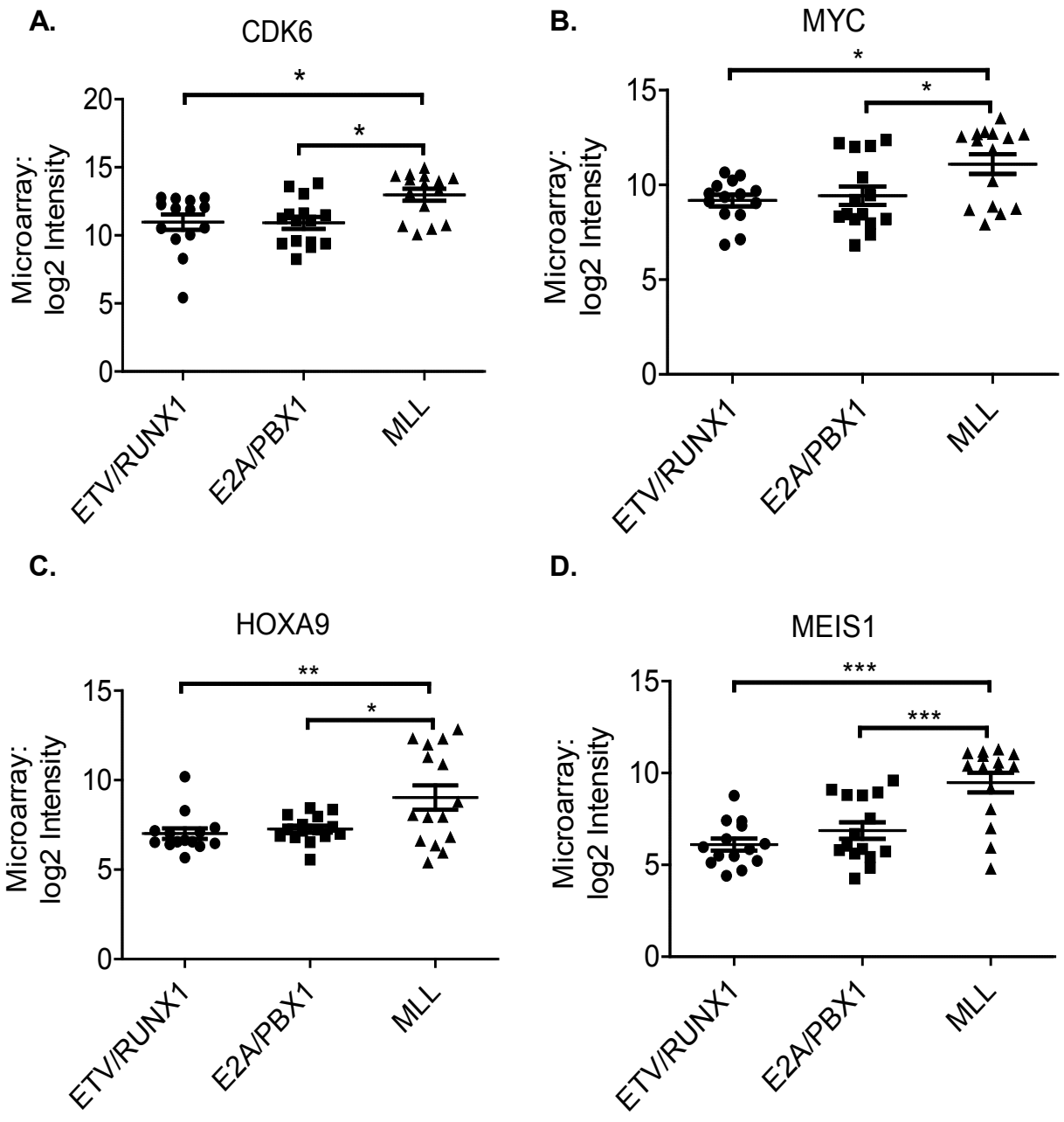

Figure S1: MLL-AF4 target gene expression by microarray. Scatter plots comparing the expression of (A) CDK6 (B) MYC (C) HOXA9 and (D) MEIS1 from the corresponding normalized fluorescence intensities on the microarray. n=14 (ETV/RUNX1); n=15 (E2A/PBX1); n=15 (MLL). (1-way ANOVA followed by Bonferroni's test, *$P < 0.05$; **$P < 0.01$;***$P < 0.001$). Data represent mean ± SD.

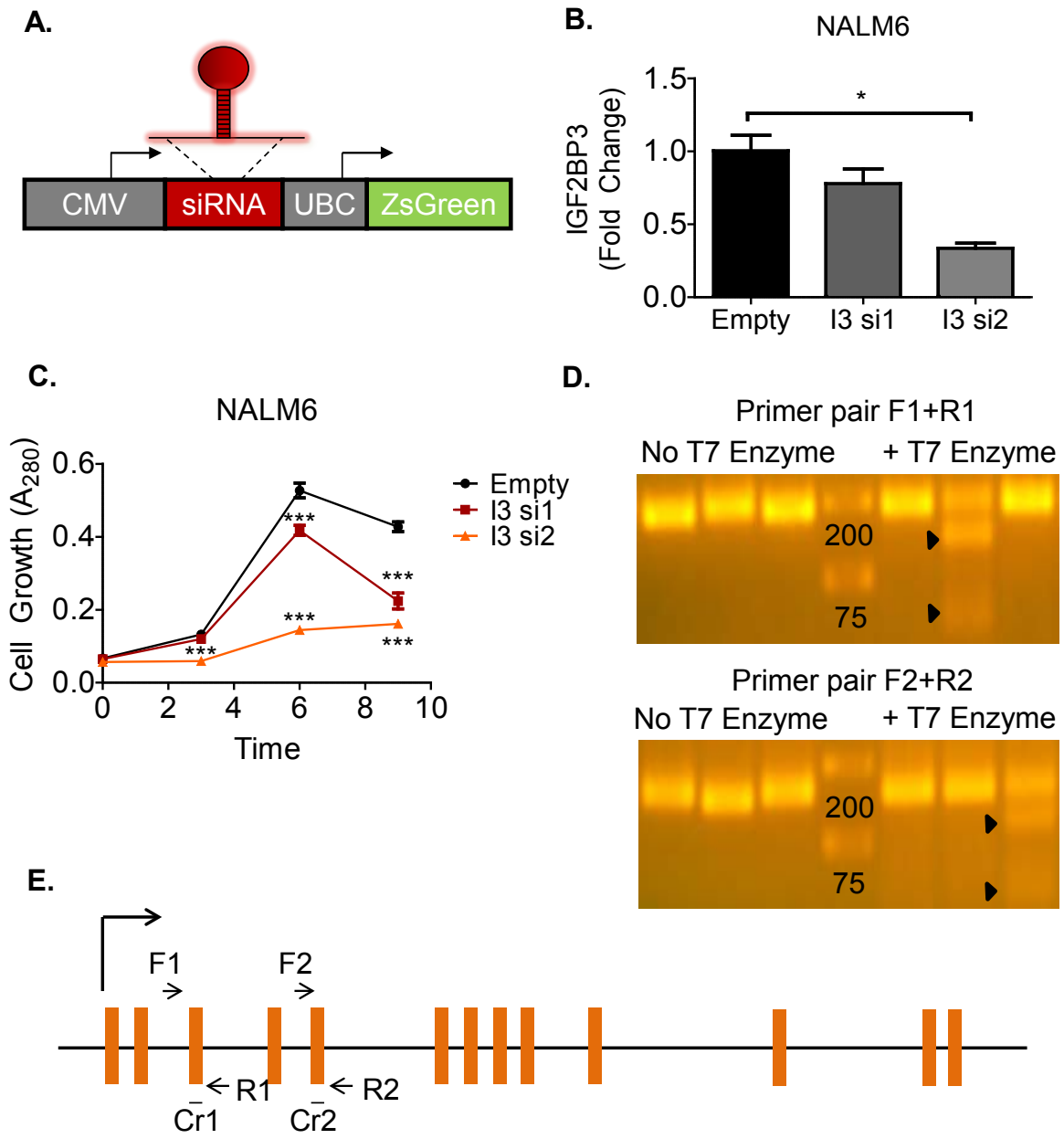

Figure S2: Knockdown of IGF2BP3 in B-ALL cell lines (A) Schematic of the lentiviral vector used for IGF2BP3 knockdown (B) IGF2BP3 knockdown by lentiviruses in NALM6 cell line (*t* test, *P < 0.05) and (C) Reduced cell proliferation (MTS assay) in NALM6 after IGF2BP3 knockdown (*t* test, ****P* < 0.001 for all comparisons) (D) T7 Endonuclease assay of PCR done using primer pair F1 and R1 (top panel) and DNA extracted from RS4;11 cells stably integrated with LentiCRISPR, Cr1 or Cr2 (Lanes 1-3 and 5-7). On addition of T7 enzyme cleavage, is seen only in the Cr1 integrated cells (arrowheads). Bottom panel shows T7 assay done using the same samples and primer pair F2 and R2. Cleavage is seen only in the Cr2 integrated cells (arrowheads) (E) Human IGF2BP3 gene structure showing the location of exons (in orange) and targets of the CRISPR guide RNAs (Cr1 and Cr2); Primer pairs F1 and R1 flanking the target site of Cr1 as well as primer pairs F2 and R2 flanking the Cr2 target site are also shown. I3, IGF2BP3. Data represent mean ± SD.

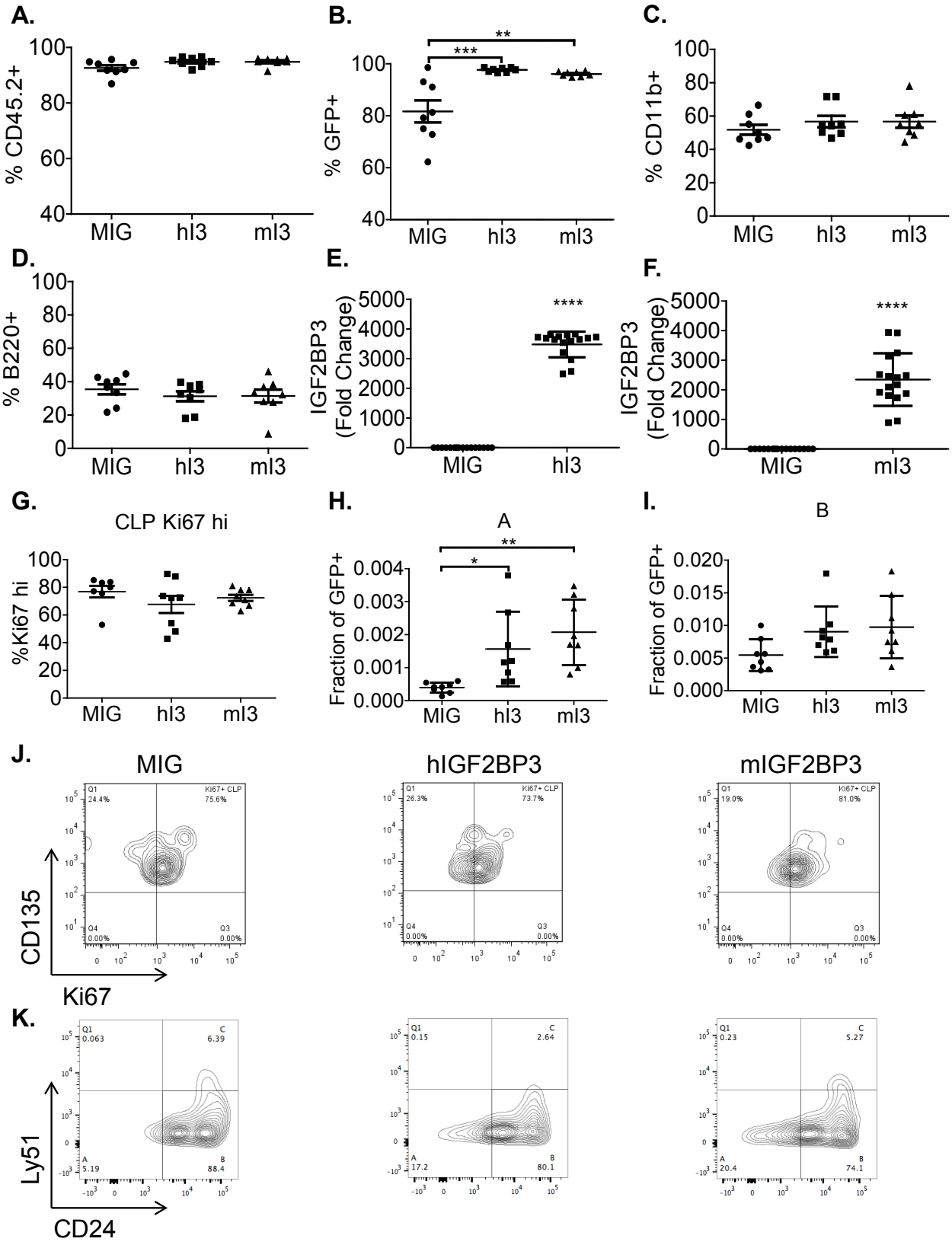
A.
% CD45.2+
100
80
60
40
MIG
hI3
mI3
B.
% GFP+
**
***
C.
% CD11b+
D.
% B220+
E.
IGF2BP3 (Fold Change)
5000
4000
3000
2000
1000
0
****
F.
G.
CLP Ki67 hi
%Ki67 hi
H.
A
Fraction of GFP+
0.004
0.003
0.002
0.001
0.000
*
I.
B
0.020
0.015
0.010
0.005
J.
MIG
hIGF2BP3
mIGF2BP3
CD135
Ki67
Q1
24.4%
KI67+ CLP
75.6%
Q4
0.00%
Q3
26.3%
73.7%
19.0%
81.0%
K.
Ly51
CD24
0.063
6.39
5.19
88.4
0.15
2.64
17.2
80.1
0.23
5.27
20.4
74.1

Figure S3: Bone marrow immunophenotypic analyses. Analysis at 24 weeks after IGF2BP3 overexpression shows (A) similar engraftment, (B) increased GFP expressing cells (1-way ANOVA followed by Bonferroni's test, $^{**}P < 0.01$;$^{***}P < 0.001$). and (C) similar numbers of myeloid and (D) B-cells. n=8 for all three groups. (E and F) Confirmation of overexpression of human and mouse IGF2BP3 in mouse bone marrow by qPCR (*t* test, $^{****}P < 0.0001$). Mouse Actin was used as internal control. n = 16 for all groups. (G) Ki67 staining of CLPs showing no significant difference and (J) representative FACS plots. (H-I) Increased Hardy fractions A (1-way ANOVA followed by Bonferroni's test, $^{*}P < 0.05$; $^{**}P < 0.01$) and B after IGF2BP3 over expression with (K) representative plots. n=8 for all three groups. hI3, human IGF2BP3; mI3, murine IGF2BP3; CLP, common lymphoid progenitor; BMT, bone marrow transplantation. Three separate BMT experiments were completed for validation. Data represent mean ± SD.

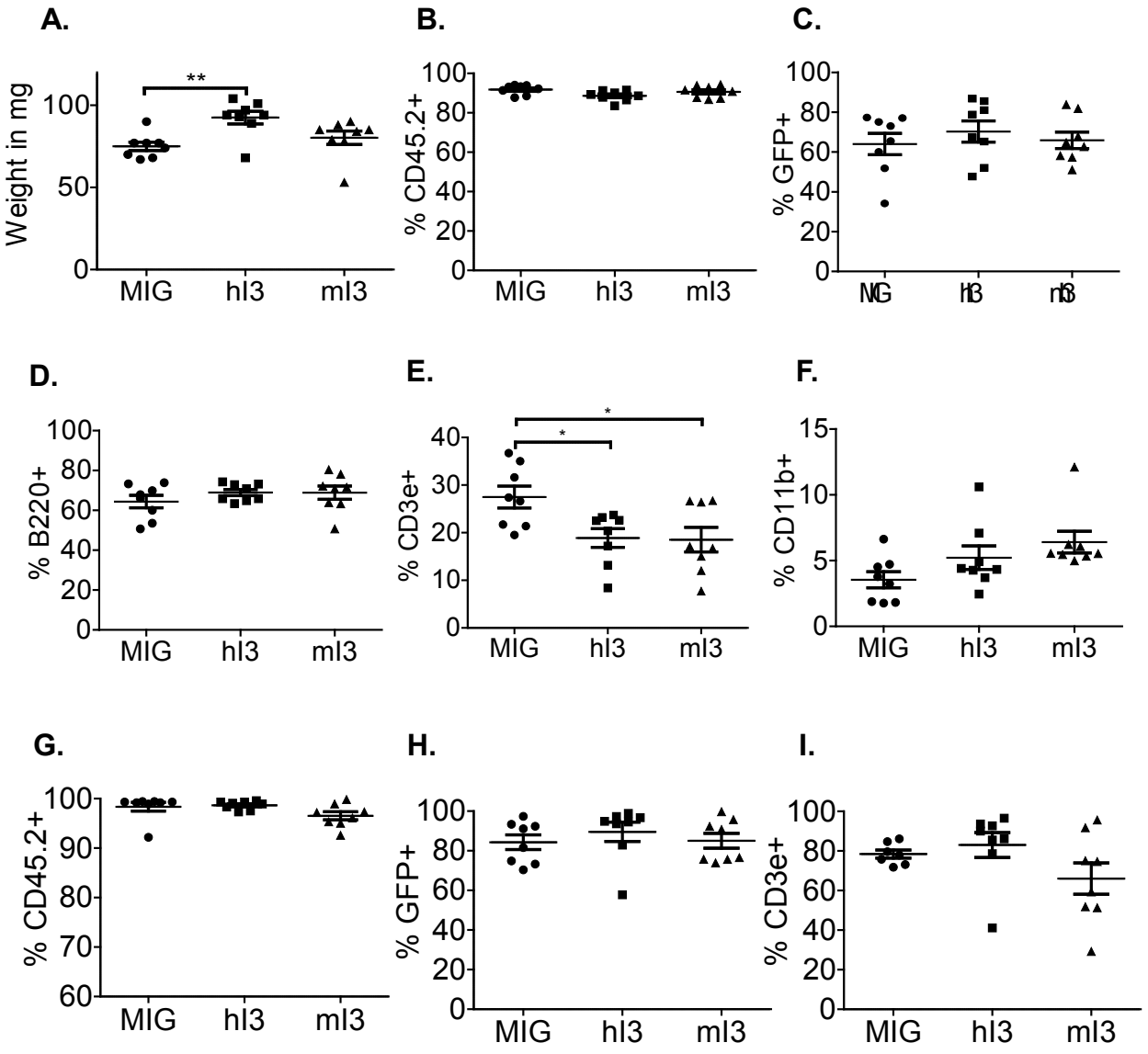

Figure S4: Immunophenotypic analyses of spleen and thymus with enforced expression of IGF2BP3 (A) Spleen analysis at the end of 27 weeks after IGF2BP3 overexpression shows significantly elevated spleen weights (1-way ANOVA followed by Bonferroni's test, $^{**}P < 0.01$), (B) similar engraftment, (C) GFP expressing cells and (D) B-cells. (E) Decreased numbers of T-cells (1-way ANOVA followed by Bonferroni's test, $^{*}P < 0.05$) and (F) elevated myeloid cells are also seen in the spleen (G-I) Enumeration of CD45.2, GFP, and CD3e+ cells, respectively, in thymi from control and human and murine IGF2BP3 overexpressing mice show no statistically significant differences. n=8 for all three groups. Three separate BMT experiments were completed for validation. Data represent mean ± SD.

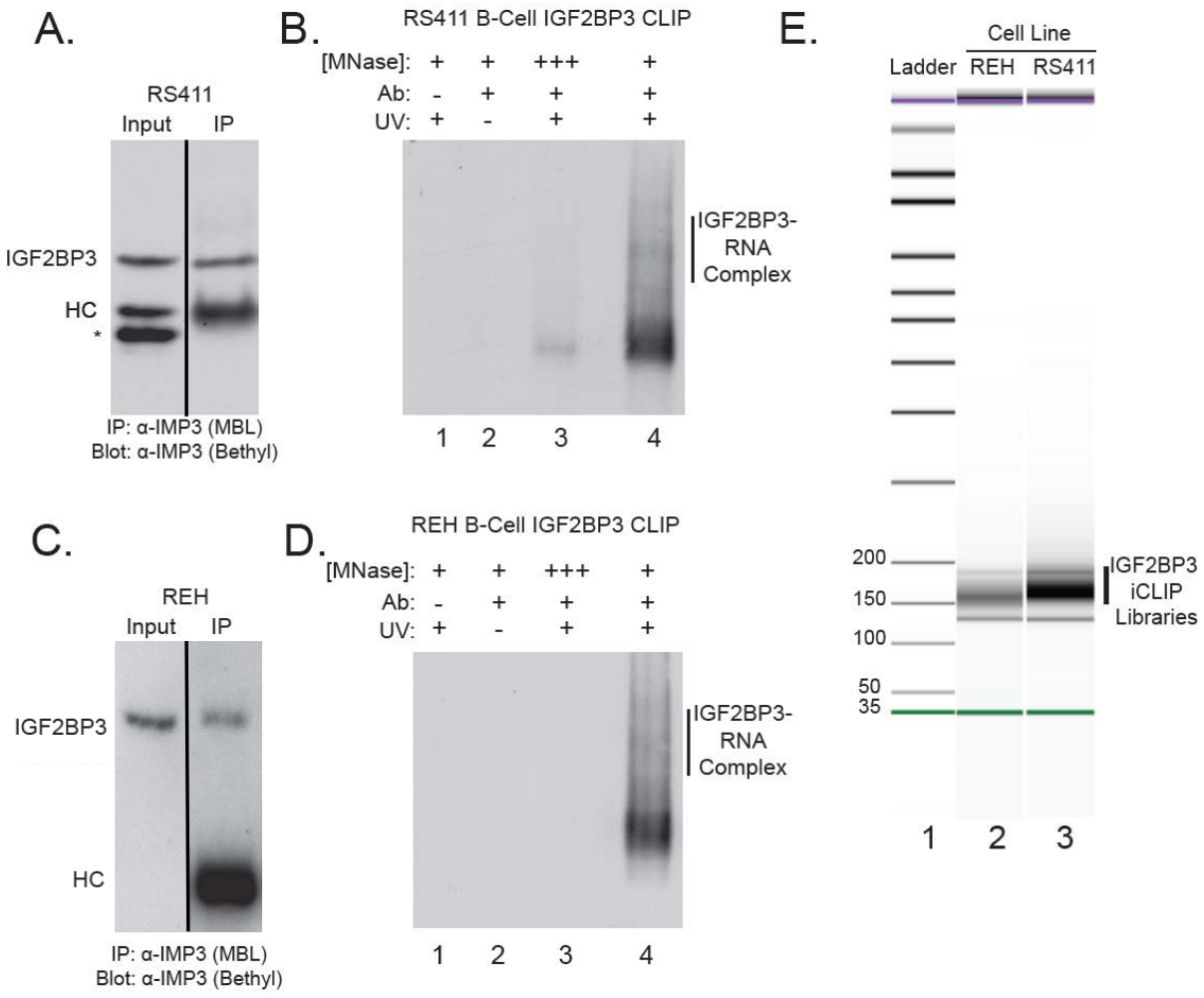

Figure S5: Purification of IGF2BP3-RNA complexes from human leukemia cell lines using crosslinking immunoprecipitation (CLIP). (A) Western blot of RS4;11 whole cell lysate and anti-IGF2BP3 immunoprecipitate. Membrane is probed with anti-IGF2BP3. IgG heavy chain (HC) and a cross-reactive protein (*) are indicated on the blot. (B) Autoradiograph of protein-RNA complexes isolated by CLIP from RS4;11 cells. UV-dependent and nuclease-sensitive IGF2BP3-RNA complexes are indicated. (C and D) As in panels A and B, but using REH cell lysates. (E) Bioanalyzer trace of pooled amplicon libraries from REH and RS4;11 cells (lanes 2 and 3, respectively). Lanes in panels (A) and (C) were run on the same gel but were noncontiguous. IMP3, IGF2BP3; MNase, micrococcal nuclease.

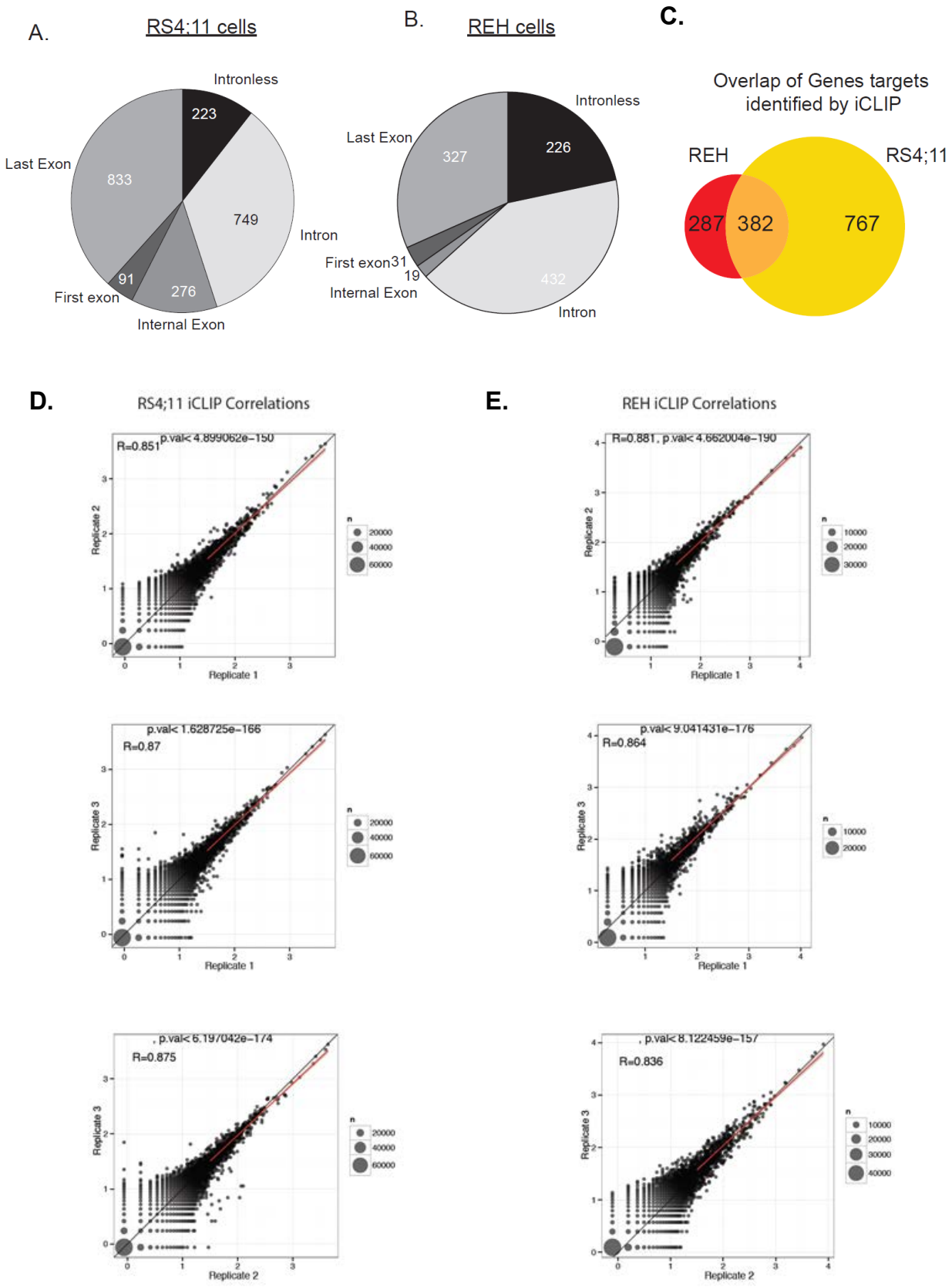
A.
RS4;11 cells
Intronless
223
Last Exon
833
749
Intron
91
First exon
276
Internal Exon
B.
REH cells
Intronless
Last Exon
327
226
First exon
31
19
Internal Exon
432
Intron
C.
Overlap of Genes targets identified by iCLIP
REH
RS4;11
287
382
767
D.
RS4;11 iCLIP Correlations
R=0.851
p.val< 4.899062e−150
Replicate 2
Replicate 1
n
20000
40000
60000
p.val< 1.628725e−166
R=0.87
Replicate 3
Replicate 1
p.val< 6.197042e−174
R=0.875
Replicate 2
E.
REH iCLIP Correlations
R=0.881, p.val< 4.662004e−190
10000
20000
30000
p.val< 9.041431e−176
R=0.864
p.val< 8.122459e−157
R=0.836
40000

Figure S6: Annotation and overlap of IGF2BP3 binding sites identified in human leukemia cell lines. (A) Annotation of peaks called in RS4;11 cells. (B) Annotation of peaks called in REH cells.(C) Pie charts showing the count of significant CLIP peaks in different regions of protein coding genes. Venn Diagram of genes identified in the iCLIP analysis of IGF2BP3 in REH (red) and RS4;11 cells (Yellow). (D and E) Correlation of replicate IGF2BP3 iCLIP experiments (D) Comparison of iCLIP from RS4;11 cells and (E) REH cells. Spearman's rank correlation coefficient (R) and *P* value are given for each comparison.

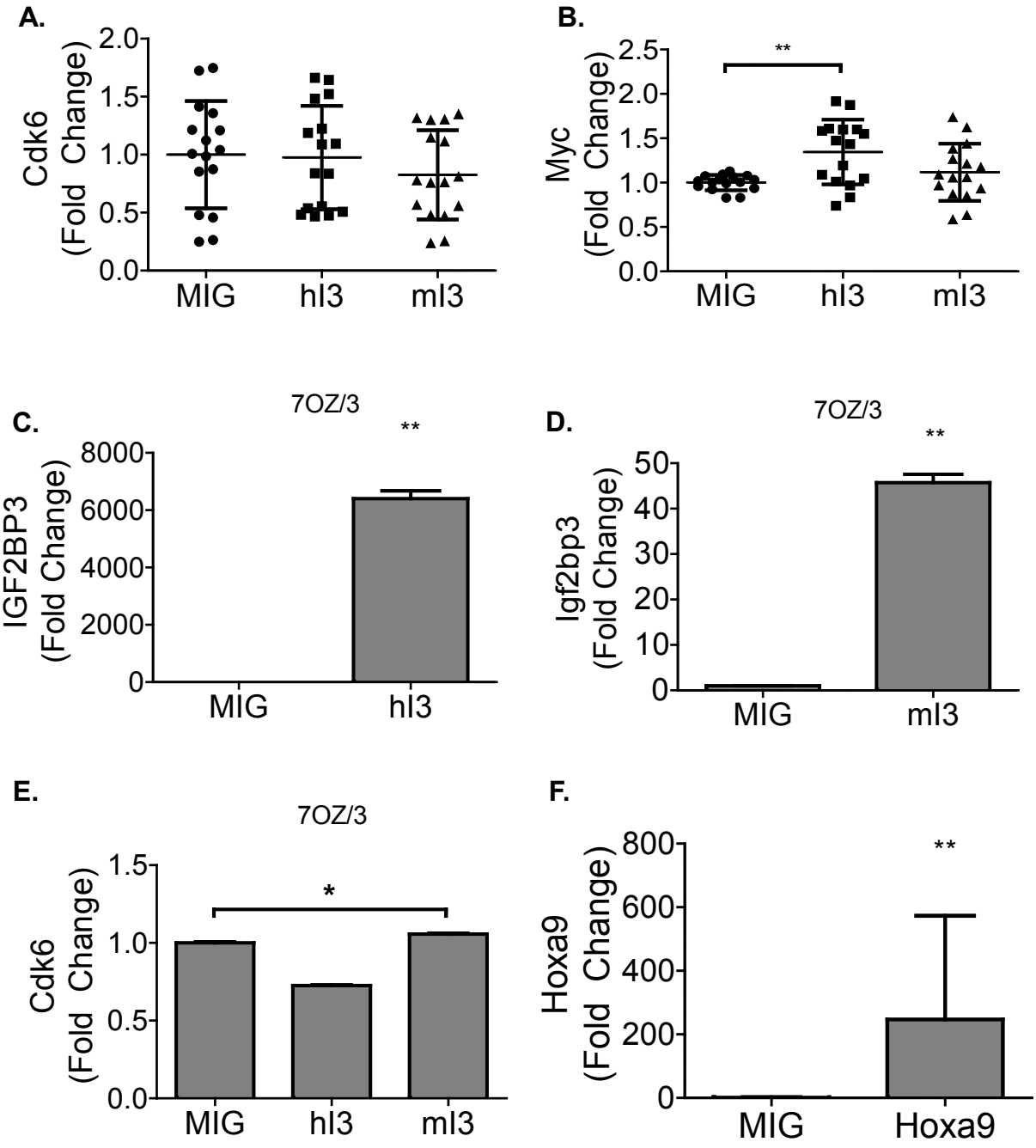

Figure S7: Expression of putative targets of IGF2BP3 (A and B) mRNA expression of Cdk6 and Myc in mouse bone marrow after IGF2BP3 over expression (1-way ANOVA followed by Bonferroni's test, $^{**}P < 0.01$). n = 16 for all groups. Three separate BMT experiments were completed for validation. (C) qPCR confirmation of overexpression of hI3 and (D) mI3 in mouse 7OZ/3 cells. (*t* test, $^{**}P = 0.0018$, $^{**}P = 0.0017$, respectively) (E) qPCR of Cdk6 in 7OZ/3 after IGF2BP3 overexpression (1-way ANOVA followed by Bonferroni's test, $^{*}P < 0.05$). (F) qPCR confirmation of overexpression of Hoxa9 in mouse bone marrow of competitive repopulation study (*t* test, $^{**}P = 0.0054$). Competitive repopulation study was completed three times for validation. Data represent mean ± SD.

Table S5: List of primers, siRNAs and CRISPR guide RNAs

Primer	Sequence
Human primers for qPCR	
qhActinF	CATGTACGTTGCTATCCAGGC
qhActinR	CTCCTTAATGTCACGCACGAT
qhL32F	GGAGCGACTGCTACGGAAG
qhL32R	GATACTGTCCAAAAGGCTGGAA
qhIGF2BP3F	CCTGGTGAAGACTGGCTACG
qhIGF2BP3R	ATCCAGCACCTCCCACTGTA
qhCDK6F	GCTGACCAGCAGTACGAATG
qhCDK6R	GCACACATCAAACAACCTGACC
qhCD44F	AGTCACAGACCTGCCCAATG
qhCD44R	AACCTCCTGAAGTGCTGCTC
q-h-POLR2AF	CATCAAGAGAGTCCAGTTCGG
q-h-POLR2AR	CCCTCAGTCGTCTCTGGGTA
MYCF	GCTGCTTAGACGCTGGATTT
MYCR	TAACGTTGAGGGGCATCG
CDK6F	TGATCAACTAGGAAAAATCTTGGA
CDK6R	GGCAACATCTCTAGGCCAGT
18s-rRNAF	CTTCCACAGGAGGCCTACAC
18s-rRNAR	CGCAAAATATGCTGGAACTTT
Mouse primers for qPCR	
qmL32F	AAG CGA AAC TGG CGG AAA C
qmL32R	TAA CCG ATG TTG GGC ATC AG
qmActin1F	GATCTGGCACCACACCTTCT
qmActin1R	GGGGTGTTGAAGGTCTCAAA
qmIGF2BP3F	GGATCGGTGTCCAAGCAGAA
qmIGF2BP3R	GCCTTCAGGGGTAGAGAGGA
qmCdk6F	TCTCACAGAGTAGTGCATCGT
qmCdk6R	CGAGGTAAGGGCCATCTGAAAA
qmMycF	TCT CCA TCC TAT GTT GCG GTC
qmMycR	TCC AAG TAA CTC GGT CAT CAT CT
CRISPR primers for T7 assay	
IMP3Cr1DNAF	TTCTGCAGGATTCGGAAACT
IMP3Cr1DNAR	GCACGGGTCATAGGAGAAGA
IMP3Cr2DNAF	GAACACTGACTCGGAAACTGC
IMP3Cr2DNAR	CACCTACCAGCCCTTCTCAG

siRNA sense strand sequence	
IGF2BP3 si1	AATTCCTGCAATGGAGATATC
IGF2BP3 si2	TTCATGATCTCCTCCTCAGCT
Cloning primers	**IGF2BP3, T7 IGF2BP3, KH, RRM into MIG: Between BglII and XhoI**
hIMP3CDS1F	atctgaGGATCCcgagaagacgaggggaacaa
hIMP3CDS1R	atgcagCTCGAGtctgtggtgggctgtttcct
mIMP3CDS1F	atctgaGGATCCtgggtcactgtgtgggtttg
mIMP3CDS1R	atgcagCTCGAGttggtttggcatctgcctct
T7IMP3F	agcataAGATCTatggcatcgatgacaggtggc
T7IMP3R	atgcagCTCGAGcaccctgaagttctcaggatc
Cloning primers	**CDK6 and MYC 3' UTR into pMirGlo: Between SacI and XhoI unless specified** **MYC 3' UTR binding site deletions into pMirGlo: Between**
CDK6UTR1F	atcgagGAGCTCgaaaacctggattcccacct
CDK6UTR1R	cgttcaCTCGAGAGTGCAGCAACCTCCATTCT
CDK6UTR2FNhe	atcgagGCTAGCGGAGGTTGCTGCACTCAGA
CDK6UTR2R	cgttcaCTCGAGTGGTGGCATATTCACTTTTAACAT
CDK6UTR3F	atcgagGAGCTCTCCAAAAGCAGGCTTTAATTG
CDK6UTR3R	cgttcaCTCGAGCCTAAGTTGTTATGCTCATATACTTCA
CDK6UTR4F	atcgagGAGCTCGCCCTAAAATACCAAAAGACCA
CDK6UTR4R	cgttcaCTCGAGTGATAAAACACCTAGATACCCAAAA
CDK6UTR5F	atcgagGAGCTCCTAAGCCCCCAAATAAGCTG
CDK6UTR5R	cgttcaCTCGAGAAGACATCCAGTTTCCAAAGGA
mycUTRpMirF	atcgagGAGCTCGGAAAAGTAAGGAAAACGATT
mycUTRpMirR	cgttcaCTCGAGTTTGGCTCAATGATATATTTG
5'MYCUTR-3R	GTACTATATATGTAACTGCTATAAACGTTTTA
3'MYCUTR-3F	AGCAGTTACATATATAGTACCTAGTATTATAG
5'MYCUTR-4R	AATCAACTTTTTAAATAAAAAAAATTAGGGT
3'MYCUTR-4F	TTTTATTTAAAAAGTTGATTTTTTTCTATTG
Cloning CRISPR guide RNAs	**Top and bottom strands to anneal and insert into LentiCRISPR**
CrIMP31T	caccgATATCCCGCCTCATTTACAG
CrIMP31B	aaacCTGTAAATGAGGCGGGATATc
CrIMP32T	caccgAGCTTGGTCCTTACTGGAAT
CrIMP32B	aaacATTCCAGTAAGGACCAAGCTc

Table S6: List of antibodies used for flow cytometry and gating schematics

Lineage staining	
CD3e (100308)	PE
CD11b (101216)	PE-Cy7
B220 (103236)	PercP-Cy 5.5
CD45.1 (110715)	APC-Cy7
CD45.2 (109813)	APC

Bone marrow HSC/LMPP staining	
CD117 (105826)	APC-Cy7
Sca1 (108123)	PerCP-Cy 5.5
CD135 (17-1351-82)	APC
CD127 (135013)	PE-Cy7
CD150 (115903)	PE
Biotin (100304,13-0041-82, 100704, 103204,108703, 116204,118103,109203)	CD3e, CD4, CD8, B220, NK1.1, Ter119, TCR beta, TCR gamma-delta
Streptavidin-Pacific Blue (48-4317-82)	
HSC	Lin- CD117 hi Sca1 hi CD150++
LMPP	Lin- CD117 hi Sca1 hi CD135+ CD127-
CLP	Lin- CD117 int Sca1 int CD135+ CD127+
For intracellular staining, CD150-PE was replaced by Ki67-PE(652403), CDK6 (sc-177) with goat anti-rabbit IgG-PE (sc-3739), or MYC-PE (sc-40 PE).	

Bone marrow Hardy staining	
B220 (103236)	PerCP-Cy 5.5
IgM (1020-09S)	PE
CD43 (BDB560663)	APC
CD24 (25-0242-80)	PE-Cy7
Ly51(108303)	APC-Cy7

Hardy Fractions	
A	B220+ IgM- CD43+ CD24- Ly51-
B	B220+ IgM- CD43+ CD24+ Ly51-
C	B220+ IgM- CD43+ CD24+ Ly51+
D	B220+ IgM- CD43-
E and F	B220+ IgM+

All antibodies were procured from Biolegend, ebioscience, Santa Cruz Biotechnology, Southern Biotech, or BD Biosciences. Catalog numbers are listed in parenthesis.

Table S1: Mapping statistics of iCLIP-Seq Reads

Abbreviations:

Stats from bowtie mappings
mapping algorithm: mapalgoT4_seVar_rptfilt_tophat_trimalgo2
mapping directory: tophat_bam
#
M: Millions of reads
K: Thousands of fragments
TotalCnt: total reads
MaxMapCnt: count of fragments with 10 mappings
MaxMapPct: MaxMapCnt/TotalCnt
MappedCnt: count of mapped fragments, INCLUDING MaxMapCnt
MappedPct: MappedCnt/TotalCnt
MultiCnt: count of multiply mapped reads but < 10 mappings
UniqCnt: count of uniquely mapped reads
SpliceCnt: count of uniquely mapped reads at splice-junctions
MultiPct: MultiCnt/MappedCnt
UniqPct: UniqCnt/MappedCnt
SplicePct: SpliceCnt/UniqCnt

#Sample	TotalCnt	MaxMapCnt	MaxMapPct	MappedCnt	MappedPct	MultiCnt	MultiPct	UniqCnt	UniqPct	SpliceCnt	SplicePct	MappedCnt (Excluding PCR dups)	MultiCnt (Excluding PCR dups)	MultiPct	UniqCnt (Excluding PCR dups)	UniqPct	SpliceCnt (Excluding PCR dups)	SplicePct	PCR DUPLICATION RATE
rs411x_imp3_jh099a	2.10M	39.11K	1.90%	1.89M	90.00%	0.30M	16.20%	1.58M	83.80%	37.24K	2.40%	1.10M	0.22M	20.30%	0.88M	79.70%	20.15K	2.30%	1.72
rs411x_imp3_jh099b	2.24M	38.58K	1.70%	1.97M	88.10%	0.32M	16.00%	1.66M	84.00%	44.54K	2.70%	1.15M	0.23M	19.70%	0.92M	80.30%	24.35K	2.60%	1.71
rs411x_imp3_jh099c	4.24M	78.06K	1.80%	3.89M	91.50%	0.52M	13.30%	3.37M	86.70%	94.86K	2.80%	1.15M	0.24M	21.20%	0.91M	78.80%	24.18K	2.70%	3.38
rehxxx_imp3_jh101a	1.69M	36.90K	2.20%	1.51M	89.50%	0.29M	19.00%	1.22M	81.00%	16.57K	1.40%	0.53M	0.16M	30.00%	0.37M	70.00%	5.07K	1.40%	2.85
rehxxx_imp3_jh101b	4.00M	74.22K	1.90%	3.72M	93.00%	0.70M	18.90%	3.02M	81.10%	38.84K	1.30%	1.28M	0.35M	27.30%	0.93M	72.70%	12.09K	1.30%	2.91
rehxxx_imp3_jh101c	2.87M	66.36K	2.30%	2.64M	92.00%	0.55M	20.70%	2.10M	79.30%	32.23K	1.50%	0.80M	0.26M	32.60%	0.54M	67.40%	7.71K	1.40%	3.3

	PCR DUPS	EXCLUDING PCR DUPS	
	MappedCnt	MappedCnt_	PCR Dup rate
rs411x_imp3_jh099a	1.89M	1.10M	1.72
rs411x_imp3_jh099b	1.97M	1.15M	1.71
rs411x_imp3_jh099c	3.89M	1.15M	3.38
rehxxx_imp3_jh101a	1.51M	0.53M	2.85
rehxxx_imp3_jh101b	3.72M	1.28M	2.91
rehxxx_imp3_jh101c	2.64M	0.80M	3.3

APPENDIX II:

“BALR-6 regulates cell growth and cell survival in B-lymphoblastic leukemia”

(reprint)

RESEARCH Open Access

BALR-6 regulates cell growth and cell survival in B-lymphoblastic leukemia

Norma I. Rodríguez-Malavé[1,2], Thilini R. Fernando[1], Parth C. Patel[1], Jorge R. Contreras[1,2], Jayanth Kumar Palanichamy[1,7], Tiffany M. Tran[1], Jaime Anguiano[1], Michael J. Davoren[5,6], Michael O. Alberti[1], Kimanh T. Pioli[1], Salemiz Sandoval[1], Gay M. Crooks[1,2,3,4] and Dinesh S. Rao[1,2,3,4*]

Abstract

Background: A new class of non-coding RNAs, known as long non-coding RNAs (lncRNAs), has been recently described. These lncRNAs are implicated to play pivotal roles in various molecular processes, including development and oncogenesis. Gene expression profiling of human B-ALL samples showed differential lncRNA expression in samples with particular cytogenetic abnormalities. One of the most promising lncRNAs identified, designated B-ALL associated long RNA-6 (BALR-6), had the highest expression in patient samples carrying the MLL rearrangement, and is the focus of this study.

Results: Here, we performed a series of experiments to define the function of BALR-6, including several novel splice forms that we identified. Functionally, siRNA-mediated knockdown of BALR-6 in human B-ALL cell lines caused reduced cell proliferation and increased cell death. Conversely, overexpression of BALR-6 isoforms in both human and mouse cell lines caused increased proliferation and decreased apoptosis. Overexpression of BALR-6 in murine bone marrow transplantation experiments caused a significant increase in early hematopoietic progenitor populations, suggesting that its dysregulation may cause developmental changes. Notably, the knockdown of BALR-6 resulted in global dysregulation of gene expression. The gene set was enriched for leukemia-associated genes, as well as for the transcriptome regulated by Specificity Protein 1 (SP1). We confirmed changes in the expression of SP1, as well as its known interactor and downstream target CREB1. Luciferase reporter assays demonstrated an enhancement of SP1-mediated transcription in the presence of BALR-6. These data provide a putative mechanism for regulation by BALR-6 in B-ALL.

Conclusions: Our findings support a role for the novel lncRNA BALR-6 in promoting cell survival in B-ALL. Furthermore, this lncRNA influences gene expression in B-ALL in a manner consistent with a function in transcriptional regulation. Specifically, our findings suggest that BALR-6 expression regulates the transcriptome downstream of SP1, and that this may underlie the function of BALR-6 in B-ALL.

Keywords: lncRNA, B-ALL, MLL, SP1, Microarray, Leukemia, RNA, Non-coding RNA

Background

The human genome produces thousands of non-coding transcripts [1]. These include the recently described class of long non-coding RNAs (lncRNAs), which have distinct chromatin signatures and epigenetic marks, designating them as unique structures that are conserved in mammals [2, 3]. More recently, comparison of lncRNA expression in zebrafish to that of mammals has suggested that although these structures retain limited overall sequence conservation among vertebrates, they show strong conservation of short stretches of sequence, chromosomal synteny and functional conservation [4]. Prior studies have shown that lncRNAs play a variety of roles in the regulation of transcription, splicing and miRNA function [5–7]. This may not be an exhaustive description of the functions of lncRNAs, as new functions are being discovered in other cellular processes [8, 9]. As might be expected, considering their roles in critical cellular functions, lncRNAs have been found to be dysregulated in cancer, with

* Correspondence: drao@mednet.ucla.edu
[1]Department of Pathology and Laboratory Medicine, UCLA, Los Angeles, USA
[2]Cellular and Molecular Pathology Ph.D. Program, UCLA, Los Angeles, USA
Full list of author information is available at the end of the article

functional roles in oncogenesis described for a handful of lncRNAs so far [10–13].

B-lymphoblastic leukemia (B-acute lymphoblastic leukemia, B-ALL) is a malignancy of precursor B-cells harboring mutations and translocations that result in dysregulated gene expression [14, 15]. We have recently completed a comprehensive description of lncRNAs in B-ALL and analyzed the association of lncRNA expression with clinicopathologic parameters. Our study showed differential lncRNA expression in samples with particular cytogenetic abnormalities [16]. One of the lncRNAs from our study, designated B-ALL associated long RNA-6 (BALR-6), was significantly upregulated in all subsets of patient samples when compared to normal CD19+ cells. Interestingly, the highest expression of BALR-6 was seen in patient samples carrying the MLL rearrangement [16]. MLL rearranged B-ALL cases have a very poor prognosis and occur in infants, making them particularly hard to treat [17].

Located on chromosome 3p24.3 in humans, *BALR-6* exists in a syntenic gene block with neighboring genes *SATB1* and *TBC1D5* that is conserved in several vertebrate species (Fig. 1a, b and d) [16]. Analysis of publically available data from the Broad Institute/ENCODE shows H3K4m3 and H3K36m3 modifications along the promoter and gene body at *LOC339862*, where BALR-6 resides, indicating that it is a transcriptional element (Fig. 1a) [4, 16, 18–20]. Alternative splicing analysis by the Swiss Institute of Bioinformatics predicted multiple transcripts expressed at this gene locus (Additional file 1: Figure S1A) [21]. Moreover, 100 Vertebrate PhastCons analyses of the *BALR-6* locus demonstrated significant conservation of the gene body, suggesting a functional transcript (Fig. 1b) [22].

To further study this lncRNA we undertook loss-of-function analyses in B-ALL cell lines and gain-of-function analyses in vivo. We found that BALR-6 is a pro-survival factor for B-ALL cell lines, and that its knockdown led to decreased growth and increased apoptosis of these cells. In vivo, overexpression of BALR-6 led to an alteration of hematopoiesis with a shift to more immature progenitor populations. Gene expression analyses of knockdown cell lines showed a differentially expressed gene set in BALR-6 knockdown cells, with enrichment for SP1 transcriptional targets and leukemogenic genes. Finally, luciferase assays demonstrated an increase in transcriptional activity when SP1 and BALR-6 were co-expressed. Together, these findings point to a role for BALR-6 in cellular survival, leukemogenesis and highlight the role of novel elements of gene regulation in B-ALL.

Results

BALR-6 knockdown inhibits proliferation of human B-ALL cell lines

To comprehensively study the function for this novel lncRNA, we first characterized the transcripts originating at the genomic locus corresponding to *BALR-6*. Using RS4;11 cell line mRNA, Rapid Amplification of cDNA Ends (RACE) uncovered multiple isoforms; from these, three were cloned and sequenced corresponding to the genomic locus as shown (Additional file 1: Figure S1A-B). Northern Blot analysis of RS4;11 DNAse treated RNA revealed the expression of two isoforms containing exon 3 and exon 5 sequences, one sized at ~3.8 Kb and the other at ~1.2 Kb (Additional file 1: Figure S1C). The annotated mRNA and new alternative splice forms, including unannotated exons, were confirmed as depicted in Fig. 1c. Isoform 1 contains several small open reading frames (ORFs), however no Kozak sequences are found in their initial ATG region, and the predicted ORFs do not resemble any known functional proteins or peptide [23]. Isoforms 2 and 3 lacked open reading frames and translation initiation sites as evaluated by EMBOSS Transeq, predicting them to be non-coding transcripts (Additional file 1: Figure S1D).

To map the murine homologous transcript, we carried out 5′RACE and 3′RACE using mRNA extracted from murine pre B-ALL cell line 70Z/3. The sequences uncovered matched the human BALR-6 sequence, confirming that there is a murine transcript originating from this same locus (Additional file 1: Figure S1E). Further analysis by BLAT showed genomic conservation of syntenic blocks in a variety of vertebrates, including *Xenopus tropicalis* (Fig. 1d). Together, these data demonstrate a highly conserved, functional and complex gene locus that expresses multiple non-coding transcripts, some yet to be discovered. During normal B cell development, BALR-6 is dynamically expressed, with high expression in pre-B cells and subsequent downregulation (Fig. 2a). This suggests that the high expression of BALR-6 in B-ALL could represent a stage-specific expression pattern in leukemia derived from early stages of B-cell development. To elucidate a cellular function for BALR-6, we first evaluated the expression levels of the transcripts in human B-ALL cell lines. BALR-6 expression was highest in RS4;11 cells and MV(411) cells, which carry the MLL-AF4 rearrangement, when compared to other lines (Fig. 2b). Additionally, RS4;11 cells treated with bromodomain and extra-terminal (BET) motif binding protein inhibitor I-BET151 [24] showed decreased levels of BALR-6 in a dose-dependent manner (Fig. 2c). Given that I-BET151 has previously been shown to inhibit transcription downstream of MLL, we propose that BALR-6 expression is induced by MLL, although this effect may not be entirely specific to MLL-AF4.

Using the approach described previously, siRNAs against the splice junctions between exons of BALR-6 were cloned into a mmu-miR-155 expression cassette (Additional file 1: Figure S2A) [4, 16, 25, 26]. We observed knockdown of all the identified transcripts in

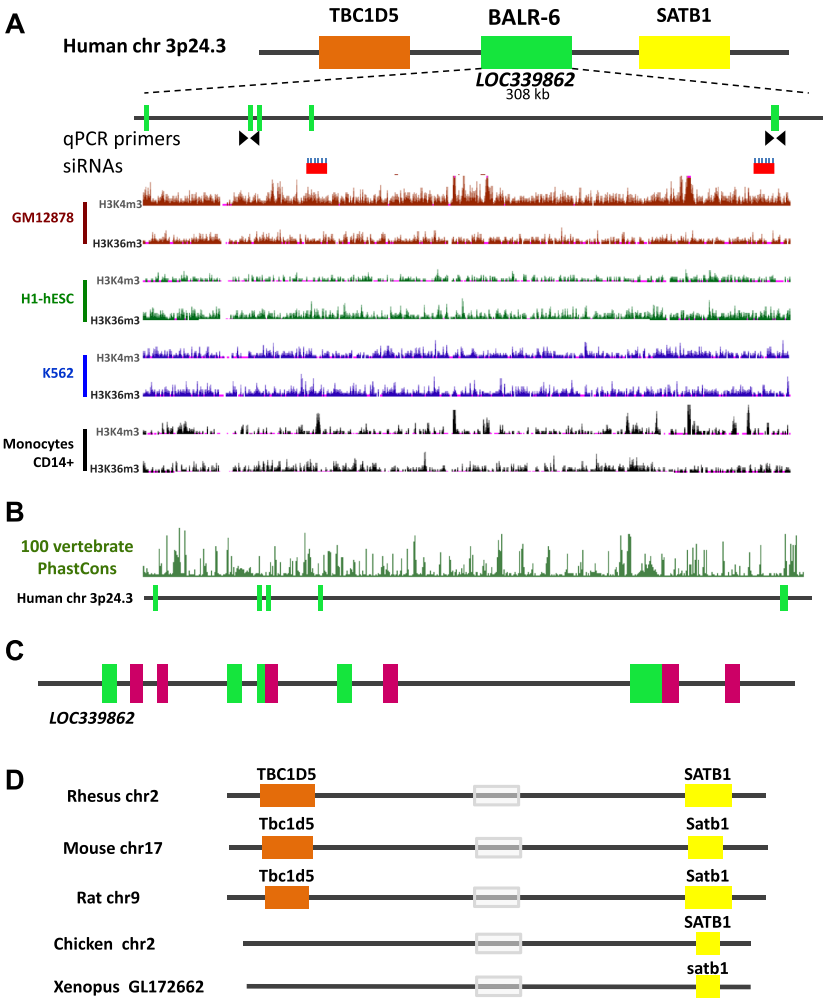

Fig. 1 Molecular characterization of *BALR-6*. **a** Top: Chromosomal location of *BALR-6* in the human genome, surrounding genes, qPCR primers, siRNAs, known annotated exons (*green boxes*), known introns (*black lines*) are shown. Bottom: Chip-Seq histone modification map from the Broad institute/ENCODE, taken from UCSC genome browser, shows H3K4m3 and H3K36m3 patterns at *LOC339862* in four different cell types indicating active transcription of the lncRNA. **b** The 100 Vertebrate PhastCons plot from the UCSC whole-genome shows conserved regions among 98 vertebrates including mice and zebrafish throughout the locus. **c** RACE discovered unannotated exons (*magenta*) depicted with known annotated exons (*green*) at *LOC339862*. **d** Schematic depicting genomic conservation of the syntenic block among multiple vertebrates, as analyzed by BLAT. Grey box indicates location of homology to *BALR-6*

multiple B-ALL cell lines (Fig. 2d and Additional file 1: Figure S2B). Transduced B-ALL cells showed a reduction in proliferation as early as 48 h after plating, with consistent reduction in proliferation observed over the full duration of the assay (up to 144 h) (Fig. 2e, f and Additional file 1: Figure S2C). siRNA-transduced B-ALL cells had significantly higher levels of apoptosis, as measured by AnnexinV, when compared with vector-transduced lines (Fig. 2g, h and Additional file 1: Figure S2D). Flow cytometry demonstrated that the siRNA2-transduced RS4;11 cell lines had an increase in Sub-G0 cells and a decrease in all other cell stages, consistent with increased apoptosis and decreased flux through the cell cycle (Fig. 2i). Together, these findings suggest a modest yet conserved role for BALR-6 in the regulation of B-ALL cell survival and proliferation.

Constitutively expressed BALR-6 supports cell survival and proliferation

To examine the effects of BALR-6 gain of function, we overexpressed the previously identified isoforms in the human B-ALL cell line Nalm-6, which has relatively low

endogenous levels of the transcript (Figs. 2b and 3a). Gene transfer was conducted via a lentiviral expression system that has proven successful in our previous studies (Additional file 1: Figure S2E) [16]. Constitutive overexpression of BALR-6 Isoforms 2 and 3 led to a significant increase in proliferation as measured by MTS (Fig. 3c). In addition to an observed increase in overall growth rate, BALR-6 Isoforms 2 and 3 caused an increase in S phase cells and G2-M cells (Fig. 3d). Furthermore, AnnexinV staining showed significantly lower numbers of apoptotic cells under basal growth conditions in cell lines overexpressing any of the BALR-6 isoforms (Additional file 1: Figure S2G).

To overexpress BALR-6 in mouse cells, we constructed a set of MSCV-based bicistronic vectors (Fig. 3b, Additional file 1: Figure S2F). Successful overexpression of these constructs in murine pre B-ALL 70Z/3 cells led to a modest increase in proliferation (Fig. 3e and f). Cell cycle analysis of these lines showed an increase of S phase cells, G2-M cells (in Isoform 3 overexpressing lines) and a reduction in Sub-G0 cells, similar to the effects in Nalm-6 cells (Fig. 3g and h). Analysis by AnnexinV staining confirmed the lower number of apoptotic cells in Isoform 3 expressing cell lines (Additional file 1: Figure S2H). Moreover, these 70Z/3 Isoform 3 overexpression lines were less vulnerable to prednisolone-induced apoptosis (Additional file 1: Figure S2I). Conversely, siRNA-transduced RS4;11 cells were more prone to prednisolone-induced apoptosis (Additional file 1: Figure S2I). Therefore, knockdown and overexpression of BALR-6 had opposing phenotypes in B-ALL cell lines, and gain-of-function phenotypes were conserved in both human and mouse cells.

Enforced BALR-6 expression promotes expansion of hematopoietic progenitor populations in vivo

Since BALR-6 is highly expressed in B-ALL, we tested the effects of constitutive expression in an in vivo model [16]. 5-FU enriched bone marrow was transduced with retrovirus expressing the BALR-6 Isoform 3 and transplanted into lethally irradiated hosts (Fig. 3 and Additional file 1: Figure S2F, 2H). Mice were followed with peripheral bleeds for 16 weeks and then sacrificed for analysis. Peripheral white blood cell counts were not statistically different between the control and experimental groups. However, mice with enforced expression of BALR-6 showed a trend towards lower red blood cell counts, hematocrit and platelet counts (Additional file 1: Figure S3A). Flow cytometry revealed a lower percentage of CD11b + myeloid cells and a higher percentage of B220+ B-cells, but no difference in CD3ε + T-cell percentage in the eGFP+ population of experimental mice (Additional file 1: Figure S3B-C).

Mice were sacrificed following 4 months of reconstitution. Gross analysis showed no changes in the thymus, spleen, livers or kidneys. Microscopic inspection of hematoxylin and eosin – stained tissues did not reveal any differences (Additional file 1: Figure S3D). In the bone marrow, qRT-PCR confirmed successful overexpression of BALR-6 (Additional file 1: Figure S4A-B). Analysis by flow cytometry revealed an increase in precursor cell populations in the eGFP+ population of the experimental mice, when compared to the control group (Fig. 4a and b, Additional file 1: Figure S5C). After exclusion of differentiated cells in the bone marrow, we observed increased relative proportion of Lin-Sca1 + c-Kit + (LSK) cells, hematopoietic stem cells (HSCs) and lymphoid-primed multipotent progenitors (LMPPs) in mice overexpressing BALR-6 (Fig. 4a and b). An increase in the relative population of Lin-Sca1^{lo}c-Kit^{lo} cells and a trend towards increased relative population of common lymphoid progenitors (CLPs) was also observed (Additional file 1: Figure S4C). The developmental pathway of B-cells in the bone marrow was investigated by the method of Hardy et al. [27]. Once again, trends towards higher relative proportions of these B-cell developmental stages were observed (fractions A-F, Additional file 1: Figure S4D). Taken together, these results suggest that BALR-6 overexpression leads to an enrichment of early developmental stage cells in murine bone marrow, indicating that its expression confers a survival advantage or increased proliferation for cells in these earlier stages.

BALR-6 regulates expression of genes involved in multiple biological processes

At the molecular level, several studies have demonstrated that many lncRNAs act as transcriptional regulators [5, 11, 23, 28, 29]. To explore whether or not BALR-6 regulates gene expression, RNA isolated from knockdown cell lines was analyzed by microarray [30, 31]. Upon siRNA mediated knockdown of BALR-6, 2499 probes showed differential expression. Of these, 1862 unambiguously mapped to 1608 unique Entrez Gene IDs. Unsupervised hierarchical clustering analysis identified differentially expressed genes in the siRNA-expressing cell lines (Fig. 5a).

Further data analysis was carried out using WebGESTALT [32, 33]. Gene Ontology (GO) slim classification of differentially expressed genes by molecular function was utilized to provide insight into the pathways in which BALR-6 is involved, with protein binding function category having the most dysregulated genes (Fig. 5b). A number of biological processes, as annotated in the GO database, were significantly dysregulated in BALR-6 knockdown cell lines, including cell death and cell proliferation (Fig. 5c). Disease associated enrichment analysis, which was inferred using GLAD4U, showed an enrichment of genes known to be dysregulated in various disease states (Fig. 5e). Of the 38 significantly associated

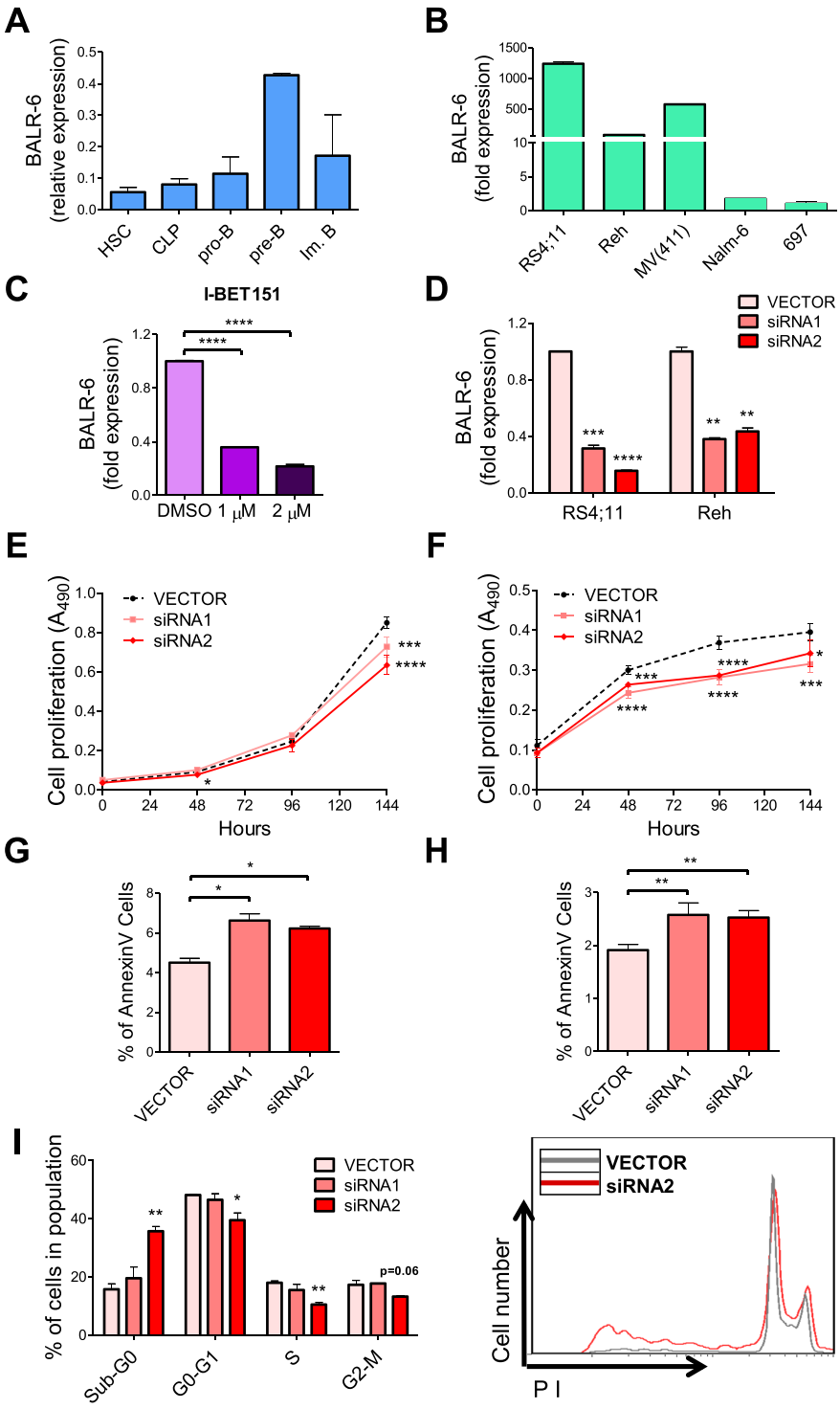

Fig. 2 (See legend on next page.)

(See figure on previous page.)
Fig. 2 BALR-6 knockdown reduces cell proliferation and increases apoptosis in human B-ALL cells. **a** BALR-6 expression in human bone marrow B-cell subsets by qRT-PCR. Normalized to ACTIN. **b** Quantitation of BALR-6 expression in human B-ALL cell lines by qRT-PCR confirming elevated levels in MLL translocated cell lines RS4;11, and MV(411). Normalized to ACTIN. **c** RS4;11 cell lines treated with 1 μM, and 2 μM of I-BET151 inhibitor for 36 h, presented a decrease in BALR-6 expression levels. Normalized to ACTIN. **d** qRT-PCR quantification of BALR-6 in RS4;11 and Reh cell lines transduced with vector control, siRNA1 or siRNA2. Normalized to ACTIN. **e**, **f** Decreased cell proliferation, upon siRNA mediated knockdown of BALR-6 in RS4;11 cells **e**, and Reh cells **f** as measured by MTS. **g**, **h** AnnexinV staining showed that siRNA mediated knockdown of BALR-6 in RS4;11 cells **g**, and Reh cells **h** resulted in an increase of apoptosis. **i** Propidium iodide staining of RS4;11 knockdown cell lines showed an increase in Sub-G0 and a decrease in G0-G1, S and G2-M cells. Representative histogram of (**i**) confirms cell cycle changes by siRNA2, shown to the right. HSC, hematopoietic stem cell; CLP, common lymphoid progenitor; pro-B, progenitor B; pre-B, precursor B; DMSO, dimethyl sulfoxide. Evaluations were made using a two-tailed *T*-test, $p < 0.05$ (*); $p < 0.005$ (**); $p < 0.0005$ (***); $p < 0.0001$ (****)

disease states, 14 were of leukemic origin. Transcription factor enrichment analysis showed a significant enrichment of genes that are predicted targets of SP1, among other transcription factors (Fig. 5d). Taken together, these data revealed the biological importance of BALR-6. A detailed description of the microarray analyses can be found in the methods.

SP1 transcriptome is modulated by BALR-6

As indicated by the transcription factor enrichment analysis, we confirmed that the expression SP1 and CREB1, a target and interactor of SP1, were dysregulated upon BALR-6 knockdown (Fig. 6a). The strongest phenotype was seen in the siRNA2-mediated knockdown, which also showed the strongest cellular phenotypes in the majority of pre B-ALL cell lines (Figs. 2d, i and 6a, Additional file 1: Figure S2B-D and Figure S5A-B). Conversely, increased levels of SP1 and CREB1 correlated with overexpression of BALR-6 isoforms in both human and murine cell lines (Nalm-6 and 70Z/3) (Fig. 6b).

To confirm our findings, a second microarray analysis was carried out with technical duplicates of RS4;11 cell lines transduced with empty vector or siRNA2. 2756 probes showed differential expression. Of these, 2280 unambiguously mapped to 2128 Entrez Gene IDs and were analyzed by hierarchical clustering (Additional file 1: Figure S6A). Enrichment analysis in WebGESTALT revealed similar GO slim classifications (Additional file 1: Figure S6B-C), and transcription factor target enrichment analysis confirmed the significant enrichment of SP1 targets seen previously (Fig. 5d, Additional file 1: Figure S6D). Additionally, enrichment of CREB1 targets was significant (Additional file 1: Figure S6D). Notably, leukemic diseases were the only ones significantly enriched in the disease association analysis (Additional file 1: Figure S6E). Together, these findings indicated a consistent change in the transcriptome, particularly downstream of SP1, upon knockdown of BALR-6 in MLL rearranged B-ALL.

To further understand the relationship of BALR-6 and SP1, we examined promoter regions of known SP1 targets (CREB1 and p21) and cloned these sequences into the luciferase reporter vector, pGL4.11 (Fig. 6c). The CREB1 promoter contained 7 putative SP1 binding sites, while the p21 promoter contained 6 such sites (Additional file 1: Figure S5C-D). Luciferase reporter assays in HEK 293 T cells with constitutive expression of SP1, Isoform 1, Isoform 3 or a combination of these vectors, revealed increased luciferase activity in both promoters (Fig. 6d and e). Notably, when SP1 and BALR-6 were co-overexpressed, we noted a strong increase in transcriptional activity with both the CREB1 and p21 promoter.

Discussion

The discovery of lncRNAs has revolutionized how we think about gene expression. The genomic organization of many lncRNAs is indeed complex. Some are found in regions overlapping with protein coding genes, while others that are exclusively intergenic [2, 4]. Some lncRNAs contain microRNAs within either their exonic or intronic sequence [34, 35]. Here, we have characterized several isoforms of a lncRNA that is overexpressed in leukemia and shows dynamic expression in hematopoietic development [16]. Expressed from a locus adjacent to genes important in lymphocyte development, BALR-6 itself is dynamically regulated during human B-cell development [36–38]. Our work significantly adds to the known repertoire of RNA molecules that are expressed from this locus, and several of these appear to be functional within a cellular context.

In this manuscript, we describe the cellular function of a second lncRNA that was discovered as being overexpressed in MLL-translocated B-ALL. In some ways, BALR-6 shows some similarities with the other lncRNA we studied, BALR-2 [16]. Indeed, knockdown of both lncRNAs led to decreased cell growth and increased apoptosis, and overexpression led to increased growth and a partial resistance to prednisolone treatment. These findings are not altogether surprising given that these lncRNAs may be contributing to the poor clinical behavior of an aggressive cytogenetic subtype of B-ALL [17]. However, there are important differences between these lncRNAs—the genomic locus for BALR-6 is more complex, there are multiple isoforms and no comparable murine transcript is described in publically available databases. Nonetheless, we have obtained fragments of a

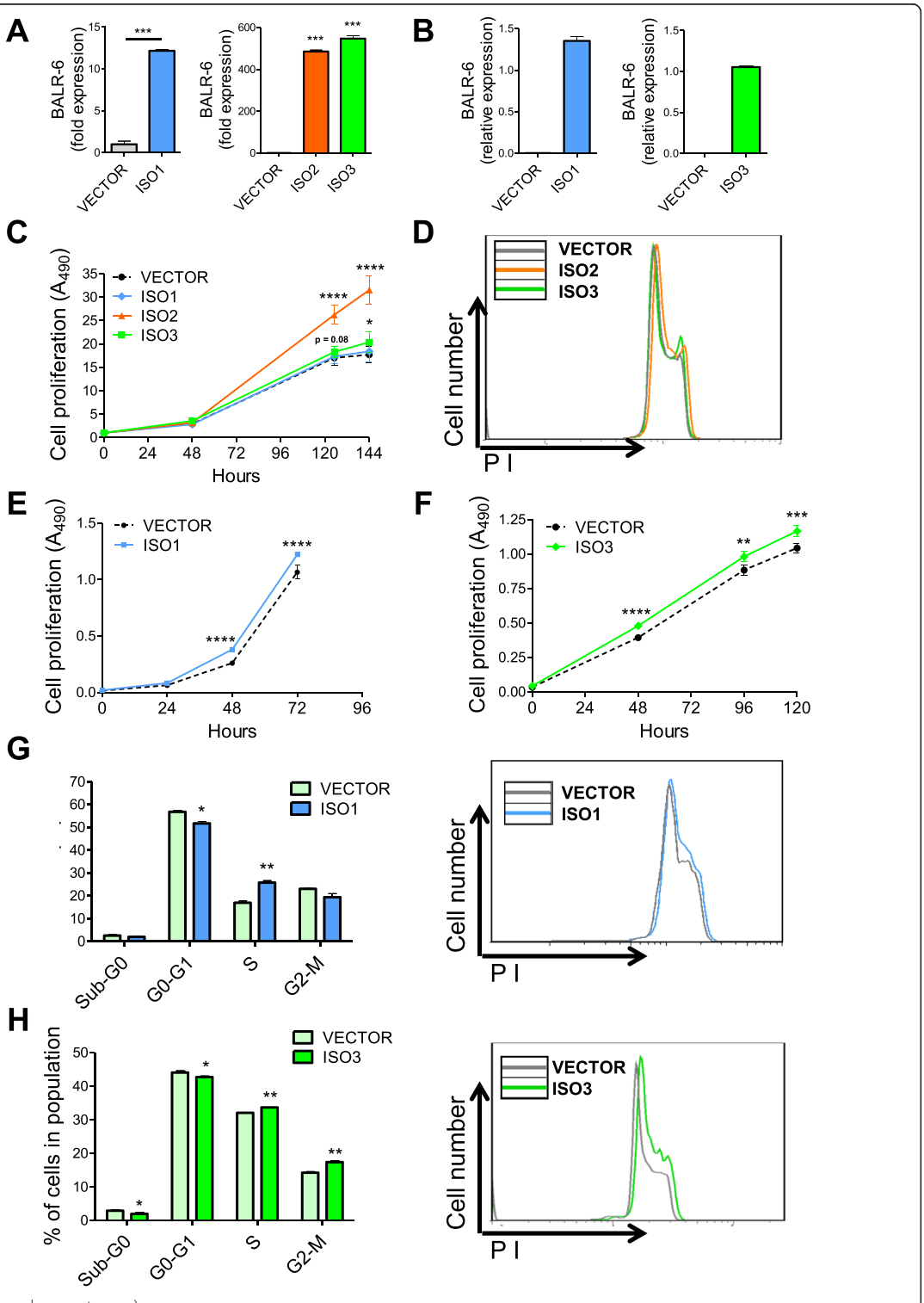

Fig. 3 (See legend on next page.)

(See figure on previous page.)
Fig. 3 BALR-6 overexpression increases proliferation in human Nalm-6 and murine 70Z/3 cells. **a** qRT-PCR quantitation of BALR-6 isoform expression in Nalm-6 human pre B-ALL cell line. Normalized to ACTIN. **b** qRT-PCR quantification of BALR-6 isoforms in 70Z/3 mouse pre B-ALL cell line. Normalized to Actin (ISO1) or L32 (ISO3). **c** Increased cell proliferation in BALR-6 overexpressing Nalm-6 cell lines, as measured by MTS. **d** Representative histogram of Nalm-6 overexpression lines, stained with propidium iodide, shows an increase in S phase cells and G2-M cells. **e**, **f** Increased cell proliferation in BALR-6 Isoform 1 (**e**) and Isoform 3 (**f**) overexpressing 70Z/3 cell lines, as measured by MTS. **g**, **h** Propidium iodide staining of 70Z/3 cells overexpressing BALR-6 Isoform 1 (**g**) and Isoform 3 (**h**), shows a consistent increase in G2-M cells, and a decrease in Sub-G0 cells. Representative histogram of figures (**g-h**) confirmed the increase in cells in the G2-M when compared to the empty vector, shown to the right. ISO1, Isoform 1; ISO2, Isoform 2; ISO3, Isoform 3. Evaluations were made using a two-tailed *T*-test, $p < 0.05$ (*); $p < 0.005$ (**); $p < 0.0005$ (***); $p < 0.0001$ (****)

low-expression transcript from murine hematopoietic cell lines that encoded portions homologous to human BALR-6. Further characterization of the murine transcripts will be the goal of future studies.

Significantly, our study is amongst the few characterizations of lncRNA dysregulation in the hematopoietic system [16, 39–41]. LncRNAs have been ascribed functions in lymphopoiesis, myelopoiesis and erythropoiesis [42–45]. Additionally, their differential expression has been described in peripheral T-cell subsets [46]. Here, we discovered the effect of BALR-6 overexpression on early hematopoietic progenitors in the marrow, including LSK cells, HSCs and LMPPs. Constitutive expression of BALR-6 isoforms led to increased survival or proliferation of normally transient bone marrow progenitor cells. Furthermore, Hardy fractions showed a trend towards being increased when compared to control, particularly those that developmentally precede the large pre B-cell stage (fraction C', early pre-B). The relative percentages of more mature B-lineage cells downstream of these developmental stages are largely normal. Despite increased proportions of early progenitor cells, passage through a checkpoint (such as the pre-BCR checkpoint) may reduce cell numbers back to baseline. This suggests that the function of BALR-6 in vivo may be in directing differentiation and adequate lymphoid cell development. The upregulation of this lncRNA causes a survival or proliferative advantage, a hallmark of leukemogenesis. Coupling BALR-6 overexpression with an appropriate oncogenic co-stimulus may lead to full-blown leukemogenesis or enhancement thereof, and this is currently an active area of investigation in the laboratory.

In line with a function in promoting the survival of early hematopoietic progenitors, BALR-6 clearly affects proliferation in cell line experiments. Upon siRNA mediated knockdown, we saw reduced cell proliferation and increased cell death. We observed the opposite effect when we constitutively expressed BALR-6 in human and murine B-ALL cell lines. Moreover, similar mechanisms may be operant in B-ALL with MLL translocations, and loss-of-function experiments in primary patient samples and mouse models of MLL-driven leukemia are areas for further investigation.

Given prior reports of lncRNAs serving to regulate transcriptional complexes, our finding that BALR-6 knockdown causes changes in the SP1 transcriptome is compelling. SP1 is a transcriptional regulator that is associated with dysregulated cell cycle arrest in multiple myeloma [47–49]. CREB1 is a well-known proto-oncogene that promotes cellular proliferation in hematopoietic cells [50, 51]. Here we demonstrate that SP1-mediated transcription at the CREB1 and p21 promoters are positively regulated by BALR-6, providing a putative mechanism for our observations of BALR-6's role in B-ALL.

Conclusions

In this study, we demonstrate that the MLL-AF4-dysregulated lncRNA, BALR-6, plays a role in cell survival and regulates hematopoietic progenitors. At the molecular level, BALR-6 regulates the transcriptome of B-ALL cell lines, likely through regulating SP1-mediated transcription. In summary, our study has several novel and unique findings that help uncover a role for a poorly understood class of molecules in a pathogenetic process. This will undoubtedly have impacts on our understanding of molecular biology within cancer cells.

Methods

Cloning and cell culture

mmu-miR-155 formatted siRNAs were cloned into BamHI and XhoI sites in the pHAGE2-CMV-ZsGreen-WPRE vector using the strategy that we have previously described to generate knockdown vectors [16, 25, 26, 52]. Using the sequence information from 5′ and 3′ RACE products we cloned full length transcripts into an MSCV-based bicistronic viral vector between the BamHI and XhoI sites, as described previously and into a pHAGE6-UBC-ZsGreen-CMV-LNC (P6UZCL) variant of the third generation lentiviral vector system, between the NotI and BamHI sites [16, 52]. Primer sequences used are listed in Additional file 2: Table S1 or mentioned previously [16]. RS4;11 and MV(411), (MLL-AF4-translocated; ATCC CRL-1873 and CRL-9591), Reh (TEL-AML1-translocated; CRL-8286), 697 (E2A-PBX1-translocated), Nalm-6, 70Z/3 (ATCC TIB-158) murine pre B-cell leukemic cell line, and the HEK 293 T cell line (ATCC CRL-11268) were grown

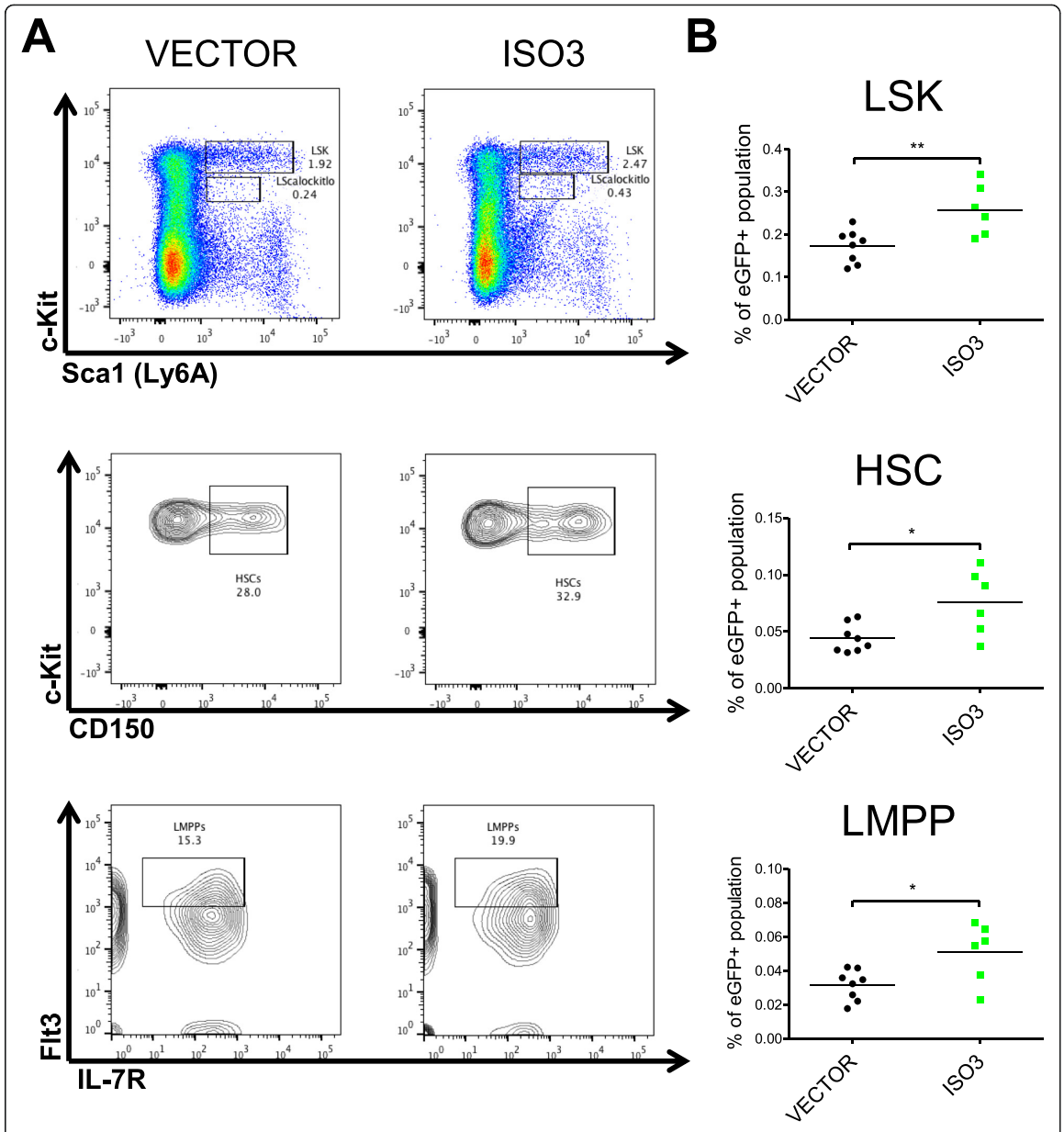

Fig. 4 BALR-6 overexpression causes an increase in hematopoietic precursor cells in vivo. **a** Representative FACS plots of hematopoietic progenitor populations LSK, HSC and LMPP in bone marrow transfer mice. **b** Quantitation of progenitor populations showing a significant increase in experimental mice when compared to control. Number of mice used in this analysis: VECTOR, $n = 8$; ISO3, $n = 6$. ISO3, Isoform 3; HSC, hematopoietic stem cell; LMPP, lymphoid primed multipotent progenitor; LSK, lineage- Sca1+ c-Kit+. Evaluations made using a two-tailed *T*-test, $p < 0.05$ (*); $p < 0.005$ (**)

in their corresponding media at 37 °C in a 5 % CO_2 incubator as previously described [16, 53].

Rapid amplification of cDNA ends (RACE)

To determine the 5′ and 3′ transcript ends of the lncRNAs, we performed RACE using First Choice RLM-RACE kit (Ambion). Using the sequence information from 5′ and 3′ RACE products, we cloned full length transcripts into P6UZCL, and into the MSCV viral vector. Primer sequences used and isoform sequences obtained are listed in Additional file 2: Table S1.

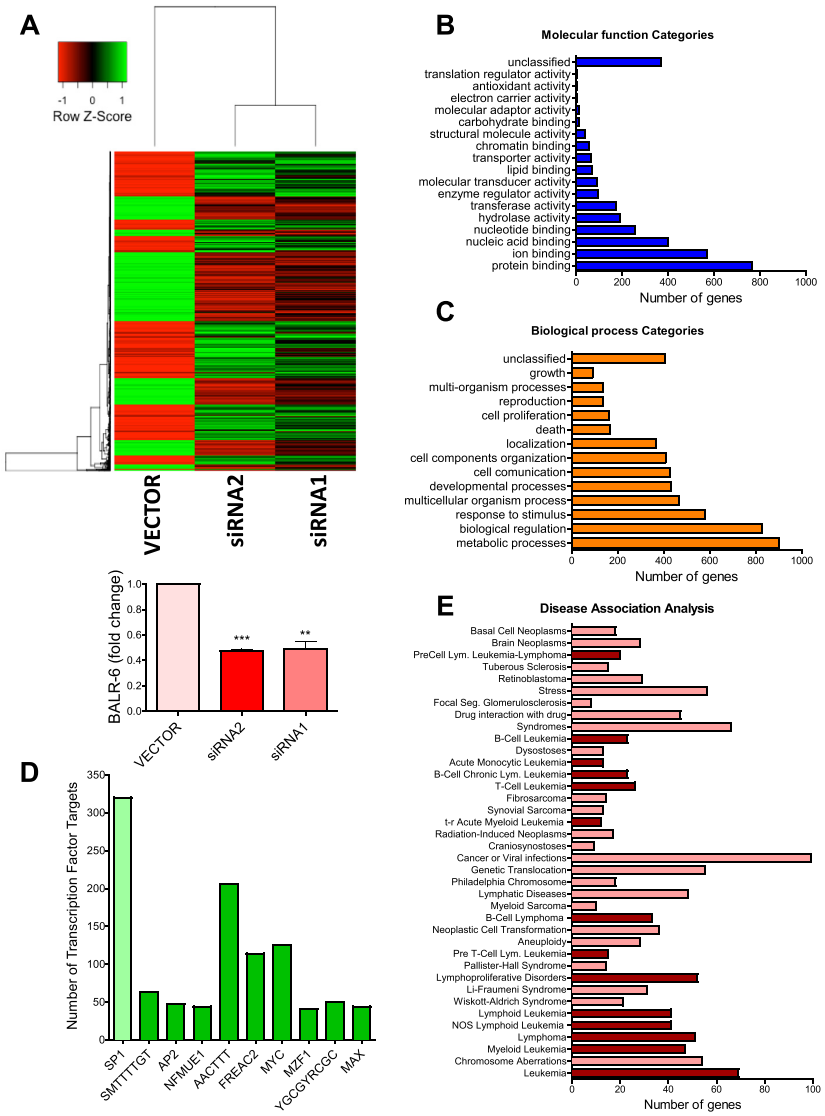

Fig. 5 BALR-6 knockdown leads to global differential expression of genes. **a** Unsupervised hierarchical gene clustering of differentially expressed genes upon BALR-6 siRNA mediated knockdown in RS4;11 cells (PPDE ≥ 95 %, fold change ≥ 1.5). qRT-PCR confirmation of BALR-6 knockdown shown below. Normalized to ACTIN. **b**, **c** Bar graphs of GO Slim classification enrichment analysis of differentially expressed genes by molecular function (**b**), and biological processes (**c**). **d** Enrichment analysis of transcription factor targets. Top ten transcription factors with a *p*-value ≤ 0.0001 are shown. SP1 had the highest number if dysregulated targets, highlighted in light green. For unknown transcription factors, binding site sequence is shown. **e** Disease association analysis by GLAD4U, revealing enrichment of genes associated to various malignancies, in particular, hematological malignancies (*dark red*). Diseases with a *p*-value ≤ 0.05 are shown.; PPDE, posterior probability of differential expression. Evaluations were made using a two-tailed *T*-test, $p < 0.005$ (**); $p < 0.0005$ (***)

Transduction and sorting of cell lines

Lentiviruses and MSCV-based retroviruses were produced to generate knockdown constructs as previously described [16, 25, 26, 52]. In brief, 5.0×10^5 cells were spin-infected at 30 °C for 90 min in the presence polybrene (4 μg/mL). Transduced cell lines were sorted for high green expression using a BD FACSAriaII cell sorter, and analysis was performed using BD FACSDiva software.

Biological assays

For pharmaco-induced assays, cells were cultured at a concentration of 1.0×10^6 cells per mL and treated for

36 h. I-BET151 was dissolved in dimethyl sulfoxide to desired concentrations. After treatment, cells were harvested for RNA extraction. For MTS proliferation assays, cells were cultured for at least 5 days before plating. Cells were plated at a density of 2500 cells per 100 μl of media in each well of a 96 well plate. Reagents were added according to the manufacturer's instructions (Promega CellTiter 96 Aqueous Non-Radioactive Cell Proliferation Assay kit) and cells were incubated at 37 °C, 5 % CO_2 for 4 h before absorbance was measured at 490 nm. For apoptosis assays, cells were plated at 5.0×10^5 cells/mL for 24 h with or without prednisolone treatment. Prednisolone (TCI America) was dissolved in dimethyl sulfoxide to desired concentrations. Cells were harvested after 24 h and stained with APC-tagged AnnexinV. For cell cycle analysis, cells were synchronized by serum starvation for 12 h (human cell lines) or 4 h (murine cell lines) then plated at 5.0×10^5 cells/mL and incubated at 37 °C, 5 % CO_2 for 24 h. Cells were harvested, fixed with EtOH and then stained with propidium iodide. AnnexinV stained and PI stained samples were analyzed using a BD FACS HTLSRII flow cytometer and further analysis was performed using FlowJo.

Luciferase assays

Promoter sequences for CREB1 and p21 were cloned upstream of synthetic firefly luciferase (luc2p) in the pGL4.11 vector. Renilla luciferase is expressed in the pGL4.75 vector downstream of the PGK promoter. HEK 293 T cells were transfected with the pGL4.75 and pGL4.11 containing reporter vectors at a 1:20 ratio (5 ng:100 ng), along with a combination of MSCV vector (empty, Isoform-1 or Isoform-3) and pCMV3 (empty or SP1-HA, Sino Biological Inc.) vector at a 1:1 ratio (200 ng:200 ng). For the last condition SP1, Isoform1 and Isoform 3 were transfected together at a ratio of 2:1:1 (200 ng:100 ng:100 ng). Co-transfections were performed with BioT (Bioland Scientific LLC) in 24 well plates as per the manufacturer's instructions. Cells were lysed after 32 h and supernatant lysate was collected as per manufacturer's instructions (Promega). The dual luciferase assay kit (Promega) was used as substrates for Renilla and firefly luciferase activity. Luminescence was measured on a Glomax-Multi Jr (Promega). The ratio of firefly to Renilla luciferase activity was calculated for all samples. The luminescence for the sample co-transfected with MSCV empty vector and pCMV3 empty vector, was used as a normalization control.

qRT-PCR and PCR

RNA from cell lines was reverse transcribed using qScript (Quantas Biosciences). Real Time quantitative PCR was performed with the StepOnePlus Real-Time PCR System (Applied Biosystems) using PerfeCTa SYBR Green FastMix reagent (Quantas Biosciences). cDNA from mice samples was amplified using KOD Master Mix (EMD Millipore) and ran on a 1.2 % agarose gel stained with ethidium bromide. Primer sequences used are listed in Additional file 2: Table S1.

Northern blot

Total RNA was separated on a 1.2 % (w/v) formaldehyde agarose gel and then blotted onto Hybond N+ nylon membranes (Amersham Biosciences) by semi-dry transfer (Bio-Rad,

Trans-Blot SD Semi-Dry Transfer Cell). DNA probes were ordered from Integrated DNA Technologies (IDT, San Diego, CA) with digoxigenin incorporated at 3′end. For ACTIN we used the RNA probe provided in the DIG Northern Starter Kit (Roche). Membranes were hybridized overnight using ULTRAhyb-Oligo Buffer (Ambion) at 37 or 42 °C with probes. Visualization was done by X-Ray film using CDP-Star reagents (Roche). X-Ray film was scanned and saved as jpeg files. Brightness and contrast was increased by 20 % for ease of visualization.

Data sources

Human genome assembly GRCh37/hg19 and the mouse genome assembly GRCm38/mm10 were used. Methylation patterns for the four cell lines were obtained from Chip-Seq data available in the UCSC genome browser generated by the Broad/ENCODE group [18–20]. Peak viewing range set from 1–50 for H3K4m3 modifications, and 1–15 for H3K36m3 modifications. Alternative splice form information was obtained from the Swiss Institute of Bioinformatics, via UCSC Genome Browser [21]. Genome alignments of RefSeq transcripts from human, mouse and other vertebrates, GenBank mRNAs and ESTs, as well as PhastCons scores were obtained from the UCSC Genome Browser [22].

Microarray data analysis

Microarray data was generated from samples of 3 different transduced RS4;11 cell lines with siRNAs against BALR-6, or the control empty vector. Samples were hybridized at the UCLA Clinical Microarray Core facility using Affymetrix HG-U133_Plus_2 microarray. The Affymetrix raw data files (.cel files) were loaded into the R program for quality control analysis. Additionally, raw hybridization intensities were normalized using the MAS5 method with the affy package in R. Normalized values were sorted by detection p-value ≤ 0.05. Differential expression analysis was performed using unpaired Bayesian comparison model (CyberT Website) [30, 31]. Data was then sorted for genes with a posterior probability of deferential expression (PPDE) ≥ 95 % and a fold change ≥ 1.5. Analysis of differentially expressed genes was carried

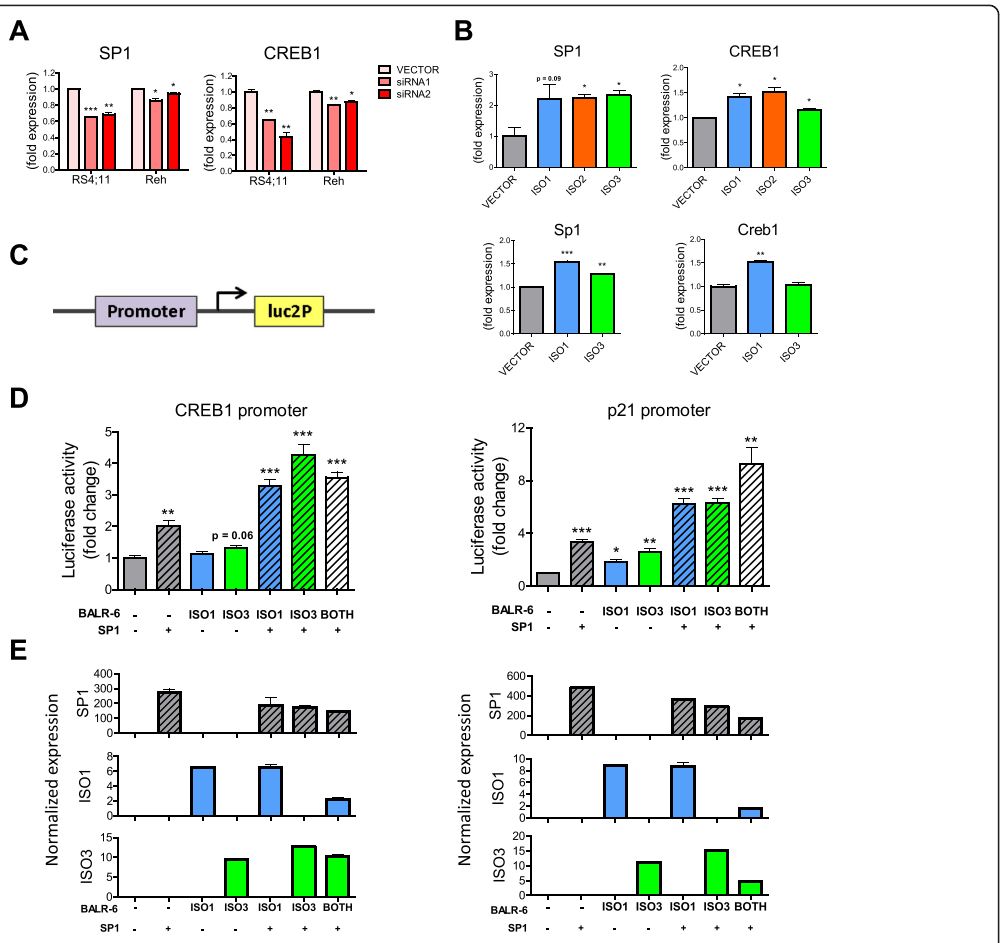

Fig. 6 SP1 transcriptome is modulated by BALR-6. **a** Confirmation of SP1 and CREB1 expression in RS4;11 microarray samples, as well as Reh knockdown cell lines. Normalized to ACTIN. (**b**) SP1 and CREB1 transcript level increase correlates with overexpression of BALR-6 in Nalm-6 cells (*top*) and 70Z/3 cells (*bottom*). Quantitation by qRT-PCR, normalized to ACTIN (Nalm-6 cells) or L32 (70Z/3 cells). **c** Schematic depicting location of cloned promoter sequences in the pGL4.11 vector system for luciferase assays. **d** Transcriptional activity at CREB1 (*left*) and p21 (*right*) promoter regions upon SP1 and/or BALR-6 overexpression, as measured by luciferase activity. **e** Quantitation of overexpression in luciferase assays (as seen in (**d**)) by qRT-PCR of respective transcripts, normalized to ACTIN. Evaluations were made using a two-tailed *T*-test, $p < 0.05$ (*); $p < 0.005$ (**); $p < 0.0005$ (***). luc2p, synthetic firefly luciferase

out using the WEB-based GEne SeT AnaLysis Toolkit (WebGESTALT, http://bioinfo.vanderbilt.edu/webgestalt/) [32, 33]. This online tool uses information from different public data sources for enrichment analysis, including the Gene Ontology data base, and GLAD4U. A second (validation) microarray was carried out, as described above, with technical duplicates for RS4;11 cell lines transduced with siRNA2 or the empty vector. For differential analysis the raw data files were loaded into the R environment and analyzed using the R library of Linear Models for Microarray Data (LIMMA). Pairwise comparison and eBayes fit was carried out. Data was then sorted for genes with a p-value ≤ 0.05. Further analysis was done as described above, using WebGESTALT.

Mice and bone marrow transplantation

Mice were housed under pathogen free conditions at the University of California, Los Angeles (UCLA). Donor mice were injected intraperitoneally with 200 mg/kg of 5-fluorouracil. After 5 days the mice were sacrificed. The bone marrow was collected under sterile conditions and plated in media enriched with IL-3, IL-6 and mSCF (Gibco). 24 h after plating, the bone marrow was spin infected twice, at 30 °C for 90 min in the presence polybrene (4 μg/mL), with retroviruses expressing the empty

MSCV vector or BALR-6 Isoform 3. Recipient mice were lethally irradiated and injected with donor bone marrow 6 h after irradiation. 8 mice were used per group. One mouse in the ISO3 group died due to engraftment failure after 2 weeks post injection. These mice were bled at 8, 12 and 16 weeks post bone marrow injection. At 16 weeks the mice were sacrificed for full analysis. For statistical analysis, one mouse was excluded due to low eGFP expression. This experiment was repeated, and had similar results. All animal studies were approved by the UCLA Animal Research Committee (ARC).

Flow cytometry of samples

At 16 weeks post bone marrow transplant, blood, bone marrow, thymus and spleen were collected from the mice under sterile conditions [53]. Single cell suspensions were lysed in red blood cell lysis buffer. Fluorochrome conjugated antibodies were used for staining (antibodies were obtained from eBiosciences, and Biolegend). Cells were stained with surface marker antibodies for 30 min at 4 °C, washed twice with 1X PBS, and finally fixed with 1 % PFA. Flow cytometry was performed at the UCLA Jonsson Comprehensive Cancer Center (JCCC) and at the BROAD Stem Cell Research Flow Core. Analysis was performed using FlowJo software. The lists of antibodies used and gating schematics are provided in Additional file 2: Table S2. Normal adult human bone marrow was obtained commercially from healthy adults (All Cells, Inc.) as previously described [51]. CD34 enrichment from human bone marrow was performed using the magnetic activated cell sorting (MACS) system (Miltenyi Biotec, San Diego, CA) prior to isolation of CD34+ subsets by flow cytometry. Bone marrow CD34 selected cells were incubated with a cocktail of antibodies as well as FITC-labeled lineage depletion antibodies (Additional file 2: Table S3). CD19 was not included in the lineage depletion cocktail used for sorting the progenitor B population. The immunophenotypic definitions used to isolate progenitors from human bone marrow CD34 selected cells are described in Additional file 2: Table S3. All populations were purified using fluorescence-activated cell sorting on a FACSAria (355, 405, 488, 561 and 633 nm lasers) (BD Immunocytometry Systems).

Additional files

Additional file 1: Figure S1. BALR-6 locus encodes numerous alternative splice forms. **Figure S2.** Knockdown and overexpression of full length BALR-6 isoforms in mammalian cell lines. **Figure S3.** Constitutive expression of BALR-6 in mice periphery. **Figure S4.** Elevated levels of immature B cell populations in mice with BALR-6 overexpression. **Figure S5.** SP1 targets in siRNA mediated knockdown cell lines. **Figure S6.** Confirmation of global differential expression findings seen in initial microarray. (PDF 1.19 mb)

Additional file 2: Tables S1. Primers and RACE sequences for BALR-6. **Table S2.** Antibodies used for bone marrow transplant flow cytometry analysis, and population gating schematics. **Tables S3.** Antibodies used for CD34 enrichment of human bone marrow flow cytometry analysis, and population gating schematics. (PDF 125 kb)

Abbreviations

BALR: B-ALL associated long RNA; chr: chromosome; CLP: common lymphoid progenitor; CMV: cytomegalovirus promoter; DMSO: dimethyl sulfoxide; eGFP: enhanced green fluorescent protein; HSC: hematopoietic stem cell; ISO1: Isoform 1; ISO2: Isoform 2; ISO3: Isoform 3; LMPP: lymphoid primed multipotent progenitor; LSK: lineage- $Sca1^+$ $c\text{-}Kit^+$; LTR: long terminal repeats; ORF: open reading frame; PFA: paraformaldehyde; PGK: phosphoglycerate kinase promoter; PPDE: posterior probability of differential expression luc2p, synthetic firefly luciferase; pre-B: precursor B; pro-B: progenitor B; UBC: ubiquitin C promoter; ZsGreen: Zoanthus green fluorescent protein.

Competing interests

The authors have no relevant competing interests.

Authors' contributions

DSR designed research, analyzed data and prepared the manuscript. GMC designed research and prepared the manuscript. NIRM designed research, performed research, analyzed data and prepared manuscript. TRF, PCP, JRC, JKP, TMT, JA, MOA, KP and SS performed research, and prepared manuscript. MJD analyzed data, and prepared manuscript. All authors read and approved the final manuscript.

Acknowledgements

We would like to thank the UCLA Clinical Microarray Core for performing the microarray hybridization experiments, Alejandro Balazs at Caltech for lentiviral vector backbones, and Ken Dorshkind for helpful discussions. Also, we thank Neha Goswami, Ella Waters, Jasmine Gajeton, Peter D. Pioli, Nolan Ung, Jennifer King and May Paing for their technical support. Very special thanks to Diana C. Márquez-Garbán at Dr. Richard Pietras lab (UCLA) for use of their facilities for some of the experiments. This research was supported by the Graduate Research Fellowship Program from the National Science Foundation DGE-1144087 (N.I.R.M.), the Eugene V. Cota-Robles Fellowship from UCLA (N.I.R.M., J.R.C.), Tumor Biology Training Grant T32 CA009056 from the National Institute of Health (NIH) (T.R.F.), the institutional Tumor Immunology Training Grants NIH T32CA009120 (J.R.C.) and NIH T32009056 (T.R.F.), the Eli and Edythe Broad Center of Regenerative Medicine and Stem Cell Research at UCLA Training Program (M.O.A.), a Career Development Award K08CA133521 (D.S.R.), the Sidney Kimmel Translational Scholar Award SKF-11-013 (D.S.R), the Irving Feintech Family Foundation/Tower Cancer Research Foundation Research Grant (D.S.R), the University of California Cancer Research Coordinating Committee (D.S.R), the Stein-Oppenheimer Endowment Award (D.S.R), NIH P01 HL073104 (G.M.C.), UCLA Broad Stem Cell Research Center (BSCRC) (D.S.R., G.M.C), NIH T32 HL086345 (S.S.) and California Institute for Regenerative Medicine (CIRM) Training Grant TG2-01169 (S.S.). Flow cytometry was performed in the BSCRC FACS Core facility, and UCLA Jonsson Comprehensive Cancer Center (JCCC) and Center for AIDS Research Flow Cytometry Core Facility that is supported by National Institutes of Health awards CA-16042 and AI-28697, and by the JCCC, the UCLA AIDS Institute, the UCLA Council of Bioscience Resources, and the David Geffen School of Medicine at UCLA.

Author details

[1]Department of Pathology and Laboratory Medicine, UCLA, Los Angeles, USA. [2]Cellular and Molecular Pathology Ph.D. Program, UCLA, Los Angeles, USA. [3]Jonsson Comprehensive Cancer Center, UCLA, Los Angeles, USA. [4]Broad Stem Cell Research Center, UCLA, 650 Charles E. Young Drive, Factor 12-272, Los Angeles, CA 90095, USA. [5]Department of Environmental Health Sciences, UCLA, Los Angeles, USA. [6]Molecular Toxicology Interdepartmental Ph.D. Program, UCLA, Los Angeles, USA. [7]All India Institute of Medical Sciences (AIIMS), New Delhi, India.

Received: 25 July 2015 Accepted: 11 December 2015
Published online: 22 December 2015

References

1. Kapranov P, Cheng J, Dike S, Nix DA, Duttagupta R, Willingham AT, et al. RNA maps reveal new RNA classes and a possible function for pervasive transcription. Science. 2007;316:1484–8.
2. Guttman M, Amit I, Garber M, French C, Lin MF, Feldser D, et al. Chromatin signature reveals over a thousand highly conserved large non-coding RNAs in mammals. Nature. 2009;458:223–7.
3. Niazi F, Valadkhan S. Computational analysis of functional long noncoding RNAs reveals lack of peptide-coding capacity and parallels with 3′ UTRs. RNA. 2012;18:825–43.
4. Ulitsky I, Shkumatava A, Jan CH, Sive H, Bartel DP. Conserved function of lincRNAs in vertebrate embryonic development despite rapid sequence evolution. Cell. 2011;147:1537–50.
5. Rinn JL, Kertesz M, Wang JK, Squazzo SL, Xu X, Brugmann SA, et al. Functional demarcation of active and silent chromatin domains in human HOX loci by noncoding RNAs. Cell. 2007;129:1311–23.
6. Tripathi V, Ellis JD, Shen Z, Song DY, Pan Q, Watt AT, et al. The nuclear-retained noncoding RNA MALAT1 regulates alternative splicing by modulating SR splicing factor phosphorylation. Mol Cell. 2010;39:925–38.
7. Cesana M, Cacchiarelli D, Legnini I, Santini T, Sthandier O, Chinappi M, et al. A long noncoding RNA controls muscle differentiation by functioning as a competing endogenous RNA. Cell. 2011;147:358–69.
8. Carrieri C, Cimatti L, Biagioli M, Beugnet A, Zucchelli S, Fedele S, et al. Long non-coding antisense RNA controls Uchl1 translation through an embedded SINEB2 repeat. Nature. 2012;491:454–7.
9. Gong C, Maquat LE. lncRNAs transactivate STAU1-mediated mRNA decay by duplexing with 3' UTRs via Alu elements. Nature. 2011;470:284–8.
10. Gupta RA, Shah N, Wang KC, Kim J, Horlings HM, Wong DJ, et al. Long non-coding RNA HOTAIR reprograms chromatin state to promote cancer metastasis. Nature. 2010;464:1071–6.
11. Prensner JR, Iyer MK, Balbin OA, Dhanasekaran SM, Cao Q, Brenner JC, et al. Transcriptome sequencing across a prostate cancer cohort identifies PCAT-1, an unannotated lincRNA implicated in disease progression. Nat Biotechnol. 2011;29:742–9.
12. Gutschner T, Hammerle M, Eissmann M, Hsu J, Kim Y, Hung G, et al. The noncoding RNA MALAT1 is a critical regulator of the metastasis phenotype of lung cancer cells. Cancer Res. 2013;73:1180–9.
13. Isin M, Dalay N. LncRNAs and neoplasia. Clin Chim Acta. 2015;444:280–8.
14. Mullighan CG, Downing JR. Global genomic characterization of acute lymphoblastic leukemia. Semin Hematol. 2009;46:3–15.
15. Mullighan CG. Molecular genetics of B-precursor acute lymphoblastic leukemia. J Clin Invest. 2012;122:3407–15.
16. Fernando TR, Rodriguez-Malave NI, Waters EV, Yan W, Casero D, Basso G, et al. LncRNA Expression Discriminates Karyotype and Predicts Survival in B-Lymphoblastic Leukemia. Mol Cancer Res. 2015;13:839–51.
17. Pui CH, Behm FG, Downing JR, Hancock ML, Shurtleff SA, Ribeiro RC, et al. 11q23/MLL rearrangement confers a poor prognosis in infants with acute lymphoblastic leukemia. J Clin Oncol. 1994;12:909–15.
18. Bernstein BE, Kamal M, Lindblad-Toh K, Bekiranov S, Bailey DK, Huebert DJ, et al. Genomic maps and comparative analysis of histone modifications in human and mouse. Cell. 2005;120:169–81.
19. Ernst J, Kheradpour P, Mikkelsen TS, Shoresh N, Ward LD, Epstein CB, et al. Mapping and analysis of chromatin state dynamics in nine human cell types. Nature. 2011;473:43–9.
20. Ram O, Goren A, Amit I, Shoresh N, Yosef N, Ernst J, et al. Combinatorial patterning of chromatin regulators uncovered by genome-wide location analysis in human cells. Cell. 2011;147:1628–39.
21. Benson DA, Karsch-Mizrachi I, Lipman DJ, Ostell J, Wheeler DL. GenBank: update. Nucleic Acids Res. 2004;32:D23–6.
22. Siepel A, Bejerano G, Pedersen JS, Hinrichs AS, Hou M, Rosenbloom K, et al. Evolutionarily conserved elements in vertebrate, insect, worm, and yeast genomes. Genome Res. 2005;15:1034–50.
23. Zhou Y, Zhong Y, Wang Y, Zhang X, Batista DL, Gejman R, et al. Activation of p53 by MEG3 non-coding RNA. J Biol Chem. 2007;282:24731–42.
24. Dawson MA, Prinjha RK, Dittmann A, Giotopoulos G, Bantscheff M, Chan WI, et al. Inhibition of BET recruitment to chromatin as an effective treatment for MLL-fusion leukaemia. Nature. 2011;478:529–33.
25. O'Connell RM, Chaudhuri AA, Rao DS, Baltimore D. Inositol phosphatase SHIP1 is a primary target of miR-155. Proc Natl Acad Sci U S A. 2009;106:7113–8.
26. Rao DS, O'Connell RM, Chaudhuri AA, Garcia-Flores Y, Geiger TL, Baltimore D. MicroRNA-34a perturbs B lymphocyte development by repressing the forkhead box transcription factor Foxp1. Immunity. 2010;33:48–59.
27. Hardy RR, Hayakawa K. B cell development pathways. Annu Rev Immunol. 2001;19:595–621.
28. Yap KL, Li S, Munoz-Cabello AM, Raguz S, Zeng L, Mujtaba S, et al. Molecular interplay of the noncoding RNA ANRIL and methylated histone H3 lysine 27 by polycomb CBX7 in transcriptional silencing of INK4a. Mol Cell. 2010;38:662–74.
29. Khalil AM, Guttman M, Huarte M, Garber M, Raj A, Rivea Morales D, et al. Many human large intergenic noncoding RNAs associate with chromatin-modifying complexes and affect gene expression. Proc Natl Acad Sci U S A. 2009;106:11667–72.
30. Baldi P, Long AD. A Bayesian framework for the analysis of microarray expression data: regularized t -test and statistical inferences of gene changes. Bioinformatics. 2001;17:509–19.
31. Kayala MA, Baldi P. Cyber-T web server: differential analysis of high-throughput data. Nucleic Acids Res. 2012;40:W553–9.
32. Zhang B, Kirov S, Snoddy J. WebGestalt: an integrated system for exploring gene sets in various biological contexts. Nucleic Acids Res. 2005;33:W741–8.
33. Wang J, Duncan D, Shi Z, Zhang B. WEB-based GEne SeT AnaLysis Toolkit (WebGestalt): update 2013. Nucleic Acids Res. 2013;41:W77–83.
34. Lerner M, Harada M, Loven J, Castro J, Davis Z, Oscier D, et al. DLEU2, frequently deleted in malignancy, functions as a critical host gene of the cell cycle inhibitory microRNAs miR-15a and miR-16-1. Exp Cell Res. 2009;315:2941–52.
35. Cai X, Cullen BR. The imprinted H19 noncoding RNA is a primary microRNA precursor. RNA. 2007;13:313–6.
36. Dickinson LA, Joh T, Kohwi Y, Kohwi-Shigematsu T. A tissue-specific MAR/SAR DNA-binding protein with unusual binding site recognition. Cell. 1992;70:631–45.
37. Will B, Vogler TO, Bartholdy B, Garrett-Bakelman F, Mayer J, Barreyro L, et al. Satb1 regulates the self-renewal of hematopoietic stem cells by promoting quiescence and repressing differentiation commitment. Nat Immunol. 2013;14:437–45.
38. Kohwi-Shigematsu T, Poterlowicz K, Ordinario E, Han HJ, Botchkarev VA, Kohwi Y. Genome organizing function of SATB1 in tumor progression. Semin Cancer Biol. 2013;23:72–9.
39. Fang K, Han BW, Chen ZH, Lin KY, Zeng CW, Li XJ, et al. A distinct set of long non-coding RNAs in childhood MLL-rearranged acute lymphoblastic leukemia: biology and epigenetic target. Hum Mol Genet. 2014;23:3278–88.
40. Garitano-Trojaola A, Agirre X, Prosper F, Fortes P. Long non-coding RNAs in haematological malignancies. Int J Mol Sci. 2013;14:15386–422.
41. Alvarez-Dominguez JR, Hu W, Gromatzky AA, Lodish HF. Long noncoding RNAs during normal and malignant hematopoiesis. Int J Hematol. 2014;99:531–41.
42. Venkatraman A, He XC, Thorvaldsen JL, Sugimura R, Perry JM, Tao F, et al. Maternal imprinting at the H19-Igf2 locus maintains adult haematopoietic stem cell quiescence. Nature. 2013;500:345–9.
43. Aoki K, Harashima A, Sano M, Yokoi T, Nakamura S, Kibata M, et al. A thymus-specific noncoding RNA, Thy-ncR1, is a cytoplasmic riboregulator of MFAP4 mRNA in immature T-cell lines. BMC Mol Biol. 2010;11:99.
44. Zhang X, Lian Z, Padden C, Gerstein MB, Rozowsky J, Snyder M, et al. A myelopoiesis-associated regulatory intergenic noncoding RNA transcript within the human HOXA cluster. Blood. 2009;113:2526–34.
45. Hu W, Yuan B, Flygare J, Lodish HF. Long noncoding RNA-mediated anti-apoptotic activity in murine erythroid terminal differentiation. Genes Dev. 2011;25:2573–8.
46. Xia F, Dong F, Yang Y, Huang A, Chen S, Sun D, et al. Dynamic transcription of long non-coding RNA genes during CD4+ T cell development and activation. PLoS One. 2014;9:e101588.
47. Fulciniti M, Amin S, Nanjappa P, Rodig S, Prabhala R, Li C, et al. Significant biological role of sp1 transactivation in multiple myeloma. Clin Cancer Res. 2011;17:6500–9.
48. Amodio N, Di Martino MT, Foresta U, Leone E, Lionetti M, Leotta M, et al. miR-29b sensitizes multiple myeloma cells to bortezomib-induced apoptosis through the activation of a feedback loop with the transcription factor Sp1. Cell Death Dis. 2012;3:e436.
49. Wang X, Yan Z, Fulciniti M, Li Y, Gkotzamanidou M, Amin SB, et al. Transcription factor-pathway coexpression analysis reveals cooperation

between SP1 and ESR1 on dysregulating cell cycle arrest in non-hyperdiploid multiple myeloma. Leukemia. 2014;28:894–903.
50. Shankar DB, Cheng JC, Kinjo K, Federman N, Moore TB, Gill A, et al. The role of CREB as a proto-oncogene in hematopoiesis and in acute myeloid leukemia. Cancer Cell. 2005;7:351–62.
51. Esparza SD, Chang J, Shankar DB, Zhang B, Nelson SF, Sakamoto KM. CREB regulates Meis1 expression in normal and malignant hematopoietic cells. Leukemia. 2008;22:665–7.
52. O'Connell RM, Balazs AB, Rao DS, Kivork C, Yang L, Baltimore D. Lentiviral vector delivery of human interleukin-7 (hIL-7) to human immune system (HIS) mice expands T lymphocyte populations. PLoS One. 2010;5:e12009.
53. Contreras JR, Palanichamy JK, Tran TM, Fernando TR, Rodriguez-Malave NI, Goswami N. MicroRNA-146a modulates B-cell oncogenesis by regulating Egr1. Oncotarget. 2015;6:11023–37.

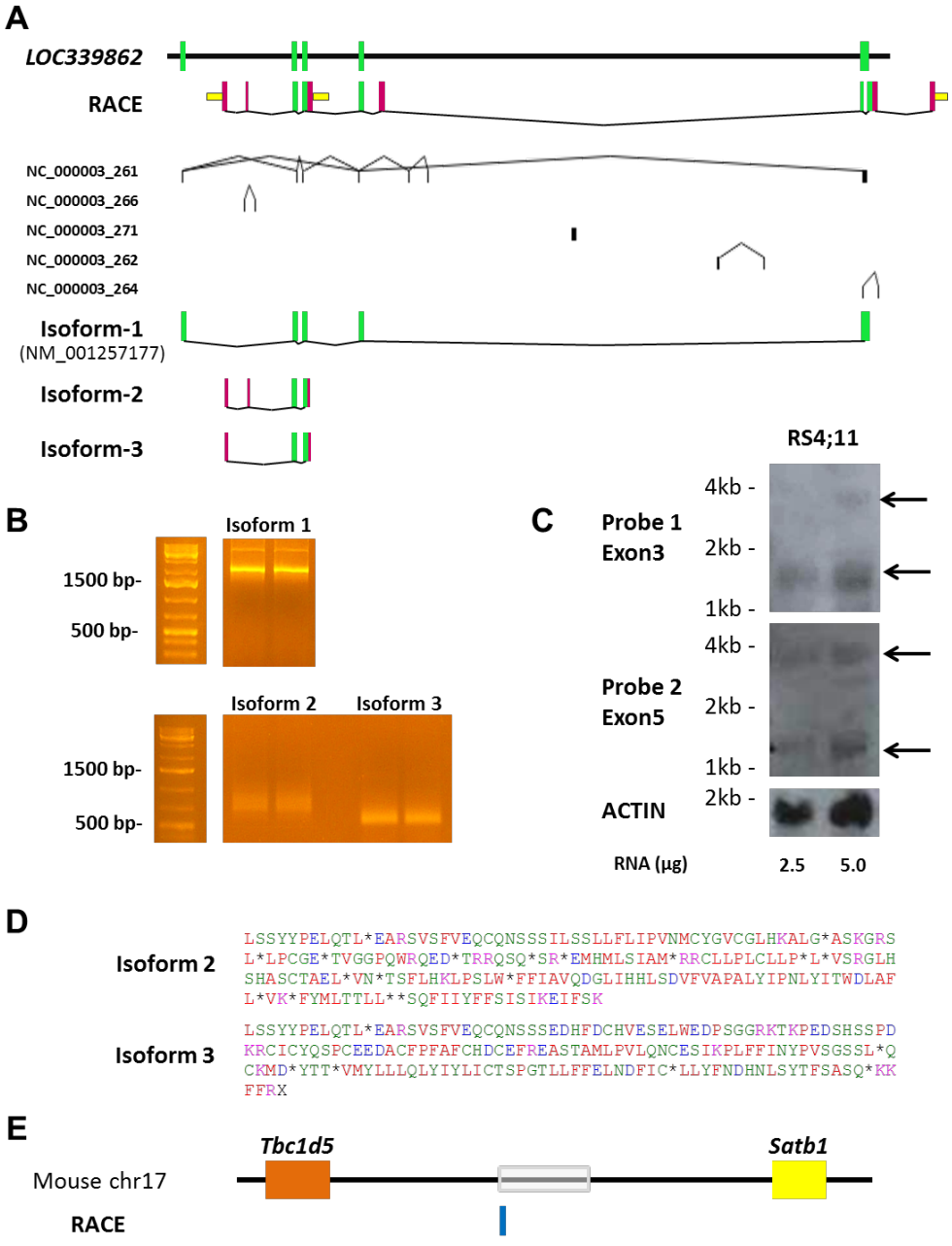

Supplemental Figure 1. BALR-6 locus encodes numerous alternative splice forms.
(**A**) Top: Diagram of RACE products obtained from *LOC339862*. 5' and 3' RACE primers are shown in yellow, with the newly discovered exons shown in magenta, as seen in Figure 1C. Known annotated exons are shown in green. Middle: Alternative splicing graph from the Swiss Institute of Bioinformatics of the predicted alternative splicing transcripts shown in the SIB Genes track. Blocks represent exons, lines indicate introns. Bottom: Schematic depiction of BALR-6 isoforms cloned from RACE sequences. Annotated exons in green, unannotated in magenta. (**B**) Gel confirmation of the isoforms cloned, including the annotated mRNA sequence (Isoform 1). (**C**) Northern blot of endogenous levels of two BALR-6 isoforms in RS4;11 cells. (**D**) EMBOSS analysis of the new isoforms confirmed lack of open reading frames, and lack of translation initiation sites. (**E**) Diagram of RACE products obtained from mouse cell lines with homology to BALR-6. chr, chromosome.

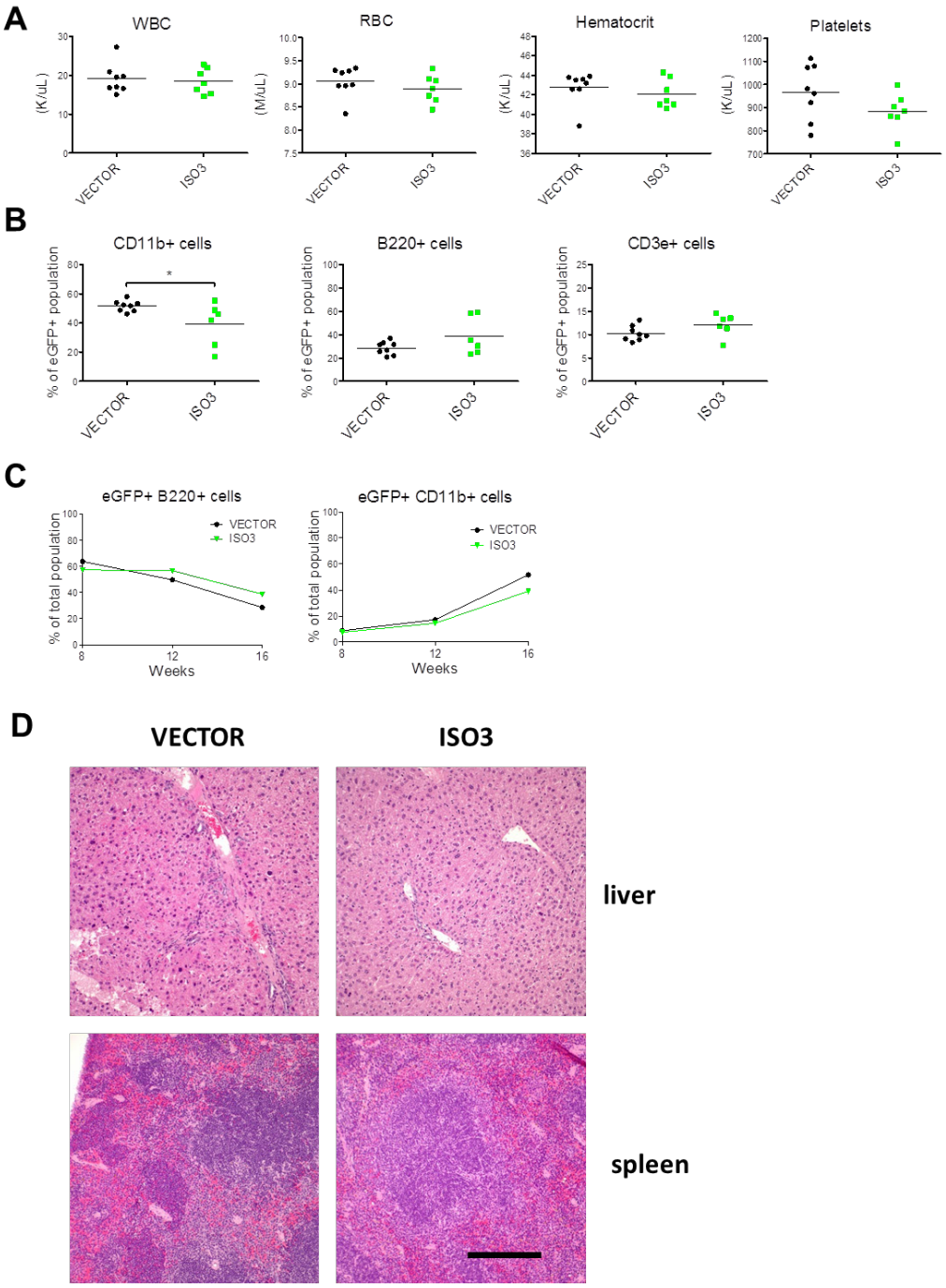

Supplemental Figure 3. Constitutive expression of BALR-6 in mice periphery.
(**A**) Peripheral white and red blood, hematocrit, and platelet cell counts. (**B**) Levels of B-cells (B220+), T-cells (CD3e+) and Myeloid cells (CD11b+) in the eGFP+ compartment of the peripheral blood at 16 weeks. (**C**) Average levels of eGFP+ B cells (B220+) and eGFP+ Myeloid (CD11b+) cells in the peripheral blood throughout the experiment. Number of mice used in this analysis: VECTOR, n=8; ISO3, n=6. (**D**) Hematoxylin and eosin stained liver and spleen samples from bone marrow transfer mice. Scale bar, 200 mm. ISO3, Isoform 3. Evaluations made using a two-tailed T-test, $p<0.05$ (*).

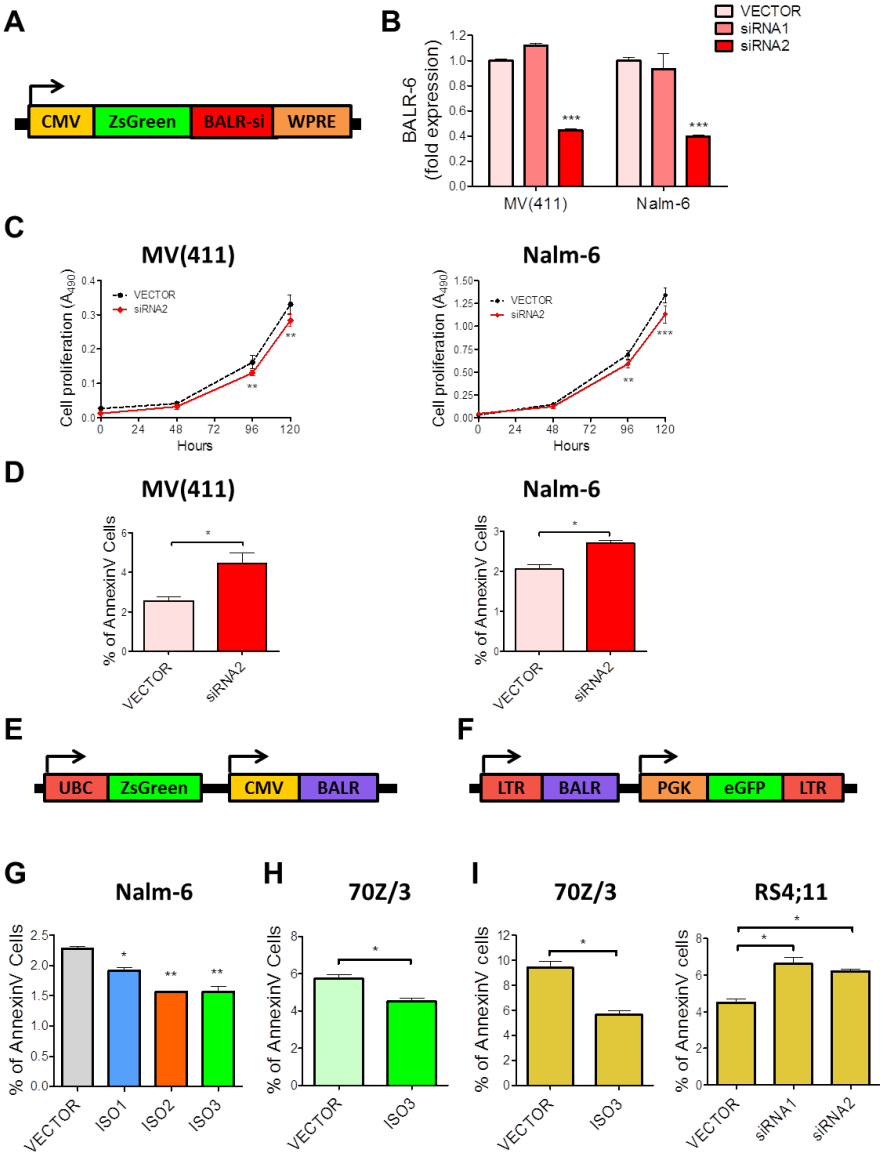

Supplemental Figure 2. Knockdown and overexpression of full length BALR-6 isoforms in mammalian cell lines.

(**A**) Schematic representation of mmu-miR-115 knockdown expression cassette. (**B**) Successful knockdown of BALR-6 using siRNA2 in MV(411), and Nalm-6 cells. (**C**) Decreased cell proliferation in transduced MV(411), and Nalm-6 lines as measured by MTS assay. (**D**) Increased apoptosis at basal levels in MV(411), and Nalm-6 stable lines as measured by AnnexinV staining. (**E-F**) Schematic representation of dual promoter phage (**E**) and MSCV (**F**) expression cassettes. (**G**) AnnexinV staining showed that Nalm-6 stably transduced with BALR-6 isoforms, had lower number of apoptotic cells at basal level. (**H**) 70Z/3 cells overexpressing BALR-6 Isoform 3 had fewer apoptotic cells at basal level, as analyzed by AnnexinV staining. (**I**) 70Z/3 cells stably transduced with BALR-6 Isoform 3, resulted in reduction of apoptosis upon treatment with 250 µg/mL prednisolone for 6 hours. The opposite effect was seen with RS4;11 cells with siRNA mediated knockdown of BALR-6 and treated with 250 µg/mL prednisolone for 24 hours. Evaluations were made using a two-tailed T-test, $p<0.05$ (*); $p<0.005$ (**); $p<0.0005$(***). UBC, ubiquitin C promoter; ZsGreen, Zoanthus green fluorescent protein; CMV, cytomegalovirus promoter; LTR, long terminal repeats; PGK, phosphoglycerate kinase promoter; eGFP, enhanced green fluorescent protein.

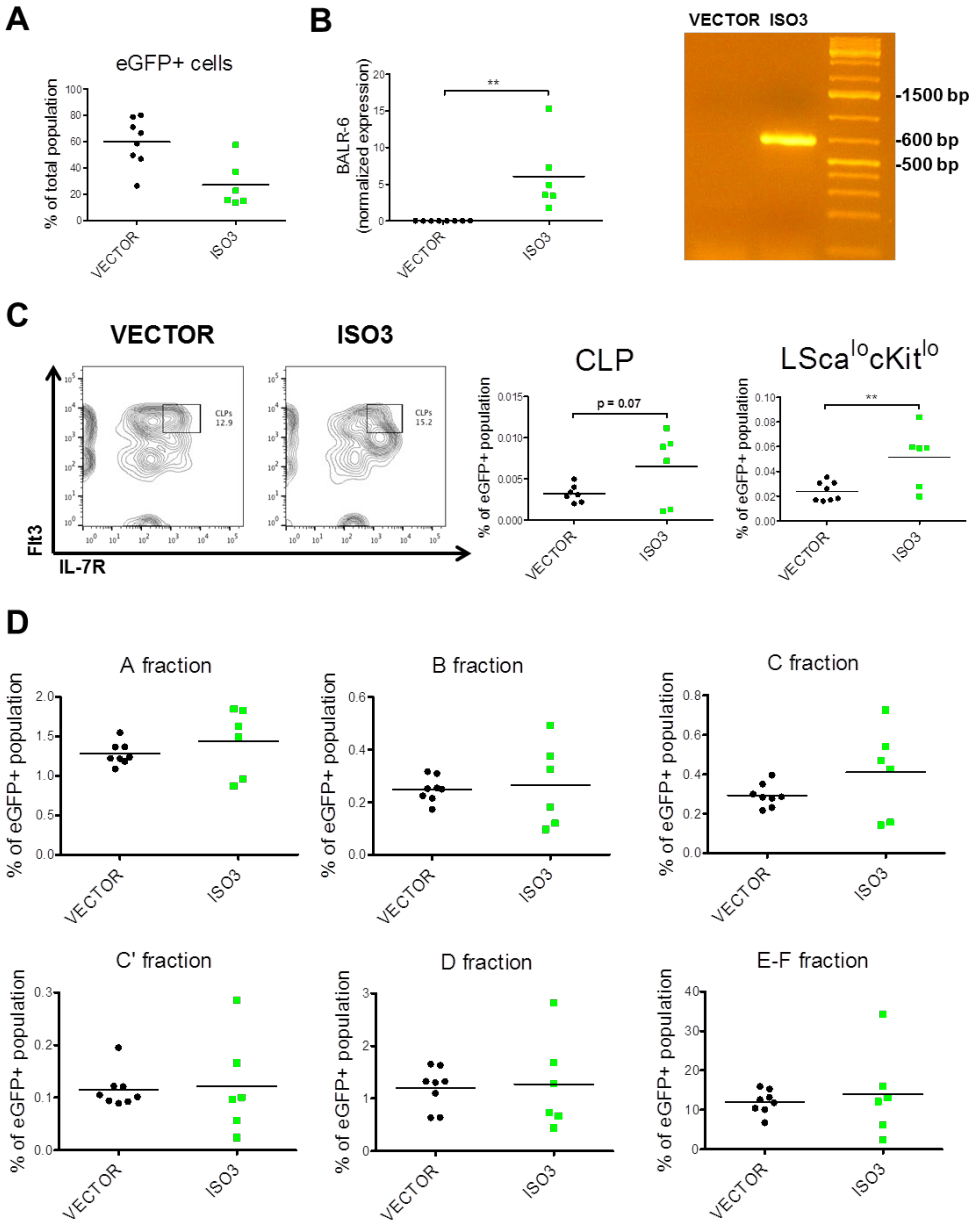

Supplemental Figure 4. Elevated levels of immature B cell populations in mice with BALR-6 overexpression.

(**A**) Levels of e+ cells in the bone marrow of experimental mice. (**B**) Expression levels of BALR-6 Isoform 3 in the experimental mice by qRT-PCR. Normalized to L32. Gel of cDNA PCR, obtained from bone marrow samples, confirming expression of full length transcript, shown to the right. (**C**) Representative FACS plots of CLP cells in the eGFP+ compartment of the experimental mice. Quantitation of the population gating and of LSca^{lo}c-Kit^{lo} cells, shown to the right. (**D**) Percentage of cells in the Hardy fractions from the eGFP+ compartment of experimental mice. Number of mice used in this analysis: VECTOR, n=8; ISO3, n=6. ISO3, Isoform 3. Evaluations made using a two-tailed T-test, $p<0.005$ (**).

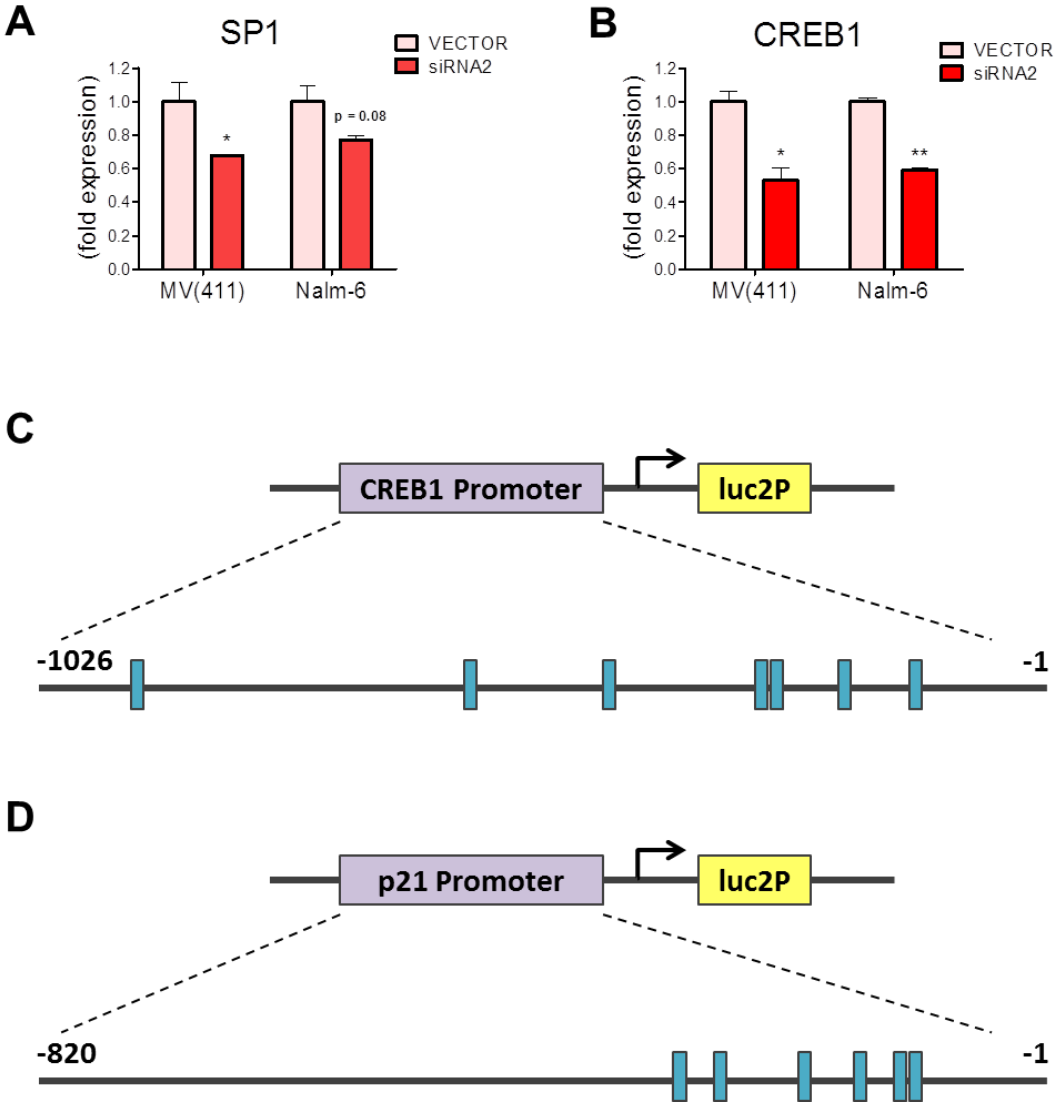

Supplemental Figure 5. SP1 targets in siRNA mediated knockdown cell lines.
(**A-B**) Transcript levels of SP1 (**A**) and CREB1 (**B**) in MV(411) and Nalm-6 knockdown cells. qRT-PCR quantitation of expression, normalized with ACTIN. Only expression levels upon siRNA2 mediated knockdown, which was successful, are shown. (**C-D**) Schematic representation of CREB1 (**C**) and p21 (**D**) promoter sequences cloned into the pGL4.11 luciferase expression vector. Promoter sequence distance shown in relation to the luc2p start codon. SP1 binding sites shown as blue boxes. luc2p, synthetic firefly luciferase.

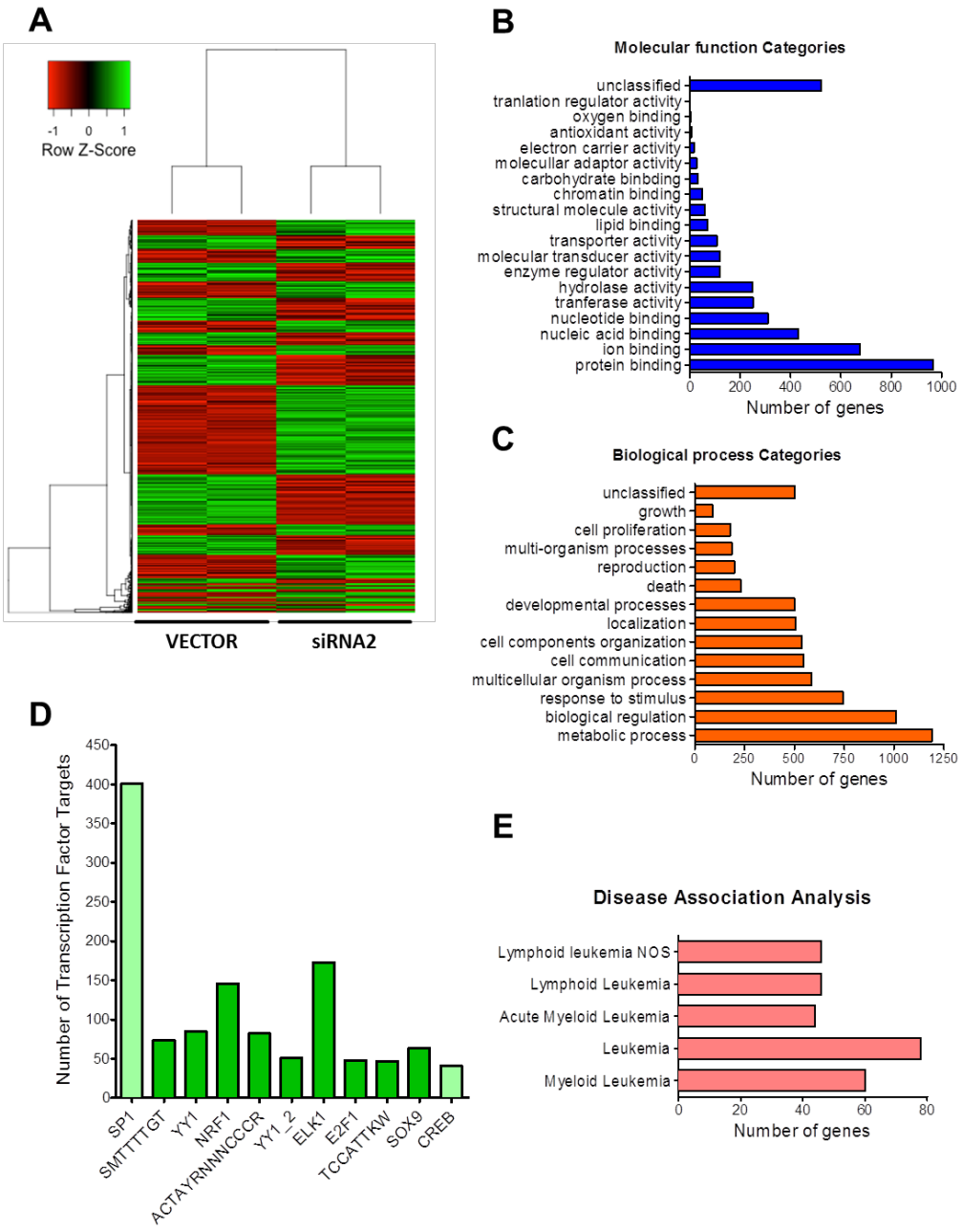

Supplemental Figure 6. Confirmation of global differential expression findings seen in initial microarray.

(**A**) Hierarchical gene clustering of differentially expressed genes in validation microarray upon siRNA2-mediated knockdown of BALR-6 in RS4;11 cells, p-value ≤ 0.05. Technical replicates of samples shown. (**B-C**) Bar graphs of GO Slim classification enrichment analysis of differentially expressed genes by molecular function (**B**) and biological processes (**C**) as analyzed by WebGESTALT. Proportions are highly similar to initial microarray. (**D**) Enrichment analysis of transcription factor targets. Top ten transcription factors with a p-value ≤ 0.02 are shown. In addition, CREB1 was shown as a significantly enriched for its targets with p-value = 0.04. For unknown transcription factors, transcription site sequence is shown. SP1 (shown in light green) had the most dysregulated targets. (**E**) Disease association analysis by GLAD4U, revealed a significant enrichment of genes solely associated to leukemic diseases, p-value ≤ 0.05.

Supplemental Table 1: Primers and RACE sequences for BALR-6

RT-qPCR primers		
BALR-6 Set 1	FOW	5' CGTGTGCTGGGGAAGGCACTG 3'
	REV	5' CCAGGCTCAGAGCAACACAGGGA 3'
BALR-6 Set 2	FOW	5' GATCACTTTGATTGCCATGTGGA 3'
	REV	5' ATCTCTTATCTGGACTACGGTGAC 3'
ACTIN	FOW	5' CATGTACGTTGCTATCCAGGC 3'
	REV	5' CTCCTTAATGTCACGCACGAT 3'
SP1	FOW	5' TGGCAGCAGTACCAATGGC 3'
	REV	5' CCAGGTAGTCCTGTCAGAACTT 3'
CREB1	FOW	5' TTAACCATGACCAATGCAGCA 3'
	REV	5' TGGTATGTTTGTACGTCTCCAGA 3'
Sp1	FOW	5' AGGGTCCGAGTCAGTCAGG 3'
	REV	5' CTCGCTGCCATTGGTACTGTT 3'
Creb1	FOW	5' TGTAGTTTGACGCGGTGTGT 3'
	REV	5' GCTGGTTGTCTGCTCCAGAT 3'
L32 (mouse)	FOW	5' AAGCGAAACTGGCGGAAAC 3'
	REV	5' TAACCGATGTTGGGCATCAG 3'
Actin	FOW	5' GCTACAGCTTCACCACCACA 3'
	REV	5' GGGGTGTTGAAGGTCTCAAA 3'
Cloning primers for P6UZCL		
NotI site-1	FOW	5'ATGGGCTTAGCTGCGGCCGCTTTCTTCATACTATCCAGAGCT CCAAA3'
BamHI site-1	REV	5'ATGGCAATTATCGGATCCTTTTTTTTTTTTCGAAAAAATTTCT TTTATTGAGATGCT3'
NotI site-2	FOW	5'ATGGCA ATTGCGGCCGCCCACGCGTCCGGGACTGAGCA 3'
BamHI site-2	REV	5'ATGGGCTGATGATCATTTTTTTTTGGTTCATAGAAAGTATTT TCTTCTAGAGTCTC3'
Cloning primers for MSCV		
HindIII_eGFP	FOW	5'ATGGGCTTAGCTAAGCTTATGGTGAGCAAGGGCGAGGAGC3'
DraIII_eGFP	REV	5'ATGGCAATTATCCACCTGGTGTTTACTTGTACAGCTCGTCCA TGCCGA3'
BclI_BglII site	FOW	5' ATGGGCTGAGGATCTCCACGCGTCCGGGACTGAGCA 3'
XhoI site-1	REV	5'ATGGCAATTCTCGAGTTTTTTTTTGGTTCATAGAAAGTATTTT CTTCTAGAGTCTC3'
BamHI_BglII site	FOW	5'ATGGGCTTAGCTGGATCCTTTCTTCATACTATCCAGAGCTCC AAA3'
XhoI site-2	REV	5'ATGGCAATTATCCTCGAGTTTTTTTTTTTTCGAAAAAATTTCT TTTATTGAGATGCT3'
Sequencing primers for MSCV		
Upstream_Puro	FOW	5' GCTGTTCTCCTCTTCCTCATCTCC 3'
Upstream_eGFP	FOW	5' CTTTATCCAGCCCTCACTCCTTCTCT 3'

RACE primers		
3-RACE_6	FOW	5' CCATGTGAAGAAGATGCTGGCTTC 3'
3-RACE_7	FOW	5' TAGGAAGCCAGAAGCGTCTCCTTT 3'
3-RACE_8	FOW	5' GGAGGCAGGAAGACTAAACCAGAA 3'
5-RACE_2	REV	5' CTCGCGAAACTCACAATCATGGCA 3'
5-RACE_4	REV	5' ATCTTCCATGTGCATGTGGCTGCA 3'
Northern probes		
BALR-6 probe 1		5'GGGCACAGAGTGTTGCATGCTCATTTCTGTTGATTTTTAATT AGCAGTAATTCATTT/3DiG_N/3'
BALR-6 probe 2		5'CTGGAAATCTAGGATCAGGACTAGCCTAAATTAGTAGATCT ATGTGATAGTATATTGGTA/3DiG_N/3'
mmu-miR-155 formatted siRNA oligos		
siRNA1		5'GAAGGCTGTATGCTGGTGAACATACCACTTACCATTGTTTTG GCCACTGACTGACAATGGTAAGGTATGTTCACCAGGACACAA GGCCTG3'
siRNA2		5'GAAGGCTGTATGCTGGACTTCTGCACACCATGCCTGGTTTTG GCCACTGACTGACCAGGCATGGTGCAGAAGTCCAGGACACAA GGCCTG3'
BALR-6 sequences		
Isoform-2		5'TTTCTTCATACTATCCAGAGCTCCAAACTTTGTAGGAAGCCA GAAGCGTCTCCTTTGTTGAACAGTGCCAAAATAGCAGCTCTAT CCTTTCCTCTCTCCTCTTTCTGATTCCAGTCAATATGTGTTATG GAGTCTGTGGTCTCCACAAGGCCTTGGGATAGGCATCCAAAG GAAGATCACTTTGATTGCCATGTGGAGAGTGAACTGTGGGAG GACCCCAGTGGAGGCAGGAAGACTAAACCAGAAGACAGTCA CAGTAGTCCAGATAAGAGATGCATATGTTATCAATCGCCATG TGAAGAAGATGCTTGCTTCCCCTTTGCCTTCTGCCATGATTGT GAGTTTCGCGAGGCCTCCACAGCCATGCTTCCTGTACTGCAGA ACTGTGAGTCAATTAAACCTCTTTTCTTCATAAATTACCCAGT CTCTGGTAGTTCTTTATAGCAGTGCAAGATGGACTAATACACC ACCTAAGTGATGTATTTGTTGCTCCAGCTCTATATATACCTAA TTTGTACATCACCTGGGACCTTGCTTTTCTTTGAGTTAAATGA TTTTATATGTTAACTACTCTACTTTAATGATCACAATTTATCAT ATACTTTTTCAGCATCTCAATAAAAGAAATTTTTTCGAAA3'
Isoform-3		5'TTTCTTCATACTATCCAGAGCTCCAAACTTTGTAGGAAGCCA GAAGCGTCTCCTTTGTTGAACAGTGCCAAAATAGCAGCTCTG AAGATCACTTTGATTGCCATGTGGAGAGTGAACTGTGGGAGG ACCCCAGTGGAGGCAGGAAGACTAAACCAGAAGACAGTCAC AGTAGTCCAGATAAGAGATGCATATGTTATCAATCGCCATGT GAAGAAGATGCTTGCTTCCCCTTTGCCTTCTGCCATGATTGTG AGTTTCGCGAGGCCTCCACAGCCATGCTTCCTGTACTGCAGAA CTGTGAGTCAATTAAACCTCTTTTCTTCATAAATTACCCAGTC TCTGGTAGTTCTTTATAGCAGTGCAAGATGGACTAATACACCA CCTAAGTGATGTATTTGTTGCTCCAGCTCTATATATACCTAAT TTGTACATCACCTGGGACCTTGCTTTTCTTTGAGTTAAATGAT TTTATATGTTAACTACTCTACTTTAATGATCACAATTTATCATA TACTTTTTCAGCATCTCAATAAAAGAAATTTTTTCGAAA3'

Supplemental Table 2: Antibodies used for bone marrow transplant flow cytometry analysis, and population gating schematics.

Marker	**Fluorochrome**
CD3e	PE
CD11b	PE-Cy7
B220	PerCP-Cy 5.5
CD117	APC-Cy7
Sca1	PerCP-Cy 5.5
CD135	APC
CD127	PE-Cy7
CD150	PE
IgM	PE
CD43	APC
CD24	PE-Cy7
Ly51	APC-Cy7
For lineage negative staining	
Biotin	CD3e, CD4, CD8, B220, NK1.1, Ter119, TCR beta, TCR gamma-delta
Streptavidin	eFluor 450 (pacific Blue)
Population	**Defined markers**
HSC	Lin- CD117 hi Sca1 hi CD150++
LMPP	Lin- CD117 hi Sca1 hi CD135+ CD127-
CLP	Lin- CD117 lo Sca1 lo CD135+ CD127+
A	B220+ IgM- CD43+ CD24- Ly51-
B	B220+ IgM- CD43+ CD24+ Ly51-
C	B220+ IgM- CD43+ CD24+ Ly51+
D	B220+ IgM- CD43-
E and F	B220+ IgM+

Antibodies were procured from eBiosciences (San Diego, CA) or Biolegend (San Diego, CA).

Supplemental Table 3: Antibodies used for CD34 enrichment of human bone marrow flow cytometry analysis, and population gating schematics.

Marker	**Fluorochrome**
CD34	APC-Cy7
CD38	APC
CD10	PE-Cy7
CD20	FITC
CD45RA	PerCP-Cy 5.5
IgM	PerCP-Cy 5.5
For lineage depletion	
FITC	CD3, CD14, CD15, CD19, CD56, and CD235a
Population	**Defined markers**
HSC	Lin- CD34+CD38-
CLP	Lin- CD34+CD10+CD45RA+
progenitor B	Lin- CD34+CD19+
precursor B	CD34-CD10+CD19+IgM-CD20-
Immature B	CD34-CD19+IgM+CD20+

Antibodies were procured from Becton Dickinson (BD, San Jose, CA) or Biolegend (San Diego, CA).